OPEN ACCESS

University of BRISTOL

This electronic thesis or dissertation has been downloaded from Explore Bristol Research, http://research-information.bristol.ac.uk

Author:
Alobaid, Hussah M S

Title:
Gonadotrophin-releasing hormone signalling: exploring the sensing of hormone concentration and dynamics

General rights
Access to the thesis is subject to the Creative Commons Attribution - NonCommercial-No Derivatives 4.0 International Public License. A copy of this may be found at https://creativecommons.org/licenses/by-nc-nd/4.0/legalcode This license sets out your rights and the restrictions that apply to your access to the thesis so it is important you read this before proceeding.

Take down policy
Some pages of this thesis may have been removed for copyright restrictions prior to having it been deposited in Explore Bristol Research. However, if you have discovered material within the thesis that you consider to be unlawful e.g. breaches of copyright (either yours or that of a third party) or any other law, including but not limited to those relating to patent, trademark, confidentiality, data protection, obscenity, defamation, libel, then please contact collections-metadata@bristol.ac.uk and include the following information in your message:

• Your contact details
• Bibliographic details for the item, including a URL
• An outline nature of the complaint

Your claim will be investigated and, where appropriate, the item in question will be removed from public view as soon as possible.

Gonadotrophin-releasing hormone signalling: exploring the sensing of hormone concentration and dynamics

Hussah M Alobaid

A thesis submitted to the University of Bristol in accordance with the requirements for award of the degree of Doctor of Philosophy in the Faculty of Health Sciences.

2019

Word counts: 62166

Publications

- Voliotis, M, Garner, KL, Alobaid, H, Tsaneva-Atanasova, K & McArdle, CA, 2018, 'Exploring Dynamics and Noise in Gonadotropin-Releasing Hormone (GnRH) Signalling: Methods and Protocols. Methods Mol Biol. 2018; 1819:405-429.
- Voliotis, M, Garner, KL, Alobaid, H, Tsaneva-Atanasova, K & McArdle, CA, 2018, 'Gonadotropin-releasing hormone signalling: An information theoretic approach'. Molecular and Cellular Endocrinology, vol 463., pp. 106-115.
- Garner, K, Voliotis, M, Alobaid, HMS, Perrett, RM, Pham, T, Tsaneva-Atanasova, K & McArdle, C, 2017, 'Information Transfer via Gonadotropin-Releasing Hormone Receptors to ERK and NFAT: Sensing GnRH and Sensing Dynamics. Journal of the Endocrine Society, vol 1., pp. 260-277.

Abstract

Gonadotrophin-releasing hormone (GnRH) is a hypothalamic neuropeptide that is secreted in pulses and acts via GnRHRs on the pituitary gonadotroph. It activates signal transduction cascades, causing a largely PKC-mediated activation of extracellular signal-regulated kinase (ERK) and Ca^{2+}-mediated activation of nuclear factor of activated T-cells (NFAT), both of which mediate GnRH effects on gonadotrophin secretion. Their activation was monitored by high content imaging (fluorescence staining for ppERK and nuclear translocation of an NFAT1c-EFP reporter). Also, GnRH effects on Egr1-zsGreen and NFAT-RE-asRed (transcriptional readouts for ERK and NFAT activation) were monitored. These responses were compared in HeLa, MCF-7 and LβT2 cells. Results revealed that effects of GnRH mediated by type I GnRHR are dependent upon cellular model, with differences in response kinetics, sensitivity to inhibitors and effects on transcription. Single cell measures of GnRH effects revealed marked cell-cell variability, implying that GnRHR signalling mechanism can be differently constructed between different cell types and between genetically identical cells within a given cell type. For further exploration of cell-cell heterogeneity, a mathematical approach that considers its impact on information transfer was used. The mutual information (MI) between GnRH concentration and measured responses (I(response; GnRH)) was used to quantify (in Bits) information transfer via GnRHRs. MI values for GnRH effects differed between HeLa and LβT2 cells, extending the idea of cell-context-dependent GnRH signalling to the amount of information transferred via the GnRHR. One bit of information can resolve two different signal values. However, the MI values for GnRH sensing were <1 Bit despite 3 Bit inputs irrespective of the cellular model used. Sensing joint pathways increased MI values, but the increase was modest, and this could be because

information transfer had been underestimated by ignoring response dynamics. This was explored by live cell imaging, tracking cells and calculating MI taking response trajectory into account in LβT2 cells. The I(NFAT1c-EFP-NF; GnRH) was ~0.4 Bits at 30 min and increased to >0.5 Bits by consideration of trajectories. The I(Ca^{2+}; GnRH) was ~0.8 Bits at ~24 sec and increased to 1 Bit by consideration of trajectories. These responses were also tracked in cells receiving two pulses of GnRH and this revealed little information gain from the 2^{nd} pulse (for both readouts). This implies that the unknown sources of cell-cell heterogeneity are relatively stable over the time course examined in this work. Most information loss occurs upstream of Ca^{2+}, and when cells were stimulated with ionomycin, the MI value was greater than any MI value reported for GnRH signalling. This suggests that the GnRHRs and their upstream effectors are a signalling node at which significant information loss occurs.

Dedication and acknowledgements

I would like to express my gratitude to my supervisors Prof. Craig McArdle and Prof. Krasimira Tsaneva-Atanasova for their guidance over the course of my study. Thank you to Dr. Gavin Welsh for his support. A special thanks to Dr. Claire Perks for her great support that she had offered during my study. Thank you to all my colleagues and friends in the Dorothy Hodgkin Building.

To my parents, I would not have achieved this step in my life without your enormous support. I am “forever” grateful to have you in my life. To every member of my family, thank you for making this journey possible.

A great thanks to the King Saud University and to the ministry of higher education at the Kingdom of Saudi Arabia for funding completely this work. Also, I would like to express a deep gratitude to the Saudi Arabian Cultural Bureau in London for their continuous guidance and support throughout my scholarship.

Above all, I give glory to Allah for watching me through to completion.

Hussah M Alobaid

Author’s declaration

I declare that the work in this dissertation was carried out in accordance with the requirements of the University's Regulations and Code of Practice for Research Degree Programmes and that it has not been submitted for any other academic award, except where indicated by specific reference in the text, the work is the candidate’s own work. Work done in collaboration with, or with the assistance of others, is indicated as such. Any views expressed in the dissertation are those of the author.

Signed:…….Date:……

Abbreviations

7TM	Seven transmembrane
αGSU	α-gonadotrophin hormone subunit
AC	Adenylyl cyclase
Ab	Antibody
Ad	Adenovirus
AFU	Arbitrary fluorescence units
ANOVA	Analysis of variance
AVPV	Anteroventral periventricular
Ca^{2+}	Calcium ion
$[Ca^{2+}]i$	Intracellular calcium ion concentration
Cn	Calcineurin
CaM	Calmodulin
CaMK	CaM-dependent protein kinase
cAMP	Cyclic adenosine monophosphate
cPKC	Conventional protein kinase C
CREB	Cyclic AMP response element binding protein
CRE	cAMP response element
Ctrl	Control
DAG	Diacylglycerol
DMEM	Dulbecco's Modified Eagle's Media
DUSP	Dual-specificity phosphatase
EGFR	Epidermal growth factor receptor
ECLs	Extracellular loops
EDTA	Ethylenediaminetetraacetic acid

EGF	Epidermal growth factor
Egr1	Early growth response1
ERK	Extracellular signal-regulated kinase
ER-α	Estrogen alpha receptor
FCS	Fetal calf serum
FD	Frequency-distribution
FSH	Follicle-stimulated hormone
FSHβ	Follicle-stimulated hormone beta subunit
GABA	Gamma-amino butyric acid
GDP	Guanosine diphosphate
GnRH	Gonadotrophin-releasing hormone
GnRHR	GnRH receptor
GPCR	G-protein coupled receptors
Grb2	Growth factor receptor-bound protein 2
GTP	Guanosine triphosphate
hr	Hour (s)
HPG	Hypothalamo-pituitary-gonadal (axis)
HH	Hypogonadotropic hypogonadism
ICLs	Intracellular loops
IEG	Immediate early gene
ICSI	Intracytoplasmic sperm injection
IHC	Immunohistochemistry
IP_3	Inositol 1, 4, 5 trisphophate
IP_3R	Inositol 1, 4, 5 trisphophate receptor
IVF	In vitro fertilisation

KNDy	Kisspeptin/neurokinin B/dynorphin
LH	luteinising hormone
MAPK	Mitogen-activated protein kinase
mGnRHR	mouse GnRHR
MEK	MAPK/ERK Kinase
MDS	Multidimensional scaling
min	Minute (s)
MI	Mutual information
msec	Millisecond
MMP	Matrix metalloproteinase
n:c	Nuclear to cytoplasmic ratio
NGS	Normal goat serum
NF	Nuclear fraction
NFAT	Nuclear factor of activated T cells
NFAT-RE	NFAT-response elements
NKB	Neurokinin B
nM	Nanomolar
PACAP	Pituitary adenylyl cyclase activating polypeptide
PBS	Phosphate buffer saline
PDBu	Phorbol 12, 13-dibutyrate
PFA	Paraformaldehyde
PGBE	Pituitary glycoprotein hormone basal element
Pfu	Plaque forming unit
PIP_2	Phosphatidylinositol 4, 5 bisphosphates
PKA	Protein kinase A

PKC	Protein kinase C
PLC	Phospholipase C
PM	Picomolar
POA	Preoptic area
PCOS	Polycystic ovarian syndrome
ppERK	Dual phosphorylated (Thr-202/Thr-204) ERK (1/2)
PSS	Physiological saline solution
QCS	Quality control system
SEM	Standard error of the mean
SLEMI	Statistical Learning Based Estimation of Mutual Information
SF-1	Steroidogenic factor 1
SOS	Son of sevenless
SV40	Simian virus 40
TNF	Tumor necrosis factor
TE	Trypsin EDTA solution

Table of contents

Table of figures

Chapter 1- Introduction

1.1. The hypothalamo-pituitary-gonadal axis

Almost all body functions are regulated directly or indirectly by the small part in the brain called hypothalamus. It is situated below the thalamus and above the brain stem and found in all mammalian brains [1]. It connects the nervous system to the endocrine system through the pituitary gland. The cycle of mammalian reproduction is controlled by a complex interplay between the hypothalamus, pituitary, and gonads [2, 3]. In 1930, Moore and Price were the first people to describe the nature of hypothalamo-pituitary-gonadal (HPG) axis by putting forward the idea that the cyclical nature of ovarian changes could be a result of a reciprocal interplay between the ovary and the anterior pituitary gland [2]. After that in 1932, Hohlweg and Junkmann demonstrated that the hypothalamus mediates the feedback action of the ovarian hormones and on the pituitary gland [4].

Gonadotrophin-releasing hormone (GnRH) is also known as a luteinising hormone-releasing hormone (LHRH), or GnRH I. It is the critical peptide hormone that controls gonadotrophin secretion and reproductive function in mammals [5]. GnRH was first isolated from mammalian hypothalamus four decades ago [6] by Roger Guillemin and Andrew Schally (Nobel Prize winner in 1977) and was described as the decapeptide pGlu-His-Trp-Ser-Tyr-Gly-Leu-Arg-Pro-Gly-NH2 [5]. Their discoveries have advanced our understanding of GnRH action leading subsequently to the development of agonist and antagonist analogues.

The human gene GNRHI is located on chromosome 8 and encodes a 92-amino acid pre-prohormone [7]. GnRH is synthesised and stored in neurons within the hypothalamus and is secreted in a pulsatile manner into the hypophyseal portal circulation [8]. GnRH binds to GnRH receptors (GnRHRs) on gonadotrophs causing

the release of luteinising hormone (LH) and follicle-stimulating hormone (FSH) that mediate gonadal steroid production [8]. These, in turn, provide feedback to the hypothalamus and pituitary to maintain the functional system [9]. The proper response of the pituitary gonadotrophs to stimulation is vital for proper action of this axis [2].

In humans and other mammals, GnRH neurons are generated in the medial olfactory placode during embryological development and migrate to the hypothalamus through the olfactory bulb [10, 11]. GnRH neurons project to the median eminence and release GnRH into the hypophysial portal blood through which it is transported to the anterior pituitary gland [12]. The median eminence subserves neurosecretion into the hypophysial portal blood, which is an essential system to hypothalamic control of the anterior pituitary gland cells [1, 3]. GnRH cells are found in the medial preoptic area (POA) and the arcuate nucleus of the hypothalamus [2, 13]. In rodents, GnRH cells are spread throughout the septal region of the brain [1, 14]. The GnRH neurons share location with other central regulators, allowing many neuroendocrine and metabolic inputs to influence the GnRH network. Studies have shown that GnRH neurons are connected to thousands of other neurons in more than 50 functionally different brain areas [15-17]. For example, studies in rodents showed that brain injections of GnRH stimulate sexual behaviours, indicating that these neurons are participated in neural circuits which control the sexual behaviour. In addition, Simerly in 2002 have reported that some brain areas that include vomeronasal inputs project axons to the anterior hypothalamus, suggesting that they synapse on GnRH neurons [18]. Overall, GnRH neurons are thought to integrate information from various sources that in turn, have an impact on many brain functions [17].

1.2. Regulation of GnRH and gonadotrophin secretion

Thousands of neurons release the neurohormone GnRH into the hypophyseal portal blood system [19, 20]. Through this system, GnRH is transported to the anterior pituitary gland where it binds to GnRHRs localised on the cell surface of gonadotrophs to modulate pituitary gonadotrophin (LH and FSH) secretion [12]. GnRH secretion occurs in synchronized pulses, typically less than 10 minutes in duration with intervals of 30 min to many hours in humans [21, 22]. LH and FSH are both glycoproteins consisting of a common α subunit (αGSU) and a distinct β subunit (LHβ and FSHβ) [12]. These gonadotrophin hormones travel through the peripheral circulation, acting on the gonads to control reproduction [23] (Figure 1.1).

There are many neurotransmitters and peptides involved in GnRH regulation [24-27]. In 2001, kisspeptin was recognised as the ligand for the G protein receptor 54 (GPR54) [28-31]. It is a 145 amino acid polypeptide that is encoded by the KISS1 gene. It has recently been identified as a main regulator of the mammalian reproductive axis [32]. Its action occurs through the kisspeptin receptor (KISS1R), stimulating the secretion of GnRH [32]. Kisspeptin neurons are found in the arcuate and anteroventral periventricular (AVPV) nuclei of the hypothalamus. These neurons projected to the medial preoptic area of the hypothalamus where the GnRH neurons are located [32]. Around 75% of GnRH neurons can express the GPR54 (i.e. kisspeptin receptor). The primary action of Kisspeptin occurs at the level of the hypothalamus stimulating GnRH secretion. However, a few studies have reported that kisspeptin can act directly on pituitary gonadotrope cells [32-37]. Mutations with KISS1R resulted in pubertal disorders in humans [38, 39]. For instance, a girl with an activating mutation in KISS1R had a prolonged activation of intracellular signalling by the mutant GPR54

and this resulted in delayed puberty [40]. Similar cases were reported in animal models characterised by pubertal delay [38, 41-43].

Kisspeptin cooperates with other neuropeptides like neurokinin B (NKB) and dynorphin to regulate the secretion of GnRH pulses [44] NKB is a hypothalamic neuropeptide that binds to the neurokinin 3 receptor (NK3R) [44]. Genetic studies demonstrated that patients with mutations in TAC3 and TACR3 genes, that encode NKB and its receptor (NK3R), respectively exhibited hypogonadotropic hypogonadism (HH, characterised by absent testes or ovaries or a reduction in their functions) due to the lack of circulating gonadotrophins [44]. Recently, a study suggested that NKB signalling mediates menopausal hot flushes [45]. β-endorphin (an endogenous opioid neuropeptide) is involved also in the regulation of the reproductive system. Studies revealed that changes in β-endorphin levels contribute to many reproductive dysfunctions [46]. For example, high levels of beta-endorphin can cause polycystic ovarian syndrome (PCOS), and low levels of β-endorphin are associated with menopause [46-49].

Dynorphin and Kisspeptin are co-localized with neurokinin B in the same hypothalamic neuronal population (termed KNDy neurons). Studies suggested that NKB has a stimulatory role in releasing LH. This effect is thought to be mediated by auto synaptic inputs of NKB on KNDy neurons which in turns stimulate the secretion of GnRH in a kisspeptin-dependent manner [50, 51]. This connection highlights the role of these neuropeptides in controlling GnRH and gonadotrophin secretion [50, 51]. In addition to the KNDy system, other neurotransmitters and peptides are shown to influence GnRH secretion. These include gamma-amino butyric acid (GABA),

vasoactive intestinal polypeptide (VIP), catecholamines, neurotensin and gonadotrophin-inhibitory hormone (GnIH) [52, 53].

Luteinising hormone and FSH act on the gonads to control reproduction. In males, LH stimulates testosterone production and acts on Leydig cells within the testes, whereas FSH acts on Sertoli cells to regulate spermatogenesis. Testosterone provides negative feedback to the hypothalamus and pituitary suppressing synthesis and secretion of LH and FSH [116]. In females, ovulation and corpus luteum formation are stimulated by LH, whereas FSH stimulates ovarian follicle formation and oestrogen secretion. Oestrogen provides either negative or positive feedback to the hypothalamus and pituitary, depending on the phase of the menstrual or oestrous cycle [116, 194]. In many species, both oestrogen and progesterone can inhibit gonadotrophin secretion during the luteal phase [195]. However, during the follicular phase, the level of oestrogen increases GnRH secretion, initiating the preovulatory gonadotrophin surge [196]. Gonadotrophins are secreted at the end of follicular phase and before ovulation, whereas both are suppressed during the luteal phase. FSH is increased during the transition phase from the luteal to follicular phase, driving the selection of dominant follicle [197].

The oestrogen alpha receptor (ER-α) is an essential receptor for sex-steroid mediated control of gonadotrophin secretion, [54]. However, GnRH neurons do not express ER-α receptor in many species. The absence of this receptor indicates that there is a need for an intermediate signalling pathway to mediate gonadal steroid feedback [196, 198]. It is most likely that the ER-α input is upstream of the GnRH neurons, including possibly on KNDy neurons. The accumulated evidence since the discovery of KNDy neuronal network suggests that this network play a pivotal role in GnRH regulation

and secretion by integrating endocrine, nutrient, and environmental signals, and thereby controls the downstream HPG axis [26, 54]. Overall, an integrated set of interactions between the hypothalamus, pituitary gland and gonads control the reproductive system in mammals. These components are regulated through feedback mechanisms that coordinate the processes causing gonadotrophin secretion, gamete production, and maintenance of the species [26, 27].

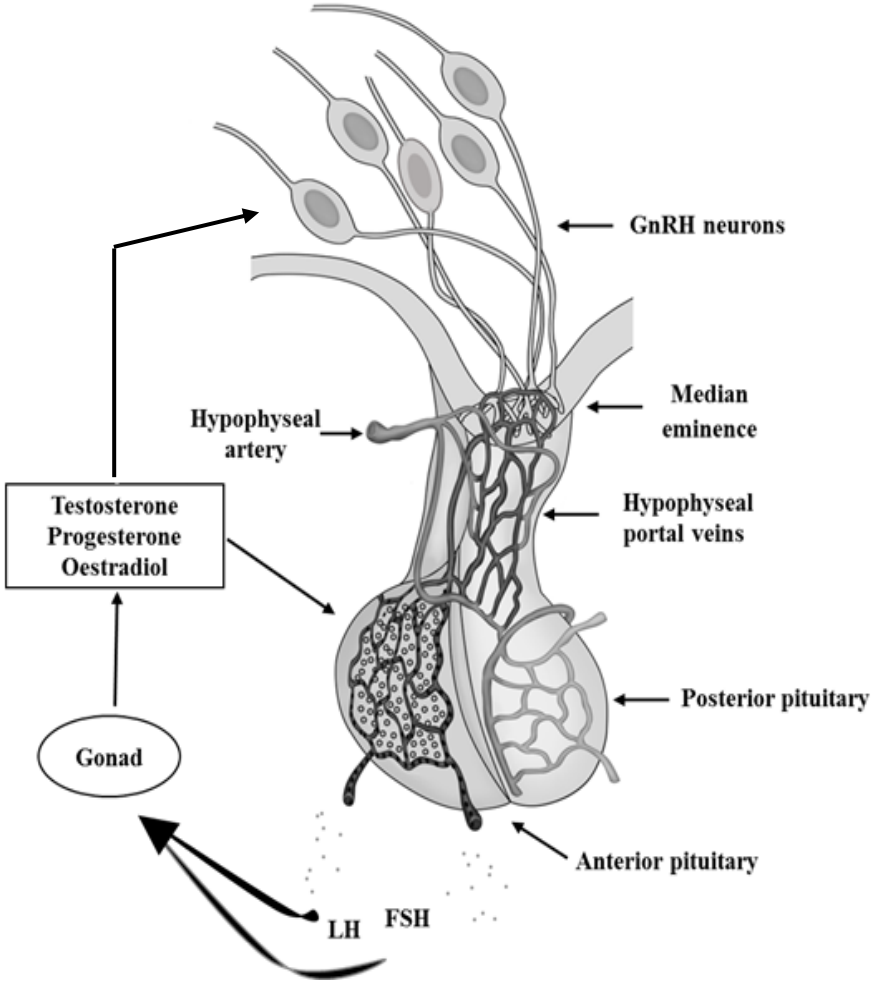

Figure 1.1. The hypothalamo-pituitary-gonadal axis

The diagram shows the HPG axis. The peptide hormone GnRH is released into the hypophyseal portal circulation from hypothalamic neurons. It acts then on gonadotrophs in the anterior pituitary for the synthesis and secretion of the gonadotrophins (LH and FSH). The gonadotrophins act on gonads stimulating the synthesis of gametogenesis and steroid hormone. These in turn feedback to the pituitary and hypothalamus.

1.3. Gonadotrophin-releasing hormone peptide

The structure of the decapeptide GnRH was first described in mammals as pGlu-His-Trp-Ser-Tyr-Gly-Leu-Arg-Pro-Gly-NH2 [5, 55-57]. In humans, the GnRH gene is located, on chromosome 8p11.2-p21 as a single gene copy. It consists of four exons that are separated by three introns [58, 59]. Numerous forms of GnRH have been identified in vertebrates and invertebrates and they are thought to have different physiological functions [60-65]. Most vertebrates express at least two types of GnRH. There are three distinct forms of GnRH and these include GnRH I which was first characterised in mammals. The second form was isolated from chicken brain and is referred to as GnRH II [66]. It is thought to be the earliest form that was conserved from primitive fish. The third form is termed GnRH III, and this has been described in fish [5]. Most vertebrate classes express GnRH I and GnRH II, whereas GnRH III is specific for teleosts [5]. Notably, although GnRH I and GnRH II are expressed by mammals (including humans), their distribution pattern different [67-69]. The GnRH II is expressed in some areas of the brain (e.g. hippocampus, caudate nucleus, and periaqueductal grey region), but the vast majority of it is expressed outside of the brain [67, 68]. The length of all known forms is 10 amino acids and the most common structural differences are at amino acids 5-8 [70]. Some major known functions of amino acids are shown in Figure 1.2.

1.4. Extra-pituitary actions of GnRH and GnRHRs

Gonadotrophin-releasing hormone acts via GnRHRs on pituitary gonadotrophs to control the synthesis and secretion of gonadotrophins [23]. However, GnRHR expression is not restricted to the pituitary [71], and GnRH is thought also to directly

regulate some extra-pituitary reproductive tissues by the activation of locally expressed GnRHRs [3]. The GnRHR expression in peripheral tissues was reported for the first time in 1981 in human placenta, by radioreceptor assay [72]. Later, a study demonstrated that GnRHR mRNA and the cDNA are found in human placenta cells [73]. The GnRH mRNA expression has also been reported in other normal reproductive tissues including breast, endometrium, prostate, and gonads, and in tumours derived from these tissues [1, 83]. Likewise, GnRHR mRNA has been shown in these tissues and in non-reproductive tissues such as skeletal muscle, blood, larynx, kidney and liver [74]. The physiological role of GnRH in many of these extra-pituitary sites is unknown. However, is thought to act in an autocrine or paracrine manner for cellular process regulation [75].

The neuropeptide hormone has a direct role in cell proliferation and a novel role in controlling tumour progression [76]. In cells derived from hormone-dependent cancers, GnRHRs were thought to mediate anti-proliferative effects. In the ovary, GnRH mediates steroidogenesis [77]. In human placenta, the peptide hormone contributes to early pregnancy [78]. GnRH can also influence the binding of spermatozoa to the zona pellucida of oocytes during fertilisation, such an effect can be inhibited by using GnRH antagonists [79, 80]. The diversity in actions shown by GnRH might be due to the divergence of signalling pathways that are caused by GnRHRs activation [76].

Early works showed that GnRHRs are expressed in testes in rat and mediate the effect of GnRH on steroidogenesis *in vitro* [81]. However, blockade of testicular GnRHRs did not change the function of Leydig cells *in vivo* [82]. No evidence was found for the expression of GnRHRs in human gonadal tissue [83].The expression of GnRHRs

is also reported in different brain areas such as the hippocampus, preoptic area, arcuate nucleus, where it is thought to regulate the releases of GnRH from the hypothalamus [74, 75]. GnRHRs are also expressed in heart in rodent and human [76, 84].

Notably, the nucleic acid sequence encoding transcripts of GnRHRs are similar in the pituitary and extra-pituitary sites [76, 85-87]. However, the expression level of the receptors in pituitary tissue is higher than in extra-pituitary cells [88, 89]. Moreover, GnRHRs can apparently signal via Gi in extra-pituitary sits rather than via Gq [90]. Furthermore, as detailed in section 3.1, there are different types of GnRHRs. Type I GnRHRs have a high affinity for GnRH, and type II GnRHRs have a low affinity for GnRH with nanomolar and micromolar dissociation constants (Kd) respectively [76, 91]. The pituitary cells express type I, whereas both type I and II have been reported to be expressed in extra-pituitary tissues [30-33].

1.5. Therapeutic use of gonadotrophin-releasing hormone analogues

Gonadotrophin-releasing hormone and its analogues have been broadly used in clinical medicine since they were identified in early 1971. The GnRH analogues are classified into two forms, agonist and antagonist. The agonists form was designed to mimic the effect of GnRH on gonadotrophin secretion. The antagonists were designed to block GnRH effects by GnRHR competition [24, 70]. The rapid degradation of GnRH was the main reason for the synthesis of GnRH analogues with agonistic or antagonistic properties to increase their potency and duration.

Pulsatile administration of GnRH agonists can be used to treat delayed puberty or infertility and can lead to induction of spermatogenesis or ovulation [12, 24, 92]. It

was successfully used to induce puberty in HH patients [93]. In recent years GnRH agonists have been used in young female patients who undergo chemotherapy, as a promising therapeutic way to treat iatrogenic ovarian failure [94]. Paradoxically, the agonists can have both stimulatory and inhibitory effects, as secretion of gonadotrophins can be inhibited by sustained stimulation [70]. High doses of GnRH agonists can be exploited to treat hormone-dependent cancers of the breast, ovary, and endometrium [95]. The agonists cause a reduction on the secretion of gonadotrophin and gonadal steroids leading to medical castration [95]. Cases like endometriosis, uterine leiomyomata, premenstrual syndrome, and POS were successfully treated using GnRH agonists on a continuous basis [24, 70], as they can inhibit ovulation and production of gonadal steroid in females [96]. Several treatment schedules use GnRH agonists in assisted reproductive technology (ART), especially in ovarian hyperstimulation *in vitro* fertilisation (IVF)/intracytoplasmic sperm injection (ICSI) treatments [95, 97]. Few side effects have been reported using the agonist (e.g. menstrual cycle disruption, a decrease in bone density) however, these effects are reversed after stopping treatment [9, 24]

Recently, the antagonist form of GnRH has been introduced into IVF and appeared to be an alternative option in preventing premature LH surge [98]. Unlike GnRH agonist, GnRH antagonists induce an immediate reduction in the levels of gonadotrophin by blocking competitively GnRHR [99]. Thus, GnRH antagonists prevent endogenous GnRH from releasing LH and FSH from the pituitary cells [98]. However, the suppression effect on gonadotrophin secretion can be rapidly reversed once the treatment discontinued [98, 100]. The difference between the two analogues make the antagonist form the logical choice to apply in IVF [100]. Moreover, the inhibitory effect of GnRH antagonists was broadly introduced in controlled ovarian

hyperstimulation (COH) for ART [99]. Like GnRH agonist, GnRH antagonists have growth inhibitory effects on many cancer cells [101]. In recent study, the effect of GnRH antagonists on treated prostate cancer cells have shown to be rapid compared to GnRH agonists [102]. Overall, GnRH analogues are clinically exploited to treat several conditions in reproductive medicine [103].

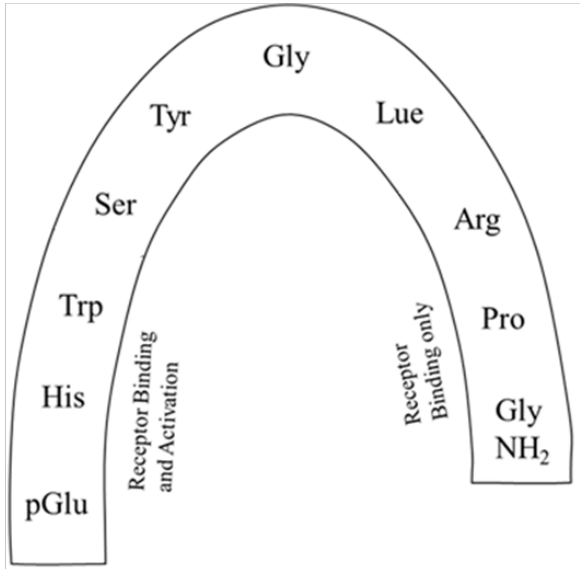

Properties of amino acids in GnRH I

pGlu Uncharged-CONHCHO-N-terminus.
His Aromaticity and imidazole required
Trp Aromaticity required
Ser Any small side chain acceptable, possible H-bonding donor
Tyr Aromaticity required, possible indirect role in binding and activation.
Gly Achirality essential to assume bent conformation and D-amino acid substitution enhances
Lue Not essential but must be uncharged.
Arg Essential for high affinity binding but not if D-amino acid in position six
Pro Essential conserved residue
Gly Small uncharged C-terminus

Figure 1.2 GnRH structure and properties of amino acids in GnRH I

The diagram represents the structure of GnRH I in a folded conformation as bound to GnRHRs. Major functions of individual amino acid residues are shown on the right. The figure is adapted from [62].

1.6. The mechanism of action of GnRH

1.6.1. Structure of GnRH receptors

Gonadotrophin-releasing hormone receptors were first cloned from a murine gonadotroph cell line [104]. Subsequently, GnRHRs have been cloned from numerous species including the rat, sheep, cow, and human. GnRHRs belong to the rhodopsin-like G-protein-coupled receptor (GPCR) superfamily [105]. The human genome encodes > 800 GPCRs [106], and they are implicated in most physiological processes. Mutations in many GPCRs are known to cause disease, and most pharmacological drugs target GPCRs [107]. GPCRs can be activated by a broad range of stimuli including ions, light, odorants, classical neurotransmitters, peptides and glycoproteins [108].

These receptors (GnRHRs) are located on the surface of the pituitary gonadotrophs, which constitute approximately 8–15% of anterior pituitary cells [109]. Three types of GnRHRs have been identified based on their sequence homology, and they have been shown to have distinct functions and distributions [19]. These are named GnRHRs I, GnRHRs II and GnRHRs III [12]. The type I GnRHRs have a high affinity for GnRH-I, while the type II and type III receptors have a higher affinity for GnRH II than for GnRH I [110]. The type I GnRHRs of humans, rats, mice, pigs, and horses share over 80% amino acid sequence homology [111]. The type II GnRHRs are functional in some mammals including monkeys, dogs and pigs, but in mice, sheep, and cows the receptor is absent [112, 113]. Some primates possess functional type I and II GnRHRs. However, although in humans both types I and II genes exist, only type I GnRHRs are expressed as functional protein. The human type II GnRHR gene is a pseudogene that is disrupted by a frame-shift and premature stop codon [114].

Therefore, the type I GnRHR is the predominant GnRHR in the human. In humans and some species, the type I GnRHR is also expressed in extra-pituitary tissues including breast, endometrium, and gonads [5, 76].

As stated above, GnRHRs belong to the GPCR family. These receptors have a characteristic seven transmembrane (7TM) α-helical domain structure with the TM domains, connected by three intracellular (ICLs) and three extracellular loops (ECLs). In general, the ECLs are implicated in ligand recognition and binding although they could have a role in GPCR signalling [115-117]. The TM domains are involved in receptor trafficking and ligand binding [118]. The ICLs and carboxy terminus are implicated in GPCR coupling to G proteins and -arrestin for signalling pathways activation [115, 119], in addition to receptor internalisation, recycling and desensitisation [120, 121]. These receptors undergo conformational changes when they bind to ligand [122]. Mammalian type I GnRHRs have peculiar features that distinguished them from other GPCR (Figure 1.3). These receptors lack the C-terminal intracellular tail that is found in all other known GPCR [123]. It was experimentally demonstrated that the type I GnRHRs are resistant to rapid homologous desensitisation upon GnRH stimulation and exhibit slow internalisation [122, 124, 125]. Moreover, when the C-terminal tail of a non-mammalian GnRHRs was fused into the rat GnRHRs, rapid desensitization and internalization occurred [126, 127]. Another structural difference between mammalian type I GnRHRs and type II or III GnRHRs is that the intracellular loop 1 is longer in type I mammalian GnRHRs than in the other types [110].

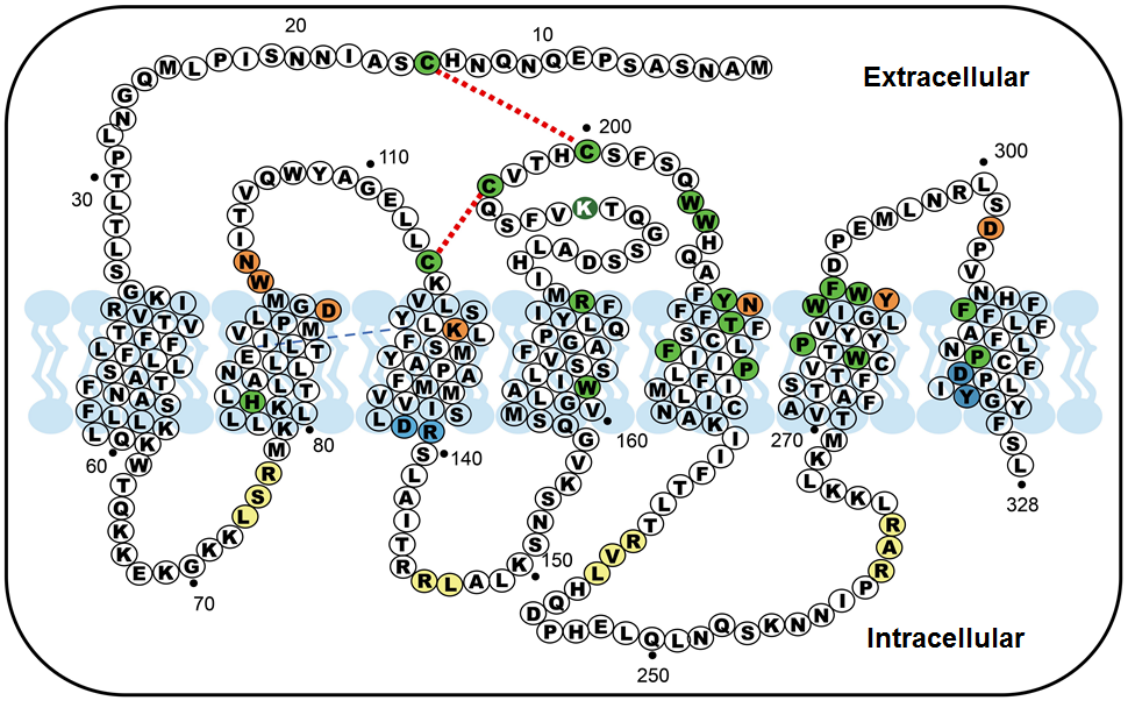

Figure 1.3. GnRHR structure in the human

The diagram shows the human GnRHR imbedded in the cell membrane, with 7TM α-helical domains connected to three ICLs and three ECLs. Residues that are implicated in receptor structure or in the formation of a binding pocket are shown in green (including residues forming disulphide bonds and glycosylation sites). Residues that are important for the activation of receptor are shown in blue. Residues implicated in G-proteins coupling are shown in yellow. The figure is reformatted from reference [128].

1.6.2. Gonadotrophin-releasing hormone receptor signalling

G-protein-coupled receptors provide a mechanism to transfer information between the extracellular and intracellular environments [129]. Heterotrimeric G-proteins are guanine nucleotide-binding proteins, acting inside cells as a molecular switch by their ability to bind to and hydrolyse guanine triphosphate (GTP) to guanine diphosphate (GDP). Heterotrimeric G-proteins are made up of α, β and γ subunits. There are more than 20 Gα subunits [120] and these are divided into four major families based on amino acid homology and effector coupling [130, 131]. These are $G\alpha_{q/11}$, $G\alpha_s$, $G\alpha_i$ and $G\alpha_{12/13}$. In general $G\alpha_{q/11}$ couples to phospholipase C (PLC) isozymes, $G\alpha_s$ activates adenylyl cyclase (AC), Gαi inhibits AC, whereas the role of $G\alpha_{12/13}$ in GnRHR signalling is unknown yet [132]. In the inactive state, Gα is bound to the G-protein βγ subunits and GDP. The interaction of the activated receptor with G-protein promotes the exchange of GDP for GTP, and this leads to dissociation of Gα from the βγ subunits. These subunits re-associate again when the GTP is hydrolysed forming the inactive heterotrimeric which terminates the signal [19].

GPCRs can be activated by a broad range of stimuli including light, glycoproteins, neurotransmitters, amino acids, and peptide hormones [61]. Activation of the heterotrimeric G-protein regulates the intracellular concentration of second messengers by modulating the activity of one or more effectors. These second messengers could be Ca^{2+} for ion channels, cyclic adenosine monophosphate (cAMP) for AC, inositol 1,4,5 triphosphate (IP_3) and diacylglycerol (DAG) for PLC [19, 133].

In general, GnRHRs interact with multiple G-protein forming a complex network of signalling proteins (Figure 1.4). In the pituitary gonadotrophs, GnRHRs act mainly via $G\alpha_{q/11}$. However, a study from Webster's laboratory revealed that $G\alpha_q$ and $G\alpha_s$ are

involved in extracellular signal-regulated kinase (ERK) regulation and LH expression [134, 135]. A recent study in LβT2 cells showed that Gαs is involved in the signalling in addition to $G\alpha_{q/11}$ [132]. In another words, the gene induction of FSHβ is mainly depended on $G\alpha_{q/11}$, and the LHβ gene expression is depended on Gαs [132]. In contrast, no evidence was shown for $G\alpha_i$ involvement in GnRHR signalling in gonadotrophs. However, in reproductive tumour cells, $G\alpha_i$ was reported to have a role in the activation of ERK and cell proliferation inhibition [136]. GnRHR-mediated G-proteins activation can be shifted from $G\alpha_s$ to $G\alpha_i$ by increasing GnRH concentration in hypothalamic neurons [137]. Accordingly, the ability of GnRHRs to activate distinct G-proteins appears to be cell context-dependent. Binding GnRH to GnRHRs on the cell surface of the gonadotroph stimulates a variety of distinct signalling cascades. ERK and nuclear factor of activated T cells (NFAT) pathways are the two main pathways that are proven to be mediated GnRH effects on gonadotrophins sections [138-141]. Therefore, the focus on this work is on the mechanism that mediates their activations. As explained, GnRHR directly activates intracellular signalling. However, a study in 2003 suggested that crosstalk with the EGFR might happen at the level of the pituitary. Roelle *et al*, showed that EGFR can be stimulated via GnRHR but the mechanism is still to be determined [71]. EGF is a protein with 53 amino acid residues, it acts via ErbB family tyrosine kinase receptors (TKR). It is capable of activating the ERK pathway through binding to and inducing phosphorylation of the EGFR, which in turn results in the phosphorylation and activation of ERK [71].

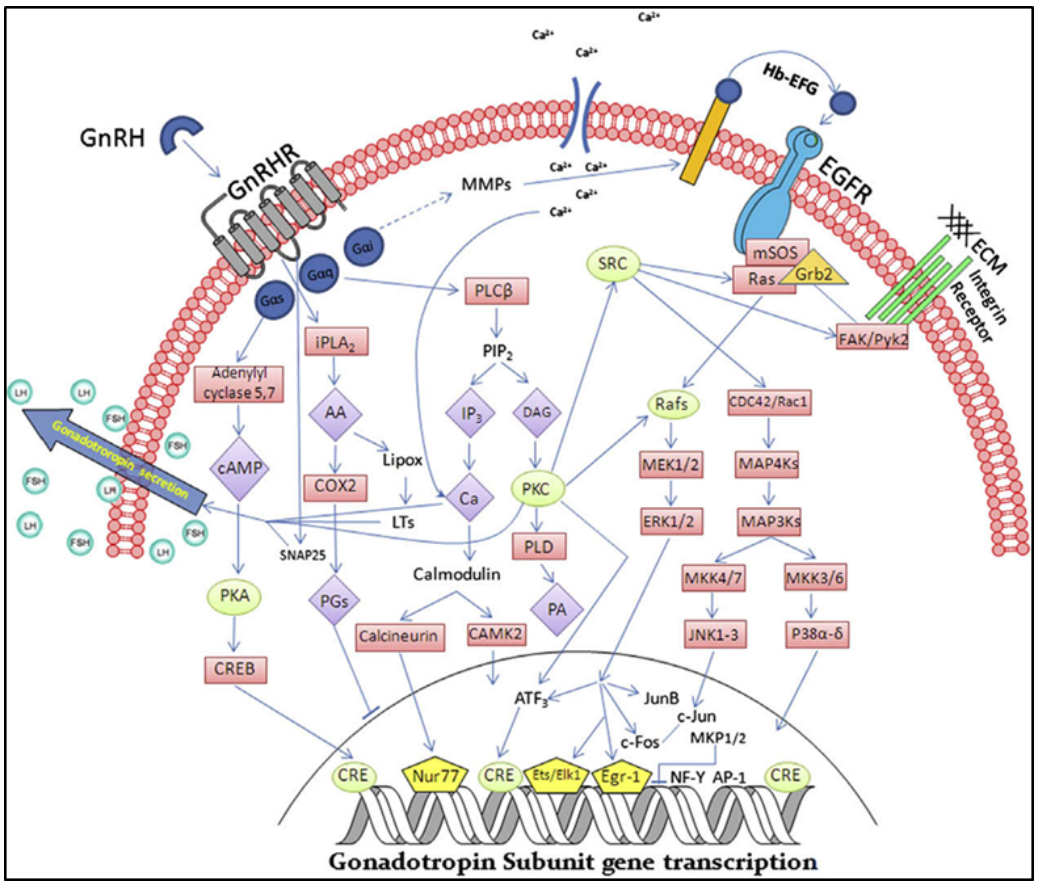

Figure 1.4. A model for GnRHR signalling

Activation of the GnRHR causes the activation of multiple G-protein subunits. Signalling downstream of PKC leads to transactivation of the epidermal growth factor (EGF) receptor and activation of MAPKs, including ERK, JNK and p38. Active MAPKs translocate to the nucleus, leading to the activation of transcription factors and rapid induction of early genes. This figure is reproduced from [120].

1.6.3. Mitogen activated protein kinase pathways

The family of mitogen-activated protein kinases (MAPKs) is made up of three central protein kinases. These are ERK, c-Jun N-terminal kinase (JNK) and p38 [142, 143]. Each of these functions in a three-tier system [2]. The MAPKs are conserved

serine/threonine kinases and are activated by a MAPK kinase (MAPKK). The MAPKK is a dual-specificity kinase which phosphorylates at Ser/Thr and Tyr sites and targets a Thr-X-Tyr motif on the MAPK. The X is glutamate (for the ERK module), proline (for the JNK module) or glycine (for the p38 module) [144]. Phosphorylation of the MAPK causes a conformational change and a significant increase (>1000-fold) in activity [139, 145, 146]. The MAPKK, is activated by a MAPKK kinase (MAPKKK) which is initiated as a result of receptor activation, or due to the interactions with GTP-binding proteins or other kinases [147]. At the end of these cascades, MAPKs phosphorylate their target proteins. Most of these are nuclear proteins including transcription factors that are implicated in many aspects of cell function [144]. Other members of the MAPK family have been identified including BMK (big mitogen-activated protein kinase) or ERK5. The ERK5 was recognised as a significant mediator of growth factor-induced cellular responses [148, 149]. The MAPKs signalling models are summarised in Figure 1.5.

Upon GnRH binding, the ERK, JNK, p38 and BMK cascades are activated [143, 145, 150]. In gonadotrophs and gonadotroph-derived cell lines GnRH causes a rapid increase in ERK (within 5 min), but its effects on JNK is slower (measurable by 10 min) [142, 151-153], and a similar effect is reported for BMK [154]. GnRH effects on p38 responses are variable, either like ERK or slightly delayed [143]. However, the mechanisms by which GnRH activate ERK are still unclear. In many models, GnRHR-stimulated ERK activation is largely mediated by PKC but in some cells of neuronal origin, it is mediated by transactivation of EGF receptors [151]. Although ERK is activated by a single kinase (MEK), it can be inactivated by at least 13 phosphatases [123]. Studies in mice with Raf1 deletion revealed that Raf1 was not required for ERK signalling in gonadotrophs [155]. Distribution of ERK signalling by

GnRH can cause perturbation of fertility in female due to the deficiency in LH biosynthesis and a failure in ovulation. In contrast the effect on LH in male mice was reported to be modest and did not have a significant impact on fertility [2].

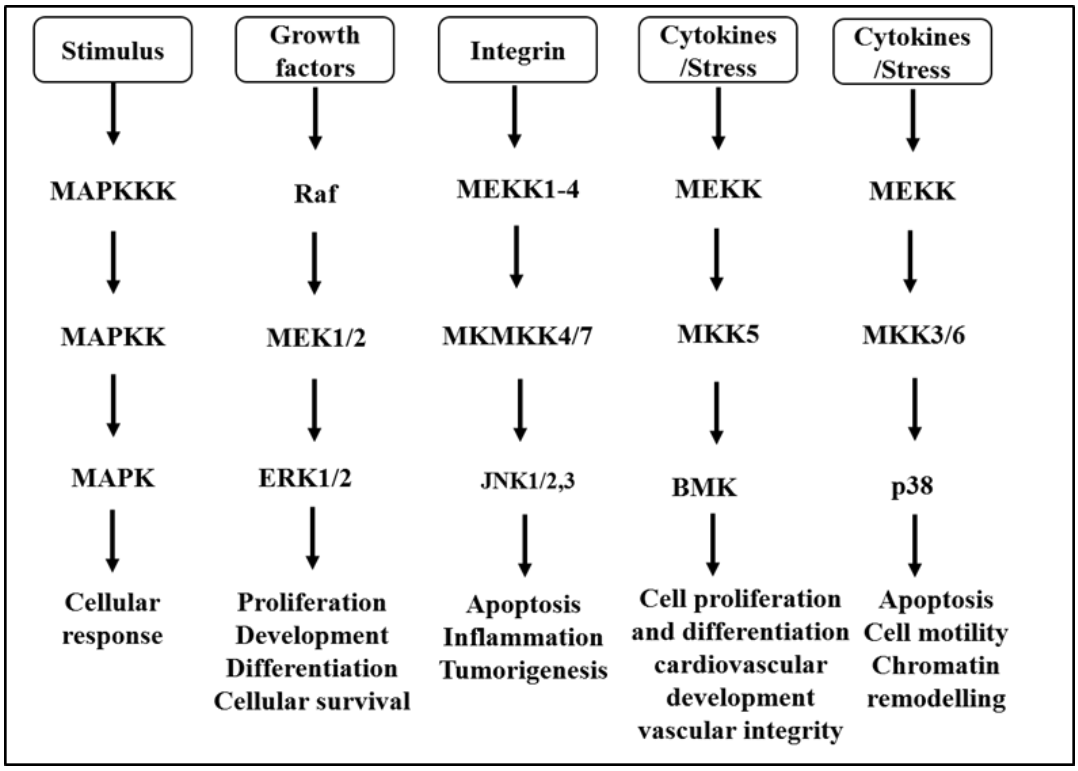

Figure 1.5. MAPK signalling models

The flow chart shows the MAPK family members and their functions. There are multiple MAPKKKs, MAPKKs, MAPKs in each module, and these can be activated by different stimuli. The figure is adapted from [144, 149, 156].

1.6.4. Ca^{2+}/calmodulin-dependent kinase pathway

GnRH typically causes a pronounced increase cytoplasmic [Ca^{2+}] concentration in its target cells. This is thought to activate the ubiquitous Ca^{2+} sensor, calmodulin, leading in turn to activation of CaMKs. The CaMKII is a common mediator of Ca^{2+} signalling

in many cell types [123, 140, 153, 157-160] that is activated by binding two Ca^{2+}-calmodulin molecules [7]. Studies in LβT2 and primary pituitary cells revealed that a single pulse of GnRH causes a rapid and transient increase in CaMK II activation [161, 162].

1.6.5. The nuclear factor of activated T cells pathway

In addition to CaMKII, Ca^{2+}-calmodulin activates a serine/threonine protein phosphatase called calcineurin (Cn, also known as protein phosphatase 3). The Cn dephosphorylates several target proteins including Ca^{2+}-dependent transcription factors of the NFAT family. It does so by dephosphorylating NFAT proteins exposing a nuclear localization sequence so that the NFATs translocate to the nucleus where they bind NFAT response elements and regulate transcription [140]. Studies showed the importance of this cascade in regulating expression of the immediate early gene products, Jun and Fos. Both of which are important for the expression of αGSU and FSHβ by GnRH [163, 164]. NFAT is a protein that belongs to a family of five members. These are NFAT1, 2, 3 and 4 (which are also known as or NFATc2, NFAT2 or NFATc1, NFAT3 or NFATc4 and NFAT4 or NFATc3, respectively) as well as NFAT5. All these forms are regulated by Ca^{2+}-calmodulin except NFAT5 that is activated in response to osmotic stress [165].

1.6.6. The protein kinase A pathway

Many GPCRs act via Gs to activate AC or via Gi to inhibit AC [132]. Adenylyl cyclase generates cAMP (from ATP) as a classic second messenger and cAMP concentration

controls the activity of protein kinase A (PKA) [132]. PKA phosphorylates and regulates numerous target proteins including the transcription factor CREB (cAMP response element binding protein).[111]. The question of whether GnRH activates Gs and/or Gi has remained controversial for decades. Although the levels of cAMP that are regulated by GnRH have little effect on gonadotrophin secretion, the gonadotrophin subunit promoters contain cAMP response elements (CRE), which might provide a mechanism for gonadotrophin subunit transcription to be activated by the cAMP/PKA pathway [5]. However, since CREB is regulated by ERK, PKC and PKA, the activation of CRE in gonadotrophin promoters could be mediated by PKC or ERK rather than the cAMP/PKA pathway [68, 94, 166].

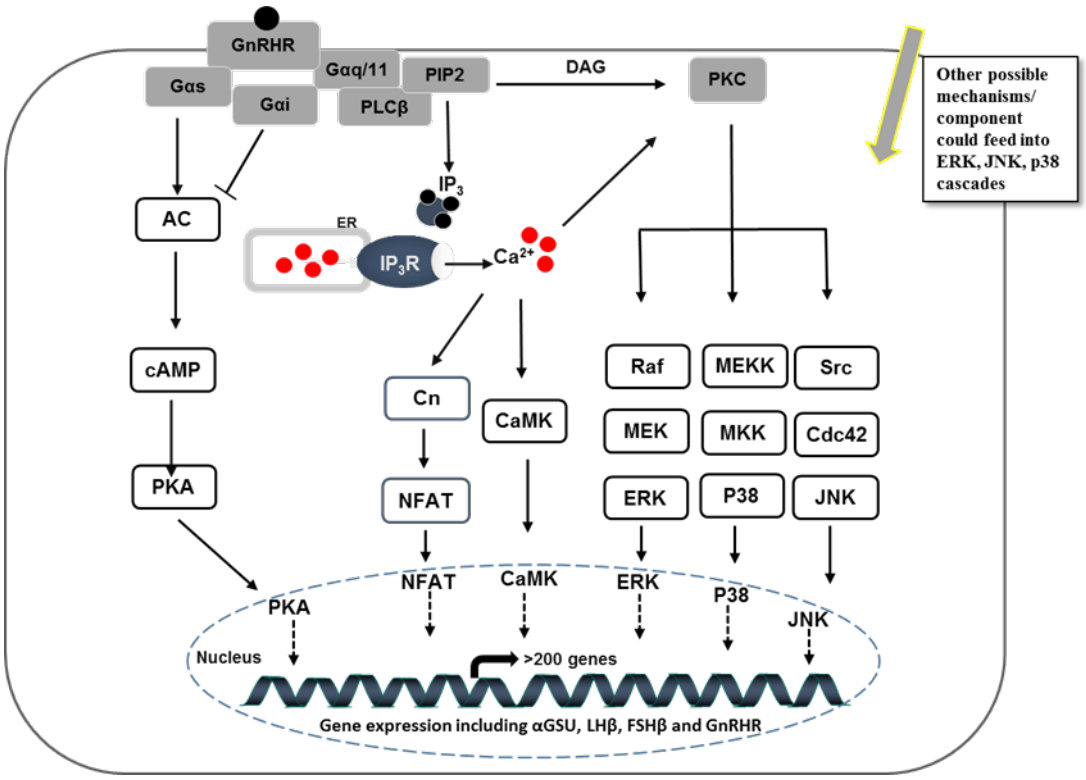

Figure 1.6. A diagram showing signal transduction pathways mediated by GnRHR

In the anterior pituitary, GnRH binds to GnRHRs on the cell surface, stimulating a variety of distinct signalling cascades, that regulate several cellular functions. These pathways are detailed above, and the figure is reformatted from [167].

1.7. Regulation of gonadotroph gene expression

Micro array studies have shown that GnRH can influence the expression of over 200 genes in its target cells [168, 169]. It regulates genes that are associated with the components in the signalling network such as the PKA, PKC subunit isoforms and GnRHRs [1]. These genes are implicated in several aspects of cellular function such as metabolism, cell growth, ion transport, signal transduction, and transcriptional regulation [170]. Studies in LβT2 cells showed that the main class of proteins affected

by GnRH treatment are transcription factors [170, 171]. Furthermore, the rapid increase in Ca^{2+} is implicated in the regulation of gene expression, as blocking Ca^{2+} channels in rat pituitary cells prevented the increases in the expression of αGSU, LHβ and FSHβ [172]. Most work in gene expression in gonadotrophs has focussed on the transcriptional control of gonadotroph signature genes. These encode αGSU, LHβ, FSHβ, and GnRHRs and are detailed below.

1.7.1. Gonadotrophin-releasing hormone receptor expression

Gonadotrophin-releasing hormone receptors are expressed by gonadotrophs that are found in the pars distalis and pars tuberalis regions of the anterior pituitary [132]. The number of GnRHRs determines the responsiveness of gonadotrophs to GnRH and it varies markedly under different physiological conditions (i.e. through the oestrous cycle and puberty) [19, 94, 173]. *In vitro* studies showed that, there are many factors that mediate GnRHR gene expression (e.g. gonadal steroids, activins and inhibins), and GnRH is the main factor that affect the expression of GnRHR gene [174, 175] at the level of mRNA [176]. Studies in rat pituitary cultures demonstrated that the expression levels of GnRHR gene are GnRH pulse frequency dependent. The levels of GnRHR mRNA were increased at all pulse frequencies and were greater with high pulse frequency (every 30 minutes) [138, 177]. Pulsatile GnRH treatment increases the number of receptors [178], while continuous treatment results in receptors internalisation [124, 179-181]. During the oestrous cycle both GnRH binding and GnRHRs expression fluctuate. The expression of both increases before ovulation which contributes to the gonadotrophin surge, then their expression declines after that [182-184].

At low cell surface densities of GnRHRs, the expression of FSHβ is optimally stimulated, and the opposite is true for LHβ that is preferentially stimulated at high cellular densities of the GnRHR [138, 185]. The number of the receptors is regulated (in part) at the transcriptional level. However, changes in GnRHR protein degradation and compartmentalisation could be significant [186]. Mutations of the GnRHR gene can disrupt pubertal development, leading to HH and impaired fertility [187-189].

Reporter studies with the 5' flanking region of the GnRHR gene have helped in understanding the molecular mechanisms that mediate GnRHR gene regulation [113, 190]. Such studies identified distinct DNA regions responsible for basal and/or GnRH-stimulated expression of the GnRHR gene [190]. The 5' flanking regions have been cloned from several mammalian species and show a high degree of cDNA sequence homology (i.e. 56% homology in rat and human, and 82% homology in rat and mouse) [191, 192]. Several cis regulatory elements have been characterised within this region. These include a GnRHR activating sequence (GRAS), an activator protein 1 (AP1) sits, a NR5A1- binding site and a Pitx1-binding site. Mutations in any of these sites can have a significant effect on basal activation of the GnRHR promotor (in rat, mouse and human) [191, 192]. Both basal and GnRH-stimulated *Gnrhr* transcription depend largely on the PKC pathway with consequent activation of ERK. However, the mechanism of which steroid hormones regulate *Gnrhr* transcription is still unknown.

1.7.2. α-glycoprotein subunit expression

The α-glycoprotein subunit (αGSU) gene is expressed during early development of the pituitary gland in various populations of cells. The αGSU is the common subunit

of the FSH and LH glycoprotein hormones [193]. Characteristic of the protein coding and 5'-flanking promoter sequences have been previously described [194, 195]. In humans and rodents, the promoter regions display a high degree of similarity [171]. Androgens are involved as a negative feedback on regulators of αGSU gene transcription [196]. Knowledge about the regulation and expression of this gene has been enhanced by the availability of the mouse gonadotroph-derived αT3-1 cells [197]. These cells express gonadotrope αGSU, GnRHRs, but not LHβ or FSHβ-subunits. In general, work on pituitary derived cells and other different model systems revealed that the effect of GnRH on αGSU expression is largely dependent on the number of GnRHRs [185, 198, 199]

GnRH activates numerous signal transduction pathways in gonadotrophs, but its effects on αGSU transcription are mediated predominantly by its ability to increase Ca^{2+} and activate the PKC pathway [200]. However, in αT3-1 cells, the ERK pathway was shown to be involved in the regulation of basal and GnRH-stimulated αGSU transcription [201]. Nevertheless, differences have been recorded between species [202]. For instance, in mouse, ERK-mediated the GnRH effect on αGSU promoter [202]. GnRH can activate another MAPKs including JNK and p38, and JNK but not p38 was reported to mediate GnRH effects on αGSU expression in LβT2 cells, αT3-1 cells and rat pituitaries [151, 172, 203, 204]

The humans basal αGSU promoter expression is mediated by several regions. These are the pituitary glycoprotein hormone basal element (PGBE), that contains the α-basal elements (αBE1 and αBE2), the gonadotroph-specific element (GSE), and cAMP response elements (CREs) [205]. In αT3-1 cells, the PGBE is the main regulatory region for basal αGSU transcription. AP-1 proteins are upregulated by

GnRH and are found to mediate GnRH effects on αGSU. The basal αGSU promoter is less active in LβT2 compared to αT3-1 cells, but the αGSU promoter activity was similar after stimulating cells with GnRH or a PKC activator [206]. Mutation studies demonstrated that two regions (between −398 and −244, and between −244 and −195 base pairs (bp)) of the human αGSU promoter are involved in basal transcription regulation. Deletion of these regions that contain SF-1 binding site abolishes the basal αGSU expression [206]. Thus, the upstream regions of -195 bp are essential for GnRH-mediated responsiveness in gonadotrophs [207, 208], and the CRE (which is the downstream of -195 bp), is not directly implicated in mediating these effects. The SF-1 is involved in mediating the transcriptional response to cAMP [208], but this is not the case in extra-pituitary tissues. Furthermore, other studies showed that in other tissues the SF-1 could be phosphorylated by activators of PKA or ERK signalling pathways [209, 210]. In humans, the αGSU promoter is highly sensitive to oestrogens. However, the mechanism appeared to be indirect, as the oestrogen response elements (ERE) is not functional [211]. Androgens seem to inhibit the activity of αGSU promoter at the CRE site via protein-protein interactions between c-Jun and activation transcription factor 2 [212]. Overall the human αGSU promoter is regulated by distinct response elements.

1.7.3. Luteinising hormone-β subunit expression

The luteinising hormone-β subunit (LHβ) gene promoter structure has been extensively characterized, giving us a great deal of information about its expression following GnRH stimulation. The proximal regions contain the following sites, two binding sites for the immediate early gene protein Egr1 and two binding sites for SF-

1, in addition to a homeodomain element which is binding site for Pitx1 [213, 214]. The latter is expressed mainly in the pituitary and thought to play a crucial role in the development of pituitary [215]. The interactions between them are essential for GnRH induction of the promoter [216]. These regions, in rat and human, share a high degree of homology [215, 217]. The expression level of LHβ changes through the oestrous cycle [172]. For example, in mouse and rat, LHβ mRNA increases at the time of preovulatory gonadotrophin surge [218, 219]. The periovulatory changes in the LHβ mRNA are coincident with the increase in GnRH secretion [220, 221]. The synthesis of LHβ mRNA was shown to be highest during proestrus (as opposed to FSHβ that was found to be greatest during late proestrus and oestrous) [220].

Egr1 is a key factor in regulating the expression of LHβ after pulsatile GnRH stimulation [216]. Studies in LβT2 cell line revealed that the expression of Egr1is stimulated at a high GnRH pulse frequency [150]. In mice with Egr1 deficiency or SF-1 knock out, a reduction in the expression of the LHβ gene and infertility was seen in both cases. However, treating SF-1 knockout mice with GnRH at high doses, induced the expression of LHβ [222-225]. In rat pituitaries, GnRH induces an increase in the expression of Egr1 mRNA, which is dependent on ERK. In mice with pituitary-specific knockouts of ERK reduced fertility. However, the effect was much more pronounced in female than male, indicating that ERK signaling is not required for male fertility [226].

1.7.4. Follicle stimulating hormone-β subunit expression

Compared to the LHβ and αGSU gene promoters, the follicle stimulating hormone-β subunit (FSHβ) gene promoter is less well characterized. This is related to the lack of

an ideal cellular model. Most studies on gonadotrophin regulation were conducted using αT3-1 cells. This cell line does not express LHβ or FSH β-subunits. However, LβT2 cells express the β-subunit of LH (in addition to GnRHR, αGSU and SF-1) and are a model for more mature gonadotrophs (as compared to αT3-1 cells). Also, by treating LβT2 cells with activin FSH can be expressed [150]. Numerous local and gonadal factors are involved in the regulation of FSHβ transcription and secretion (e.g. activins, inhibins, follistatin and many steroids) [172, 227-229]. Both activins and inhibins belong to the transforming growth factor-β (TGF-β) family and are produced by the pituitary and gonads [230]. Inhibins can suppress FSH secretion independently of LH [172]. Follistatin is a glycoprotein hormone that binds activins with high-affinity and blocks activin receptor engagement. Notably, follistatin and activin are also produced in extra-pituitary sites. However, the mechanism of their effect in the pituitary is mainly autocrine and paracrine [172]. FSHβ mRNA increases during the proestrus FSH surge [172, 220, 221]. However, the increase occurs after the increase of LHβ. Studies in mouse and rat showed that the FSHβ mRNA was greatest during late proestrus and oestrous [218, 219].

Since the development of LβT2 cell line, several groups have conducted experiments for further investigation of the gonadotrophin regulation, and this led to the discovery of a GnRH-RE in the proximal FSHβ promoter region. It is relatively conserved in humans and has a partial (CRE)/AP-1 sit [231-233]. This site is thought to provide GnRH responsiveness to the FSHβ promoter [234-236]. Furthermore, a study in 2010 on LβT2 cells revealed that the expression of FSHβ in response to low GnRH pulse frequencies is largely dependent on binding CREB to the CRE/AP1 site [237]. In 2015, it was shown that mice with cFos deficiency exhibited a significant reduction in the expression level of FSHβ, LHβ, αGSU and GnRHR mRNA, and none of these

were recovered by GnRH treatment [238]. A more recent study, in 2017, has identified cJun dimerisation protein 2 (Jdp2) as a novel repressor of GnRH-mediated FSHβ expression in LβT2 cells [239]. Jonak and his group found that Jdp2 acts as a negative regulator. It does that by binding directly to the FSHβ promoter forming a complex with cJun to stop cJun-cFos dimerisation, and indirectly by reducing the expression of cJun [239].

1.8. Desensitisation to GnRH

The amount of GPCRs localised on the plasma membrane is tightly controlled by endocytic pathways [240]. These pathways are clathrin-dependent, clathrin-independent, caveolin-dependent and caveolin-independent mechanisms [241, 242]. Typically, upon GPCRs activation, cytoplasmic signalling is initiated and GPCR kinases are activated (GRKs) [243]. This causes agonist-bound receptor phosphorylation and facilitates binding to β-arrestins. The process occurs in the C-terminal tails and within seconds preventing more G-protein coupling and causing receptor desensitisation. Thus, arrestins act as terminators of GPCR signaling [244] [245]. Next, the GPCR/arrestins complex is internalised via clathrin-coated vesicles (CCV), from where it can be recycled to the cell surface or directed to the lysosome for degradation [241, 244].

The internalization process is dynamic and involves adaptor proteins. As explained, the formation of the vesicles is mediated by clathrin [246]. Clathrin molecules have heavy and light chains and three such dimers form a clathrin triskelion. The CCV is coated with these clathrin polymers and association adaptor proteins which together form a frame around the vesicle [247, 248]. The separation of the vesicle from the

plasma membrane is initiated by recruitment of dynamin with polymerised actin. The dynamin creates a coil around the vesicles' neck that twists upon GTP hydrolysis to facilitate the separation of the vesicle [248]. A summary of these steps is shown in figure 1.7.

Sustained stimulation with GnRH cause desensitisation of GnRH-stimulated gonadotrophin secretion as well as internalisation of GnRHR into CCV and a reduction in the number of cell surface of GnRHRs [249]. It was therefore expected that this model (Figure 1.7) would be relevant to GnRHR regulation. However, the GRK-mediated phosphorylation of GPCR typically occurs in the C-terminal tail, and the type I mammalian GnRHR lack this feature. The absence of the C-terminal tail raised the question of how this type of receptor is regulated [76, 120]. Early work revealed that the mammalian GnRHRs are internalised through coated and uncoated membrane vesicles. However, the nature of the coated structure is not defined yet. Some studies demonstrated that the internalisation process may occur in a clathrin-dependent manner [250]. Studies in rat GnRHRs demonstrated the mechanism of internalisation is dynamin-dependent, but it is dynamin-independent for human GnRHRs [110, 251]. In general, mammalian type I GnRHRs do not undergo rapid homologous desensitisation, do not show agonist-induced internalisation and they are arrestin-independent.

Type II GnRHRs possess the C-terminal tail and do undergo rapid desensitisation. Where studied, these receptors do recruit β-arrestins, and internalise through clathrin-coated pits in different ways [110]. For instance, studies on a bullfrog showed that the internalisation was independent of β-arrestin but dependent on dynamin. In a marmoset type II receptor, the internalisation process was shown to be clathrin and

caveolin and independent on β-arrestins [166]. In COS-7 cells (fibroblast cells derived from monkey) transfected with chicken GnRHRs, the internalisation shown to be in a clathrin-independent [252]. Addition of Xenopus laevis C-terminal tail to the human GnRHR (which lacks the tail) facilitated arrestin- and dynamin-dependent internalisation [181].

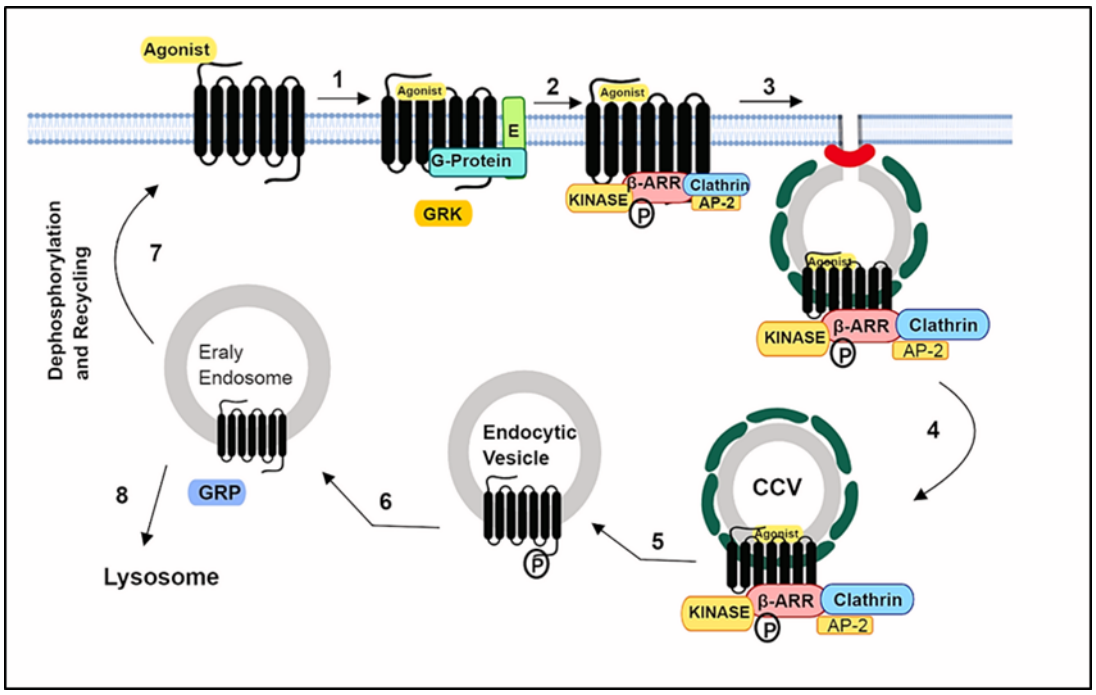

Figure 1.7. Desensitisation, internalisation and cycling of GPCRs

Following agonist binding, G-proteins and effectors (E) are recruited (1). The active receptors are phosphorylated (P) on S and T residues in their C-terminus or ICLs by GRKs (2). This causes the recruitment of β-arrestins (β-ARR). Arrestins target the receptor to clathrin-coated pits (3) that are removed by dynamin (shown in red), forming a clathrin-coated vesicles (CCV) (4). The clathrin is removed from the CCV, and the uncoated vesicle merges with early endosome (5). The receptor is dephosphorylated by GPCR phosphatases (GRP, 6), and is then recycled back to the cell membrane (7) or targeted to lysosomes for degradation and down regulation (8).

1.9. GnRHR trafficking to the plasma membrane

The synthesis of protein is regulated at the transcriptional, translational and post-translational levels by multiple signalling pathways [253]. Proteins are synthesised and processed in the endoplasmic reticulum (ER) and Golgi apparatus [254]. In the ER a strict quality control system (QCS) checks the correct folding and structural

integrity of nascent proteins before their translocation to the Golgi [255]. Consequently, only properly assembled and folded proteins reach their destination. In addition, the QCS also stops the aggregation of defective proteins that might interfere with normal cell function. The strict system does this using several strategies including the action of endogenous protein chaperones [255].

GnRHRs are subjected to structural and conformational scrutiny at the ER prior to trafficking to the plasma membrane [256]. Any mutations in these integral membrane proteins could result in misfolding and degradation of the defective protein receptor [253]. Molecular chaperones can prevent accumulation or interactions between misfolded proteins and other molecules [257]

The expression levels of human GnRHR (hGnRHRs) at the cell surface are found to be relatively low, compared to other GnRHRs. The reason for that is thought to be related to the inefficient exit from the ER. An early study demonstrated that when MCF-7 cells (breast cancer cells) were transduced with hGnRHRs Xenopus laevis GnRHRs, the proportion of the expression level of hGnRHRs was < 1% compared to 40-60% in Xenopus laevis GnRHRs [256, 258]. The low expression level of hGnRHR is a consequence of the absence of a consensus N-glycosylation site which is found in rodent (e.g. mouse and rat). The addition of this site to the hGnRHRs increased their expressions at the surface [259], and fusing the Xenopus laevis C-terminal tail to hGnRHRs had shown to have a similar effect on hGnRHRs (increasing the expression levels of the receptors at the cell surface) [199, 259].

1.10. Dynamics of GnRH signalling

Gonadotrophin releasing hormone is secreted in pulses which are required to establish and maintain normal gonadal function [77]. Its effects on LH and FSH secretion are largely dependent on pulse frequency [138, 260, 261]. Early studies showed that high levels or continuous stimulation of the pituitary with GnRH suppress gonadotrophin secretion [138]. This can be restored by restoration of GnRH pulses [262-264]. The pattern of GnRH secretion develops during life phases. It is transiently active during the neonatal period, quiescent during infancy and childhood, then increases during puberty [23]. GnRH has a half-life of approximately 2-4 min in blood, due to rapid degradation by peptidase [265]. As a result of this rapid degradation, GnRH is not easily detected in the general circulation. However, circulating LH and electrical activity in hypothalamic neurons are often used as measurements from which the dynamic of GnRH secretion can be inferred [94, 266] However, in some species GnRH pulses have been measured directly in the portal circulation [266-270].

In humans and other primates, GnRH pulses are less than 10 min in duration with intervals of 30 min to many hours [21]. The frequency of GnRH pulses differs under different physiological situations which contributes to changing reproductive status [271]. For instance, increasing GnRH pulse frequency in males stimulates gametogenesis and gonadal steroid at puberty. In females, the GnRH pulse frequency differs over the menstrual cycle. It increases before ovulation generating the preovulatory gonadotrophin surge [7]. GnRH has different effects during different time-scales. Within seconds of stimulation, GnRH increases the cytoplasmic Ca^{2+} concentration and increases LH and FSH secretion from pre-existing stores in

secretory vesicles. However, its effect on the expression of αGSU, LHβ, and FSHβ occurs over hours to days.

Gonadotrophins are secreted by exocytosis and this can occur via constitutive or regulated secretion pathways [272]. In constitutive secretion proteins are packaged into small vesicles in the Golgi, which move to the cell surface and fuse directly with the plasma membrane, so constitutive secretion does not require an extracellular stimulus [272, 273]. In contrast, with regulated secretion, proteins are packaged tightly into dense vesicles that fuse in the plasma membrane after appropriate stimulation [272]. The primary stimulus for this regulated exocytosis is an increase in the $[Ca^{2+}]^i$. However, there is an important difference between LH and FSH secretion. The majority of LH is released through the regulated pathway and is dependent on GnRH-induced Ca^{2+} mobilisation [272]. Whereas, FSH tends to be constitutively secreted and is dependent on the rate of FSH synthesis. Thus, GnRH-stimulated increases in $[Ca^{2+}]^i$ has a rapid and pronounced effect on LH secretion and relatively minor effect on FSH secretion. Consequently, when gonadotrophins were measured in hypophyseal and peripheral blood there was high synchrony between pulses of GnRH and LH and much less synchrony between pulses of GnRH and FSH [273].

Overall, disruption of signalling pathways of GnRH, FSH, and LH can result in reproductive disorders. For example, rapid GnRH pulses result in an increase in the ratio of LH to FSH that contributes to excessive ovarian androgen production and ovulatory dysfunction seen in a case termed POS. This syndrome also was shown to be associated with obesity, and impaired glucose tolerance. On the other hand, low pulse frequencies of GnRH and abnormal levels of serum gonadotrophin contribute to hypothalamic amenorrhea.

1.11. Heterogeneity, noise and information in cell signalling

Cells receive information via signalling pathways that are devoted to conveying environmental information [274]. Cell signalling pathways have traditionally been investigated using conventional metrics that depend largely on measuring the average responses from a large number of cells [152]. These include measurements of hormone secretion from large populations of cultured cells, levels of proteins in cell populations by western blotting, or measurement of reporter gene expression in cell populations. These traditional methods are useful in mapping the signalling pathways but ignore cell-cell variability that often has physiological implications [152]. The recent advance in biological research methods has provided researchers with several methods to give a better view of the behaviours of single cells. For example, imaging-based experimental readouts have been increasingly used, and these revealed marked cell-cell variability [153, 275]. Early GnRH signalling studies revealed cell-cell heterogeneity in secretory responses of gonadotrophs to GnRH as well as in Ca^{2+} responses of gonadotrophs and gonadotroph-derived cell lines to GnRH [276-278]. In general, variability between cells in dynamic responses to stimuli was seen ubiquitously [279-282]

The biological system is diverse in nature. Such diversity can generally be perplexing [283], particularly, when it is displayed by the same type of cells that have identical genomes. If it is assumed that if the genetic composition of a cell defines the phenotypic responses to environmental input, the same type of cells would be expected to display similar responses to the same input [283]. However, this is not the case as such heterogeneity is seen in genetically identical cells. Recent studies revealed that the intrinsic thermal fluctuations of biochemical reactions are the main

source of variability [284-287]. The heterogeneity appears to be an intrinsic feature of the signalling pathways and responses measured [288]. Heterogeneity is an inevitable consequence of the stochastic nature of biochemical processes [288]. For example, any given molecule of ERK2 is either inside or outside the nucleus and has either been activated or not by dual phosphorylation. Thus, when measuring the response of ERK2 in a single cell, variability in the amount and activity of signalling proteins is seen between cells.

Little is known about the biological importance of this heterogeneity. However, it is a central aspect to be considered when studying the behaviour of cells [289]. This is because each cell has to sense environment for the appropriate decision [286], and the decisions taken by individual cells are what defines the activity of tissues in health and disease. A recent study in PC12 cells stimulated by growth factors (NGF and EGF) demonstrated this diversity [290].The study measured the response of individual cells to the activity of ERK and Akt. The results revealed that cells use a combinatorial signalling system to control cell fate and that this was dependent on the activities of ERK and Akt between different cells within the cell population [290]. A similar observation has been reported related to the responses of single cells to therapy and outcomes to medical intervention [291]. It was shown that, if a drug is designed to target rapidly proliferating cells, then variability between cell can leave some relatively unresponsive cells unaffected or unscathed, which might reduce the sensitivity to the follow-up treatments [285] as can be seen in cancer stem cells [291]

Many studies have reported that such heterogeneity has a remarkable impact on cellular function and development. It shapes the mechanism of signal transduction, gene expression and metabolism [12, 286, 292]. For instance, it can destroy the fidelity

of transferred signals or degrade the concentration of ligand via networks. It possibly drives cells to dramatical changes in phenotypic states as seen in pathological cases like cancer [286], and contributes to producing random mutations [285, 289]. On the other hand, stochasticity can lead identical cells to generate different molecule number and different physiological states [285]. This in turn, offers a mechanism for a population to increase the variety of its phenotypic and can even provide adaptability to a stressful or fluctuating environment [293-295]. Consequently, cell-cell heterogeneity can be advantageous to a biological system as well as disadvantageous in certain circumstances.

1.12. Information theory

Despite the functional importance of cell-cell heterogeneity, analytical methods for interrogating its impact have been lacking. Recently, a statistical measure derived from information theory named mutual information (MI) has increasingly being applied in cell biology. MI can be used to explore the influence of various sources of noise on the information transmitted through signalling pathways [283, 296]. Information theory was first developed in 1948 by Claude Shannon as an attempt to understand the efficiency of information transmission through communication channels [297]. Shannon proposed that information can be quantified in term of the entropy [298], and the information that flows through channels can be measured using MI [274]. In particular, MI measures the reliability with which a system input (S) can be inferred from the output (Z) [153] and is defined as:

$$I(Z;S) = H(S) - H(S \mid Z),$$

where H(S) denotes the entropy of S, and H(S|Z) denotes the conditional entropy of S given Z. It is worthwhile mentioning that MI is an appropriate measure of statistical association even in the case of a nonlinear relationship between input and output variables, a prevalent characteristic of signalling networks [274]. MI is often measured in Bits, where 1Bit of information intuitively means that the system can resolve unambiguously two different signal values [292].

In the context of cell biology, MI between an environmental variable (e.g. extracellular levels of GnRH) and a signalling response (e.g. NFAT translocation to the nucleus) measures the uncertainty about the environment that is eliminated by signalling. Consequently, rather than MI focusing on identification of signalling intermediates in a pathway, it works on quantifying the amount of information that the pathway transfers. Figure 1.8 illustrates the principle with emphasis on how cell-cell heterogeneity could impact information transfer (i.e. the reliability of hormone sensing in this example). Recently, a few research groups have applied this approach to quantify transferred information through signalling pathways. This provided us with more insights into cell signalling, and some of the key insights are outlined below.

First a remarkable amount of available information is lost through signalling. A recent work provided the first quantification of information transfer via GnRHR revealed that although there was 3 Bits of information available, <1 Bit was transferred via GnRHR to ERK or NFAT [153]. Studies on different receptors and with different ligands and effectors in different cell types indicated that signalling pathways act as noisy communication channels, where loss of information was reported through

signalling networks [152, 153, 281, 296, 299]. The noise referred to here is the cell-cell heterogeneity that results on a pronounced loss of information through signalling. The obvious indication from such a work is that despite the graded responses in population average over a broad range of stimulus, individual cells cannot distinguish between two different states of the environment. Thus, it is possible that the techniques used led to underestimate transferred information. Consequently, work on Chapter 5 and Chapter 6 addresses the questions of where information is lost and the extent to which the methods used might impact information transfer.

Second, equating the size of the response to information transfer is not acceptable in signalling cell studies. As shown in Figure 1.8, for response B, the transferred information would be higher for the large response than the small one. For response A, transferred information would be identical for both (large and small responses) [292]. Thus, where the average response and cell-cell variability scale right with one another, it might indicate that desensitisation has happened even though the reliability of the cells in sensing their environment has not changed. Notably, information cannot be gained via signalling and any increase in the size of the response via signalling pathways must be related to an increase in heterogeneity and cannot lead to an increase the reliability with which cells sense the stimulus

Third, several studies have considered the role of negative feedback as a mechanism that can relieve (but not always) the limitation in losing such information. A study found that by reducing the basal activity, the negative feedback could enhance information transfer [287]. A recent study considered the effect of rapid and slow negative feedback on the quantity of information transfer. It showed that negative feedback can reduce information transfer by reducing the dynamic range for the

system output and can also protect information transfer by reducing cell-cell variability [152].

Fourth, sensing multiple pathways within a network was considered as a mechanism that cells do to mitigate loss. For example, in the case of activating a receptor that causes the activation of ERK and Akt pathways, the extreme scenarios would be either there is no correlation between ERK and Akt responses or a perfect correlation. in the former scenario, sensing both pathways will provide a substantial increase in transferred information and would be the opposite in the latter case. A similar observation was reported for the ERK-dependent and ERK-independent activation of CREB by NGF or PACAP [300], where sensing growth factors through multiple pathways did not increase transferred information. Instead, it protected the cells from loss of environment sensing on perturbation of individual signalling pathways.

Finally, snapshot data might be underestimated transferred information. Consider a situation where cells are stimulated for example at 5 time points. The estimated MI value could be high at early time point (time 2) and reduce later (time 3). This clearly does not mean that the cells gain less information during time 2 than during time 3, instead it just shows that the later snapshot data underestimate the information gained over the entire stimulation period. In the same manner, the time 2 snapshot data could underestimate the information transferred over this period, suggesting that cells could gain information by sensing response trajectories over time as illustrated in Figure 1.9, and shown here [152]. This has been an important driver for the application of information theoretic approaches to live cell imaging data.

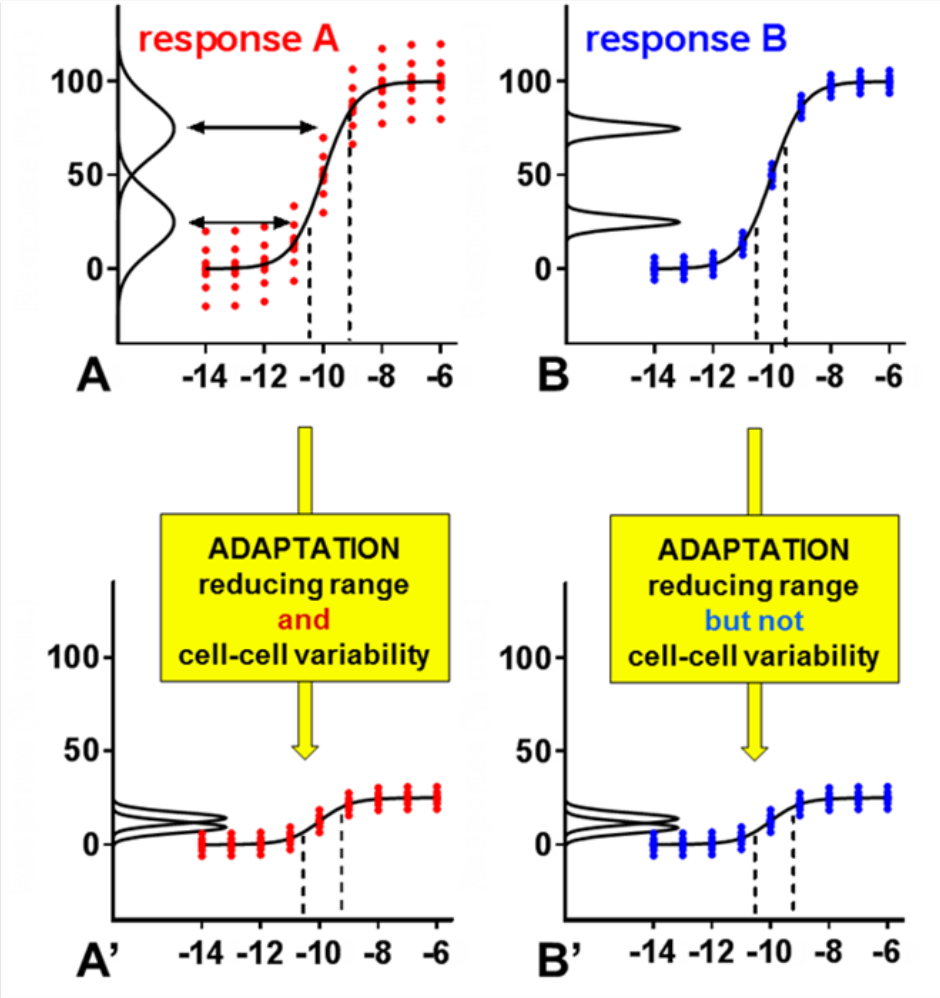

Figure 1.8. Variability between cells and transferred information

As shown the population average response is similar in A and B. However, the cell-cell variability is higher in A than B. This is illustrated in red dots (individual cells), and black lines on the y-axis (frequency distribution). The black dotted lines and arrows represent two concentrations of a stimulus. The frequency distributions in A overlap, indicating that there is an area of uncertainty where individual cell cannot distinguish between two equally probable states of the environment. The uncertainty is not seen in B. The quality of the signal that can be inferred from the response is higher in B than A. Consequently, MI value will be expected to be greater in B than A. In the case where cells adapt to their environment as a result of negative feedback loops, a reduction in population-averaged response and variability between cells occurs (A→A′). However, the quality of sensing is not reduced. The opposite is true for B→B′, were the population averaged response is reduced but not the variability between cells. The quality of sensing reduced as well, as the frequency-distribution plots overlap. Thus, consideration of population averaged responses alone cannot be equated to information transfer (or in this case, the reliability of hormone sensing). The figure is reproduced from [292].

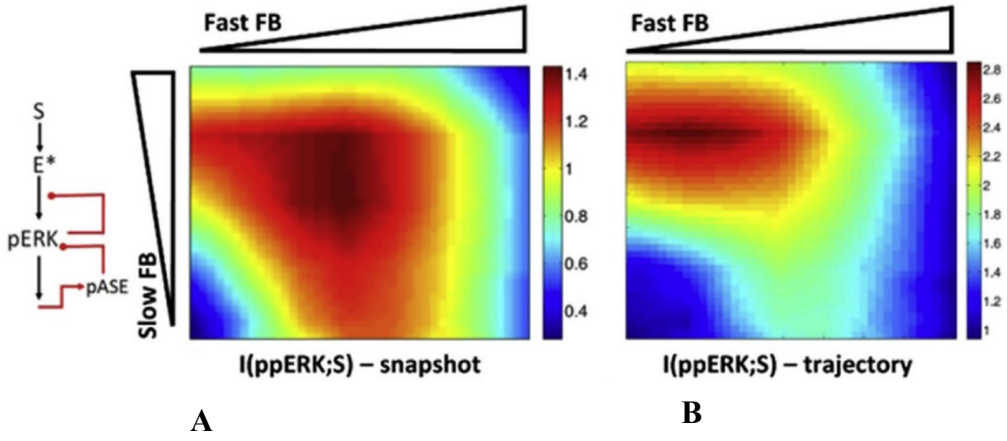

Figure 1.9. Stochastic modelling of ERK signaling.

The figure shows a heat map of population-averaged responses of ppERK for single cells with varied fast and low feedback (FB) at 3.5 and 0-4 (log_{10} scale), respectively. The simulations were run for 60 min. A predicted I(ppERK; S) for 10 min snapshot data is shown in A. MI was calculated taking response trajectories into account (shown in B). The calculated MI values reveal that maximum information transfer at intermediate feedback levels and information is increasing with trajectories (from 1.4 Bits to 2.8 Bits). The cartoon in the left shows system simulated, with stimulus (S) that activates an upstream effector (E) which in turns catalyses the pERK. The fast FB loop represents ERK-dependent inhibition of E*/pERK. The slow FB loop represents pERK-driven phosphatase expression and causing dephosphorylation of pERK. The figure is reproduced from [153].

1.13. Cell lines

In this work, different cells lines were used for the GnRHR signalling study. These are HeLa, MCF-7 and LβT2 cells. The HeLa cell line is the first immortalised human cell line established in culture [301]. It is a human epithelial cell line derived from cervical cancer cells that were obtained from Henrietta Lack in 1951. HeLa cells are widely used as a model for studying human cellular and molecular biology [301] and have been largely used for GnRHR signalling studies [152, 199, 256, 302]. However, this cell line has some disadvantages. The most significant one is that these cells can contaminate aggressively other cell cultures in a laboratory [303]. Thus, great care should be taken when working with this cell line. Another issue is that these cells do not have a normal karyotype as found in humans [303-305]. A normal cell contains 46 chromosomes, but the HeLa genome comprises of 76-80 chromosomes (due to the infection by human papillomavirus) and around 25 chromosomes are abnormal [301, 304, 305].

The second cell line is the MCF-7. These cells are breast cancer cells that were derived from a woman with breast adenocarcinoma in the Michigan Cancer Foundation [306, 307]. This cell line is largely popular due to its exquisite sensitivity to hormones through the expression of the ER, which makes it an ideal model for hormone response studies [308, 309]. Reports have shown that this cell line can be used to study PI3K, MAPK and to detect ERK and Akt phosphorylation [310, 311]. Furthermore, numerous groups have described GnRHR signalling in hormone-dependent cancer-derived cell lines [258, 312]. MCF-7 cells are like HeLa cells, they are easily grown and can display a high degree of homogeneity [313]. However, although these cells appear to be morphologically identical, genetically they are described to have a

karyotype containing 69 chromosomes [313, 314]. Both HeLa and MCF-7 cell lines do not express the endogenous GnRHR, but studies have shown that cells can heterogeneously express the receptor by transducing them with Ad mGnRHR [152, 153, 258, 302, 315, 316]. In addition to that, these cell types acquire many of the properties of cancer cells. Despite that *in vitro* systems are isolated from the complexity of the endocrine environment; these models have significantly contributed to our knowledge.

The third cell line is LßT2 cells. These are a mouse gonadotroph-derived cell line that was produced by targeted oncogenesis with Simian Virus 40 (SV40) T antigen in transgenic mice [197]. These cells display similar characteristic of mature gonadotrophs (i.e. express αGSU, the LHβ subunit and GnRHRs). Moreover, they can express FSHβ when cells treated with activin A [150]. Consequently, the LßT2 cell line is an important model for GnRHR-signalling pathways study [317]. Nevertheless, SV40 T antigen causes cell immortalisation [318] by interacting with a wide range of target proteins, like proteins phosphatase 2A and protein phosphatase 1. In most cells and tissue these two proteins account for >90% of Ser/ Thr phosphatase activity [319]. Moreover, the small SV40 cause the inhibition of protein phosphatase 2A [320], which is reported to affect ERK and MEK activities. This cell line has been largely used to study the regulation of gonadotrophin and GnRH signalling [135, 150, 315, 321, 322].

1.14. Aim

The hypothalamic neuropeptide hormone (GnRH) is the primary regulator of mammalian reproductive function [20]. It is secreted in a pulsatile manner, and acts via GPCRs on gonadotrophs within the anterior pituitary [15]. Binding of GnRH to its cognate receptor causes the activation of PLC and consequent activation of a signalling network including two major pathways (i.e. the GnRHRs/Gq/PLC/Ca^{2+}/ CaM/Cn/NFAT and GnRHRs/Gq/PLC/KC/ERK pathways) [209]. GnRHRs were cloned first in the early 90's since then numerous studies have been conducted investigating its function in heterologous expression systems. In addition to gonadotrophs, GnRHRs have been found to be expressed in many cell types. The effects of GnRH are cell context-dependent. This implies that the GnRH signalling system can be different in different cell types, resulting in input-output relationships differences between these cells. These observations raise two questions. First, what is the optimal cellular model to study the mechanisms of GnRH action. Second, by comparing GnRH signalling in different cell types, would that provide us with additional insight into the mechanisms of signalling networks that mediate GnRH effect on cells.

Single cell measures revealed marked variation from cell-cell in the responses to the same stimulus. This heterogeneity suggests that differences in network components from one cell to another result in different outcomes, just as they do for large cell populations with different cell types. Thus, the overall aim of the work here was to advance our understanding of GnRH signalling by exploring differences in responses between different cell types as well as between individual cells of a given cell type.

In the first two chapters, a conventional approach for GnRH signalling was followed, comparing three different cell types with emphasis on response kinetics (Chapter 3) and the use of pharmacological inhibitors (Chapter 4). Then the emphasis was placed on cell-cell variability in responses with the use of the of information theoretic approach to quantify information transferred via GnRHRs in fixed cells (Chapter 5) and in live cells to explore the importance of stimulus and response dynamics (Chapter 6). Specific aims of each of the results chapters and experimental approaches were as follows:

The principle aims of the experiments described in Chapter 3 was to determine the effects of GnRH on the two main signalling pathways, as well as transcriptional readouts for both. This was achieved by automated fluorescence microscopy with an INCell to monitor the signalling in large numbers of fixed cells. Given the possibility of cell context-dependent signalling [22], the work was done in different cell lines. These are HeLa and MCF-7 cells (extra-pituitary cell lines) and LßT2 cells (pituitary-derived cell line). An additional aim was to quantify ERK and NFAT1c-EFP activities in response to PDBu (PKC activator) and EGF.

The work continued in Chapter 4 using the same cellular models and experimental readouts as used in Chapter 3. Here the aim was to use pharmacological inhibitors that target ERK and NFAT pathways for further delineation of the network architecture.

The experiments described in Chapter 3 and Chapter 4 do not define information transfer via GnRHR, thus an information theoretic approach was applied in Chapter 5. The statistical measure (MI) was used to quantify information transferred via GnRHRs to ERK and NFAT. An additional aim here was to quantify the information that cells can gain by sensing multiple pathways within the network. The information

was compared in three cellular models using distinct readouts (transcriptional and non-transcriptional) for their activation.

The aim of the experiments described in Chapter 6 was to determine whether cells gain additional information by sensing response dynamics, using live cell monitoring of Ca^{2+} responses and Ca^{2+}-driven NFAT1c-EFP translocation in GnRH stimulated cells. Additional aims of the work described in Chapter 6 were to determine how much information is gained by sensing repeated GnRH pulses and by sensing GnRHR-independent stimuli.

Chapter 2- General materials and methods

Suppliers

All products and reagents were purchased from Sigma Aldrich, UK, except those listed below.

Product	Company
Matrigel basement membrane complex 10 ml	BD Bioscience, Oxford, UK
PDBu, AG1478, Ro31-8425, PD184352	Calbiochem (Merck), Nottingham, UK
Alexa Fluor® 546 Goat anti-mouse IgG, highly cross-adsorbed **Alexa Fluor® 488 Goat anti-mouse IgG, highly cross-adsorbed**	Cell Signalling Technology (New England Biolabs), Hitchin, UK
Plasticware	Corning Life Sciences, distributed by Appleton Woods, Birmingham, UK, or Fisher Scientific, Loughborough UK
HeLa cell line **MCF-7 cell line**	European Collection of Cell Cultures, Salisbury, Wiltshire, UK
LβT2 cell line	Kindly provided by Prof. P.L. Mellon, University of California San Diego, San Diego, CA
Hoechst 33258	GE Healthcare, Amersham, UK
Fluo-4, AM, cell permeant	Invitrogen Ltd., Paisley, UK
Rhod-3 Calcium Imaging Kit **FBS**	Life Technologies Authenticated

Standard solutions

Culture Medium

DMEM

10% (v/v) FCS

100 U/mL penicillin and 0.1 mg/mL streptomycin

Gonadotrophin-Releasing Hormone

Stored in sterilised ddH_2O at -20ºC

Serum Starvation Medium

DMEM

0.1 (v/v) FCS

100 U/mL penicillin 0.1 mg/mL streptomycin

Phosphate Buffered Saline

5 x 0.5 g tablets dissolved in 1 litre ddH_2O

Phorbol 12, 13 dibutyrate

Stored in DMSO at -20 ºC

4% Paraformaldehyde

4% (w/v) in PBS aliquot into 20 ml and store at -20 ºC

Physiological Salt Solution

20 mM HEPES

137 mM NaCl

5 mM KCl

2 mM $MgCl_2$

1.8 mM $CaCl_2$

5.6 mM glucose

1 mg/mL BSA

0.5 mM$NaH2PO_4$

1 mM$NaHCO_3$

0.03 mM Phenol red

(pH 7.4)

Rhod-3 Loading Buffer

100x PowerLoad concentrate

100 mM Rhod-3 AM

2.5 mM probenecid

PSS buffer

2.1. Experimental models

As explained in Chapter 1, three different types of cells were used in this work; HeLa, MCF-7 and LβT2 cells. HeLa cells are a human cervical cancer-derived cell line that has been extensively used for GnRHR signalling studies [152, 199, 256, 302]. MCF-7 cells are breast cancer cells derived from breast adenocarcinoma [258, 312]. LßT2 cells are a mouse gonadotroph-derived cell line that was produced by targeted oncogenesis with SV40 T antigen in transgenic mice [197]. These cells can express αGSU, the LHβ subunit and GnRHRs [323].

Since LβT2 cells are derived from transgenic mice they are genetically modified, and most experiments described here involved further genetic modification (i.e. viral transduction) of cells. The work was undertaken with approval of the University of Bristol's Biological and Genetic Modification Safety Committee (Project #4509)

2.2. Cell culture

All three cell lines were routinely maintained in Culture Medium consisting of Dulbecco's Modified Eagle's Media supplemented with 10% (v/v) fetal calf serum (FCS) 100 U/mL penicillin and 0.1 mg/mL streptomycin in T75 flask. Cells were maintained in a humidified atmosphere of 5% CO_2 at 37°C. Cells were passaged upon reaching >70% confluence (approximately two to three times per week). Cells were subcultured by removal of medium, washing with 5 ml phosphate buffer saline (PBS) at room temperature, then incubating for around 3 min with 2 ml TE (0.25% trypsin, 0.03% ethylenediaminetetraacetic acid (EDTA) in PBS) until cells detached. Cells were then dispersed by repeat pipetting with 8 ml of cell medium. The suspended cells

(typically, 2.5 ml) were added into a T75 flask containing approximately 12 ml of fresh culture medium and supplemented as above.

For some experiments, cells were cultured in 96-well plates. After trypsinisation as outlined above they were counted and suspended in an appropriate volume of culture medium so that they could be seeded in Costar black-walled 96-well culture plates at 100 µl/well with 5000 HeLa or MCF-7 cell/well, or with 10.000 LβT2 cells/well.

The LβT2 cells were routinely cultured as described above except that cultured plates were coated with Matrigel to improve cell attachment. Matrigel was stored in 200 µl aliquots at -20°C and for use, a single aliquot was thawed on ice and then added to DMEM (with no additions) at 4°C. 3 ml of the solution was used to coat each T75 flask, and 30 µl was used to coat each well of a 96-well plate. The Matrigel was left at room temperature for 1 hr to solidify and then any residual liquid was removed by aspiration [315].

2.3. Adenoviral transduction

Several recombinant adenoviruses (Ad) were used to express proteins of interest in cells. These included Ad for expression of mouse GnRHR (Ad mGnRHR) and Ad for expression of an NFAT1c-emerald green fluorescent protein (EFP) (Ad NFAT1c-EFP) which was used as a readout for GnRH-mediated activation of Ca^{2+}/CaM/Cn pathway. Ad for expression of a reporter with Egr1 promoter driving expression zsGreen fluorophore (Ad Egr1-zsGreen) and another reporter in which NFAT response elements drive expression asRed fluorophore (Ad NFAT-RE-as Red). These were used as transcriptional readouts of ERK and NFAT pathways respectively. The

Ad used were engineered as described here [140, 141, 180] and the stock solutions were stored with PBS at -80°C.

Ad transduction was performed with cells cultured in 96-well plates as described under section 2.2. On the day after seeding into culture plates, the Culture Medium was replaced with DMEM containing 2% (v/v) FCS and the appropriate Ad (Ad mGnRHR, Ad NFAT1c-EFP, Ad Egr1-zsGreen or Ad NFAT-RE-asRed). These Ad were used at the range of 1 to 10 plaque-forming units per nanolitre (pfu/nl) except Ad mGnRHR, was used at 25 pfu/nl [22, 180, 324]. After 4-6 hr at 37°C Transduction Medium was removed and replaced with DMEM containing 0.1% (v/v) FCS (Serum Starvation Medium). Cells were then incubated overnight before stimulation. The removed Transduction Medium was immediately treated with Virkon to destroy any remaining Ad.

2.4. Cell treatments for fixed cell imaging.

For acute stimulations, 25µl of Serum Starvation Medium containing 5x concentrated stimulus was added to each well that contained 100 µl of the Serum Starvation Medium. Stimulations were at 37°C and were terminated by removal of this medium and addition of ice-cold 4% (w/v) paraformaldehyde (PFA) in phosphate-buffered saline (PBS). The stimuli and stimulation periods are outlined in the figure legends. For most experiments, cells were stimulated with varied concentrations of GnRH, PDBu or EGF and for periods of 5 min to 8 hr.

2.5. Delineating network architecture with pharmacological inhibitors.

The mechanism of GnRH, PDBu, and EGF action were explored with pharmacological agents to further characterise ERK and NFAT signalling in the three cell lines. The drugs that were used here are a) Cetrorelix, a GnRH antagonist [325], b) AG1478, an inhibitor of EGFR signalling that competitively blocks the ATP binding pocket of the EGFR [158, 326], c) Ro31-8425, a reversible and highly selective inhibitor of protein kinase C that blocks the ATP binding site [158] d) PD184352, that inhibits MEK1/2 [316], by binding a hydrophobic pocket and altering the Mg-ATP binding site of MEK1/2. This induces a conformational change in unphosphorylated MEK1/2 that prevents its activation [327], and e) Cyclosporine A (CsA) a potent immunosuppressant drug that inhibits calcineurin [111] by binding cyclophilin, and forming a complex that inhibits the phosphatase activity of calcineurin. The phosphatase calcineurin is required for the regulation of nuclear translocation and activation of NFAT transcription factors [111].

Cells were cultured as described above. Inhibitors were applied in a volume of 25 µl/well for 30 min at 37°C. The antagonists were 4x concentrated in Serum Starvation Medium and were used at a concentration of 10^{-6} M for Cetrorelix, Ro31-8425, and CsA, and at a concentration of 10^{-7} M for AG1478 and PD184352. Cells were then stimulated with GnRH, PDBu or EGF in the continued presence of inhibitors in the cells for times outlined in the figure legends.

2.6. Immunocytochemistry and fluorescence imaging with fixed cells

2.6.1. Immunohistochemical quantification of total ERK and ppERK using a high content imaging platform

Following culture and stimulation as outlined above, the stimulation medium was removed, and cells were fixed with ice-cold 4% (w/v) PFA in PBS for 5 min at 4°C. They were then permeabilized with ice-cold 100% methanol for 5 min at -20°C and then washed with PBS at room temperate. Cells were blocked with 5% normal goat serum (NGS) in PBS for 1-2 hr at room temperature. Cells were then incubated overnight at 4°C in PBS with primary antibody (30 µl/well). The primary antibody (1°Ab) used was monoclonal mouse antibody (1:200 dilution in PBS) recognizing ppERK or monoclonal rabbit antibody (1:300 dilution in PBS) recognizing total ERK. The 1°Ab was removed, and plates were washed 3x with 100 µl PBS at room temperature. Cells were then incubated with secondary antibody (2°Ab) for 90 min at room temperature. The 2°Ab used was green Alexa-488-conjugated goat anti-mouse (1:200 in PBS) or red Alexa-546-conjugated goat anti-rabbit (1:300 in PBS, 30 µl per well). Plates were then washed 3x with PBS and nuclei were stained with 4', 6-Diamidino-2-Phenyindole, Dilactate (DAPI, 1:5000 in PBS) and incubated for 20 min at room temperature. Fluorescence images were then obtained and analysed as described below. If images are not obtained immediately, cells could be stored for several days at 4°C with 200 µl PBS/well to prevent drying of the cells, and plates were covered with aluminium foil to prevent degradation of fluorophores.

2.6.2. Quantification of NFAT1c-EFP translocation using a high content imaging platform.

Cells were treated as described above except that HeLa and MCF-7 cells were transduced with Ad NFAT1c-EFP and Ad mGnRHR, while LβT2 cells were transduced with Ad NFAT1c-EFP alone. After stimulation, they were fixed and stained with DAPI but were not processed for immunohistochemistry (IHC) as EFP fluorescence was used for quantification of nuclear and cytoplasmic NFAT1c-EFP.

2.6.3. Monitoring Egr1-driven zsGreen and NFAT-RE driven asRed expression.

Cells were treated as described earlier except that the HeLa and MCF-7 cells were transduced with Ad Egr1-zsGreen, Ad NFAT-RE-asRed and Ad mGnRHR, while LβT2 cells were transduced with Ad Egr1-zsGreen, Ad NFAT-RE-asRed. Cells were stimulated with GnRH as outlined in figure legends for a period of 4-6 hr at 37°C Cells were then fixed and stained with DAPI. However, cells were not processed for IHC as zsGreen, and asRed fluorescence were captured directly for quantification.

2.7. Live cells imaging experiments.

2.7.1. Imaging NFAT1c-EFP translocation in response to single and two pulses of GnRH in LßT2 cells.

LβT2 cells were cultured and transduced with Ad NFATc1-EFP in 96-well plates as described under Section 2.2 and 2.3. On the day of imaging, the Culture Medium was replaced with live cell imaging buffer (Physiological Salt Solution-PSS), which is

composed of [20 mM HEPES (pH 7.4), 137 mM NaCl, 5 mM KCl, 2 mM $MgCl_2$, 1.8 mM $CaCl_2$, 5.6 mM glucose, 1 mg/mL bovine serum albumin, 0.5 μM NaH_2PO_4 and 1mM$NaHCO_3$] and nuclei were stained with 400 nM Hoechst 33342 dye in PPS for 30 min at 37°C. The Hoechst dye is membrane permeant so can be used for live cells, while DAPI is not and is therefore only used for fixed/permeabilized cells. Cells were then imaged at 37°C both before and during stimulation with GnRH.

In the single pulse experiment, cells were imaged for an hour, and images were collected every 2 min for the first half hour then every 5 min for the next half hour. For the two pulses experiments, LβT2 cells received two pulses of GnRH. The first one lasted for 15 min, and images were collected every 2 min. Next, the plate was taken out of the microscope stage to terminate the GnRH effect by extensive washing with PSS buffer (4x 100 μl/well). Then the plate was returned to the stage and cells were imaged for 130 min, before receiving the second pulse of GnRH which lasted for a further 30 min and images were collected every 2 min.

In both experiments (single and repeated pulses), images were collected by moving from one well to the next then returning to the first well. Accordingly, multiple wells were imaged in parallel (12 well). Notably, the addition of the stimulus was done automatically by the machine. This allows for better temperature control and reduce delay in imaging. On the other hand, the use of 5% CO_2 atmosphere is not possible, therefore, HEPES-buffered PSS was used.

2.7.2. Live cell imaging of cytoplasmic [Ca^{2+}]

A fluorescent green dye (Fluo-4 AM) was used to quantify the intracellular Ca^{2+} concentrations. Fluo-4 is an improved analogue of Fluo-3, where two chlorine substituents in Fluo-3 are replaced by fluorine in Fluo-4. This modification increases fluorescence excitation at 488 nm, so that higher signalling levels result. The Ca^{2+} indicator is hydrophilic and does not cross lipid membranes freely, so it is modified by addition of acetoxymethyl (AM) esters. During the incubation period the Fluo-4AM enters cells, and then the endogenous esterase enzyme cleaves the AM hydrophobic component, causing the dye to be trapped inside the cell (Figure 2.1).

Cells were cultured and plated as described earlier (Section 2.2). On the day of imaging, cells were incubated for 30 min at 37°C in PSS containing 5 mM Fluo-4 AM, and 400 nM Hoechst. The cells were then washed three times with PSS to remove any additional indicator from the extracellular solution. Cells were then left in clean PSS for 10 min in the INCell Analyser 2200 at 37°C to recover prior to imaging. Cells were then auto injected with a stimulus. Images were collected from multiple wells in a single plate as described above for NFAT1c-EFP imaging. However, time intervals were shorter (images captured every 20 sec for 10 min) so only 3 wells were imaged per plate.

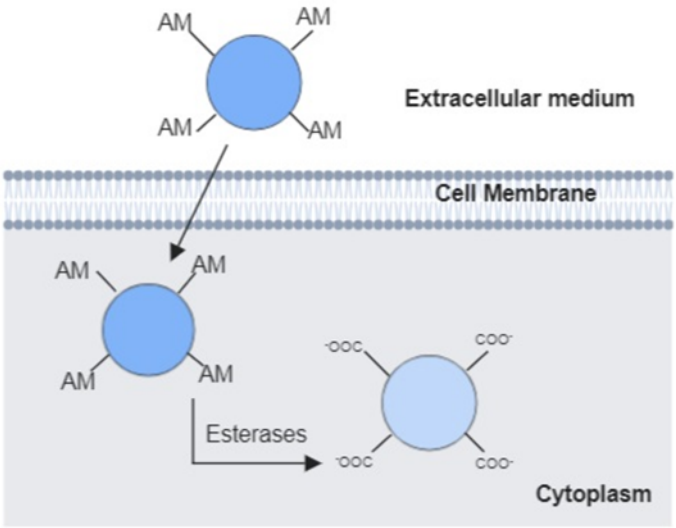

Figure 2.1. A scheme showing the process of loading Fluo-4AM inside cells

The large circle represents the fluorescent dye core. The carboxylic groups are protected as AM esters which makes the dye neutral so that they can cross the cell membrane. Inside the cell, the AM groups are cleaved by esterases generating the charged and membrane impermeant Fluo-4 molecules that are trapped inside the cell.

2.7.3. Live cell imaging of cytoplasmic [Ca^{2+}] in combination with NFAT1c-EFP.

Ad NFAT1c-EFP transduced LβT2 cells were incubated at 37°C for 60 min in loading buffer composed of 100x PowerLoad concentrate, 100 mM Rhod-3 AM and 2.5 mM probenecid. The PowerLoad concentrate is an optimized form of nonionic, pluronic surfactant polyols. It helps the Rhod-3 AM to be soluble in the PSS buffer. The water-soluble probenecid increases dye retention by suppression efflux of fluorescent dyes via anion pumps that are found on the cell membrane. These components together maximize the loading of dye into cells and reduce background fluorescence [328, 329]

After the incubation period, cells were washed 3x with PSS buffer, followed by a further 20 min incubation with Hoechst for nuclei staining. Cells were then left 10 min in INCell Analyzer 2200 to recover prior to imaging. The images were collected every 30 sec for 30 min, then every 120 sec for 20 min.

2.8. Image acquisition and image Analysis

Digital images were acquired with INCell Analyser 1000 and 2200 high-content imaging platforms (GE Healthcare). High content imaging systems are increasingly used as cell-based assays for drug discovery as well as for interrogation of signalling pathways. This is largely because they can offer higher throughput and more rigorous quantification than other cell-based or microscopy-based assay systems. The ability to determine amount and localisation of signalling molecules in large numbers of individual cells is of particular importance for consideration of cell-cell heterogeneity, as described in Chapter 1.

For the InCell 1000 experiments, images were captured using a 10x objective and a 61002 trichroic mirror. Excitation and emission filters were 360 ± 40 nm and 460 ± 40 nm for DAPI, 475 ± 20 nm and 535 ± 50 nm for Alexa 488, EFP, and zsGreen and 535 ± 50 nm and 620 ± 60 nm for Alexa 546 and asRed. Three fields of view were imaged per well each 0.602 mm^2. Exposure time for each fluorophore was determined individually to obtain clear images whilst keeping exposure times short (<1 sec).

The INCell Analyser 2200 was used for the live cell imaging experiments described here. This system uses LEDs for excitations (as opposed to the Xenon lamp light source used by the INCell Analyser 1000. Additionally, exposure times are reduced,

and speed is increased with the INCell Analyser 2200. The blue channel was used to image Hoechst or DAPI with excitation filter of 590/18x, and emission filter of 452/48 m. The FITC channel was used to image NFAT1c-EFP and or Fluo-4 AM with excitation and emission filters of 475/28x and 512/23 m, respectively. The Texas Red channel was used to image Rhod-3 with excitation and emission filters of 575/25x and 620/30 m, respectively.

INCell Analyser Investigator software (Workstation 3.7.1, GE Healthcare) was used to analyse the images. Multi-Target Analysis (an automated image analysis algorithm) was used to define areas of interest (i.e. perimeters of individual nuclei and cells). Where cells grow close to one another delineation of cell perimeters can be unreliable and for this reason, a "collar" was used (i.e. the cytoplasm was defined by adding a 3 μm collar around the nucleus). However, LβT2 cells tend to grow in clusters, as shown in figure 2.2 and image analysis can fail to separate individual nuclei. Where individual nuclei are not accurately delineated, perimeters are drawn around large, elongated or irregularly shaped regions that represent multiple overlapping nuclei. In order to exclude these from the analysis additional filters were applied to exclude cells that have nuclear area >180 um^2 and a nuclear roundness index >1.25, as illustrated in figure 2.2.

2.9. Data presentation and routine statistical analysis

For most experiments, full concentration-response curves were constructed at multiple time points. Each concentration was applied to duplicated or triplicate wells, so data were pooled from all replicated wells. Each experiment was routinely repeated three to four times reporting means and SEMs for "n" separate experiments. For population

average responses, images were routinely collected for two to three fields of view per well. This provided thousands of individual cells for each treatment in each experiment and was used for frequency-distribution (FD) plots.

Whole cells or nuclear fluorophore intensities are reported in arbitrary fluorescence units (AFU). The INCell workstation software generates an Excel spreadsheet (.xls file) that contains fluorescence intensity measures for each of the regions segmented and for each fluorophore. The file shows the measures for each well, for each field of view and for each cell. Graphs were plotted using GraphPad Prism [version 7]. Two-way ANOVAs were used to examine if a specific drug is a significant source of variation. Then, separate One-way ANOVAs were applied to test for significant differences over time. Post-hoc tests were also used to test for differences between groups, as outlined in the figure legends.

For the NFAT1c-EFP translocation assay, the distribution of the fluorophore was described either as a nuclear: cytoplasmic ratio (n:c) or as nuclear fraction (NF). Nuclear: cytoplasmic ratios are often used in work of this nature [140, 302] but can yield misleading results when fluorophore expression levels are low. For this reason, NFAT1c-EFP NF values are used for the data described in chapters 4 and 5. For live cell imaging of Fluo-4 and Rhod-3, cell-cell variability in fluorophore uptake will influence the single cell fluorescence measures. For this reason, responses were normalised to the fluorescence (background subtracted) in each individual cell before stimulation [330].

Statistical analysis was performed using GraphPad Prism 7 (GraphPad Software Inc, CA), and analysis was by one or two-way ANOVA (using Bonferonni's post-hoc test).

P<0.05 was accepted as statistically significant. Curve fitting was done using non-linear regression.

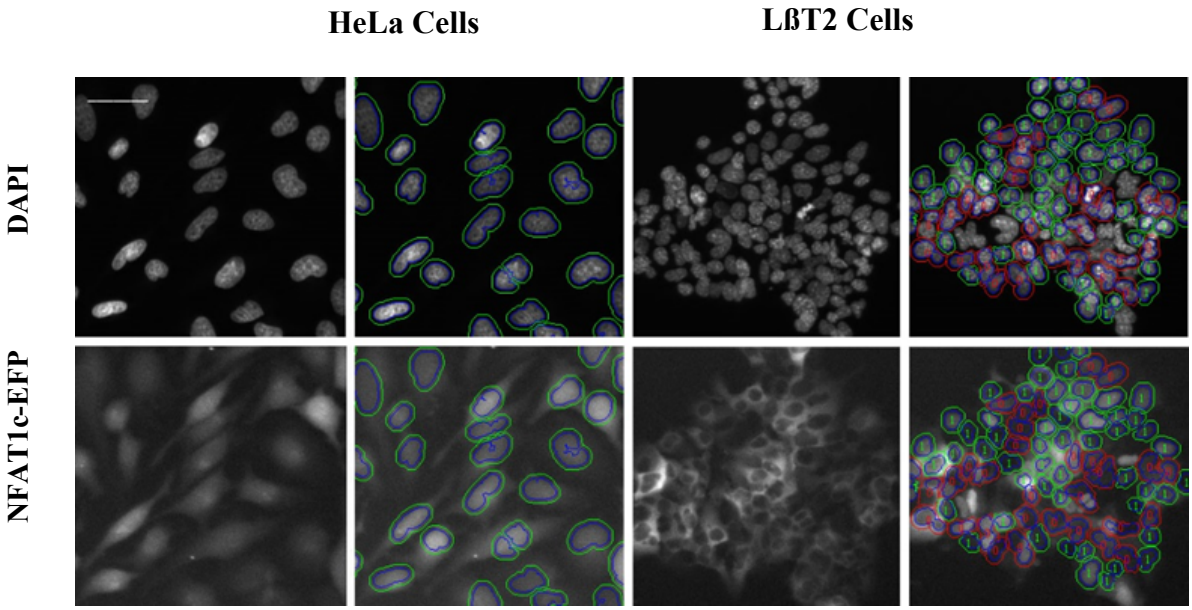

Figure 2 2. Semi-automated image acquisition and analysis for HeLa and LßT2 cells

Semi-automated software (Workstation 3.7.1) was used for cell segmentation as described under section 2.8. The cytoplasm perimeter (green) was defined by adding a 3 µm collar to the nucleus (blue). HeLa cells are well-separated making segmentation simple, but LβT2 cells grow in tightly packed groups. Thus, additional filters were applied. Cells with a nuclear area ≥180 um^2 and nuclear form factor ≥ 1.25 were excluded (for example, the cell marked 0 in red), whereas cells marked 1 in green were included. The images shown are from cropped image fields. Each field typically contains 100 to 600 cells for HeLa and MCF-7 cells and up to 1500 LβT2 cells. Scale bar 30µm.

2.10. Cell tracking

For live cell imaging experiments, the Excel file generated by the INCell Analyzer software shows single cell measures. This file is imported into MatLab R2017a (MathWorks) to track the response of individual cells over time. The tracking algorithm matches the geometric centre of the nuclei between sequential images in the time stack (i.e. tracking is based on the x-y position of the nuclei identified by the image analysis algorithms). In preliminary experiments the use of alternative cell measures (nuclear area and nuclear stain intensity) were also considered for cell tracking but these offered no improvement over simply tracking using cell position (Appendix, tables 1 and 2). Cells are paired with a probability which depends exponentially on their Euclidean distance from one-another, and Markov chain Monte Carlo analysis was used to find the most likely matching configuration for each pair of images [153]. Responses of tracked cells were plotted and inspected to remove those for which the tracking had failed. In addition, outliers (approximately 5% of cells) were removed from the NFAT1c-EFP experiments. These were cells in which time 0 NFAT1c-NF values were <0.4 or >0.55 (see Appendix, Figure 1).

For the dual pulse live cell imaging experiments, it was necessary to combine image stacks before tracking, as detailed in figure 2.3. The INCell analyser 2200 can add treatments automatically but cannot do the washing step between the two pulses. Thus, the plate was taken out of the stage before repeat stimulation to wash off a stimulus manually before returning it to the stage. Accordingly, two separate folders of digital images were generated, and these folders were combined using Notepad^{++} (Text editor, Microsoft) and MatLab R-2017a. Cell tracking was then precisely as described above for the single pulse experiments.

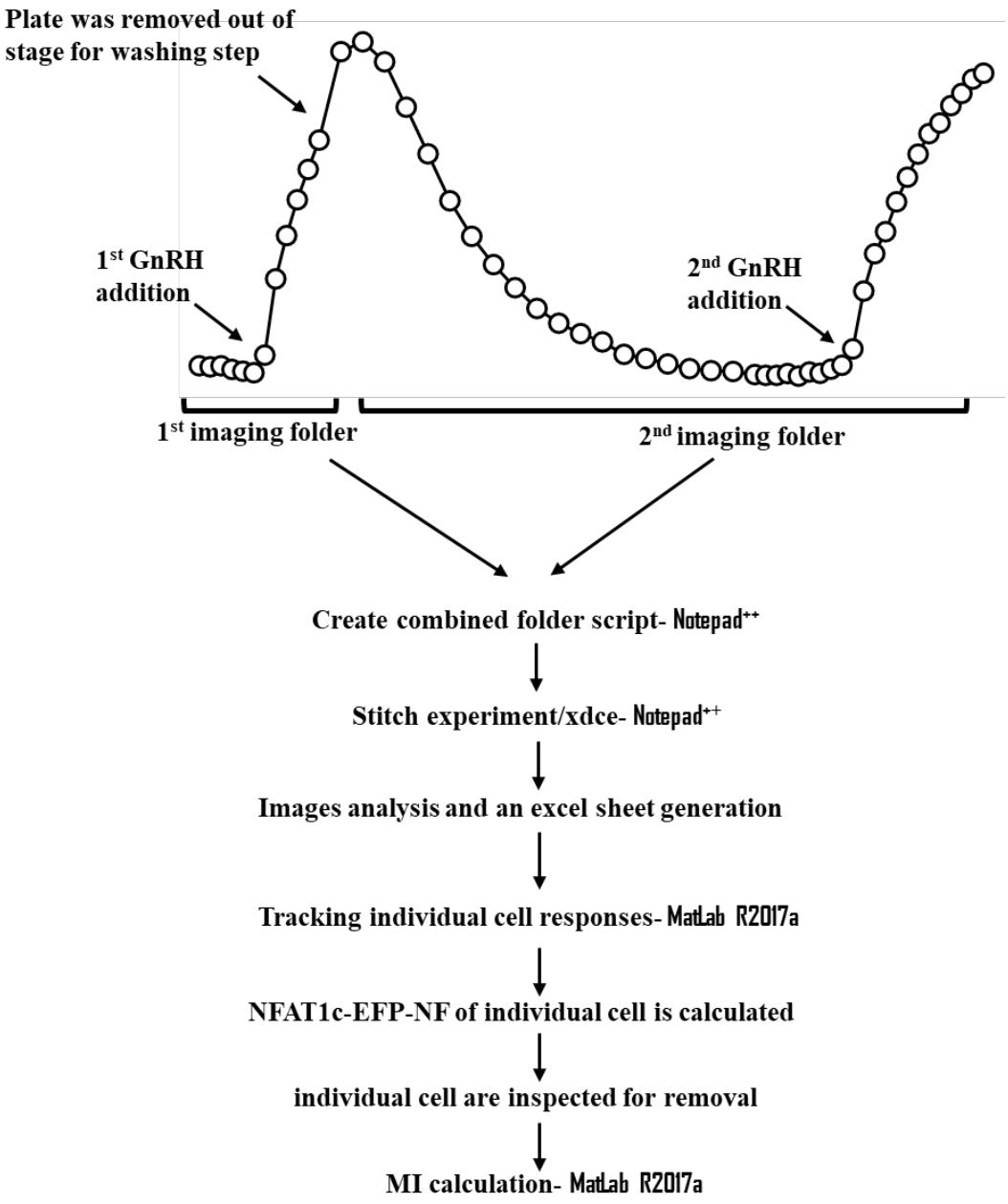

Figure 2.3. Steps required to calculate MI for the two-pulse LßT2 experiments

The INCell analyser 2200 can add treatments automatically but cannot do the washing step between the two pulses. Therefore, the plate was removed from the stage before repeat stimulation to wash off a stimulus manually. Accordingly, two separate folders of digital images were generated, and these folders were stitched together before MI calculation following the steps shown in the figure. The curve is representing the response of NFAT1c-EFP to GnRH.

2.11. Single cell analysis and calculation of mutual information

Mutual information (MI) was calculated between stimulus and the experimental measures using readouts as proxies for concentration levels based on fluorescence intensity. This was done at each time point and using single cell measures from complete concentration response curves. MI was estimated using the formula:

$$I(Z;S) = H(Z) - H(Z|S)$$

Where I: is the MI between a signal (S) and a response (Z), H(Z): is the unconditional entropy of the response, and H(Z|S): is the conditional entropy [298]. The Bayesian method which was proposed by Nemenman *et al*. [331] was used for entropy terms estimation, and for providing error bars of these estimations. The method is designed for discrete data, so that ERK and NFAT cell measures were discretized by binning them into 30 equally sized bins.

For joint pathways MI estimation, data were collected (as described earlier) for nuclear ppERK and NFAT1c-EFP-NF in the same cells, or for Egr1-driven zsGreen and NFAT-RE driven asRed, also in the same cells. This provides an opportunity to calculate the MI between stimulus and each individual experimental measure, as well as the joint MI between the stimulus and the paired outputs (ppERK and NFAT1c-EFP-NF or asRed and zsGreen) as previously shown, except that in this case, the response (Z) is interpreted as a two-dimensional vector.

Similarly, for trajectory calculation, we use an "N" dimensional vector, where N is the number of sampling points. Alternatively, we calculated the MI between stimulus and entire trajectory by compressing single cell response trajectories (N time points)

to two dimensions using multidimensional scaling (MDS) [292]. We do that to assess additional information gained by consideration of the response trajectories.

For the two pulses experiments, the maximum value of NFAT1c-EFP-NF during each pulse was used to measure the responses (Z1 and Z2) to the first and second pulse. Information I(Z1; GnRH) was calculated, and the additional information from the response to the second pulse was calculated using the following formula:

$$I(Z2;S|Z1) = I(Z1;GnRH)2\ I(Z1;Z2) + I(Z1;Z2|GnRH),$$

Here the I(Z1; Z2) is MI between the individual cell responses in pulses 1 and 2. The I(Z1;Z2|GnRH) is the MI between the individual cell responses in pulses 1 and 2 conditioned on the concentration of GnRH.

Chapter 3- Concentration dependencies and kinetics of ERK and NFAT1c-EFP responses

3.1. Background

Gonadotrophin-releasing hormone mediates central control of reproduction. It does so, by acting through GPCRs on the anterior pituitary gland to stimulate the synthesis and secretion of gonadotrophins [180]. Type I mammalian GnRHRs are different from other GPCRs in that the receptors signal in an arrestin-independent manner and do not undergo rapid desensitisation [133, 302]. Binding of GnRH to its receptor causes a Gq-mediated activation of PLC with consequent elevation of cytoplasmic Ca^{2+} concentration and activation of PKC [24]. This Ca^{2+} causes a rapid increase in the exocytotic release of LH and FSH but also causes a calmodulin and calcineurin-mediated activation of the Ca^{2+}-dependent transcription factor NFAT [140, 163].

GnRH also activates the Raf/MEK/ERK cascade [157, 165]. This is largely PKC-mediated, and ERK has pronounced effects on gene expression, that are in part Egr1-mediated [226]. Accordingly, nuclear translocation of an NFAT1c-EFP reporter or NFAT-RE-driven gene expression can be used as readouts for activation of the GnRHR/Gq/PLC/Ca^{2+}/CaM/Cn/NFAT pathway, just as activating phosphorylation of ERK or Egr1-driven gene expression can be used as readouts for activation of the GnRHR/Gq/PLC/PKC/ERK pathway.

The initial aim of the work described in this chapter was to determine the effects of GnRH on the two major signalling pathways outlined above, and this was achieved by automated fluorescence microscopy with an INCell 1000 or an INCell 2200. The GnRH effect on the downstream readouts for activation of ERK and NFAT was also explored. Given the possibility of cell context-dependent signalling [332] the work was done in three cellular models (HeLa, LβT2, and MCF-7 cells). Additional aim was to quantify ERK and NFAT1c-EFP activities in response to EGF and the PKC

activator (PDBu). This is because both EGFR and PKC were reported to be implicated in GnRH signalling (see Chapter 1).

3.2. Materials and methods

Distinct stimuli were used to monitor their effects on ERK activation and to define dose-dependencies and response kinetics in different cell lines. This was done by indirect immunofluorescence, using primary antibodies directed to total ERK or ppERK and fluorophore-labelled secondary antibodies. Also, the nuclear translocation of NFAT1c-EFP was monitored by transducing cells with Ad NFAT1c-EFP. Images were obtained by automated fluorescence microscopy using a 10x objective. For all experiments, multiple fields were collected for each well, and two to four wells were run for each treatment, thus, the images show only a small proportion of the cells analysed (approximately 0.3%).

3.3. Results

3.3.1. GnRH Effects on ERK signalling in Ad mGnRHR transduced HeLa cells.

Figure 3.1 shows representative images for DAPI (nuclear stain, blue channel), ppERK (active ERK, green channel) and total ERK (red channel) in control cells and in cells stimulated for 5 min with 10^{-7} M GnRH. As shown in figure 3.1A, GnRH caused a pronounced increase in ppERK stain intensity, particularly in the cell nucleus, but did not cause any obvious change in total ERK stain intensity. Analysing the images revealed that GnRH caused a clear concentration-dependent increase in

nuclear ppERK (ppERK-n) that was most pronounced at 5 min and reduced thereafter (Figure 3.1B). The ppERK-n was 295.01 ± 19.13 AFU in unstimulated cells and went up significantly to 459.01 ± 18.10 AFU with 10^{-6} M GnRH at 5 min.

To better illustrate response kinetics, these data were re-plotted against time (Figure 3.1D) and this revealed that GnRH effects were maximal at 5 min and had reduced to control (pre-stimulation) values by 60 min. Two-way ANOVAs of the data in figure 3.1B revealed that GnRH concentration and time are both significant sources of variation ($P<0.05$, $F(21,42) = 14.29$). Post-hoc tests comparing responses with GnRH to control measures with no GnRH revealed statistically significant responses ($P<0.05$) with 10^{-9}-10^{-6} M GnRH at 5 and 15 min and with 10^{-8}-10^{-6} M GnRH at 30 min. However, two-way ANOVAs of the total ERK data in figure 3.1C revealed that neither GnRH concentration nor time is significant sources of variation ($P>0.05$). These data reveal that GnRH increases ppERK measures by increasing the proportion of ERK that is dual phosphorylated, rather than by increasing the total amount of ERK present.

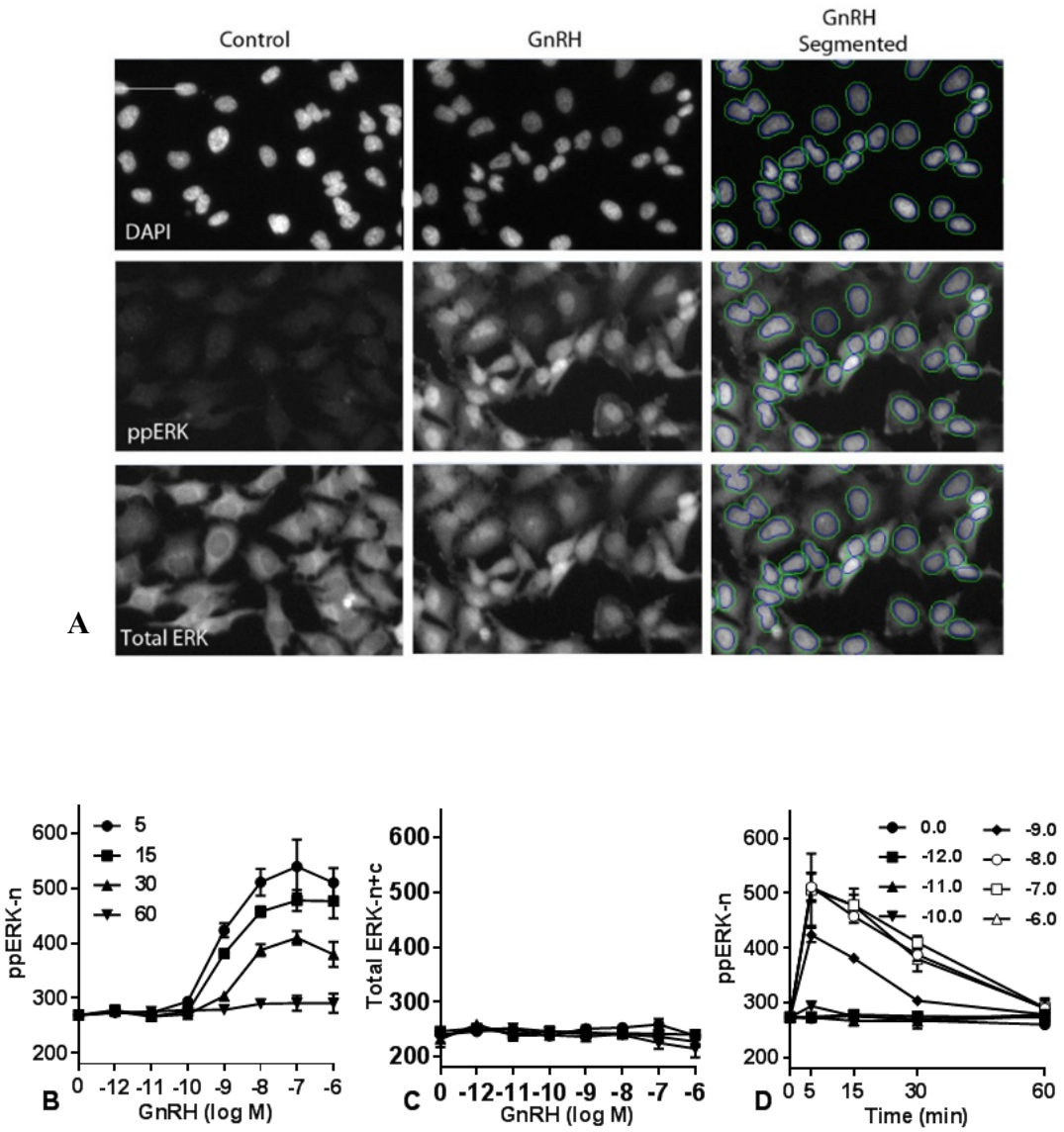

Figure 3.1. GnRH Effects on ERK signalling in Ad mGnRHR transduced HeLa cells.

The cells were plated as described in Chapter 2. They were then stimulated for 5, 15, 30 or 60 min with 0 or 10^{-12}–10^{-6} M GnRH before being fixed and stained for ppERK, total ERK and with DAPI (nuclei). Digital images were acquired using an INCell 1000. Panel A shows representative images of DAPI, ppERK and total ERK. The right-hand images show an example of the automated image segmentation used to define perimeters of the nuclei and cells (perimeters superimposed over GnRH treated cells) using automated image analysis algorithms. Scale bar, 30 μm. Image analysis algorithms were used to determine fluorophore intensity in areas of interest (nuclei and cytoplasm). Panel B shows ppERK-n in AFU. Panel C shows total ERK-n+c in AFU. Panel D shows the same data as B but re-plotted against time for each GnRH concentration (legend shows log M GnRH concentration). The figures show means ± SEMs for 3 replicate experiments (n=3) each of which was from an experiment with triplicate wells for each condition and three fields of view/well.

The image analysis for the data in figure 3.1 provides measures of all three fluorophores in the nucleus and the cytoplasm. This could be expressed and presented in several different ways. For figure 3.2A ppERK-n was plotted, but the analysis also yields measures of cytoplasmic ppERK and whole cell (nuclear + cytoplasmic) ppERK, and these are compared in figure 3.2. For each measure, GnRH caused a clear concentration and time-dependent increase in ppERK although stain intensities were generally higher in the nucleus than in the cytoplasm (compare Figures 3.2B and 3.2B). However, the responses were qualitatively similar, and the results of the statistical analysis were also similar. Two-way ANOVAs of the data in panel B revealed that GnRH concentration and time are both significant sources of variation ($P<0.05$, F (21,42) = 11.52). Post-hoc tests comparing responses with GnRH to control measures with no GnRH revealed statistically significant responses ($P<0.05$) with 10^{-9}-10^{-6} M GnRH at 5 and 15 min and with 10^{-8}–10^{-6} M GnRH at 30 min. The log EC_{50} (M) values were -9.60 ± 0.32, -9.06 ± 0.66, and -9.12 ± 0.92 at 5, 15 and 30 min respectively.

Two-way ANOVAs of the data in figure 3.2C revealed that GnRH concentration and time are both significant sources of variation ($P<0.05$, F (21,42) = 13.40). Post-hoc tests comparing responses with GnRH to control measures with no GnRH revealed statistically significant responses ($P<0.05$) with 10^{-9}–10^{-6} M GnRH at 5 and 15 min and with 10^{-8} -10^{-6} M GnRH at 30 min. This suggests that the effects of GnRH do not appreciably differ between these cellular compartments. For subsequent experiments ppERK-n was used as the main experimental end-point, reasoning that this would be sensitive to both activation and nuclear translocation of ppERK and may be more reliable as nuclear perimeters are readily defined using the DAPI stain.

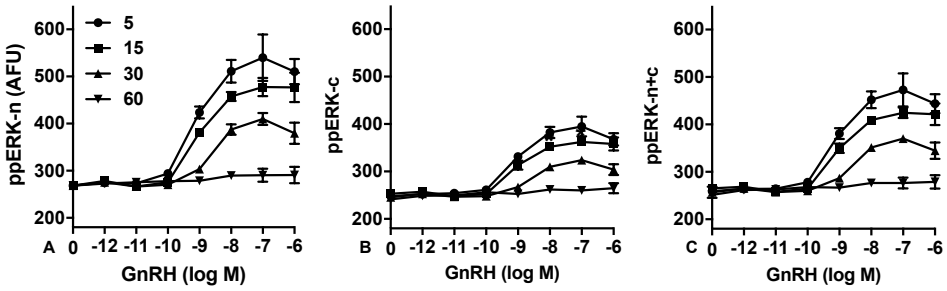

Figure 3.2. Comparison of 3 different measures for the effect of GnRH on ppERK in Ad mGnRHR transduced Hela cells.

The cells were cultured and processed as described above. Panel A shows ppERK-n stain intensity in AFU and is reproduced from figure 3.1 for comparison. Panel B and C show population averaged ppERK-c and ppERK-n+c in AFU respectively. The results show means ± SEMs, n=3, each with triplicate wells and three fields of view/well.

3.3.2. PDBu effects on ERK signalling in Ad mGnRHR transduced Hela cells.

Phorbol 12,13-dibutyrate (PDBu) activates conventional PKC (cPKC) by mimicking the actions of DAG. PKC regulates different signal transduction pathways including the ERK pathway [333]. Images in figure 3.3A revealed that PDBu caused a pronounced increase in ppERK stain intensity in the cell nucleus and had no effect in total ERK stain intensity.

PDBu caused a clear concentration-dependent increase in ppERK-n levels. In unstimulated cells, the ppERK-n levels were 264.28 ± 11.91 AFU and went up remarkably to around 499.04 ± 2.41 AFU in cells stimulated with 10^{-6} M PDBu. Two-way ANOVAs of the data in panel B revealed that PDBu concentration and time are both significant sources of variation ($P<0.05$, F (21,42) = 21.02). Post-hoc tests

comparing responses with PDBu to control measures revealed statistically significant responses ($P<0.05$) with 10^{-7}-10^{-6} M PDBu at 5, 15, 30 min and ($P<0.05$) with 10^{-7}-10^{-6} M PDBu at 60 min. The data were re-plotted against time (Figure 6C). This revealed that PDBu effects were maximum at 5 min and reduced to control values by 60 min. The log EC_{50} (M) values were -6.85 ± 0.25, -7.06 ± 0.11, -7.24 ± 0.25, and -8.10 ± 0.17 at 5, 15, 30 and 60 min respectively.

Total ERK levels were not changed by PDBu as shown in figure 3.3C, demonstrating that PDBu (like GnRH) increases ppERK measures by increasing the proportion of ERK that is dual phosphorylated, instead of increasing the total amount of ERK present. Two-way ANOVAs of the total ERK data revealed that neither PDBu concentration nor time is significant sources of variation ($P>0.05$).

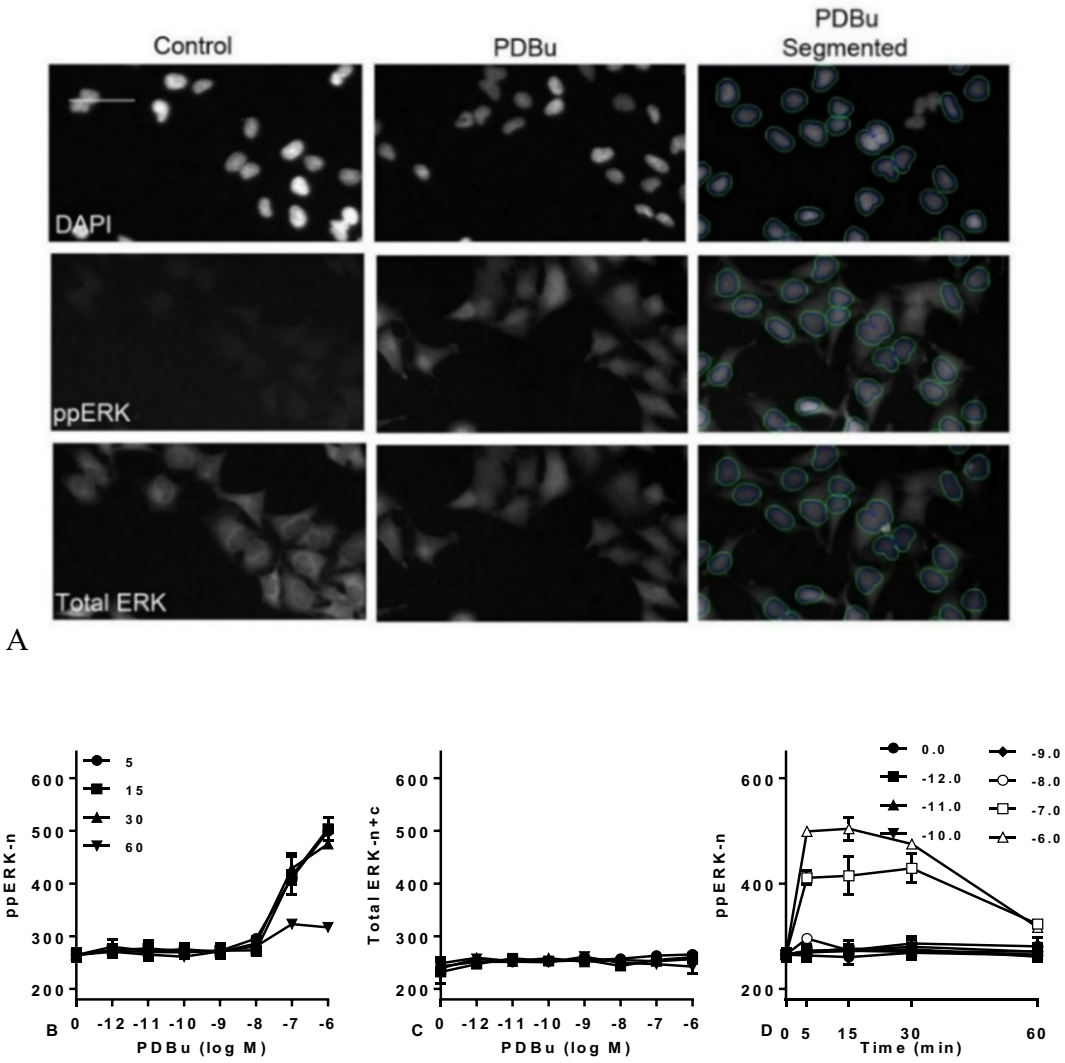

Figure 3.3. PDBU effects on ERK signalling in Ad mGnRHR transduced HeLa cells.

Cells were cultured and treated as described in Chapter 2. Panel A shows representative images of DAPI, ppERK and total ERK stained cells cultured under control condition or stimulated 5 min with 10^{-7} M PDBu. The right-hand images show an example of the automated image segmentation used to define perimeters of the nuclei and cells (perimeters superimposed over PDBu treated cells). Scale bar, 30 μm. Panels B and C show population averaged ppERK-n and total ERK-n+c in AFU. Panel D shows the same data as A but re-plotted against time (legend shows log M PDBu concentration). The figures show means ± SEMs, n=3 each with triplicate wells for each condition and three fields of view/well.

3.3.3. EGF effects on ERK signalling in Ad mGnRHR transduced HeLa cells.

Effects of EGF on ERK were also monitored in HeLa cells. Images in figure 3.4A showed that EGF triggered a marked increase in ppERK stain intensity in the cell nucleus but did not cause any obvious change in total ERK stain intensity. EGF caused a clear concentration-dependent increase in ppERK-n, peaking at 5 min, and reducing subsequently (Figure 3.4B). In control cells, the ppERK levels were 272.81 ± 7.02 AFU, and this increased to around 557.72 ± 67.81 AFU with 10^{-8} M EGF.

Two-way ANOVAs of the data in panel B revealed that EGF concentration and time are both significant sources of variation ($P<0.05$, F (21,42) = 17.36). Post-hoc tests comparing responses with EGF to control measures revealed statistically significant responses ($P<0.05$) with 10^{-10}–10^{-7} M EGF at 5 and 15 min ($P<0.05$) and with 10^{-10} M EGF at 30 min. The EC_{50} values were -9.42 ± 1.03, -9.65 ± 1.21, -10.51 ± 3.01 and -7.88 ± 1.21 at 5, 15, 30 and 60 min respectively. These data were re-plotted against time for better illustration of the response kinetics (Figure 3.4D) and demonstrated that EGF effects were maximal at 5 min and then declined over the time to near the basal levels (by 60 min).

Two-way ANOVAs of the total ERK data in (Figure 3.4C) revealed that neither EGF concentration nor time are significant sources of variation ($P>0.05$), indicating that EGF increased the proportion of ERK that is dual phosphorylated, not the total amount of ERK present

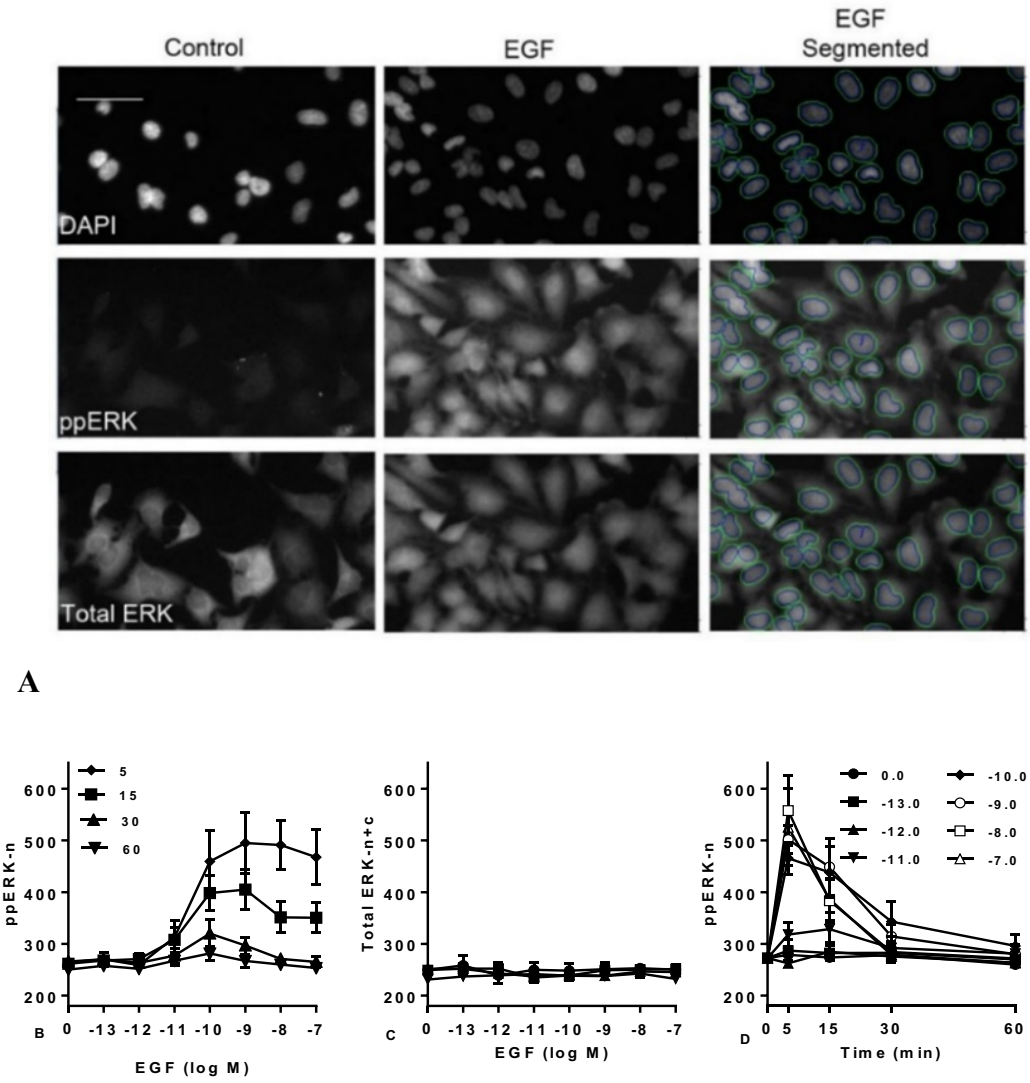

Figure 3.4. EGF effects on ERK signalling in in Ad mGnRHR transduced HeLa cells.

Cells were cultured as described in Chapter 2. They were then stimulated with the indicated times and concentrations of EGF. Cells were fixed and stained for ppERK, total ERK, and nuclei. Representative images of DAPI, ppERK and total ERK stained cells cultured under control condition or stimulated with 10^{-7} M EGF for 5 min are shown in A. The right-hand images show an example of the automated image segmentation used to define perimeters of the nuclei and cells. Scale bar, 30 μm. Panels B and C show population averaged ppERK-n and total ERK-n+c in AFU. Panel D shows the same data as A but re-plotted against time. The figures show means ± SEMs, n=3 separate experiments each of which was performed in triplicate wells for each condition and with three fields of view/well.

3.3.4. GnRH Effects on ppERK and NFAT1c-EFP translocation in Ad mGnRHR transduced HeLa cells.

The nuclear translocation of NFAT1c-EFP used here as a cellular readout for activation of the Ca^{2+}/CaM/Cn pathway. HeLa cells were cultured and treated as described in Chapter 2. Nuclear translocation of the NFAT1c-EFP reporter was followed by calculating the ratio of the nucleus: cytoplasm (NFAT1c-EFP-n:c). Representative images for DAPI (blue channel), NFAT1c-EFP (green channel) and ppERK (red channel) in control cells and cells stimulated for 60 min with 10^{-7} M GnRH are shown in Figure 3.5A. The images demonstrate that NFAT1c-EFP was mostly cytoplasmic in unstimulated cells and translocated to the nucleus in GnRH stimulated cells.

The data in Figure 3.5 demonstrates that GnRH caused a clear concentration-dependent increase in ppERK-n stain intensity. In untreated cells, the ppERK-n was approximately 295.12 ± 19.13 AFU and increased to a maximum of 458.85 ± 19.10 AFU at 5 min in cells stimulated with 10^{-6} M GnRH. Two-way ANOVAs of ppERK data (Figure 3.5B) revealed that GnRH concentration and time are both significant sources of variation ($P<0.05$, F (14,28) =6.21). Post-hoc tests comparing responses with GnRH to control measures with no GnRH revealed statistically significant responses ($P<0.05$) with 10^{-9}–10^{-6} M GnRH at 5, 20 and 60 min. Re-plotting data against time (Figure 3.5C) showed that GnRH effects on ppERK-n levels were maximal at 5 min then gradually declined over the time. The log EC_{50} values were -9.60 ± 0.33, -9 ± 0.71 and -8.10 ± 0.17 at 5, 20 and 60 min respectively.

The NFAT1c-EFP translocation responses were measured in the same cells and these are shown in figure 3.5D and E, where GnRH caused a clear concentration-dependent

increase in NFAT1c-EFP translocation. The NFAT1c-EFP-n:c was 1.40 ± 0.13 under control condition and was increased to a maximum of 1.77 ± 0.24 by GnRH, with a log (EC_{50}, M) values of -10.31± 1.12 at 5 min, -8.94 ± 0.41 at 20 min, and -9.35 ± 0.45 at 60 min. Two-way ANOVAs revealed that GnRH concentration is a significant source of variation ($P<0.05$), whereas time is not ($P>0.05$, F (14, 28) =1.65). Post-hoc tests comparing responses with GnRH to control measures with no GnRH revealed statistically significant responses ($P<0.05$) with 10^{-8} –10^{-6} M GnRH at 5 and 20 min and with 10^{-8} –10^{-7} M GnRH at 60 min. To better illustrate response kinetics, these data were re-plotted against time (Figure 3.5E). GnRH effects were seen at 5 min and increased gradually over 20 min, then remained constant until 60 min (end-point of stimulation).

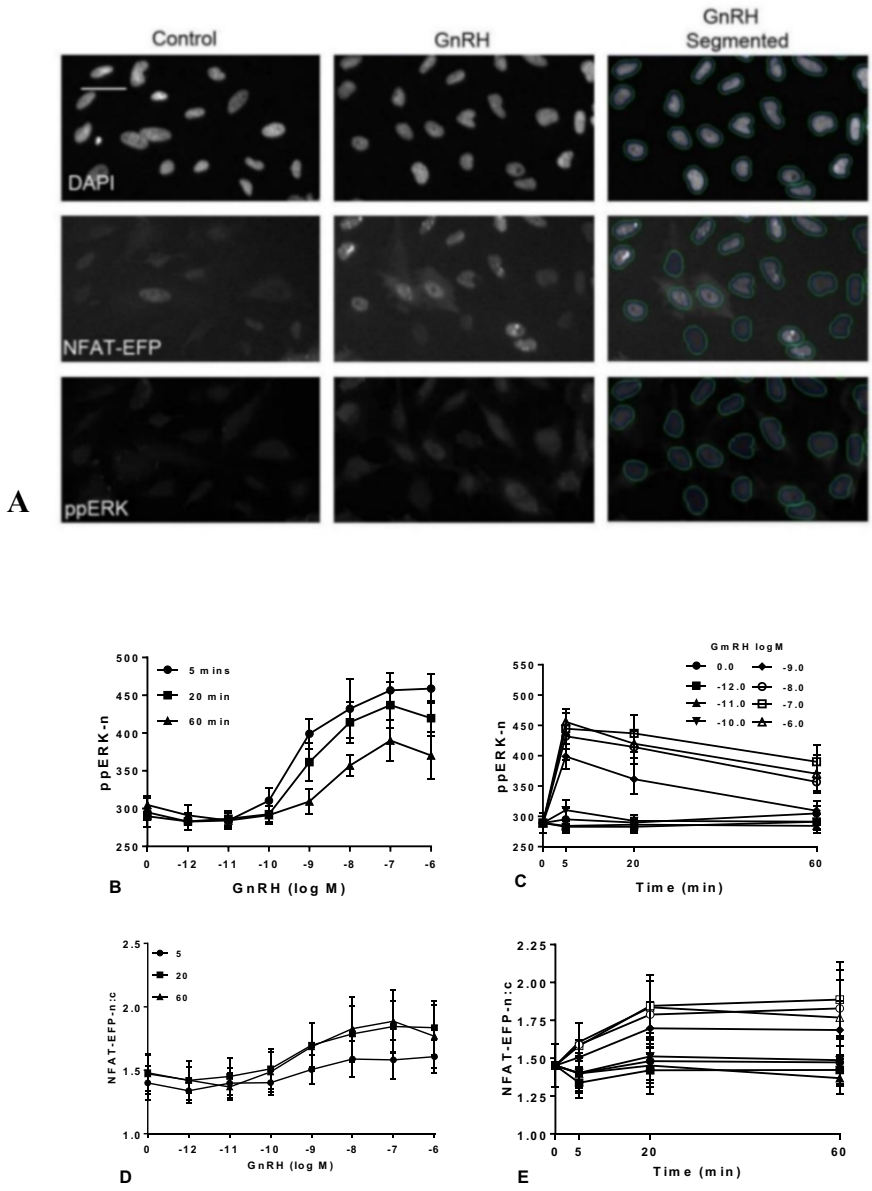

Figure 3.5. GnRH effects of NFAT1c-EFP translocation in Ad mGnRHR transduced HeLa cells.

Cells were cultured and treated as described in Chapter 2. Representative images of DAPI, ppERK and NFAT1c-EFP cultured under control condition or stimulated with 10^{-7} M GnRH for 60 min are shown in A. The right-hand images show an example of the automated image segmentation used to define perimeters of the nuclei and cells. Scale bar, 30 μm. Panels B and D show population average responses of ppERK-n in AFU and NFAT1c-EFP-n:c. Panels C and E the same data as B and D but re-plotted against time. The figures show means ±SEMs, n=3, with quadruplicate wells for each condition and three fields of view/well.

3.3.5. Quantifying GnRH effects on Egr1 driven zsGreen and NFAT-RE driven asRed expression in Ad mGnRHR transduced HeLa cells.

Figure 3.6A shows representative images of DAPI, Egr1-zsGreen (green channel) and NFAT-RE- asRed (red channel) in control cells and cells stimulated for 8 hr with 10^{-7} M GnRH. GnRH increased the expression of both fluorophores (Egr1-zsGreen and NFAT-RE-asRed). GnRH caused a clear concentration-dependent increase in the Egr1-zsGreen-n+c that was 213.31 ± 0.31 AFU in control cells and went up to approximately 260.25 ± 17.88 AFU after being stimulated by 10^{-7} M GnRH. Two-way ANOVAs of the data in figure 3.6B revealed that GnRH concentration but not time is both significant sources of variation ($P<0.05$, F (14,42) =5.00). Post-hoc tests comparing responses with GnRH to control measures with no GnRH revealed statistically significant responses ($P<0.05$) with 10^{-8} –10^{-6}M GnRH. These data were re-plotted against time showing that GnRH effects were maximal at 6 and 8 hr (Figure 3.6C) and the log EC_{50} values were -8.16 ± 0.04 at 6 hr and -8.01 ± 0.12 at 8 hr.

For NFAT-RE-asRed, as shown in figure 3.6D, GnRH caused a clear concentration-dependent increase in the NFAT-RE-asRed-n+c. The expression of NFAT-RE-asRed-n+c was around 199.81 ± 4.11 AFU in control cells and moved up during 8 hr to 315.02 ± 24.50 with 10^{-7} M GnRH. Re-plotting against time (Figure 3.6E), the NFAT-RE asRed-n+c levels were observed at 4 hr and peaked at 8 hr (end point of stimulation). Two-way ANOVAs showed that GnRH concentration (but not time) is a significant source of variation ($P<0.05$, F (14,24) =3.64). Post-hoc tests comparing responses with GnRH to control measures with no GnRH revealed statistically significant responses ($P<0.01$) with 10^{-8}–10^{-6} M GnRH at 4, 6 and 8 hr. Studies in dose-response showed that the log EC_{50} (M) values were similar during the examined

period. The log EC_{50} values were -8.61 ± 0.31, -7.30 ± 0.41, and -8.72 ± 0.56 at 4, 6, and 8 hr respectively.

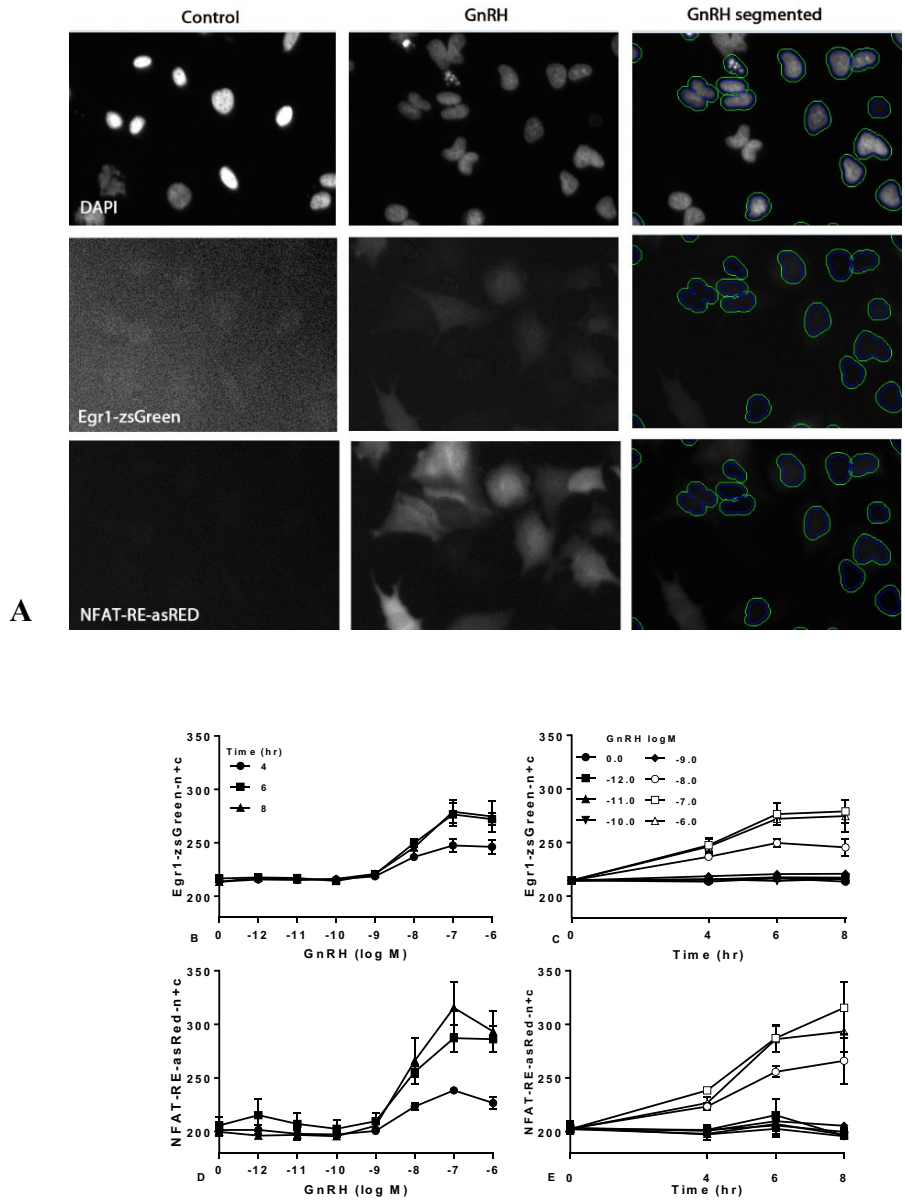

Figure 3.6. Quantifying GnRH effects on Egr1 driven zsGreen and NFAT-RE driven asRed expression in Ad mGnRHR transduced HeLa cells.

Cells were transduced with Ad Egr1-zsGreen, Ad NFAT-RE-asRed, and Ad mGnRHR, prior to serum starvation overnight. They were then stimulated for 4, 6 or 8 hr with 0 or 10^{-12} -10^{-6} M GnRH. They were then fixed and stained with DAPI (nuclei). Digital images and analysis were used as described in Chapter 2. Representative images of DAPI, Egr1-zsGreen and NFAT-RE-asRed in cells cultured under control condition or stimulated 8 hr with 10^{-7} M GnRH are shown in A. The right-hand images show an example of the automated image segmentation used to define perimeters of the nuclei and cells. Scale bar 3 μm. Panels B and D show population averaged responses of Egr1-zsGreen-n+c and NFAT-RE-asRed-n+c in AFU. These data are re-plotted against time in panel C and E. The figures show means ± SEMs, n=3, each with quadruplicate wells for each condition and three fields of view/well.

3.3.6. GnRH effects on NFAT1c-EFP and ERK activation in LβT2 cells.

LβT2 cells express endogenous GnRHRs, so they were transduced with Ad NFAT1c-EFP alone then treated as described in Chapter 2. The NFAT1c-EFP translocation and ppERK levels were monitored in the same cells. Representative images for DAPI, NFAT1c-EFP, and ppERK in control cells and cells stimulated for 60 min with 10^{-7} M GnRH are shown in figure 3.7A. These revealed that NFAT1c-EFP was largely cytoplasmic in unstimulated cells and translocated to the nucleus in response to GnRH.

GnRH caused a clear concentration-dependent increase in NFAT1c-EFP translocation. The NFAT1c-EFP-n:c was approximately 0.73 ± 0.12 and increased by 10^{-7} M GnRH to a maximum of 3.02 ± 0.62 at 60 min. For a better illustration of the kinetics, data were re-plotted against time (Figure 3.7C), and these show that GnRH effects on NFAT1c-EFP location were observed at 20 min and peaked at 60 min. Two-way ANOVAs of the data in panel B revealed that GnRH concentration is a significant source of variation ($P<0.05$, F (7,14) =15.82). Post-hoc tests comparing responses with GnRH to control measures with no GnRH revealed statistically significant responses ($P<0.05$) with 10^{-9} –10^{-6} M GnRH at 5 and 20 min and with 10^{-8}–10^{-6} M GnRH at 60 min. The log EC_{50} (M) values were similar with -10.01 ± 0.50 at 5 min, and -9.41 ± 0.15 at 20 and -9.10 ± 0.50 at 60 min.

The ppERK was measured in the same cells and these shown in figure 3.7D. GnRH caused a clear concentration-dependent increase in ppERK-n stain intensity in stimulated cells (176.15 ± 1.72 AFU for control, 228.10 ± 12.02 AFU for 10^{-6} M GnRH). For better illustration, the response kinetics of these data were re-plotted against time (Figure 3.7E). These indicated that GnRH effects on ppERK-n levels

were rapid within 5 min and were maintained at similar levels for 60 min. Two-way ANOVAs of ppERK data in figure 3.7D revealed that GnRH concentration and time are both significant sources of variation ($P<0.05$, F (14,28) =2.54). Post-hoc tests comparing responses with GnRH to control measures with no GnRH revealed statistically significant responses ($P<0.05$) with 10^{-9}-10^{-6} M GnRH at 5 min and with 10^{-8}– 10^{-6} M GnRH at 20 and 60 min. The log EC_{50} (M) values were similar with -8.45 ± 0.16 at 5, -8.16 ± 0.04 at 20 min, and -7.34 ± 0.56 at 60 min.

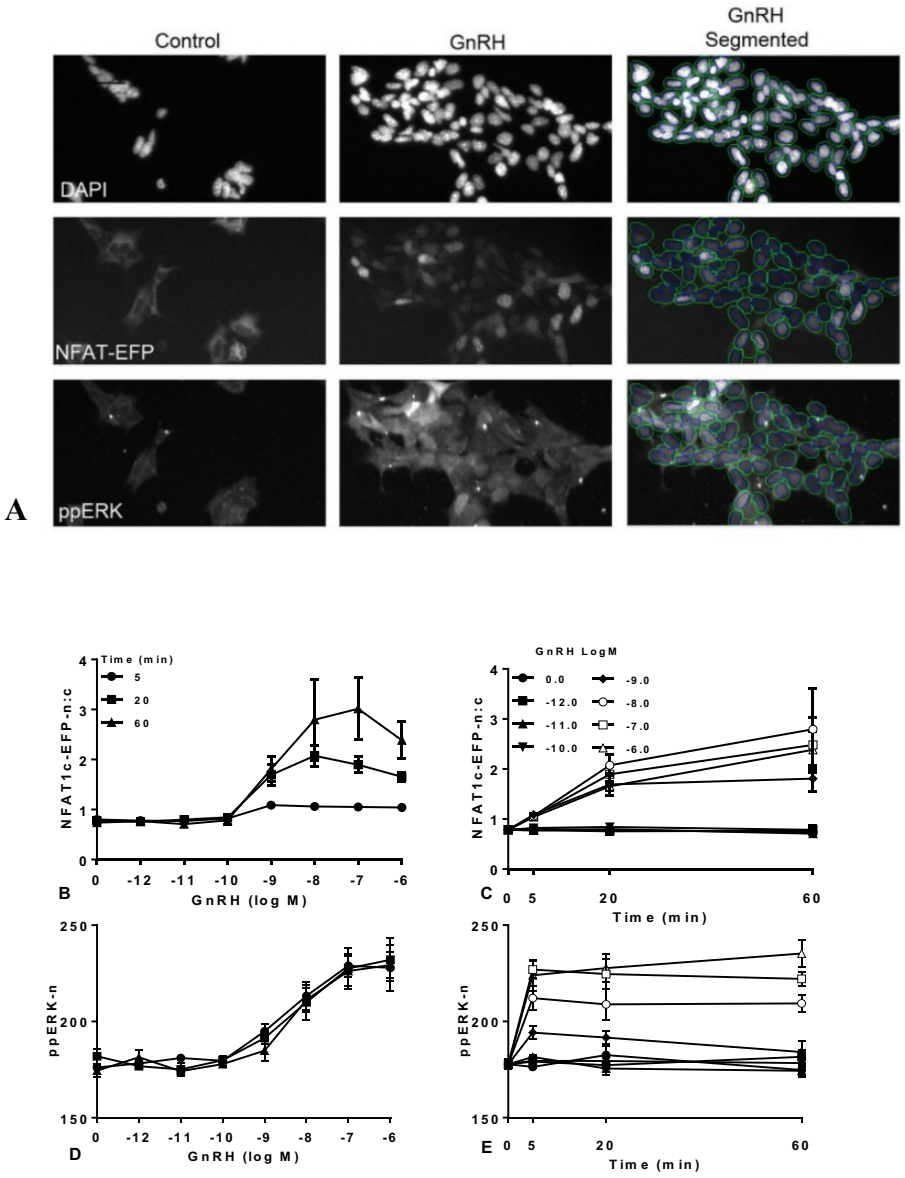

Figure 3.7. Quantifying GnRH effects on NFAT1c-EFP location and the activation of NFAT and ppERK levels in LβT2 cells.

Cells were treated for the indicated times and with the indicated concentrations of GnRH. They were then fixed and stained for ppERK and nuclei. Digital images and analysis were as described in Chapter 2. Representative image of DAPI, NFAT1c-EFP and ppERK in cells cultured under control condition or stimulated 60 min with 10^{-7} M GnRH are shown in A. Scale bar, 3 μm. Panel B shows NFAT1c-EFP-n:c. panel D shows ppERK-n stain intensity in AFU. Panels C and E represent the same data as B and D respectively but re-plotted against time. The figures show means ±SEMs, n=3-4, each with quadruplicate wells for each condition and three fields of view/well.

3.3.7. GnRH effects on Egr1 driven zsGreen and NFAT-RE driven asRed expression in LβT2 cells.

LβT2 cells were transduced with Ad Egr1-zsGreen, and Ad NFAT-RE-asRed then treated as described in Chapter 2. The representative images in Figure 3.8A illustrates DAPI, Egr1-driven zsGreen, and NFAT-RE-driven asRed expression in control cells and cells stimulated for 8hr with 10^{-7} M GnRH. The stimulus led to an increase in Egr1-driven zsGreen expression in the nucleus and cytoplasm (Egr1-zsGreen-n+c) and NFAT-RE-driven asRED expression in the nucleus and cytoplasm (NFAT-RE-asRed-n+c.

As shown in figure 3.8A, GnRH caused a clear concentration-dependent increase in Egr1-zsGreen-n+c. This rose from 216.64 ± 0.80 AFU to 1049.35 ± 110.41 AFU after being stimulated by GnRH, and the effect was maximal at 8 hr with 10^{-6} M GnRH. The log EC_{50} (M) values were similar at all the indicated times (-7.72). These data were re-plotted against time (Figure 3.8C), revealing that GnRH effects were seen at 4 hr and were maximal at 8 hr. Two-way ANOVAs of the data in figure 3.8B showed that GnRH concentration and time are both significant sources of variation ($P<0.05$, F (14,28) =6.72). Post-hoc tests comparing responses with GnRH to control measures with no GnRH revealed statistically significant responses ($P<0.05$) with 10^{-8} –10^{-6} M GnRH.

Effects of GnRH on NFAT-RE-driven asRed expression are shown in figure 3.8D. GnRH caused a clear concentration-dependent increase in NFAT-RE-asRed-n+c, which was most pronounced at 8 hr (from 140.71 ± 0.61 to 153.10 ± 4.10), with a log EC_{50} (M) value of -8.56 ± 0.32. To better illustrate response kinetics, data were re-plotted against time, and this shows that GnRH effects on NFAT-RE-asRed-n+c levels

were like its effects on Egr1-zsGreen. The effect was seen at 4 hr and continued to rise until 8 hr, where the experiment was ended. However, the response on the former was lower than the latter (compare Figure 3.8C and Figure 3.8E). Two-way ANOVAs of NFAT-RE-asRed-n+c revealed that GnRH concentration and time are both significant sources of variation ($P<0.05$, F (14,28) =2.76). Post-hoc tests comparing responses with GnRH to control measures with no GnRH showed statistically significant responses ($P<0.05$) with 10^{-8} –10^{-6} M GnRH at 4 and 6 hr, and with 10^{-8} – 10^{-6} M GnRH at 8 hr.

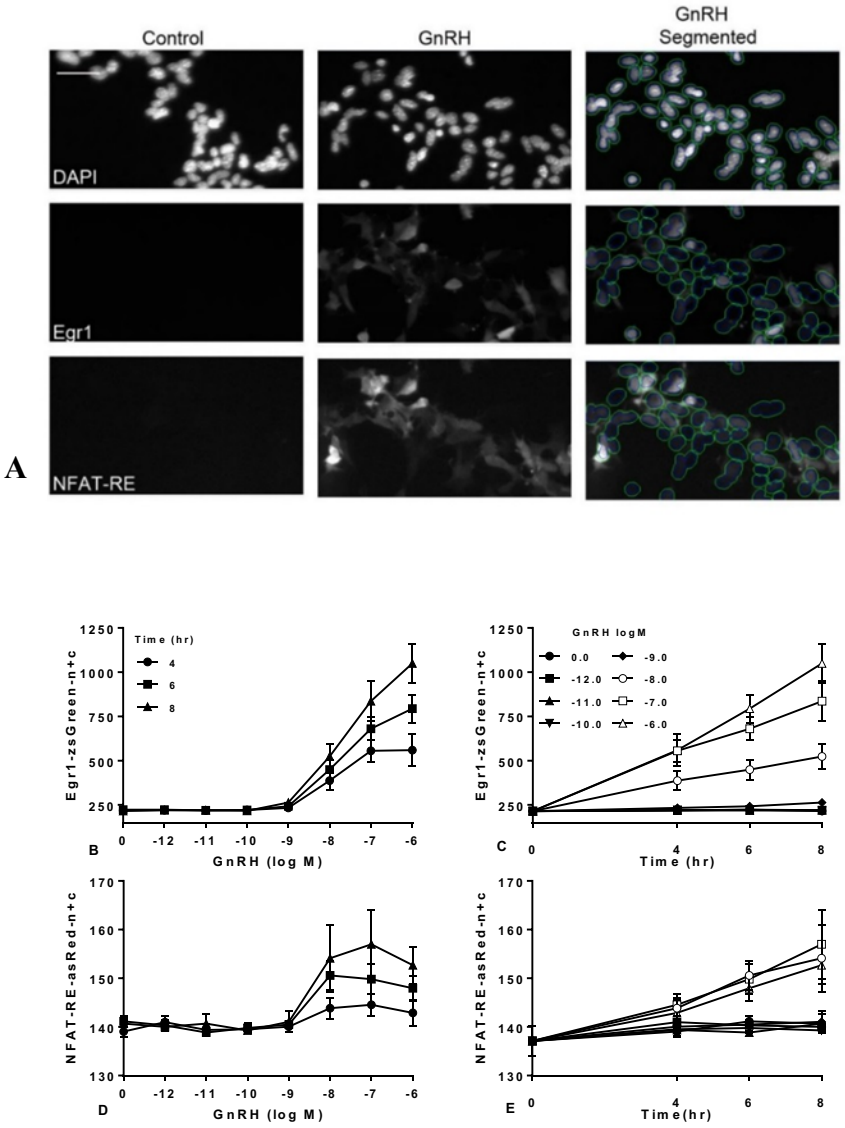

Figure 3.8. GnRH effects on Egr1 driven zsGreen and NFAT-RE driven asRed expression in LβT2 cells.

Cells were cultured and treated as described in Chapter 2. Representative images for DAPI, Egr1-zsGreen, and NFAT-RE-asRed for cells cultured under control condition or stimulated 8 hr with 10^{-7} M GnRH are shown in A. The right-hand images show an example of the automated image segmentation used to define perimeters of the nuclei and cells. Scale bar, 3 μm. Panels B and D show population average responses of Egr1-zsGreen-n+c and NFAT-RE-asRed-n+c in AFU. Panels C and E show the same data as B and D respectively but re-plotted against time. The figures show means ± SEMs, n=3-4, each with quadruplicate wells for each condition and three fields of view/well.

3.3.8. GnRH effects on NFAT and ERK activation in Ad mGnRHR transduced MCF-7 cells.

Some studies have shown that breast cancer lines express the endogenous GnRHRs [325]. However, work in our lab has revealed no evidence for endogenous GnRHRs in MCF7 cells, although functional GnRHRs could be expressed in these cells by adenoviral transduction [325]. Thus, these cells were treated similarly to HeLa cells.

Figure 3.9 shows that the effect of GnRH on NFAT1c-EFP translocation was rapid then remained sustained during the examined period (60 min). In control cells, the NFAT1c-n:c was 0.45 ± 0.01 and increased significantly to a maximum of 0.63 ± 0.01 with 10^{-6} M GnRH. The effect of GnRH on NFAT1c-EFP-n:c was dose-dependent, and the maximum effect was seen at 60 min with 10^{-8} –10^{-6} M GnRH, with a log EC_{50} (M) value of -9.18 ± 0.11. Two-way ANOVAs of the data in figure 3.9 revealed that only GnRH concentration is a significant source of variation ($P<0.05$, F (2,24) = 452.00). Post-hoc tests comparing responses with GnRH to control measures with no GnRH revealed statistically significant responses ($P<0.05$) with 10^{-9}–10^{-6} M GnRH at 5, 20 and 60 min.

For ERK dual phosphorylation, GnRH caused a clear concentration-dependent increase in ppERK-n. That was rapid and transient (peaking at 5 min and returning to basal conditions by 60 min). The level of ppERK-n increased significantly from 935.65 ± 61.36 AFU to 1467.21 ± 132.12 AFU with 10^{-6} M. Two-way ANOVAs of ppERK data revealed that GnRH concentration and time are both significant sources of variation ($P<0.05$, F (14,56) =11.86). Post-hoc tests comparing responses with GnRH to control measures with no GnRH revealed statistically significant responses ($P<0.05$) with 10^{-9}-10^{-6} M GnRH at 5 min but not for 20 and 60 min. The log EC_{50}

(M) values were –7.87 ± 0.31 at 5 min, –8.03 ± 0.01 at 20 min, and -10.65 ± 0.65 at 60 min.

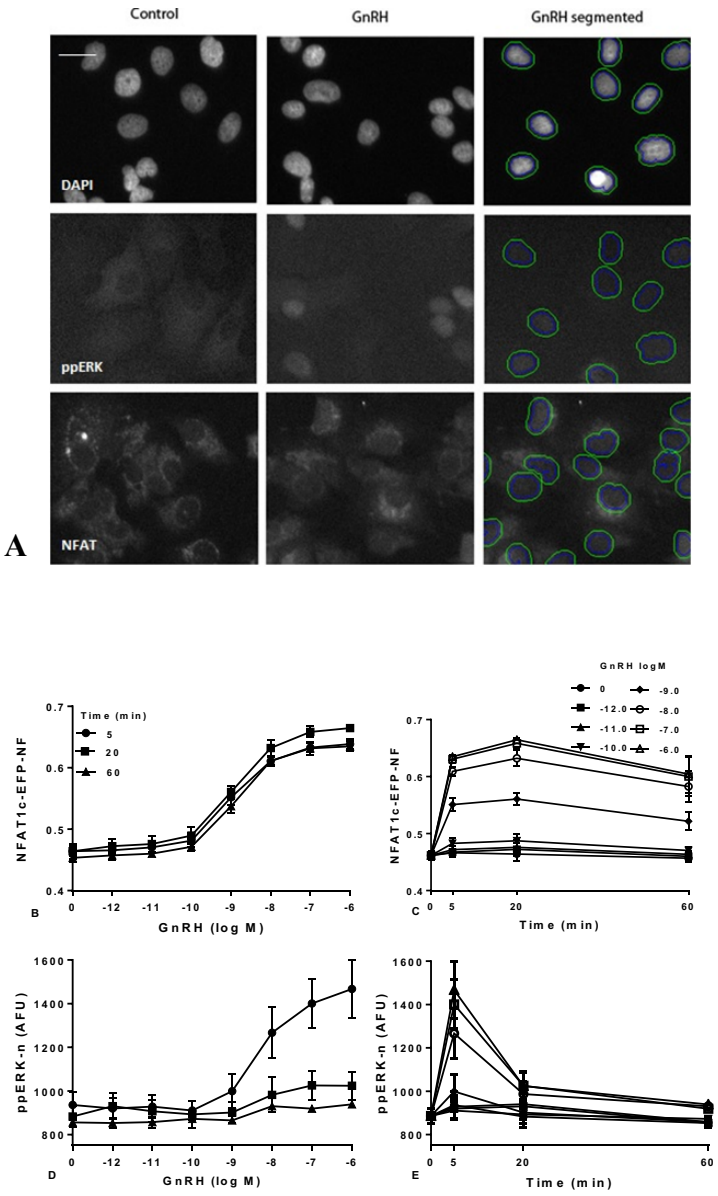

Figure 3.9. GnRH effects on the activation of NFAT and ERK in Ad mGnRHR transduced MCF-7 cells.

Cells were treated as described in Chapter 2 and were stimulated for the indicated times and concentrations. Representative images of DAPI, NFAT1c-EFP, and ppERK in cells cultured under control condition or stimulated 5 min for ppERK and 60 min for NFAT1c-EFP with 10^{-7} M GnRH are shown in A. Scale bar, 3 μm. Panels B and D show population average responses of NFAT1c-EFP-NF and ppERK-n stain intensity. Panels C and E show the same data as B and D respectively but re-plotted against time. The figures show means ±SEMs, n=4, each with quadruplicate wells for each condition and two fields of view/well.

3.3.9. GnRH effects on Egr1 driven zsGreen and NFAT-RE driven asRed expression in Ad mGnRHR transduced MCF-7 cells.

The effects of GnRH on Egr1 driven zsGreen and NFAT driven as Red expression were quantified in the same cells. The representative images in figure 3.10A, demonstrate DAPI, Egr1-zsGreen and NFAT-RE-asRed expression in control cells and cells stimulated for 8 hr with 10^{-7} M GnRH. GnRH caused a pronounced increase in NFAT-RE driven asRed expression in the whole cell but did not cause any obvious change in Egr1-driven zsGreen expression.

GnRH caused a concentration-dependent increase in NFAT-RE-asRed-n+c, that was seen at 4 hr and was most pronounced at 8 hr (Figure 3.10D). The expression level of NFAT-RE-asRed was 318.28 ± 2.3 AFU under control condition and increased significantly to 340.44 ± 3.61 AFU after being stimulated with 10^{-7} M GnRH at 8 hr (Figure 3.10D). Two-way ANOVAs of the data in panel D revealed that GnRH concentration and time are a significant source of variation ($P<0.05$, $F(14,56) = 6.10$). Post-hoc tests comparing responses with GnRH to control measures with no GnRH revealed statistically significant responses ($P<0.01$) with 10^{-8} –10^{-6} M GnRH at 6 and 8 hr. The EC_{50} (M) values for NFAT-RE-asRed were -9.12 ± 0.44 at 4 hr, -9.12 ± 1.12 at 6 and -8.72 ± 0.45 at 8 hr.

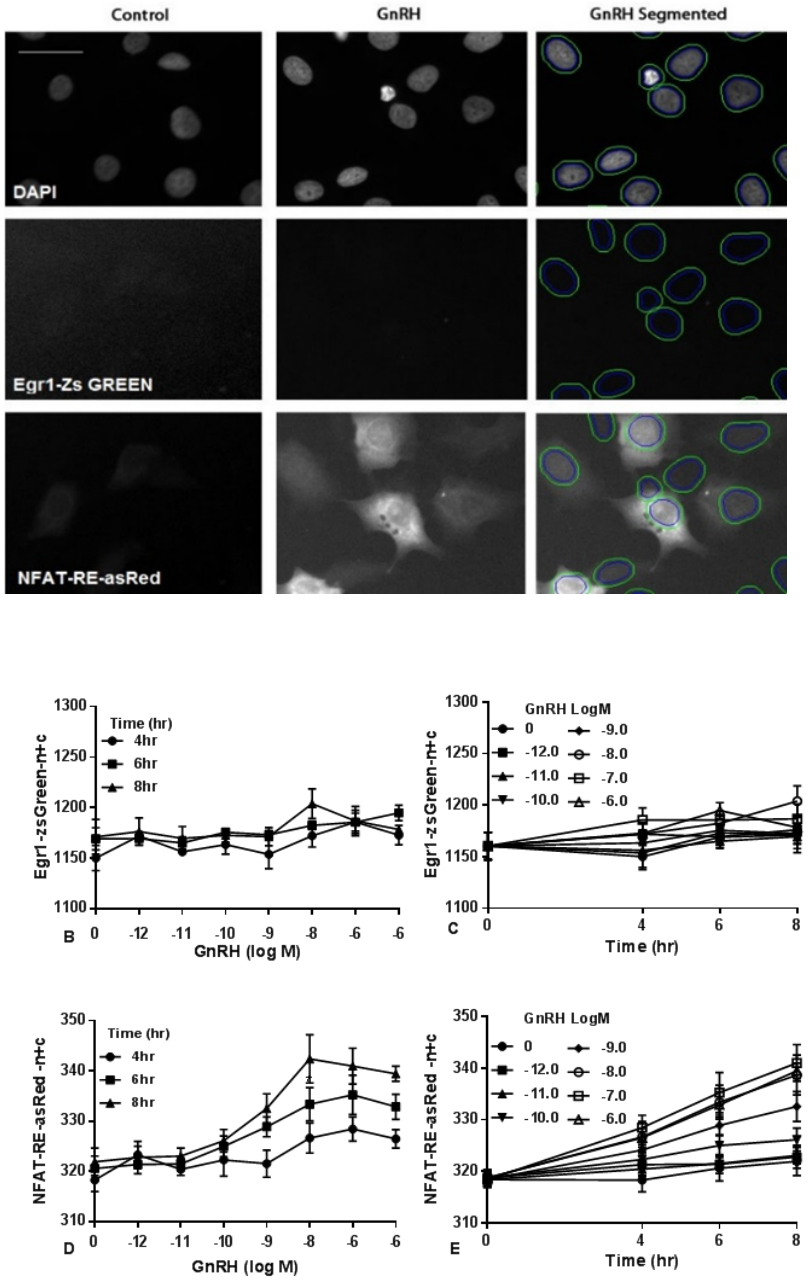

Figure 3.10. GnRH effects on Egr1 driven zsGreen and NFAT-RE driven asRed transcription in Ad mGnRHR transduced MCF-7 cells.

Cells were cultured and treated as described in Chapter 2. Representative images for DAPI, Egr1 driven zsGreen expression, and NFAT-RE driven asRed expression for cells cultured under control condition or stimulated 8 hr with 10^{-7} M GnRH are shown in A. The right-hand images show an example of the automated image segmentation used to define perimeters of the nuclei and cells. Scale bar, 3 µm. Panels B and D show population average responses of Egr1-zsGreen-n+c and NFAT-RE-asRed-n+c in AFU. These data are re-plotted against time in panel C and E. The figures show means ± SEMs, n=4, each with quadruplicate wells for each condition and two fields of view/well.

3.3.10. Comparing the effect of GnRH, PDBu, and EGF on ERK and NFAT1c-EFP activation in LβT2 cells.

The effect of GnRH, PDBu, and EGF on ppERK activation and nuclear translocation of NFAT1c-EFP in LβT2 cells are compared and illustrated in figure 3.11. Stimulating the cells with 10^{-7} M GnRH or 10^{-6} M PDBu resulted in a sustained effect on the level of the ppERK-n, which was most pronounced at 30 min with GnRH and 15 min with PDBu, and the responses remained elevated during the observed period. In control cells, the ppERK-n level was 162.41 ± 1.62 AFU, and this was increased significantly to around 243.62 ± 19.27 AFU by GnRH (Figure 3.11A), and up to 206.71 ± 6.14 AFU by PDBu (Figure 3.11B). In contrast, stimulation with 10^{-8} M EGF (Figure 3.11C), induced a rapid and transient increase of the ppERK-n, which was 165.422 ± 4.23 AFU and increased to 262.31 ± 5.31 AFU after being stimulated with EGF. The response peaked at 5 min then declined to the basal level by 60 min.

Two-way ANOVAs of the ppERK data (Figure 3.11 A, B and C) revealed that concentration and time are both significant sources of variation ($P<0.05$, $F(4,16)=14.76$ (GnRH), $F(4,16)=36.44$ (PDBu) and $F(4,16)=247.20$ (EGF)). Bonferroni's multiple comparisons test (comparing the responses with GnRH or PDBu to control measures) showed that both stimuli are significant sources of variation ($P<0.05$) at all the indicated times. However, comparing the responses of ppERK-n with EGF to control measures showed that EGF is a statistically significant response ($P<0.05$) at 5 and 15 min but not for the 30 or 60 min.

The NFAT1c-EFP translocation in response to the same stimuli was measured in parallel. As shown in figure 3.11D, GnRH caused a time-dependent increase in the NFAT1c-EFP from approximately 0.78 ± 0.02 to 1.86 ± 0.12, with a maximum

response at 30 min. Notably, neither PDBu nor EGF had any effect on the nuclear translocation of NFAT-EFP in this cell line (Figure 3.11E and F). Two-way ANOVAs of the NFAT-EFP data in the data in panel D revealed that concentration and time are both significant sources of variation ($P<0.05$, and F (4,16) = 46,87 GnRH, F (4,16) = 46.87). Comparing the responses with GnRH to control measures for each time by Bonferroni's multiple comparisons test revealed statistically significant responses ($P<0.05$) with 10^{-7} M GnRH at all the indicated times. However, neither concentration of PDBu, and EGF nor time was a significant source of variation ($P>0.05$).

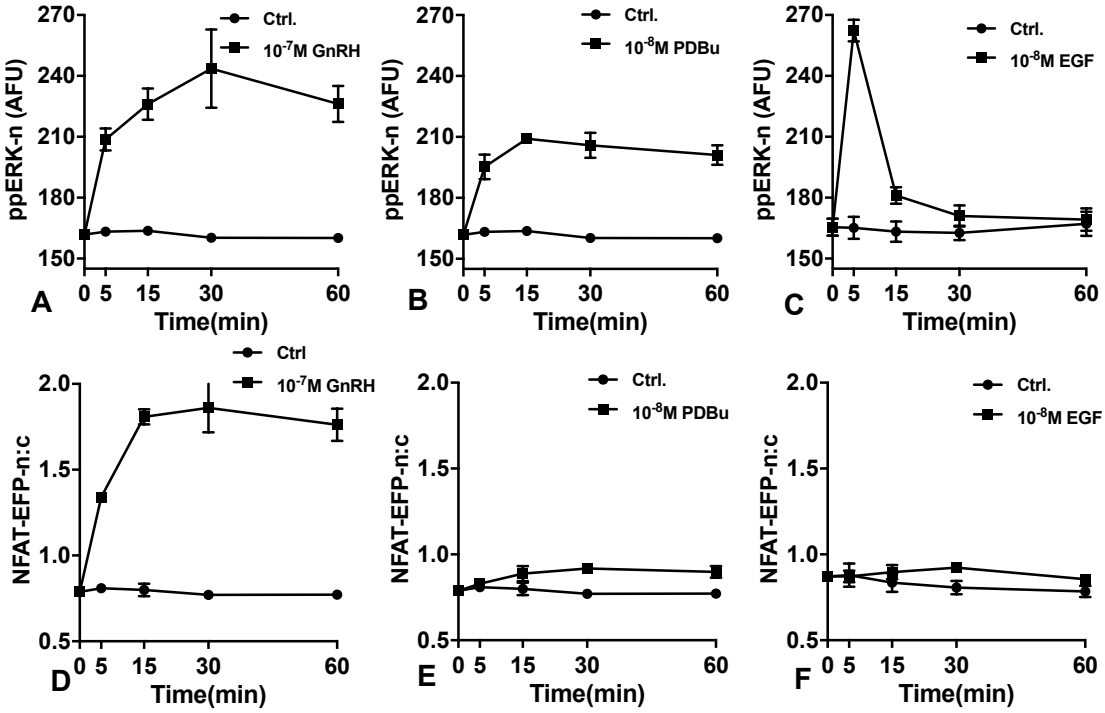

Figure 3.11. Comparison of the effect of GnRH, PDBu and EGF on the activation of ERK and NFAT1c-EFP in LβT2 cells.

Cells were plated as described in Chapter 2. They were then stimulated with 10^{-7} M GnRH, 10^{-8} M PDBu or 10^{-8} M EGF, for the indicated times, before being fixed and stained for ppERK and nuclei. The cells were imaged using an automated fluorescence microscope. Data shown are the ppERK-n in AFU and NFAT1c-EFP-n:c. The results show the means ± SEMs, n=3-4, with triplicate wells and three fields of view/well.

3.3.11. Comparing the effect of GnRH, PDBu, and EGF on ERK and NFAT1c-EFP in HeLa cells.

As shown in figure 3.12A and C, GnRH and EGF had a transient effect on ppERK in HeLa cells that peaked at 5 min and returned to control values by 60 min. The response was substantially higher with EGF than with GnRH. In untreated cells, ppERK-n levels were 163.71 ± 2.14 AFU and increased to 209.18 ± 0.25 AFU and 232.56 ± 6.45 AFU following stimulation with 10^{-7} M GnRH and 10^{-8} M EGF, respectively (Figure 3.12A and C). Stimulating cells with 10^{-6} M PDBu rapidly increased the level of ppERK-n from 162.33 ± 2.04 AFU to 233.23 ± 8.15 AFU by 5 min then gradually declined but did not return to basal conditions during the observed period (Figure 3.12B).

Two-way ANOVAs showed that both variables (concentration and time) are significant source of variation ($P<0.05$, and F (4,16) =44.46 (GnRH), F (4,24) =103.80 (PDBu) and F (4,24) =114.80 (EGF)). Post-hoc tests comparing responses with GnRH, PDBu or EGF to control measures for each time showed that GnRH and EGF concentration are statistically significant sources of variation ($P<0.05$) at 5, 15, 30 min but not for the 60 min. However, PDBu effect is significant ($P<0.05$) at all the indicated times.

The effect of these stimuli on NFAT1c-EFP translocation was measured in parallel (Figure 3.12 D, E and F). GnRH caused a time-dependent increase in NFAT1c-EFP-n:c. In this cell line, a concentration of 10^{-7} M GnRH resulted in significant increase in NFAT1c-EFP-n:c (2.6-fold). The response was observed at 5 min, peaked at around 15 min, and remained elevated during the observed period. Stimulating the cells with 10^{-8} M EGF caused a transient increase in NFAT1c-EFP-n:c (1.5-fold). This effect

was most pronounced at 5 min and declined to the basal level by 60 min (Figure 3.12F). However, no effect of PDBu on NFAT1c-EFP translocation was observed (Figure 3.12E).

Two-way ANOVAs of the NFAT1c-EFP-n:c data in figure 3.12D, E and F, were performed and revealed that concentration (of GnRH and EGF but not for PDBu), and time are both significant sources of variation ($P<0.05$, F (4,16) =68.36 (GnRH) and F (4,24) =80.80 (EGF)). Post-hoc tests comparing responses with GnRH and EGF to control measures revealed statistically significant responses ($P<0.05$) of NFAT1c-EFP with 10^{-7} M GnRH at all the indicated times, whereas with 10^{-8}M EGF the response is statistically significant ($P<0.05$) at 5, 15 and 30 but not for 60.

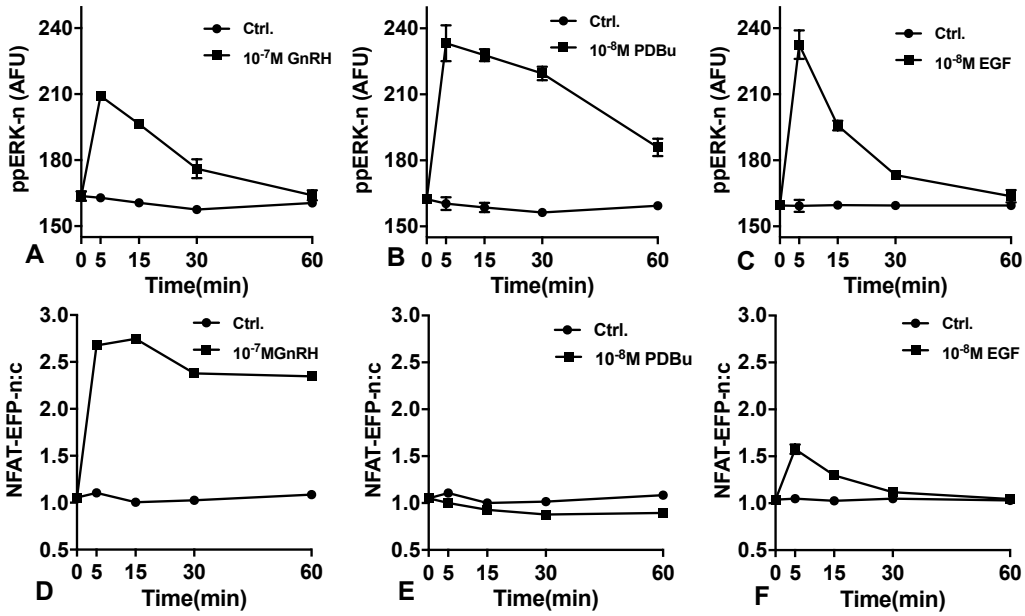

Figure 3.12. Comparison of the effect of GnRH, PDBu and EGF on the activation of ERK and NFAT1c-EFP in Ad mGnRHR transduced HeLa cells.

Cells were cultured and treated as described in Chapter 2. Cells were then stimulated with GnRH PDBu, or EGF at the indicated time and concentrations, before being fixed, stained for ppERK and nuclei. Data shown are ppERK-n (in AFU) and NFAT1c-EFP-n:c. The figures show means ± SEMs, n=3-4, each from an experiment with triplicate wells and three fields of view/well.

3.3.12. Comparing the effect of GnRH, PDBu, and EGF on ERK and NFAT1c-EFP in MCF-7 cells

Figure 3.13 illustrates the response of ppERK in MCF7 cells stimulated with GnRH, PDBu or EGF. Rapid and transient ERK phosphorylation was observed after stimulating cells with 10^{-7} M GnRH and 10^{-8} M EGF. The responses peaked at 5 min and returned to the control value by 60 min (Figure 3.13A and C). The ppERK-n level was considerably higher in cells treated with EGF than with GnRH. It was increased by 1.2- and 1.7-fold change following treatment with GnRH and EGF, respectively (Figure 3.13A and C). The ppERK response to PDBu (10^{-6} M) was more sustained. It peaked at 5 min and remained elevated throughout the time course (Figure 3.13B).

Two-way ANOVAs for the ppERK data in the top panels (Figure 3.13A, B and C) revealed that time is a significant source of variation ($P<0.05$) in cells stimulated by GnRH, whereas concentration is not. However, in cells stimulated by PDBu or EGF, both variables are significant sources of variation ($P<0.05$, F (4,24) = 68.7.91 (GnRH) F (4,32) =23.15 (PDBu) F (4,32) =95.19 (EGF)). Post-hoc tests comparing responses with GnRH, PDBu and EGF to control measures showed that GnRH concentration (panel A) is statistically significant sources of variation ($P<0.05$) at 5, 15, 30 min but not for the 60 min, of the PDBu (in panel B) is statistically significant source of variation ($P<0.01$) at all the indicated times, whereas EGF concentration effect is statistically significant at only 5 and 15min.

GnRH caused NFAT1c-EFP translocation in this cell line. The response peaked at 5 min and remained steady throughout the observed period. The NFAT1c-EFP-n:c increased substantially from 1 to 2.2 after being stimulated with GnRH (Figure

3.13D). However, no measurable effect of EGF or PDBu on NFAT1c-EFP nuclear translocation was observed here (Figure 3.13E and F).

Two-way ANOVAs for the NFAT1c-EFP data (Figure 3.13D, E and F) showed that concentration and time are both significant sources of variation ($P<0.05$, F (4,24) =12.33) in cell treated with GnRH but not with PDBu or EGF. Post-hoc tests comparing responses with GnRH to control measures for each time revealed statistically significant responses ($P<0.05$) with 10^{-7} M GnRH at all the indicated time points.

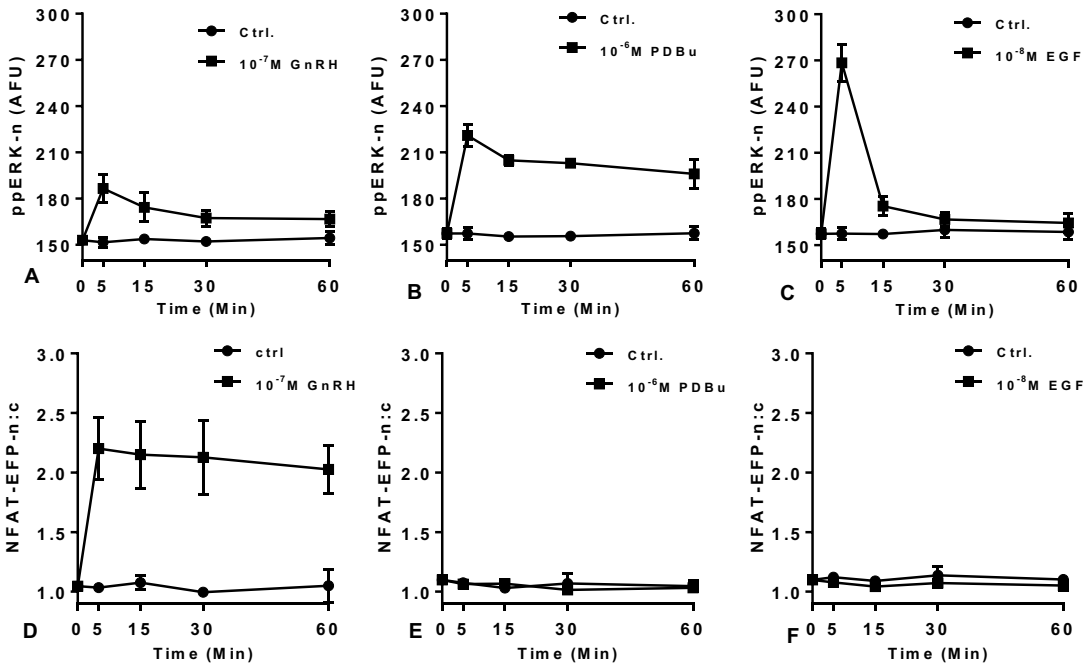

Figure 3.13. Comparison of the effect of GnRH, PDBu and EGF on the activation of ERK and NFAT in Ad mGnRHR transduced MCF-7 cells.

Cells were cultured and treated as described in Chapter 2. Data shown are the ppERK-n (in AFU) and NFAT1c-EFP1c-n:c. The figures show means ± SEMs, n=4-5, each from an experiment with triplicate wells and with three fields of view/well.

3.3.13. Comparing the effects of GnRH on ERK and NFAT1c-EFP and their transcriptions readouts in HeLa, LβT2 and MCF-7 cells.

As shown in figure 3.14, two-way ANOVAs revealed that concentration and time are both significant sources of variation ($P<0.05$), and comparing the responses of ppERK with GnRH to control measures for each time showed that in LβT2 and HeLa cells the responses were significant different at all the indicated times (Figure 3.14A and B). However, in MCF-7 cells (Figure 3.14F), the GnRH effect was significant for the 5, 15 and 30 min data (but not for the 60 min data).

For the NFAT1c-EFP data (panels D, E, and F), two-way ANOVAs revealed that both variables are significant sources of variation in all three cell lines ($P<0.05$). Post-hoc tests comparing responses with GnRH to control measures for each time revealed that the GnRH effect on NFAT1c-EFP was statistically significant ($P<0.05$) with 10^{-7} M at all the time points and in the three cell lines examined here.

Effect of GnRH on Egr1- and NFAT-RE driven expression of zsGreen and asRed respectively are also shown in figure 3.15. Two-way ANOVAs revealed that concentration and time are both significant sources of variation in all three cell lines ($P<0.05$). Comparing responses with and without GnRH for each time revealed that GnRH effect on Egr1-zsGreen-n+c was statistically significant with 10^{-7} M at 4, 6 and 8 hr in both HeLa cells and LβT2 cells but not in MCF-7 cells ($P<0.05$). Two-way ANOVAs of the low panels (figure 13.14D, E and F) revealed that concentration and time are both significant sources of variation for HeLa cells ($P<0.05$, F (3,9) = 6.12, and only concentration is significant sources of variation for LβT2 with $P<0.05$). Comparing the responses of NFAT-RE-asRed with GnRH to control measures for each time showed that in LβT2 and HeLa cells the responses were significant at 4, 6, and 8hr (but not for the 2hr data). For MCF-7 cells data, GnRH had no effect on the expression level of both measurements.

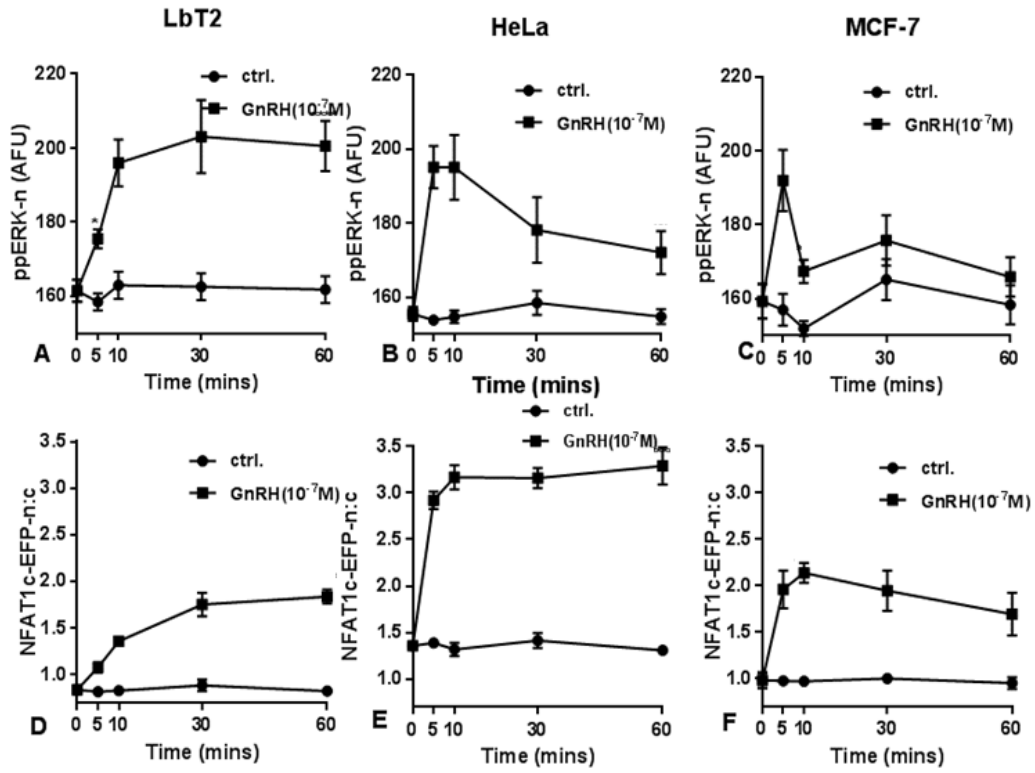

Figure 3.14. Comparing the effect of GnRH on ppERK and NFAT1c-EFP in three different cell lines

Cells were cultured as described above and treated with 0 or 10^{-7} M GnRH for the indicated times. Cells were then fixed and stained for ppERK and cell nuclei (DAPI). Image acquisition and analysis were performed as described in Chapter 2. The data shown are the ppERK-n (in AFU) and NFAT1c-EFP-n:c. The results show the means ± SEMs from 3 to 4 separate experiments (n=3-4), with triplicate wells and with three fields of view/well.

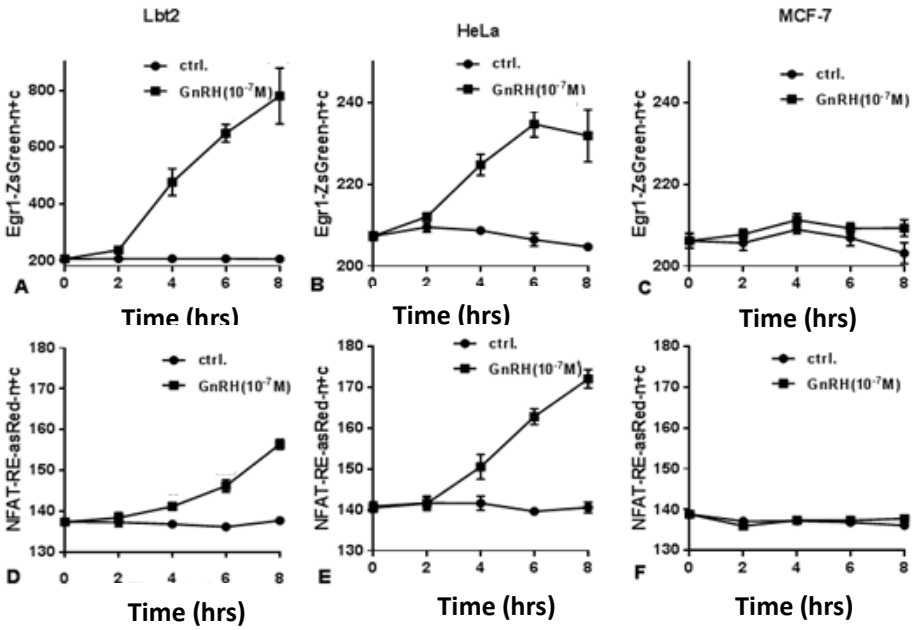

Figure 3.15. Comparing the effect of GnRH on Egr1 driven zsGreen and NFAT-RE driven asRed expression in three different cell lines

Cells were cultured and treated as described in Chapter 2. Cells were then stimulated with 0 or 10^{-7} M GnRH for the indicated times. Cells were next fixed and stained for cell nuclei (DAPI). Image acquisition and analysis were performed as described in Chapter 2. The data shown are the NFAT-RE-asRed-n+c and Egr1-ZsGreen-n+c (in AFU). The results show the means ± SEMs, (n=3-4), with triplicate wells and with three fields of view/well.

3.4. Discussion

Type I mammalian GnRHRs are $G\alpha_{q/11}$ coupled receptors. Their activation leads to the activation of both ERK and NFAT pathways [8, 25]. The aim of the experiments described in this chapter was to determine the effects of GnRH on the two pathways, and this was achieved by automated fluorescence microscopy. An additional aim was to monitor the responses of both ERK and NFAT1c-EFP to EGF and PKC activator. The work was performed in three different cell lines, LßT2 cells that express the endogenous GnRHRs, and HeLa and MCF-7 cells where both do not express GnRHR, therefore they had to be transduced with Ad mGnRHRs.

The key findings are that similar effects of GnRH on ppERK were seen in the extra-pituitary cell lines (HeLa and MCF-7 cells), the effect was rapid and transient (maximal at 5 min and returned to the control level by 60 min). In contrast, in the pituitary-derived cell line (LßT2 cells), the response was slower in onset and remained elevated throughout the observed period (Figure 3.13A-C). These findings are in accord with other studies that described the transient kinetics of ERK in both HeLa [316, 327] and MCF-7 cells [325]. A difference in these studies is that the cells were transfected either with Ad human GnRHR or Ad sheep GnRHR instead of Ad mGnRHR (which is used in this work to allow for direct comparison with the endogenous mGnRHRs of LβT2 cells). However, mammalian GnRHRs of humans, mice, horse, and sheep share more than 80% amino acid homology and have similar mechanisms for signalling [111].

The difference in kinetics observed in these cell lines are not related to the differences in receptor affinity. The dose-response analysis showed similar potencies log EC_{50} (M) values of -8 to -10 during the examined times (5, 20 and 60 min) in HeLa, MCF-

7 and LβT2 cells, which is in accord with previous studies in HeLa and MCF-7 cells [133, 316, 334]. The response of NFAT1c-EFP to GnRH was similar in the three cell lines. Though, the response in HeLa cells was greater than in the other two cell types, and the log EC_{50} (M) values was largely similar (-9 to -10, Figure 3.5, 3.7 and 3.9).

The differences observed here between cell lines could be related to the way that cells were immortalised as explained in Chapter 1 (Section 1.13). The extra-pituitary cell lines are derived from carcinomas [335-337]. On the other hand, LßT2 cells were immortalised from large and small SV40 T antigen. SV40 T antigen causes cell immortalisation [318] by interacting with a wide range of target proteins, like proteins phosphatase 2A and protein phosphatase 1. In most cells and tissue these two proteins account >90% of Ser/ Thr phosphatase activity [319]. Moreover, the small SV40 cause the inhibition of proteins phosphatase 2A [320], which is reported to affect the ERK and MEK activities [338].

Promoters of the genes encoding LHß, FSHß and αGSU have sites that can be regulated by both ERK and NFAT [123]. In order to investigate Ca^{2+}/calcineurin/ calmodulin- and PLC/PKC/ERK-directed transcriptional activity directly, GnRH-mediated activation of the Egr1 promoter and the NFAT-RE was examined in the three cell lines. GnRH increased the expression levels of the fluorescent proteins (zsGreen and asRed) that were used as readouts of Egr1 and NFAT-RE respectively. These responses had relatively similar kinetics in both HeLa and LβT2 cells. However, the expression levels of Egr1-zsGreen were greater than NFAT-RE-asRed in LβT2 (Figure 3.6 and Figure 3.8). The potencies were comparable for each reporter with EC_{50} values of approximately 10^{-7}. In the MCF-7 cell line, GnRH had little effect on Egr1 driven zsGreen expression and there was no effect of GnRH on NFAT-RE-asRed

expression (Figure 3.10). This low or absent expression might be related to that the stimulation period is not enough and signals can be observed if cells stimulated over 8 hr. For example, the effect of GnRH on ERE driven luciferase reporter gene in LβT2 was observed after a period of 18-24 hr [339].

These variances in the expression levels of Egr1-zsGreen that were observed between the three cell types are likely related to the duration of the signalling to ERK that may affect the downstream process [341, 342]. The signal duration likely influences the transcription and activity of immediate early genes, such as c-Fos, and Egr1 [341]. Thus, the differences could be explained by that, the transient response of ERK in HeLa cells resulted in an increase in the Egr1-driven zsGreen expression, but ERK declined before the Egr-1zsGreen is accumulated further. On the other hand, the sustained ERK response that was seen in LβT2 cells could allow for more accumulation of Egr1-zsGreen [342]. However, different mechanisms could also be involved such as protection of ERK phosphorylation by specific interacting proteins or crosstalk with other signalling pathways [343]. Such differences emphasise the importance of examining different cell lines on signalling pathways studies.

For further validation of the effect of GnRH, EGF and PDBu on the measurements, an extra step was conducted. As shown in Figure 3.11 to Figure 3.14, cells were subjected to a single dose of the stimulus and measured its effect on ppERK, NFAT-1c-EFP and their transcriptions readouts at different time points. The main findings are that activation of ERK was shown to be stimulus dependent (transient by GnRH and EGF and sustained by PKC activator). Similarly, GnRH caused a sustained effect on the NFAT1c-EFP translocation, whereas EGF caused a transient response in only HeLa cells (Figure 3.12). PDBu had no effect on NFAT1c-EFP translocation in any

of the examined cell lines. These findings imply that EGF is functionally linked to the PLCγ pathway in HeLa cells and provides evidence for coupling between EGFR and PLCγ. On the other hand, EGF did not signal to NFAT in LβT2 and MCF-7 cell lines (Figure 3.11, 3.12 and 3.13). These differences are likely related to the variation in the activation mechanisms, scaffolding proteins and the balance of kinases and phosphatase in the cells. These factors play a crucial role in shaping responses [36]. The transient response that are resulted by EGF it could be related to the dynamics of its receptor [39]. A more likely explanation is that EGFR undergoes rapid cell-dependent agonist-induced internalisation upon stimulation by EGF, terminating ERK activation [39]. However, mammalian GnRHRs do not undergo rapid homologous receptor desensitisation [302, 344]. Notably, regarding the expression of Egr1-zsGreen and NFAT-RE-asRed in MCF-7 cells, an opposite result was obtained (Compare Figure 1.10 C and E with Figure 1.14 C and F), GnRH caused the expression of NFAT-RE-asRed and no effect on Egr-1zsGreen (Figure 1.10), whereas GnRH had no effect on both measurements (Figure 1.14). The main reason is unknown and thus, various inhibitors were used in next chapter for further investigations of the signalling pathways in these cell lines

To sum up, ERK activation kinetics were found to be stimulus specific, while PDBu caused sustained ERK activation, EGF caused transient activation. GnRH effects were dependent upon cell context, with GnRH causing transient responses in the HeLa and MCF-7 cells and a sustained response in LβT2 cells. Regarding NFAT1c-EFP the response was sustained with GnRH in all three cell types. In spite of the fact that PKC is thought to mediate elevation of cytoplasmic Ca^{2+} in pituitary cells [345], PDBu did not signal to NFAT in any of the examined cell lines. EGF effects were also context-specific with a small increase in NFAT1c-EFP caused in HeLa cells. GnRH-induced

Egr1- driven zsGreen expression, and NFAT-RE- driven asRed expression in both LßT2 and HeLa cells. However, the effect on Egr1-zsGreen was greater in LßT2 than in HeLa cells. In contrast, in MCF-7 cells, GnRH had little effect on NFAT-RE-asRed and no effect on Egr1-zsGreen was observed in this cell line (summarised in Table 3.1). These differences presumably reflect differences in the identity or concentration of signalling components in the three cellular models explored. Therefore, the experiments described in the following chapter were planned to use pharmacological inhibitors for better delineation of the signalling network.

Measurement	HeLa cells	LβT2 cells	MCF-7 cells
ERK	Transient	Sustained	Transient
NFAT1c-EFP	Sustained	Sustained	Sustained
Egr1-zsGreen	Sustained	Sustained	No effect
NFAT-RE-asRed	Sustained	Sustained	Sustained

Table 3.1. Summary of the GnRH effect on ERK, NFAT1c-EFP, Egr1-zsGreen and NFAT-RE-asRed in three cell lines.

Stimulating cells with GnRH caused transient ERK activation in HeLa and MCF-7 cells and sustained effect in LβT2 cells. However, its effect on NFAT1c-EFP translocation was found to be sustained in all three cell types. GnRH-caused Egr1-driven zsGreen expression, and NFAT-RE- driven asRed expression in LßT2 and HeLa cells, but the effect was greater on Egr1-zsGreen in LßT2 than in HeLa cells. In contrast, the effect of GnRH in MCF-7 cells shown to be relatively low on NFAT-RE-asRed and no effect on Egr1-zsGreen was observed in this cell line.

Chapter 4- Using pharmacological inhibitors to define GnRH signalling mechanisms

4.1. Background

The substantial role of GnRH in the reproductive system has made it a major target for the treatment of infertility and sex steroid hormone-dependent diseases [346, 347]. GnRH interacts with its cognate receptor in the plasma membrane and utilises various signalling mechanisms for the activation of ERK and NFAT [6, 133, 158]. The fine control of ERK or NFAT signalling is involved in the regulation of numerous genes that implicated in the LHß, FSHß, and αGSU expression [348-350]. GnRHRs are also expressed in extra-pituitary sites such as steroid hormone-dependent cancer cells including prostate, ovary, and mammary [76]. In these sites, GnRH has been shown to have a direct effect in cell proliferation and a novel role in controlling tumor progression [199, 351, 352].

The previous chapter (Chapter 3) described the use of a high content imaging approach to interrogate intracellular signalling in HeLa, MCF-7, and LβT2 cell lines, with immunofluorescence used to monitor ppERK and fluorescent reporters used to monitor effector activation and effector-driven transcription. The data reveal activation of the Ca^{2+}/CaM/Cn/NFAT and Raf/MEK/ERK cascades by GnRH, but also reveal marked context-dependence of signalling. Such differences imply that there are differences in network topology between these models and are consistent with the large body of evidence showing that GnRH signalling is dependent on cellular context [131, 133, 332]. The differences in ppERK response kinetics could conceivably reflect differences in strength of negative feedback pathways known to shape ERK responses in other systems [353-355] or differences in reliance on EGF-receptor transactivation for ERK activation.

This chapter documents a series of experiments using the same cellular models and experimental readouts as used for Chapter 3, but with additional use of pharmacological inhibitors to further delineate the network architecture for ERK and NFAT signalling downstream of the GnRHR.

4.2. Materials and methods

Pharmacological inhibitors were used to further probe the signalling networks in LβT2, HeLa, and MCF-7 cell lines. The inhibitors used here are a) Cetrorelix, is a synthetic decapeptide that competes specifically with GnRH for binding receptors on the anterior pituitary cells. Thus, it prevents the action of GnRH in releasing LH and FSH [356], b) AG1478, an inhibitor of EGFR signalling that competitively blocks the ATP binding pocket of the EGFR [357] c) Ro31-8425, a reversible and highly selective inhibitor of protein kinase C that blocks the ATP binding site [358], d) PD184352, a MEK1/2 inhibitor that is a highly selective non-competitive inhibitor. It does that preventing the activation of MAPKK1 by Raf or MEK kinase with an IC50 of 2-7μM [359], and e) cyclosporine A (CsA) a potent immunosuppressant drug that inhibits calcineurin by binding cyclophilin, and forming a complex that inhibits the phosphatase activity of calcineurin [360, 361]. These molecules were applied for a 30 min pre-treatment, then cells were stimulated with the concentrations and for the times outlined under the figures.

4.3. Results

4.3.1 Effect of pharmacological inhibition on GnRH signalling in LβT2 cells.

Cells were subjected to the above inhibitors prior to stimulation with 10^{-7} M GnRH (Figure 4.1). As shown, pre-treatment of the cells with the indicated inhibitors caused variable reductions in GnRH signalling to ERK, NFAT1c-EFP, Egr1-zsGreen, and NFAT-RE-asRed.

Two-way ANOVAs of the data in each panel of figure 4.1 revealed that stimulus, inhibitor and stimulus-inhibitor interactions were significant sources of variation ($P<0.05$). Post-hoc tests revealed that GnRH caused a significant increase in ppERK-n (from 153.12 ± 2.10 to 223.11 ± 4.25 AFU) and that this effect was significantly inhibited by PD184352, RO31-8425 and Cetrorelix, but not by AG1478 or CsA (Figure 4.1A). Similarly, GnRH caused a significant increase in Egr1-zsGreen (from 205.10 ± 1.21 to 808.11 ± 4.00 AFU) and this effect was inhibited by PD184352 and Cetrorelix but not by AG1478 or CsA (Figure 4.1B). Notably, although R031-8425 caused a 30% reduction in the GnRH effect on Egr1-zsGreen this effect was not significant ($P>0.05$). It also caused a 70% reduction in ppERK-n response but that was statistically significant ($P<0.05$).

Of the data in panel C and D, post-hoc tests revealed that GnRH caused a significant increase in NFAT1c-EFP-n:c (from 0.84 ± 0.03 to 1.22 ± 0.11 AFU) and that this effect was significantly inhibited by Cetrorelix and CsA but not by PD184353, RO31-8425, or AG1478 (Figure 4.1C). Similar effect was seen in NFAT-RE-asRed (Figure 4.1D). GnRH caused a significant increase in NFAT-RE-asRed (from 137 ± 1AFU to 156 ± 0.85 AFU) and this effect was completely abrogated by Cetrorelix and CsA but not by the other treatments. Notably, CsA inhibited totally the GnRH effect on NFAT1c-EFP translocation (100% reduction) and had a similar inhibition effect on NFAT-RE-asRed (70% reduction) and that was statistically significant ($P<0.05$).

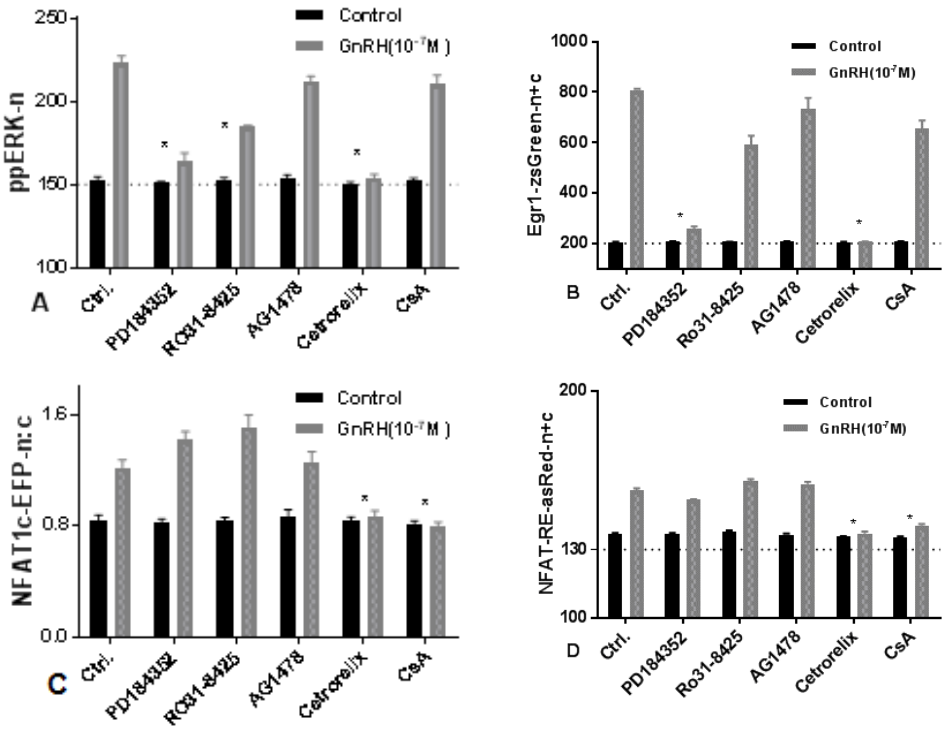

Figure 4.1. Effect of pharmacological inhibition on GnRH signalling in LβT2 cells.

LβT2 cells were cultured and treated as described in Chapter 2. Then the indicated inhibitors were applied for 30 min prior to stimulation for 5 min (in A and D) or 6 hr (in B and E) with 0 or 10^{-7} M GnRH. The cells were then fixed and stained for ppERK and nuclei. The figures show means ±SEMs, n=3, each with triplicate wells for each condition and three fields of view/well. The black columns represent the unstimulated group where the cells were subjected only to the inhibitors, except for the control group (Ctrl) without inhibitor. The grey columns represent cells subjected to the inhibitors prior to GnRH stimulation. The star (*) shows significant inhibition of GnRH signalling ($P<0.05$) in cells subjected to inhibitors (grey columns) comparing to Ctrl (the first grey column). The F (5,20) = 62.93 (A), The F (5,20) = 188.30 (B), F (5,20) = 33.28 (C), F (5,20) = 99.77 (D). The dotted lines represent the background values for each measurement.

4.3.2 Effect of pharmacological inhibition on PDBu signalling in LβT2 cells.

Two-way ANOVAs of the data in panel A and panel B in figure 4.2 revealed that stimulus, inhibitor and stimulus-inhibitor interactions were significant sources of variation. Post-hoc tests showed that PDBu caused a significant increase in ppERK-n (from 152.12 ± 2.10 AFU to 201.05 ± 0.57 AFU). This effect was significantly inhibited by PD184352 and RO31-8425, but not by the other drugs. In the same way, PDBu caused a significant increase in Egr1-zsGreen (from 205.21 ± 1.10 AFU to 808.13 ± 4.44 AFU) and this effect was inhibited by PD184352 (~70% reduction), and RO31-8425 (~80% reduction) but not by AG1478, Cetrorelix or CsA (Figure 4.2D).

Of the data in panel C and D, separate two-way ANOVAs revealed that neither stimulus nor inhibitor is significant sources of variation. PDBu had no effect on NFAT1c-EFP translocation or on the NFAT-RE-asRed expression in this cell line (Figure 4.2C and D).

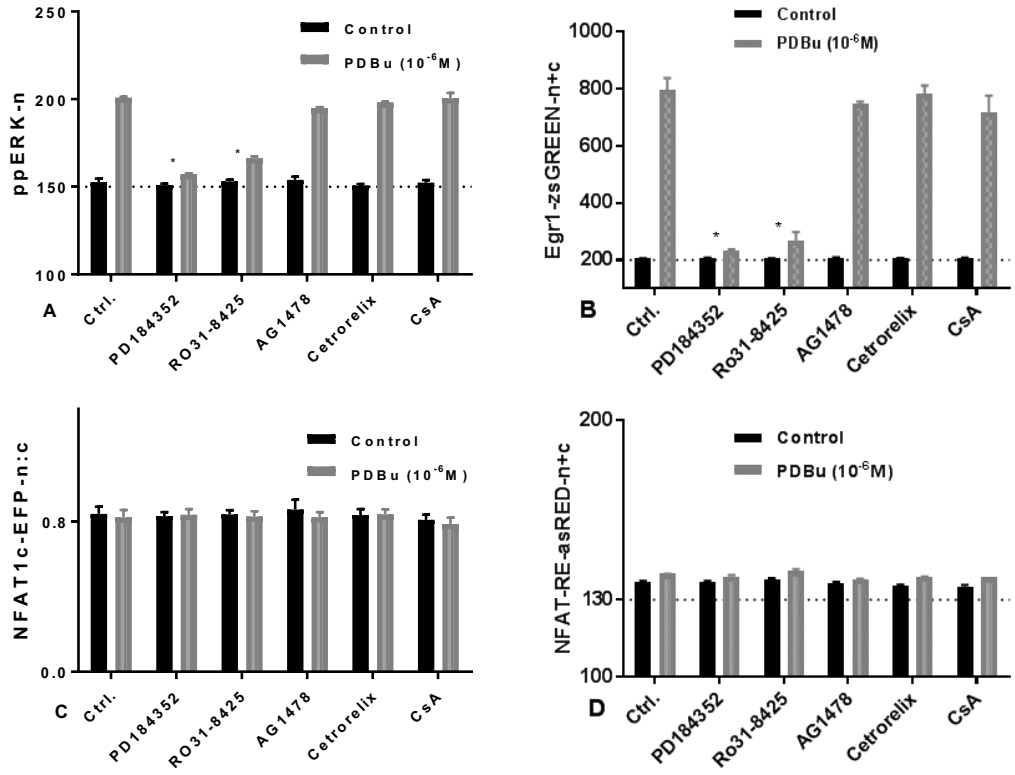

Figure 4.2. Effect of pharmacological inhibition on PDBu signalling in LβT2 cells.

Cells were cultured and treated as described in Chapter 2. Then the indicated inhibitors were applied for 30 min prior to stimulation for 5 min (in A and C) or 6 hr (in B and D) with 0 or 10^{-6} M PDBu. The cells were then fixed and stained for ppERK and nuclei. Digital images and analysis were acquired as detailed under section 2.8. The figures show means ±SEMs, n=3, each with triplicate wells for each condition and three fields of view/well. The black columns represent the unstimulated group where the cells were subjected only to the inhibitors, except for the control group (Ctrl) without inhibitor. The grey columns represent cells subjected to the inhibitors prior to GnRH stimulation. The star (*) shows significant inhibition of GnRH signalling ($P<0.05$) in cells subjected to inhibitors (grey columns) comparing to Ctrl (the first grey column). The F (5,20) = 173.7 (A), F (5,20) = 119.60 (B). The dotted lines represent the background values for each measurement.

4.3.3 Effect of pharmacological inhibition on EGF signalling in LβT2 cells.

LβT2 cells were subjected to different inhibitors (outlined in figure 4.3) prior to stimulation with 10^{-8}M EGF. As shown, pre-treatment of the cells with the indicated inhibitors caused variable reductions in EGF signalling to ERK, NFAT1c-EFP, Egr1zsGreen, and NFAT-RE-asRed.

Two-way ANOVAs of the data in panels A and B revealed that stimulus, inhibitor and stimulus-inhibitor interactions were significant sources of variation. Post-hoc tests showed that EGF caused a significant increase in ppERK-n (from 152 ± 2 AFU to 270 ± 5 AFU) and that effect was significantly inhibited by PD184352 and AG1478 (60% reduction), but not by RO31-8425, Cetrorelix or CsA (Figure 4.3A). Similarly, EGF caused a significant increase in Egr1-zsGreen-n+c (from 205.21 ± 1.01 to 238.02 ± 0.03 AFU) and this effect was abrogated by PD184352 and AG1478 (Figure 4.3B). Both Cetrorelix and R031-8425 caused a 30% reduction in the EGF effect on Egr1-zsGreen, although this effect was small, statistically was. significant ($P<0.05$).

Two-way ANOVAs of the data in panel C and D revealed that stimulus, inhibitors, and stimulus-inhibitor interaction were not significant sources of variation. As shown in figure 4.3, there was no measurable effect of EGF on the NFAT1c-EFP translocation or NFAT-RE-asRed, suggesting that the agonist is not signalling to NFAT via EGFR in this context.

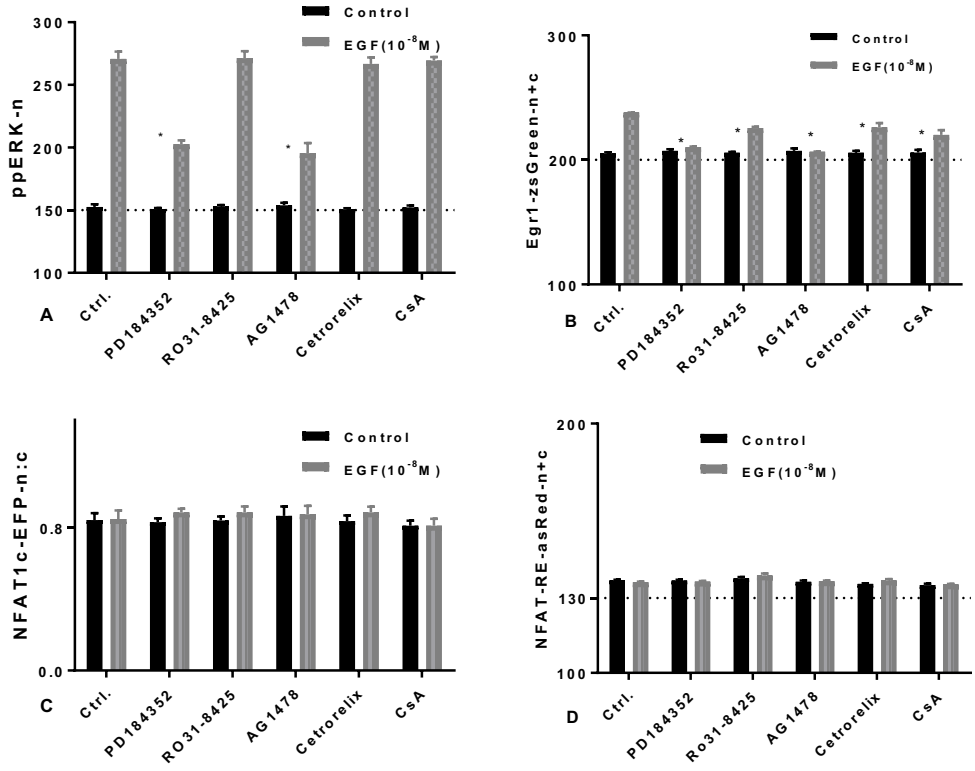

Figure 4.3. Effect of pharmacological inhibition on EGF signalling in LβT2 cells.

Cells were cultured and treated as described in Chapter 2. Then the indicated inhibitors were applied for 30 min prior to stimulation for 5 min (in A and C) or 6 hr (in B and D) with 0 or 10^{-8}M EGF. They were then fixed and stained for ppERK and nuclei. The figures show means ±SEMs, n=3, each with triplicate wells for each condition and three fields of view/well. The black columns represent the unstimulated group where the cells were subjected only to the inhibitors, except for the control group (Ctrl) without inhibitor. The grey columns represent cells subjected to the inhibitors prior to GnRH stimulation. The star (*) shows significant inhibition of GnRH signalling ($P<0.05$) in cells subjected to inhibitors (grey columns) comparing to Ctrl (the first grey column). The F (5,20) = 18.25 (A), F (5,20) = 45.84 (B). The dotted lines represent the background values for each measurement.

4.3.4 Pharmacological inhibition of GnRH signalling in Ad mGnRHR transduced HeLa cells.

The mechanism of GnRH signalling to ERK and NFAT was also examined in this cell line. As shown in figure 4.4, separate two-way ANOVAs of the data in panels A and B revealed that stimulus, inhibitor and stimulus-inhibitor interactions were significant sources of variation. Post-hoc tests revealed that GnRH caused a significant increase in ppERK-n from 157.03 ± 0.67 AFU to 241.12 ± 1.20 AFU, and that this effect was significantly inhibited by Cetrorelix. Although GnRH resulted in a significant increase in ppERK-n in cells treated with PD184352 (178.45 ± 7.50 AFU) and in cells treated with RO31-8425 (196.40 ± 1.60 AFU), the increase was decreased compared to control cells by 70% and 50%, respectively ($P<0.05$). Similar GnRH effect was seen on EGr1-zsGreen (Figure 4.1D). GnRH caused a significant increase in Egr1-zsGreen (from 208.65 ± 4.10 AFU to 234.03 ± 7.14 AFU) and this effect was completely abrogated by PD184352, RO31-8425, and Cetrorelix but not by the other treatments.

Of the data in panel C, Two-way ANOVAs revealed that stimulus, inhibitor and stimulus-inhibitor interactions were significant sources of variation. Post-hoc tests revealed that GnRH caused a significant increase in NFAT1c-EFP-n:c translocation (from 0.84 ± 0.03 to 1.22 ± 0.05) and that this effect was significantly inhibited by Cetrorelix and CsA (100% reduction). Likewise, GnRH caused a significant increase in NFAT-RE-asRed-n+c, from 139.24 ± 2.15 AFU to 173.10 ± 4.06 AFU, and this effect was completely abrogated by Cetrorelix and CsA (Figure 4.4D).

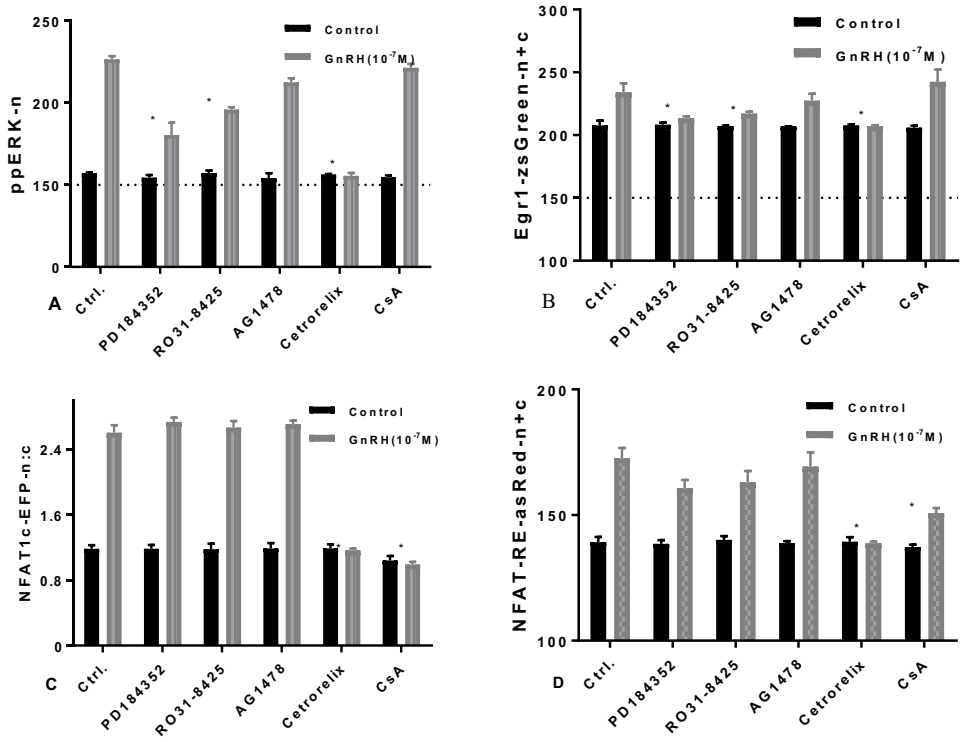

Figure 4.4. Pharmacological inhibition of GnRH signalling in Ad mGnRHR transduced HeLa Cells

LβT2 cells were cultured and treated as described in Chapter 2. Then the indicated inhibitors were applied for 30 min prior to stimulation for 5 min (in A and D) or 6 hr (in B and E) with 0 or 10^{-7}M GnRH. The cells were then fixed and stained for ppERK and nuclei. The figures show means ±SEMs, n=3, each with triplicate wells for each condition and three fields of view/well. The black columns represent the unstimulated group where the cells were subjected only to the inhibitors, except for the control group (Ctrl) without inhibitor. The grey columns represent cells subjected to the inhibitors prior to GnRH stimulation. The star (*) shows significant inhibition of GnRH signalling ($P<0.05$) in cells subjected to inhibitors (grey columns) comparing to Ctrl (the first grey column). The F (5,20) = 44.68 (A), F (5,20) = 7.43 (B), F (5,20) = 147.30 (C), F (5,20) = 23.70 (D). The dotted lines represent the background values for each measurement.

4.3.5 Pharmacological inhibition of PDBu signalling in Ad mGnRHR transduced HeLa Cells

As shown in figure 4.5, pre-treatment of the cells with the indicated inhibitors caused variable reductions in PDBu signalling to ERK, Egr1-zsGreen, and NFAT-RE-asRed. Separate two-way ANOVAs of the data in panels A and B revealed that stimulus, inhibitor and stimulus-inhibitor interactions were significant sources of variation. Post-hoc tests demonstrated that PDBu caused a significant increase in ppERK-n (from 137 ± 0.5 to 240 ± 1.2 AFU) and that this effect was significantly reduced by PD184352 and RO31-8425, but not by AG1478, Cetrorelix or CsA (Figure 4.5A). In PD184352-treated and RO31-8425-treated cells, although PDBu caused a significant increase in ppERK-n, the increase was statistically decreased compared to control cells (70% reduction, $P<0.05$). Similarly, PDBu caused a significant increase in Egr1-zsGreen (from 207 ± 2.8 to 360 ± 13 AFU) and this effect was inhibited by PD184352 and R031-8425 (Figure 4.5B). The PKC inhibitor is abrogated the effect of PDBu -mediated Egr1-zsGreen expression (220 ± 8 AFU, ~95% reduction). In PD184352-treated cells, although PDBu resulted in a significant increase in Egr1-zsGreen expression, the increase was statistically decreased compared to control cells (257 ± 4 AFU, 65% reduction).

Of the data in panel C and D, Two-way ANOVAs revealed that neither stimulus nor inhibitor were significant sources of variation. PDBu had no effect on NFAT1c-EFP translocation. Two-way ANOVAs of the data in panel D revealed that only stimulus was a significant source of variation. PDBu caused a significant increase in NFAT-RE-asRed (from 138.26 ± 1.73 to 159.10 ± 5.38 AFU). A partial reduction by ~30%

on the expression level of NFAT-RE-asRed was observed in cells treated with PD184352 or Ro31-8425, however, this effect was not significant (P>0.05).

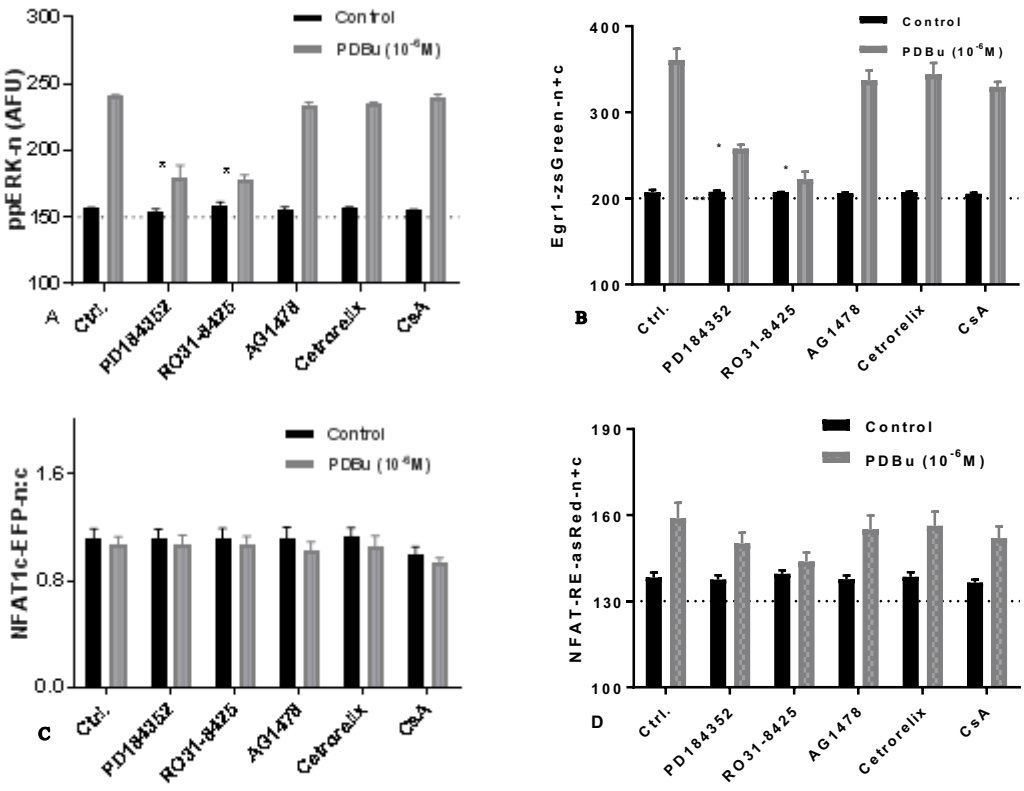

Figure 4.5. Pharmacological inhibition of PDBu signalling in Ad mGnRHR transduced HeLa cells.

Cells were cultured as described in Chapter 2. Then the indicated inhibitors were applied for 30 min prior to stimulation for 5 min (in A and D) or 6 hr (in B and E) with 0 or 10^{-6} M PDBu, they were then fixed and stained for ppERK and nuclei. The figures show means ±SEMs, n=3-4, each with triplicate wells for each condition and three fields of view/well. The black columns represent the unstimulated group where the cells were subjected only to the inhibitors, except for the control group (Ctrl) without inhibitor. The grey columns represent cells subjected to the inhibitors prior to GnRH stimulation. The star (*) shows significant inhibition of GnRH signalling (P<0.05) in cells subjected to inhibitors (grey columns) comparing to Ctrl (the first grey column). The F (5,30) = 45.00 (A), F (5,20) = 11.21 (B), F (5,30) = 13.40 (D). The dotted line represents the background values for each measurement.

4.3.6 Pharmacological inhibition of EGF signalling in Ad mGnRHR transduced HeLa cells.

HeLa cells were subjected to different inhibitors (outlined in figure 4.6) prior to stimulation with 10^{-8} M EGF. Pre-treatment of the cells with the indicated inhibitors caused variable reductions in EGF signalling to ERK and NFAT1c-EFP.

As shown in figure 4.6, two-way ANOVAs of the data in panel A revealed that stimulus, inhibitor and stimulus-inhibitor interactions are significant sources of variation. Post-hoc tests revealed that EGF caused a significant increase in ppERK-n (from 156.74 ± 0.56 to 244.02 ± 4.10). Comparing the effect of EGF in the control group to the treated one revealed that EGF signalled significantly under all tested condition. A partial reduction by ~25% was observed in AG1478-treated cells, however, this effect was not significant ($P>0.05$). In contrast, EGF had no significant effect on Egr1-driven zsGreen expression in HeLa cells ($P>0.05$).

Two-way ANOVAs of the data in panel C revealed that stimulus, inhibitors, and stimulus-inhibitor interaction were significant sources of variation. As shown in figure 4.6C, post-hoc tests revealed that EGF caused a significant increase in NFAT1c-EFP-n:c (from 1.12 ± 0.06 to 2.00 ± 0.12), and this effect was significantly inhibited by AG1478 and CsA (100% reduction) but not by PD184352, RO31-8425 or Cetrorelix (Figure 4.3C). On the other hand, EGF had no effect on NFAT-RE- driven asRed expression ($P>0.05$).

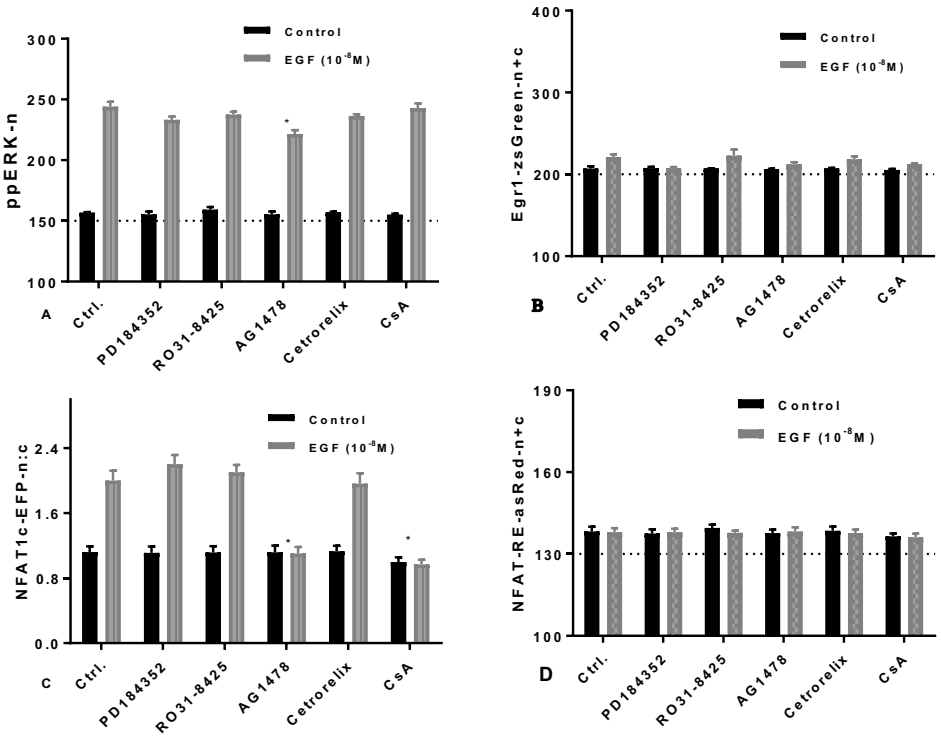

Figure 4.6. Pharmacological inhibition of EGF signalling in Ad mGnRHR transduced HeLa cells.

HeLa cells were cultured and treated as described in Chapter 2. Then the indicated inhibitors were applied for 30 min prior to stimulation for 5 min (in A and D) or 6 hr (in B and E) with 0 or 10^{-8} M EGF. Cells were then fixed and stained for ppERK and nuclei. The figures show means ±SEMs, n=3, each with triplicate wells for each condition and three fields of view/well. The black columns represent the unstimulated group where the cells were subjected only to the inhibitors, except for the control group (Ctrl) without inhibitor. The grey columns represent cells subjected to the inhibitors prior to GnRH stimulation. The star (*) shows significant inhibition of GnRH signalling ($P<0.05$) in cells subjected to inhibitors (grey columns) comparing to Ctrl (the first grey column). The F (5,30) = 7.61 (A), F (5,30) = 77.78 (C). The dotted lines represent the background values for each measurement.

4.3.7 Pharmacological inhibition of GnRH signalling in Ad mGnRHR transduced MCF-7 cells.

Separate two-way ANOVAs of the data in figure 4.7, panels A and C revealed that stimulus, inhibitor and stimulus-inhibitor interaction were a significant source of variation. Post-hoc tests revealed that EGF caused a significant increase in ppERK-n (from 157.41 ± 3.23 to 193.12 ± 10.42). This effect was significantly reduced by PD184352 and Cetrorelix but not by RO31-8425, AG1478, or CsA (Figure 4.7A). R031-8425 caused a 30% reduction in the GnRH effect on Egr1-zsGreen but this effect did not reach statistical significance ($P>0.05$). Likewise, post-hoc test showed a marked increase in NFAT1c-EFP-n:c by GnRH (from 1.12 ± 0.13 to 1.61 ± 0.21). This effect was significantly reduced by both Cetrorelix and CsA (100% reduction).

Of the data in panels B and D, separate two-way ANOVAs revealed that neither stimulus nor inhibitor were a significant source of variation. GnRH had no effect on Egr1 driven zsGreen expression or NFAT-RE-driven asRed expression ($P>0.05$).

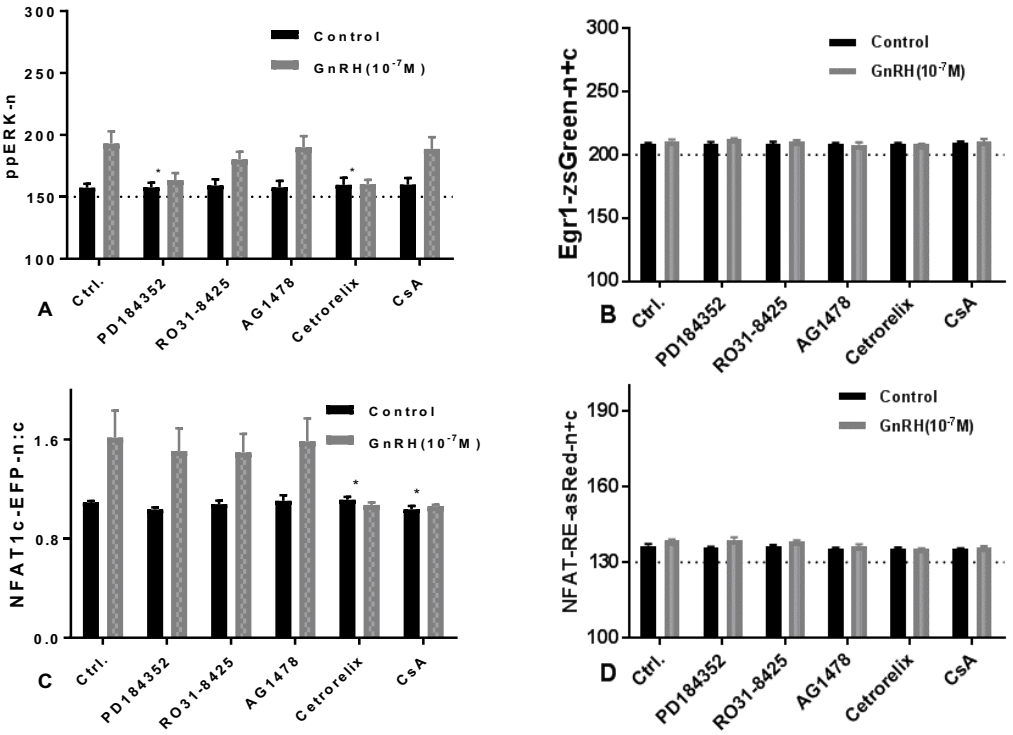

Figure 4.7. Pharmacological inhibition of GnRH signalling in Ad mGnRHR transduced MCF-7 cells.

Cells were cultured as described earlier. The cells were stimulated with 0 or 10^{-7} M GnRH for 5min (A and B) or 6 hr (C and D), they were then fixed and stained for ppERK and nuclei. Digital images and analysis were acquired (detailed under section 2.8). The figures show means ±SEMs, n=3, each with triplicate wells for each condition and three fields of view/well. The black columns represent the unstimulated group cells where the cells were subjected only to the inhibitors, except (Ctrl). The grey columns represent cells subjected to the inhibitors prior to GnRH stimulation. The star (*) shows significant inhibition of GnRH signalling ($P<0.05$) in cells subjected to inhibitors (grey columns) comparing to Ctrl (the first grey column). The F (5,30) = 17.50 (A), F (5,30) = 6.10 (C). The dotted lines represent the background values for each measurement.

4.3.8 Pharmacological inhibition of PDBu signalling in MCF-7 cells

As shown in figure 4.8, pre-treatment of the cells with the indicated inhibitors caused variable reductions in PDBu signalling to ERK, NFAT1c-EFP, Egr1zsGreen, and NFAT-RE-asRed. Separate two-way ANOVAs of the data in panel A and B revealed stimulus, inhibitor and stimulus-inhibitor interactions were significant sources of variation. Post-hoc tests revealed that PDBu caused a significant increase in ppERK-n (from 157.40 ± 3.23 to 219.46 ± 12.63 AFU) and that this effect was significantly inhibited by PD184352 and RO31-8425, but not by AG1478, Cetrorelix or CsA (Figure 4.8A). Similarly, PDBu caused a significant increase in Egr1-zsGreen (from 208.21 ± 1.2 4to 240.31 ± 5.15 AFU), and this effect was inhibited by PD184352 and R031-8425 (Figure 4.8B).

On the other hand, separate two-way ANOVAs of the data in panel C and D revealed that neither stimulus nor inhibitor were significant sources of variation. As shown, PDBu had no effect on NFAT1c-EFP translocation, and no measurable effect on the NFAT-RE-asRed expression was observed in this cell line ($P>0.05$).

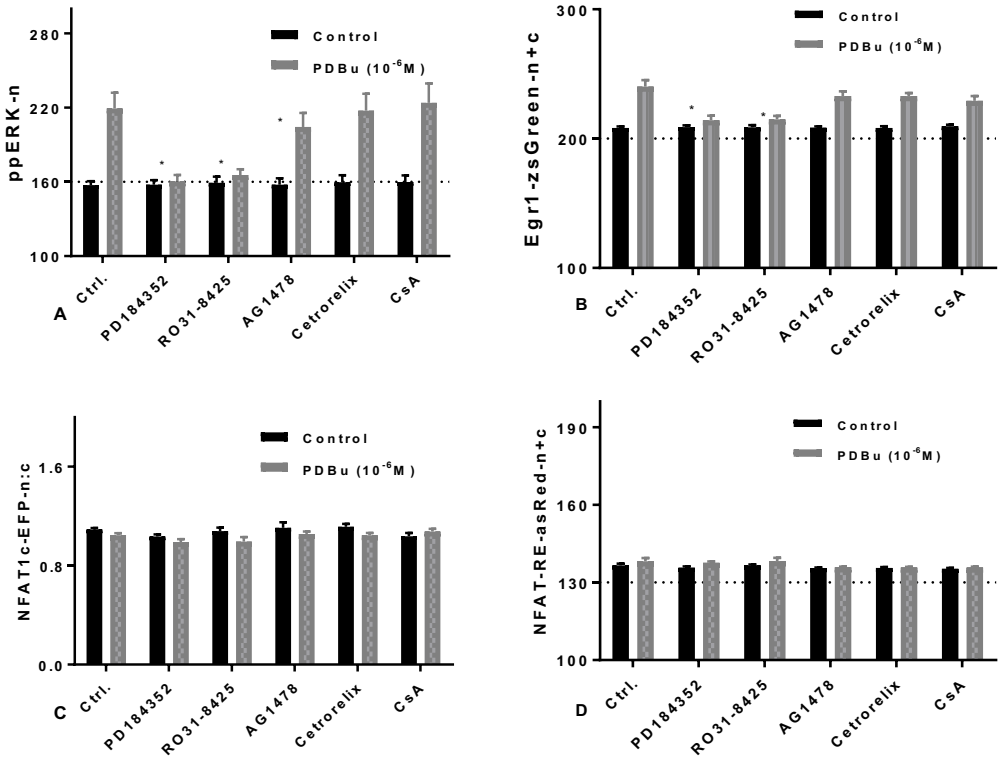

Figure 4.8. Pharmacological inhibition of PDBu signalling in MCF-7 cells

Cells were cultured as described earlier. The cells were stimulated with 0 or 10^{-6} M PDBu for 5min (A and B) or 6 hr (C and D), they were then fixed and stained for ppERK and nuclei. Digital images and analysis were acquired (detailed under section 2.8). The figures show means ±SEMs, n=3,5, each with triplicate wells for each condition and three fields of view/well. The black columns represent the unstimulated group cells where the cells subjected only to the inhibitors, except (Ctrl). The grey columns represent cells subjected to the inhibitors prior to GnRH stimulation. The star (*) shows significant inhibition of GnRH signalling ($P<0.05$) in cells subjected to inhibitors (grey columns) comparing to Ctrl (the first grey column). The F (5,30) = 23.26 (A), F (5,30) = 46.63 (B). The dotted lines represent the background values for each measurement.

4.3.9 Pharmacological inhibition of EGF signalling in MCF-7 cells.

Two-way ANOVAs show that stimulus, inhibitors, and stimulus-inhibitor interaction were significant sources of variation (Figure 4.9). Post-hoc test showed that EGF caused a significant increase in ppERK. The ppERK-n level increased from 157.40 ± 3.23 AFU to 253.31 ± 20.10 AFU. Comparing the effect of EGF in the control group to the treated one revealed that the effect of EGF-mediated ERK signalling was significantly inhibited by PD18435 and AG1478 but not by RO31-8425, RO31-8425, Cetrorelix, or CsA. Notably, although in PD184352-treated and AG1478-treated cells EGF resulted in a significant increase in ppERK-n, the increase was statistically decrease compared to control cells. The ppERK-n was 199.34 ± 14.01 AFU (60% reduction) by MEK inhibitor, and 182.02 ± 11.27 AFU by EGFR inhibitor (70% reduction). In contrast, no measurable effect of EGF on the other measurements (Egr1-zsGreen, NAFT1c-EFP, NFAT-RE-asRed) was observed in this cell line (Figure 4.9B, C and D).

The effects of these inhibitors on ERK and NFAT activities and their transcriptional readouts (Egr1-zsGreen and NFAT-RE-asRed) in the three cellular models are summarised in figure 4.10.

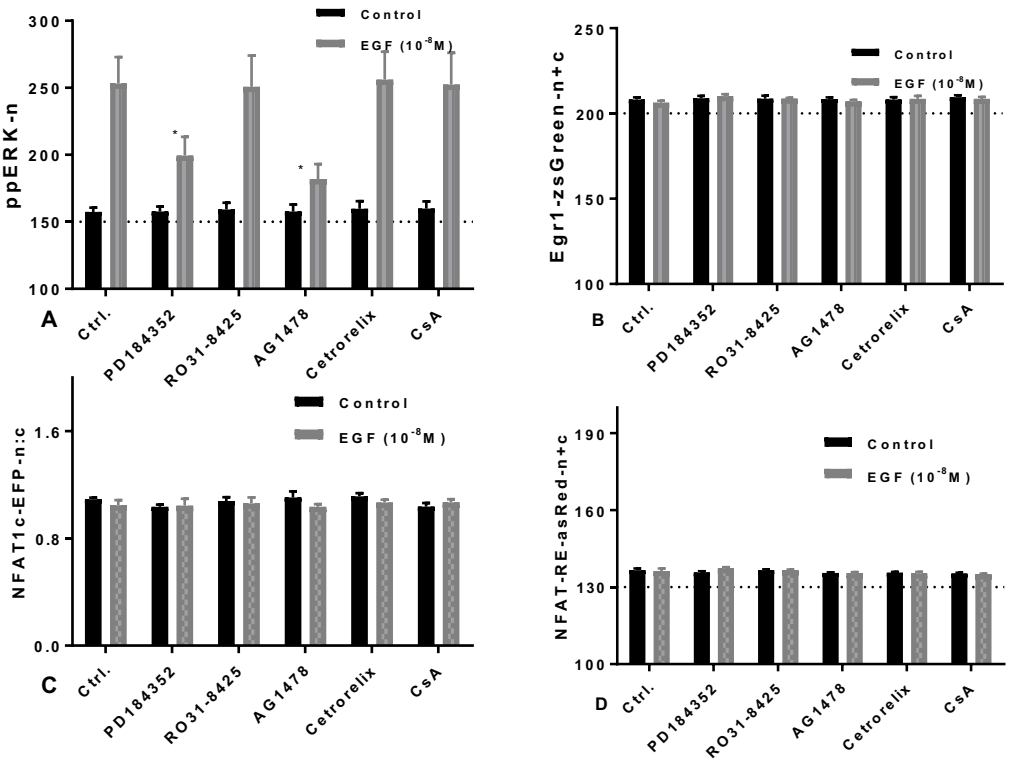

Figure 4.9. Pharmacological inhibition of EGF signalling in MCF-7 cells.

Cells were cultured as described in chapter 2. The cells were stimulated with 0 or 10^{-8} M PDBu for 5min (A and B) or 6 hr (C and D), they were then fixed and stained for ppERK and nuclei. Digital images and analysis were acquired as detailed under section 2.8. The figures show means ±SEMs, n=3, each with triplicate wells for each condition and three fields of view/well. The black columns represent the unstimulated group cells where the cells subjected only to the inhibitors, except (Ctrl). The grey columns represent cells subjected to the inhibitors prior to EGF stimulation. The star (*) shows significant inhibition of GnRH signalling ($P<0.05$) in cells subjected to inhibitors (grey columns) comparing to Ctrl (the first grey column). The F (5,30) = 11.02 (A). The dotted lines represent the background values for each measurement.

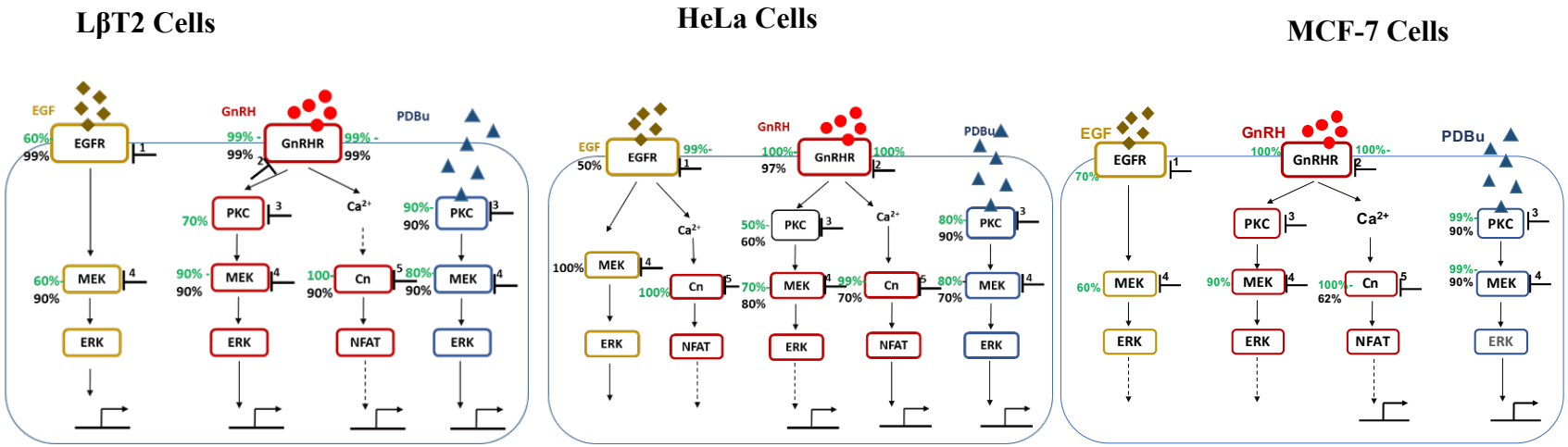

Figure 4.10. A schematic diagram of signalling pathway in LßT2, HeLa, and MCF-7 cells

Coloured boxes show proteins identified as mediators by sensitivity to inhibitors (i.e. >50% inhibition in ppERK and/or Egr1-zsGreen assays, or in NFAT1c-EFP and NFAT-RE-asRed assays). The numbers from 1-5 represent the drugs that inhibit 1-EGFR (AG1478), 2-GnRHR (Cetrorelix), 3-PKC (RO318425), 4-MEK (PD184352) and 5-AC (Cyclosporine A). The green numbers show the ~% reduction of ERK or NFAT activity in cells subjected to inhibitors. The black numbers show % reduction of the Egr1-zsGreen or NFAT-RE-asRed expression in cells subjected to inhibitors. No measurable effect of EGF on NFAT-RE-asRed in the three cell lines was observed. Thus, the transcriptional response is excluded here. For the MCF-7 cell line, ANOVAs reveal no significant effect of EGF or GnRH on Egr1-zsGreen responses and the GnRH effect on the NFAT1c-EFP response was very small. Accordingly, the inhibitor- sensitivity and % inhibition data are based solely on ppERK and NFAT1c-EFB- n:c readouts. The percentage numbers (approximate numbers) were calculated by working out the difference in expression level between Ctrl (grey column, Figure 4.1-4.9) and treated groups, where cells subjected to inhibitors prior to stimulation with GnRH, EGF or PDBu (grey columns, Figure 4.1-4.9). Then divided the number by the original number and multiply the answer by 100.

4.4. Discussion

The hypothalamic neuropeptide GnRH-I acts on GPCRs on the anterior pituitary gonadotrophs. It causes a PKC-mediated activation of ERK and Ca^{2+}-mediated activation of NFAT, both of which mediate GnRH effects on gonadotrophin expression [2, 24, 123, 140]. GnRHR signalling has been shown to be dependent on cell context but that the reasons for this are unknown. This dependence was clearly seen in Chapter 3, where the kinetics of responses to GnRH differed in LβT2, HeLa and MCF-7 cells. Thus, the aim of this chapter was to further delineate network architecture in three cell lines using pharmacological inhibitors.

The effects of GnRHR agonists were previously demonstrated to be mimicked by GnRHR antagonists in hormone dependent cancer cells [351, 362-366], and this suggested that there might be no dichotomy between GnRHR agonists and antagonists in these cells. An explanation was that GnRHR ligands were acting through other receptor types, such as type II GnRHRs in hormone-dependent cancer cells [351]. However, the data here argue against this idea. This is because cetrorelix had no measurable effect a lone on any of the experimental readouts or in any of the cell types examined. The GnRHRs antagonists always blocked GnRH effects in all cell types. GnRH is the endogenous ligand for type I mammalian GnRHR and cetrorelix is a type I GnRHR antagonist. Thus, the data obtained here all indicate that GnRH is acting via type I GnRHR (endogenous or exogenous) in the three examined cell lines.

In primary pituitary cell cultures, the GnRHR acts mainly via $G\alpha_{q/11}$, driving the activation of ERK and NFAT pathways [145]. However, there is also evidence showing that GnRHRs can act via other G-proteins such as G_i and G_s in different cell

types (see Chapter 1, section 1.5.2) [362]. On the other hand, it was argued that GnRHRs do not act via $G\alpha_{q/11}$ in breast cancer cells [256]. Work here using NFAT translocation and NFAT-RE-driven asRed expression (as downstream readouts for Ca^{2+} mobilisation) and using ERK activation (as a downstream readout for PKC activation) revealed that GnRH activates these pathways in both HeLa and LβT2 cells. In MCF-7 cell line although GnRH activated ERK and NFAT pathways, its effect on the downstream transcriptional readouts of both ERK and NFAT was not significant. The results indicated that GnRH activates $G\alpha_{q/11}$ in all of them.

The use of CsA (Cn inhibitor) inhibited significantly GnRH effects on NFAT but not on ppERK in all three cell types (Figure 4.1, 4.4 and 4.7). These observations indicate that the two reporters of NFAT activation can both be used as a readout for Ca^{2+} elevation that drives the activation of CaM/Cn/NFAT pathway. In a similar way, the MEK inhibitor inhibited the effects of both GnRH and PDBu on ppERK. It also prevented their effects on Egr1-zsGreen responses in all three cell types, which implies that GnRH causes a PKC-mediated activation of ERK in these cells and that the Egr1-zsGreen is a reliable readout for ERK activation. However, the MEK inhibitor did not prevent GnRH effects on NFAT1c-EFP or NFAT-RE-asRed. In some systems PKC activation can modulate the function of Ca^{2+} ion channel increasing cytoplasmic Ca^{2+} concentration but this did not occur, as PDBu failed to activate either NFAT readout in all three cell lines [345].

Gonadotrophin releasing hormone is reported to cause a PKC-mediated transactivation of EGFR ligands and an EGFR-mediated activation of ERK in some cells [332, 367]. In fact, EGF was shown to stimulate ppERK in LβT2, HeLa and MCF-7 cells (Figure 3.11, Figure 3.12 and Figure 3.13), and the effect of GnRH on

ppERK was inhibited by RO-318425 (Figure 4.1, Figure 4.4 and Figure 4.7), which is consistent with the above observation. However, these results here do not examine the involvement of EGFR in ERK activation by GnRH. The AG1478 (EGFR inhibitor) inhibited the effects of EGF on the responses of ppERK and/or Egr1-zsGreen responses in all three cell types, showing both efficacy and specificity. AG1478 also, had no effect on PDBu or GnRH mediated ppERK activation in any of the cell types. Consequently, PKC activation seems not to cause sufficient EGFR activation for ERK activation in any of the examined cells here. GnRH causes a PKC-mediated ERK activation but EGFR-independent activation of ERK in LβT2 cells and HeLa cells.

The experimental results that are obtained from EGF-stimulated HeLa cells (Figure 4.6) revealed some interesting observations. EGF-mediated ppERK was not significantly inhibited by PKC inhibitor or MEK inhibitor, but the stimulus failed to increase Egr1-zsGreen expression in these cells. The underline reason behind this effect is unknown, but it contrasts with the effect of these inhibitors on PDBu (Figure 4.5), demonstrating efficacy of the inhibiters in these cells. However, the lack of the expression of Egr1-zsGreen might be related to the transient response of ppERK to EGF in these cells [341, 342]. In other words, if a sustained response is required for Egr1-zsGreen activation, this would explain the absence of transcriptional response to EGF here, it would also raise the possibility that inhibitors could also be more effective when a more sustained ppERK activation occurs. Another surprising observation is that EGF caused a marked increase in NFAT1c-EFP translocation in these cells. The effect was inhibited by AG1478, that might reflect PLCγ -mediated Ca^{2+} mobilisation by EGFR. The effect was only seen in HeLa cells extending the concept of context-dependent signalling to these receptors. Another interesting

observation was that GnRH and EGF both increased ppERK levels but failed to increase Egr1-zsGreen responses in MCF7 cells. Given that these cells are cancer cells, it could be a consequence of a protein found in these cells acts as corepressor binding and activating a specific repressor, which in turn binds to the promotor preventing the initiation of transcription of that gene [368]. In general, these observations could be a related to the way that cells were immortalised as described in Chapter 3. Overall, we can conclude that HeLa and MCF-7 cells might well be unsuited to further work on transcription regulation by GnRH, because GnRH did not measurable increase the expression of either transcriptional reporter in these cells.

To sum-up, in the three cell lines, GnRH-mediated ERK and NFAT signalling are GnRHR-dependent. PDBu-mediated ERK signalling is dependent on MEK and PKC, but no sign of signal to NFAT following PKC activator. EGF caused NFAT translocation in HeLa cells, but not in the other two cell lines. The context-dependence of GnRH signalling that was seen in Chapter 3 in comparison of response kinetics, can be extended to differential sensitivity to inhibitors (summarised in figure 4.10), but no evidence was seen here for GnRH acting via EGFR transactivation in any of the examined cell types. However, despite the % reduction in response that was given by an inhibitor, it does not tell us anything about the relative importance of any given effector or pathway for GnRH signalling. Therefore, in the following chapters a statistical measure derived from information theory is used as alternative approach to quantify information transfer via GnRHRs.

Chapter 5- Sensing GnRH: An information theoretic approach

5.1. Background

Most work on cell signalling mechanisms is based on the measurement of average responses from large cell populations, despite cell-cell variation. This variability is critical for cells behaviour, as each cell has to sense the environment for appropriate decisions [275, 282, 285, 300]. Information theoretic approaches that take cell-cell variability into account are increasingly being used in cell biology to study the effect of this heterogeneity on transferred information through signalling pathways [153]. Here, information can be quantified as the uncertainty about the environment that is removed by signalling, and one way of doing this is to calculate MI between system inputs and outputs [292].

In Chapter 4, the use of pharmacological inhibitors helped to map the network architecture of ERK and NFAT in the three cellular models (HeLa, LβT2 and MCF-7 cells), but the percentage reduction given by the inhibitors (summarised in Figure 4.10), did not tell us how much information transferred through each pathway. Accordingly, the focus was placed here on the use of the information theoretic approach as a tool that might provide biologist with better insight into the route carrying most information, so that can be targeted for therapeutic manipulation.

The aim of this chapter was using MI to quantify information transfer via GnRHRs to ERK or NFAT, using two distinct readouts (transcriptional and non-transcriptional) for their activation. The work here was done based on the following hypotheses: First, the amount of information transfer might be specific to the cellular model, and to test this hypothesis, different cell types were used (LßT2, HeLa and MCF-7 cells). Second, GnRHRs activate a bifurcating signalling system, and cells might gain additional information by sensing multiple pathways within the network. To investigate this

hypothesis, joint MI between GnRH concentration and responses measured in the same cells were calculated. Third, the conditions of the chosen assay might lead to underestimation of MI values, so the protocols used were validated.

5.2. Materials and methods

For MI measurement, at first, full concentration-response curves were constructed in three cell lines and at 3 time points. Images were collected from 2-3 fields of view per well and the individual cells measures were used to calculate MI between GnRH concentration and the experimental readouts at each time point. The images used for this analysis are from experiments already described in Chapter 3 and for which population averaged responses have been reported in figures 3.5, 3.6, 3.7, 3,8, 3,9 and 3.10. In these experiments ppERK and NFAT1c-EFP measures were determined in the same cells, enabling measurement not only of I(ppERK; GnRH) and I(NFAT1c-EFP; GnRH) but also of joint MI (as described in Chapter 2).

In a similar way, cells expressing the Egr1-zsGreen and NFAT-RE-asRed (imaging readouts for ERK-driven and NFAT-driven transcription, respectively) were used for calculation of I(Egr1-zsGreen; GnRH) and I(NFAT-RE-asRed; GnRH), as well as joint MI. The high content imaging platform used provides the same experimental measures for each individual cell (approximately 100 to 600 cells per well for HeLa and MCF-7 cells and up to 1500 cells per well for LβT2 cells) and this enables calculation of frequency-distribution (FD) plots. Notably, an MI of 1 is obtained when 2 different states of the environment can be unambiguously distinguished, and this would require that two FD plots do not overlap.

5.3. Results

5.3.1. Measurement of GnRHR-mediated information transfer to ERK or NFAT1c-EFP in Ad mGnRHR transduced HeLa cells.

HeLa cells transduced with Ad NFAT1c-EFP and Ad mGnRHRs were stimulated with varied concentrations of GnRH for 5, 20 or 60 min before staining for nuclei and ppERK. The cells were then imaged for calculation of the nuclear fraction (NF) of NFAT1c-EFP as well as nuclear ppERK stain intensity (ppERK-n). This chapter describes re-analysis of the experiments shown in Chapter 3 and the population averaged data are repeated here for simplicity. As shown in figure 5.1A, GnRH caused a concentration and time-dependent increase in ppERK that was rapid and transient (i.e. maximal at 5 min but reduced by 60 min) as well as a concentration and time-dependent increase in nuclear translocation of NFAT1c-EFP (Figure 5.1B) that was slower in onset (maximum at 20 min) and was more sustained (comparable at 20 and 60 min).

Binning individual cells according to the log of the ppERK-n (Figure 5.1D) showed cell-cell variation in the ppERK levels. GnRH increased the population averaged ppERK levels by shifting the FD plots rightward. There was no evidence for such distinct cell populations, as cells showed a graded response, rather than an all-or-nothing response. In a similar way, individual cells in figure 5.1E were binned according to the NF of the NFAT1c-EFP, and these revealed pronounced cell-cell variation, a rightward shift of FD plots on stimulation by GnRH. The pronounced overlaps between the FD plots for stimulated and unstimulated cells suggest that MI values will be low. As shown in Figure 5.1C, I(ppERK; GnRH) values were maximal at 5 min (0.49 ± 0.04 Bits) reduced to 0.18 ± 0.01 Bits by 60 min (Figure 5.1 E).

I(NFAT1c-EFP-NF; GnRH) values were 0.16 ± 0.03 Bits at 5 min and increased to 0.30 ± 0.04 Bits by 60 min (Figure 5.1C).

In the above data, MI values were always less than 1 Bit despite system inputs of 3 Bits (i.e. 2^3 different GnRH concentrations) implying that most information is lost through signalling networks. However, it is possible that information loss is mitigated by the joint sensing of multiple pathways within the network. The Joint MI values were comparable at all time points with 0.52 ± 0.01 Bits at 5 min, 0.44 ± 0.08 Bits at 20 min and 0.30 ± 0.04 Bits at 60 min and were always greater than MI values for either response alone. Thus, additional information was gained by joint sensing, but the increase was small.

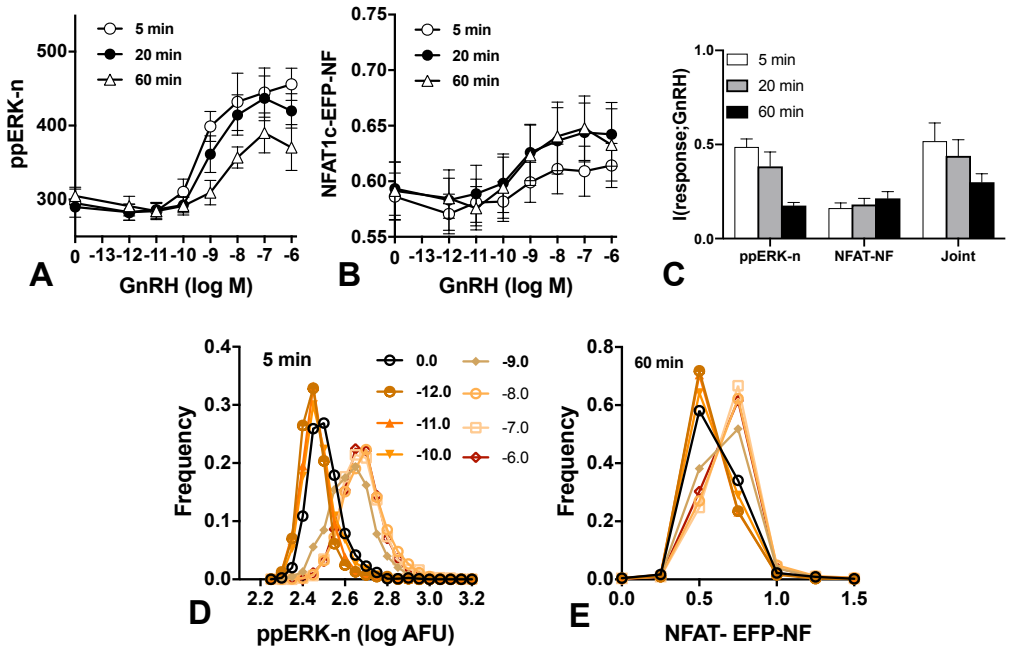

Figure 5.1. Measurement of GnRHR-mediated information transfer to ERK or NFAT1c-EFP in Ad mGnRHR transduced HeLa cells.

Cells were cultured and treated as described in Chapter 2. They were then stimulated for 5, 20 or 60 min with 0 or 10^{-12} – 10^{-6} M GnRH before being fixed and stained (nuclei and ppERK) and used for digital image acquisition and analysis. Panels A and B show population averaged ppERK-n in AFU, and NFAT1c-EFP-NF values (mean ± SEM, n=3) and are repeated from figure 3.5 for simplicity. Single cell data from complete concentration-response curves were then used to calculate the MI between GnRH and ppERK-n or NFAT1c-EFP-NF as well as the joint MI for GnRH sensing by both pathways (Panel C). Representative FD plots are shown for cells stimulated 5 min (D) or 60 min (E) with the indicated concentrations of GnRH.

5.3.2. Measurement of GnRHR-mediated information transfer to Egr1-zsGreen or NFAT-RE-asRed in Ad mGnRHR transduced HeLa cells

HeLa cells were transduced with Ad mGnRHR, Ad Egr1-zsGreen and Ad NFAT-RE-asRed. The cells were then stimulated with different concentration of GnRH for 4, 6, and 8 hr, before being imaged and analysed as described in Chapter 2. As shown in figure 5.2A and B, GnRH caused concentration and time-dependent increases in Egr1 driven zsGreen expression and NFAT-RE driven asRed expression. The expression levels were relatively similar in both (seen at 4 hr and peaked at 8 hr).

Binning individual cells according to the log of the Egr1-zsGreen-n+c showed pronounced variation between cells in the Egr1-zsGreen levels. GnRH increased the population averaged Egr1-zsGreen levels by shifting the FD plots rightward. There was no evidence for distinct cell population as the data showed graded responses rather than an all-or-nothing response (Figure 5.2D). In the same way, binning individual cells according to the log of the NFAT-RE-asRed-n+c revealed pronounced cell-cell variation, a rightward shift on stimulation by GnRH and no evidence for distinct GnRH responsive and GnRH non-responsive cell populations (Figure 5.2E).

The pronounced overlaps between the FD plots for stimulated and unstimulated cells suggest that MI values will be low. As shown in figure 5.2C, the I(Egr1-zsGreen-n+c; GnRH) values was 0.19 ± 0.02 Bits at 4 hr, increased slightly to 0.24 ± 0.03 Bits at 6 hr and remined sustained for the next two hr. The I(NFAT-RE-asRed; GnRH) values were gradually increased over the time. The MI values were 0.14 ± 0.02 Bits at 4 hr, 0.22 ± 0.3 Bits at 6 hr and 0.26 ± 0.05 Bits at 8hr. However, the joint MI values were higher than MI values for each response alone (0.30 ± 0.03 Bits at 4hr increased to 0.40 ± 0.07 Bits by 8 hr).

As shown, the MI values were always <1 Bit despite system inputs of 3 Bits. However, since the Egr1-zsGreen and NFAT-RE-asRed were measured in the same cells, sensing both pathways were possible. The Joint MI values were comparable at all time points (0.34 ± 0.03 Bits at 4 and 6 hr and 0.40 ± 0.07 Bits at 8 hr) and were always greater than MI values for either response alone (Figure 5.2C).

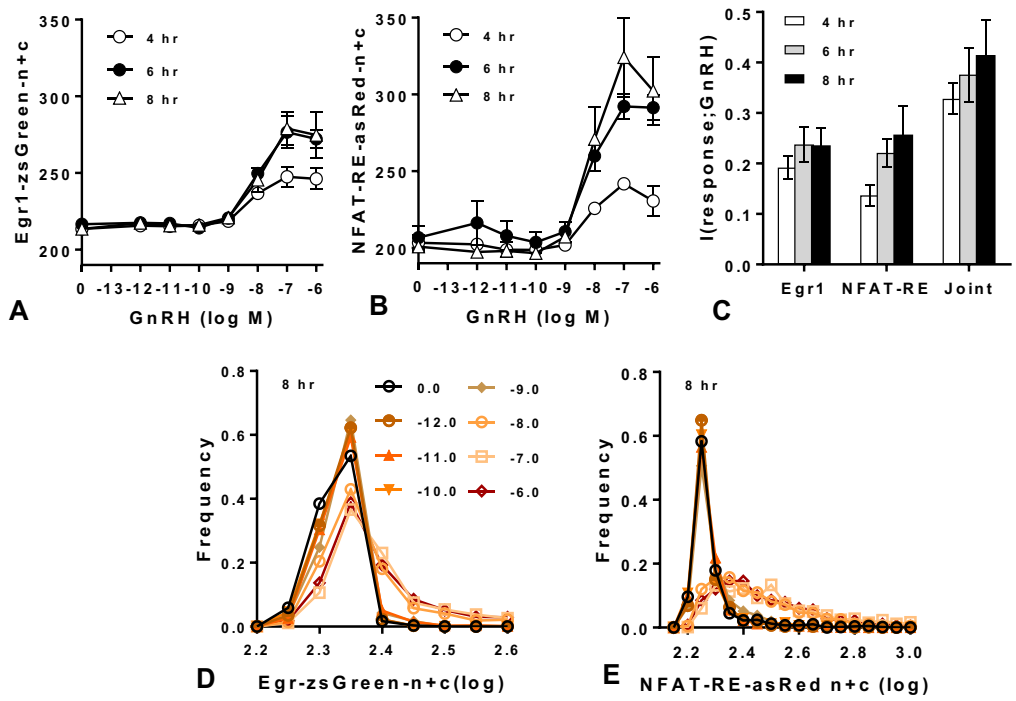

Figure 5.2. Measurement of GnRHR-mediated information transfer to Egr-1driven zsGreen or NFAT-RE driven asRed expressions in HeLa cells

Cells were cultured as described in Chapter 2 and stimulated with GnRH for the indicated times and with the indicated concentrations. The cells were then fixed and stained (nuclei) and used for digital image acquisition and analysis. A and B show population average Egr1-zsGreen-n+c and NFAT-RE-asRed-n+c values in AFU (means ± SEMs, n=3-4), and are repeated from figure 3.5 Chapter 3 for simplicity. Single cell data from complete concentration-response curves were then used to calculate the MI between GnRH and Egr1-zsGreen-n+c or NFAT-RE-asRed-n+c, as well as the joint MI for GnRH sensing by both pathways, and these are shown in panel C. Representative FD plots are shown in D and E for cells stimulated 8 hr with the indicated concentrations of GnRH.

5.3.3. Measurement of GnRHR-mediated information transfer to ERK or NFAT1c-EFP in LßT2 cells.

LßT2 cells transduced with Ad NFAT1c-EFP were stimulated with varied concentrations of GnRH for 5, 20 or 60 min before staining for nuclei and ppERK. The cells were then imaged for calculation of the NFAT1c-EFP-NF, as well as nuclear ppERK stain intensity. As shown in figure 5.3A, GnRH caused a concentration and time-dependent increase in ppERK-n, that was rapid and sustained (maximal at 5 min and maintained at a similar level for 60). GnRH also caused concentration and time-dependent increase in the nuclear translocation of NFAT1c-EFP-NF, which was slower in onset and was maximum at 60 min (Figure 5.1B).

Binning individual cells according to the log of the ppERK-n stain intensity revealed pronounced cell-cell variation in the ppERK levels. GnRH increased the population averaged ppERK levels by shifting the FD plots rightward. No evidence was found for GnRH responsive and GnRH non-responsive cell populations, as a graded response rather than an all-or-nothing response was seen (Figure 5.3D). Likewise, binning individual cells according to the NF of the NFAT1c-EFP revealed pronounced cell-cell variation and a rightward shift on stimulation by GnRH. No evidence was found for such distinct cell populations (Figure 5.3E).

The pronounced overlaps between the FD plots for stimulated and unstimulated cells suggest that MI values will be low. As shown in figure 5.3C, the I(ppERK; GnRH) values were comparable at all time points (0.41 ± 0.03 Bits at 5, 20 and 60 min). The I(NFAT1c-EFP-NF; GnRH) values were 0.20 ± 0.1 Bits at 5 min (lower than ppERK at the same time) and increased to 0.52 ± 0.03 Bits by 60 (Figure 5.3C). The Joint MI values were comparable at all time points and were greater than MI values for either

response alone. The values were 0.58 ± 0.08 Bits at 5 min and 0.7 ± 0.1 Bits at 60 min.

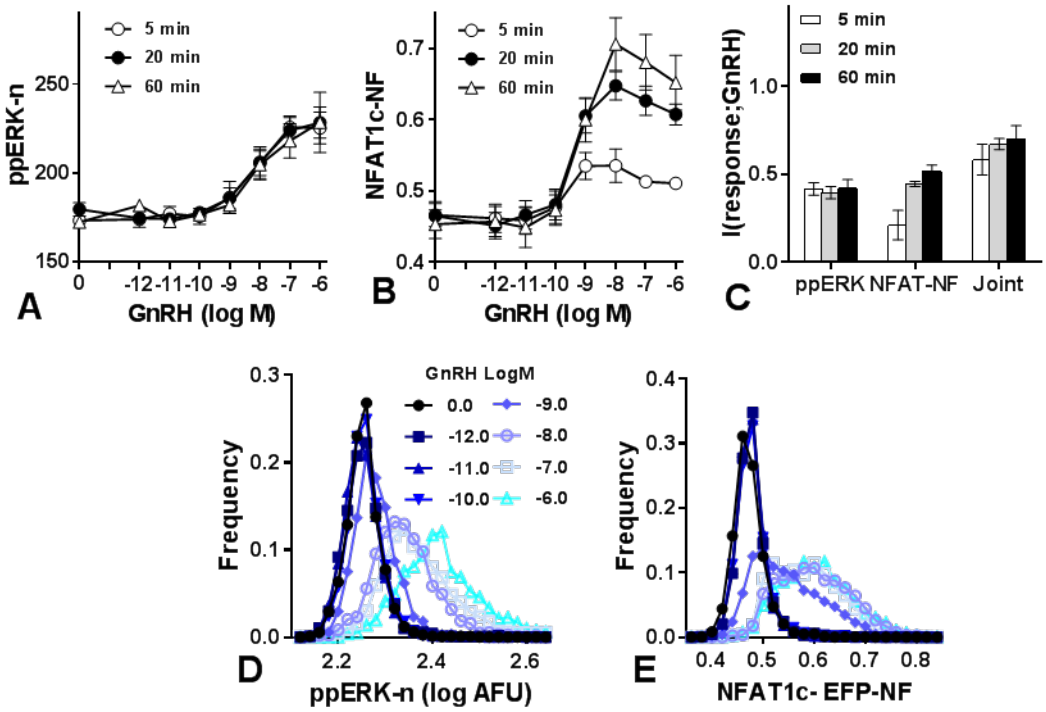

Figure 5.3. Measurement of GnRHR-mediated information transfer to ERK or NFAT1c-EFP in LßT2 cells

LßT2 Cells were cultured and treated as described in Chapter 2. They were then stimulated for 5, 20 or 60 min with 0 or 10^{-12} – 10^{-6} M GnRH before being fixed and stained (nuclei and ppERK) and used for digital image acquisition and analysis. A and B show population averaged ppERK-n in AFU, and NFAT1c-EFP-NF values (mean ± SEM, n=3) and are repeated from figure 3.7 for simplicity. Single cell data from complete concentration-response curves were then used to calculate the MI between GnRH and ppERK-n or NFAT1c-EFP-NF, as well as the joint MI for GnRH sensing by both pathways (Panel C). Representative FD are shown in panel D and E for cells stimulated 60 min with the indicated concentrations of GnRH.

5.3.4. Measurement of GnRHR-mediated information transfer to Egr1-zsGreen or NFAT-RE-asRed in LßT2 cells

LβT2 cells transduced with Ad Egr1-zsGreen and Ad NFAT-RE-asRed were stimulated with varied concentrations of GnRH for 4, 6 and 8 hr before staining for nuclei. The cells were then imaged and analysed as describe in Chapter 2. As shown in figure 5.4A and B, GnRH caused concentration and time-dependent increases in Egr1 driven zsGreen and NFAT-RE driven as Red expression. The responses of both readouts were slow in onset and peaked at 8 hr.

Binning individual cells according to the log of the Egr1-zsGreen-n+c stain intensity revealed pronounced cell-cell variation in the Egr1-zsGreen levels, and that GnRH increased the population averaged Egr1-zsGreen levels by shifting the FD plots rightward (Figure 5.4D). Similarly, binning individual cells according to the log of the NFAT-RE-asRed-n+c revealed pronounced cell-cell variation, a rightward shift on stimulation by GnRH (Figure 5.4E). No evidence was found for GnRH responsive and GnRH non-responsive cell populations, as the data showed graded responses rather than an all-or-nothing response (Figure 5.4D and E).

Figure 5.4C shows that the I(Egr1-zsGreen; GnRH) values were similar at all time points (~0.8 Bits). However, although the I(NFAT-RE-asRed; GnRH) values were gradually increased over the time, the MI values were considerably lower than I(Egr1-zsGreen; GnRH). The I(NFAT-RE-asRed; GnRH) values were 0.20 ± 0.03 Bits at 4 hr and increased to 0.35 ± 0.06 Bits by 8 hr. The joint MI values were higher than MI values for each response alone (0.90 ± 0.05 Bits at 4 hr increased to 1.00 ± 0.02 Bits by 8hr).

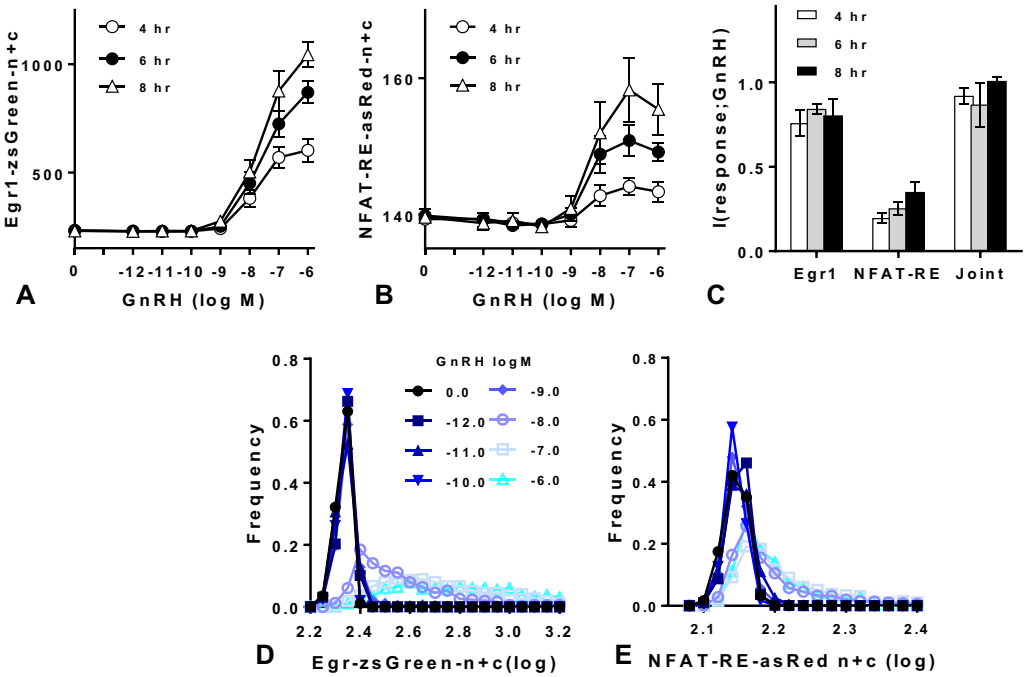

Figure 5.4. Measurement of GnRHR-mediated information transfer to Egr1-zsGreen or NFAT-RE-asRed in LßT2 cells

Cells were cultured as described in Chapter 2 and stimulated with GnRH for the indicated times and concentrations. Cells were then fixed and stained (nuclei) and used for digital image acquisition and analysis. A and B show population average Egr1-zsGreen-n+c and NFAT-RE-asRed-n+c values in AFU (means ± SEMs, n=3-4), and are repeated from Figure 3.8 for simplicity. Single-cell data from complete concentration-response curves were then used to calculate the MI between GnRH and Egr1-zsGreen-n+c or NFAT-RE-asRed-n+c, as well as the joint MI for GnRH sensing by both pathways. These values are shown in panel C. Single cell data were also used to generate FD plots by binning log-transformed Egr1-zsGreen and NFAT-RE-asRed values. Representative FD are shown in D and E for cells stimulated 8hr with the indicated concentrations of GnRH.

5.3.5. Measurement of GnRHR-mediated information transfer to ERK and NFAT1c-EFP in Ad mGnRHR transduced MCF-7 cells

MCF-7 cells transduced with Ad mGnRHR, Ad NFAT1c-EFP were stimulated with varied concentrations of GnRH at 5, 20 or 60 min, then fixed and stained for nuclei and ppERK. The cells were then imaged for calculation of the nuclear fraction of NFAT1c-EFP as well as nuclear ppERK stain intensity. As shown in figure 5.5A, GnRH caused a concentration and time-dependent increases ppERK-n that was rapid and transient (the maximal effect was at 5 min and returned to the basal condition by 60 min). Also, GnRH caused a concentration and time-dependent increase in the nuclear translocation of NFAT1c-EFP. The GnRH effect on NFAT1c-EFP translocation was rapid (like the ppERK response at the same time) but remained sustained during the examined period (60 min).

Binning individual cells according to the log of the ppERK-n stain intensity revealed pronounced cell-cell variation in the ppERK levels and that GnRH increased the population averaged ppERK levels by shifting the FD plots rightward (Figure 5.5D). No evidence was seen for GnRH responsive and GnRH non-responsive cell populations (the responses were graded). For the NFAT1c-EFP-NF data in Figure 5.5.C, the individual cells revealed pronounced cell-cell variation, a rightward shift on stimulation by GnRH and no evidence for GnRH responsive and GnRH non-responsive cell populations (Figure 5.5E).

The I(ppERK; GnRH) values were maximal at 5 min with 0.10 ± 0.03 Bits and reduced to 0.05 ± 0.01 Bits by 60 min. The I(NFAT1c-EFP-NF; GnRH) values were higher than I(ppERK; GnRH) values (~0.25 Bits during all time points, Figure 5.5C).

However, the joint MI values were higher than MI values for either response alone (~ 0.3 Bits).

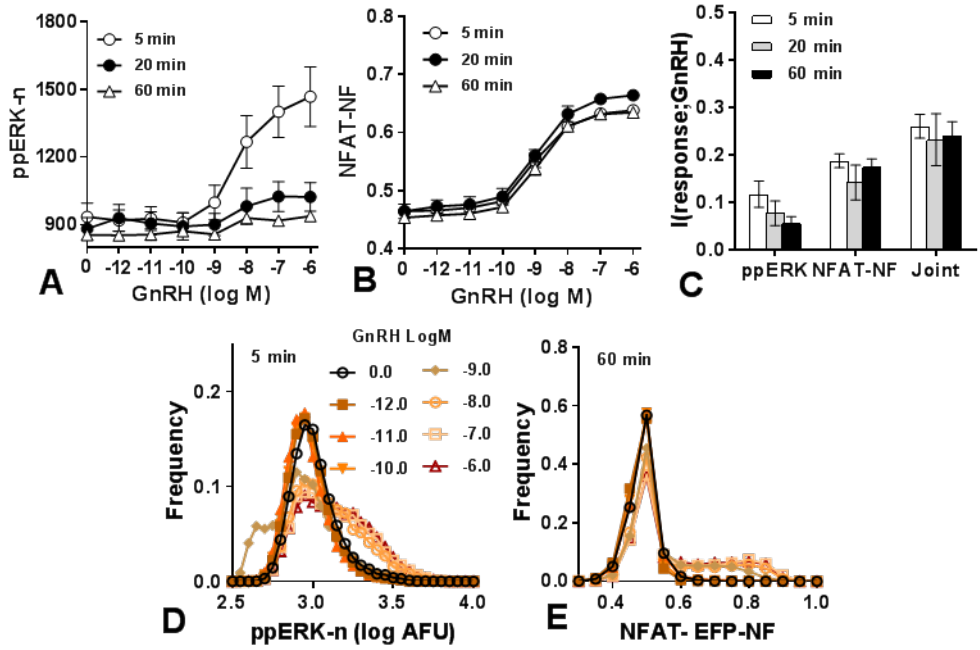

Figure 5.5. Measurement of GnRHR-mediated information transfer to ERK or NFAT1c in Ad mGnRHR transduced MCF-7 cells

Cells were cultured and treated as described in Chapter 2. They were then stimulated for 5, 20 or 60 min with 0 or 10^{-12} – 10^{-6} M GnRH before being fixed and stained (nuclei and ppERK) and used for digital image acquisition and analysis. A and B show population averaged ppERK-n in AFU, and NFAT1c-EFP-NF values (mean ± SEM, n=3) and are repeated from Figure 3.9 for simplicity. Single cell data from complete concentration-response curves were then used to calculate the MI between GnRH and ppERK-n or NFAT1c-EFP-NF, as well as the joint MI for GnRH sensing by both pathways (Panel C). Representative FD plots are shown for cells stimulated 5 min (D) or 60 min (E) with the indicated concentrations of GnRH.

5.3.6. Measurement of GnRHR-mediated information transfer to Egr1-zsGreen or NFAT-RE-asRed in MCF-7 cells

MCF-7 cells transduced with Ad Egr1-zsGreen and Ad NFAT-RE-asRed in addition to Ad mGnRHR were stimulated with varied concentrations of GnRH for 4, 6 and 8 hr before staining for nuclei. The cells were then imaged and analysed as describe in Chapter 2. As shown in figure 5.5A, GnRH had no effect on Egr1 driven zsGreen expression. Whereas, GnRH caused a concentration and time dependent increase NFAT-RE-driven asRed expression. Although the effect was relatively small, it was statistically significant ($P<0.05$) as detailed in Chapter 3.

Since GnRH had no measurable effect on the expression level of Egr1-zsGreen, binning individual cells according to the log of the Egr1-zsGreen-n+c stain intensity revealed no cell-cell variation (no response to GnRH concentrations, Figure 5.6 D). Thus, MI values were considerably small (~ 0.02 Bits). In a similar way, binning individual cells (in Figure 5.5D) according to the log of the NFAT-RE-asRed-n+c revealed that the effects of GnRH on NFAT-RE-asRed were considerably low. The overlap between the FD plots remained (Figure 5.6E). Accordingly, MI values were expected to be small. As shown in figure 5.6C, the I(NFAT-RE-asRed; GnRH) values were maximum ~0.03 Bits at 8 hr.

However, considering the possibility of mitigating the lost information by sensing multiple pathways within the network, and since Egr1-zsGreen and NFAT-RE-asRed responses were measured in the same cells, joint MI values were calculated for this data set, and these were higher than MI values for each response alone (0.12 ± 0.01 Bits at 4 hr and increased to 0.20 ± 0.03 Bits by 8 hr).

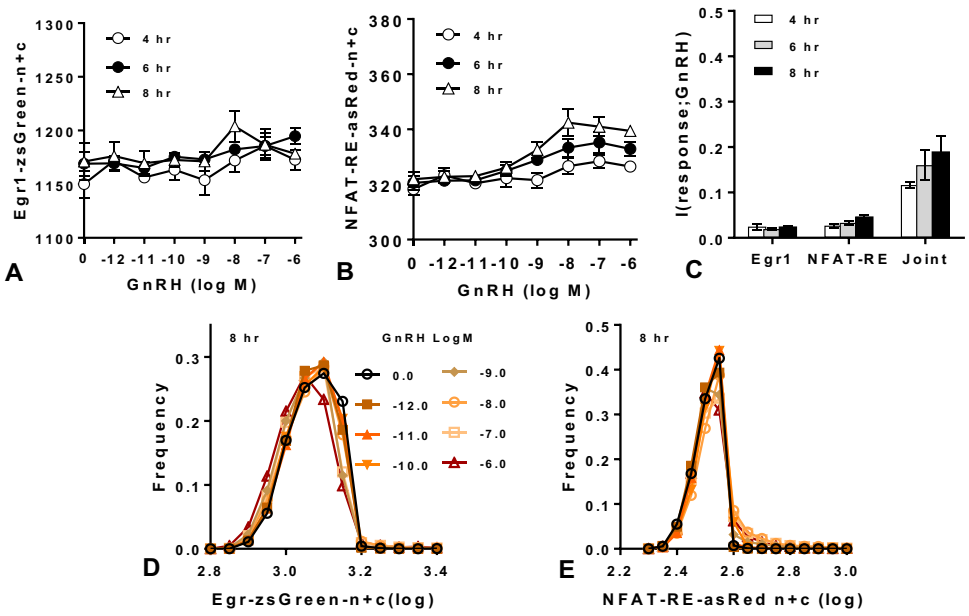

Figure 5.6. Measurement of GnRHR-mediated information transfer to Egr1-zsGreen or NFAT-RE-asRed in MCF-7 cells.

Cells were cultured as described in Chapter 2 and stimulated with GnRH for the indicated times and at the indicated concentrations. The cells were then fixed and stained (nuclei) and used for digital image acquisition and analysis. A and B show population average Egr1-zsGreen-n+c and NFAT-RE-asRed-n+c values in AFU, (means ± SEMs, n=3-4), and are repeated from Figure 3.9 for simplicity. Single-cell data from complete concentration-response curves were then used to calculate the MI between GnRH and Egr1-zsGreen-n+c or NFAT-RE-asRed-n+c, as well as the joint MI for GnRH sensing by both pathways (panel C). Single cell data were also used to generate FD plots by binning log-transformed Egr1-zsGreen and NFAT-RE-asRed values. Representative FD plots are shown in D and E for cells stimulated 8hr with the indicated concentrations of GnRH.

5.3.7. Optimizing procedures for an ERK activation assay using MI measurements

The statistical measure (MI) is used to estimate information transfer via GnRHR to ERK or NFAT (for example). Information could be lost through the cascade. Also, a technical source could contribute to a loss of information by using inappropriate choice of technology. Thus, the protocol used for ERK staining was optimised to maximised estimate MI. LßT2 cells were cultured as described in Chapter 2. On the following day, cells were stimulated with 0 or 10^{-7} M GnRH. They were then fixed and stained for ppERK with varied dilutions of 1°Ab and 2°Ab. The 1°Ab used was monoclonal mouse antibody, diluted in PBS at 1:200, 1:400, 1:800, 1:1600 or 1:3200. Cells were then incubated with 2°Ab green Alexa-488-conjugated goat anti-mouse diluted in PBS at 1:200, 1:400 or 1:800. Images were acquired with INCell 1000 Analyser at the acquisition time of 1000 millisecond (msec).

As shown in figure 5.7, reducing the 1°Ab and 2°Ab dilutions increased the ppERK levels over a broad range of GnRH concentrations. For example, in cells stimulated by GnRH and stained with 1°Ab at the dilution of 1:200, the ppERK levels were increased from ~200 AFU to ~ 300 AFU, and 500 AFU with 2°Ab diluted at 1:800, 1:400 and 1:200 respectively. However, the single cell data used for the calculation of MI showed that the estimated MI values did not differ under all tested conditions (0.6 to 0.7 Bits). Routinely, we are working in these ranges. For all other experiments reported in this thesis, ppERK was stained with 1°Ab at the dilution of 1:400 or 1:800 and with 2°Ab diluted at 1:200 or 1:400.

5.3.8. Optimizing the acquisition time for an ERK activation assay using MI measurements

The exposure time is one of the parameters that need to be considered carefully when acquiring a digital image. As the length of the exposure time affects pixel intensity and image brightness, it will ultimately affect the signal to noise ratio. In other words, if acquisition time is too short it will not be possible to resolve images from background noise, and if it is too long, the detectors could theoretically become saturated. Thus, the acquisition time for an ERK activation assay was optimised as well. LβT2 cells were cultured as usual, stimulated with 0 or 10^{-7} M GnRH, fixed and stained for ppERK with varied dilutions of 1°Ab (1:200, 1:400, 1:800, 1:1600 or 1:3200). Then cells were incubated with 2°Ab at 1:200. The cells were then imaged using INCell 1000 Analyser at the acquisition time of 1, 3, 10, 30, 100, 300, 1000, 3000 and 10000 msec.

As shown in figure 5.8 A-D, no signal was acquired with cells imaged at the exposure time of 3, 10, 30 msec. The obtained values were increased by increasing the exposure time (Figure 5.8 E-I). The single cell data measures used for the calculation of MI showed that the MI values were maximum in cells imaged at the exposure time of 100, 300, 1000 and 3000 msec, and lower values were obtained when cells imaged at the acquisition time 10000 msec (Figure 5.8J).

Overall, the obtained results shown in figure 5.7 and 5.8 indicate that the choices of assay's conditions do not underestimate our MI values, as we are routinely staining cells for ppERK with 1°Ab diluted at 1:400 or 1:800, and with 2°Ab diluted at 1:200, and images were acquiring at 1000 msec. In another experiments, images were collected using different objectives (10X, 20X and 40X lenses, data are not shown).

The estimated MI for ppERK or NFAT1c-EFP translocation responses were not reduced, although MI values were lower with a 4X objective. Also, in another experiments (Craig McArdle personal communication) imaging more fields of view to increase the cell numbers did not increase MI values with these assays. Taken together these observations we can conclude that MI values are not underestimated by using sub optimal assay conditions, and MI estimates can be used to optimise assay conditions.

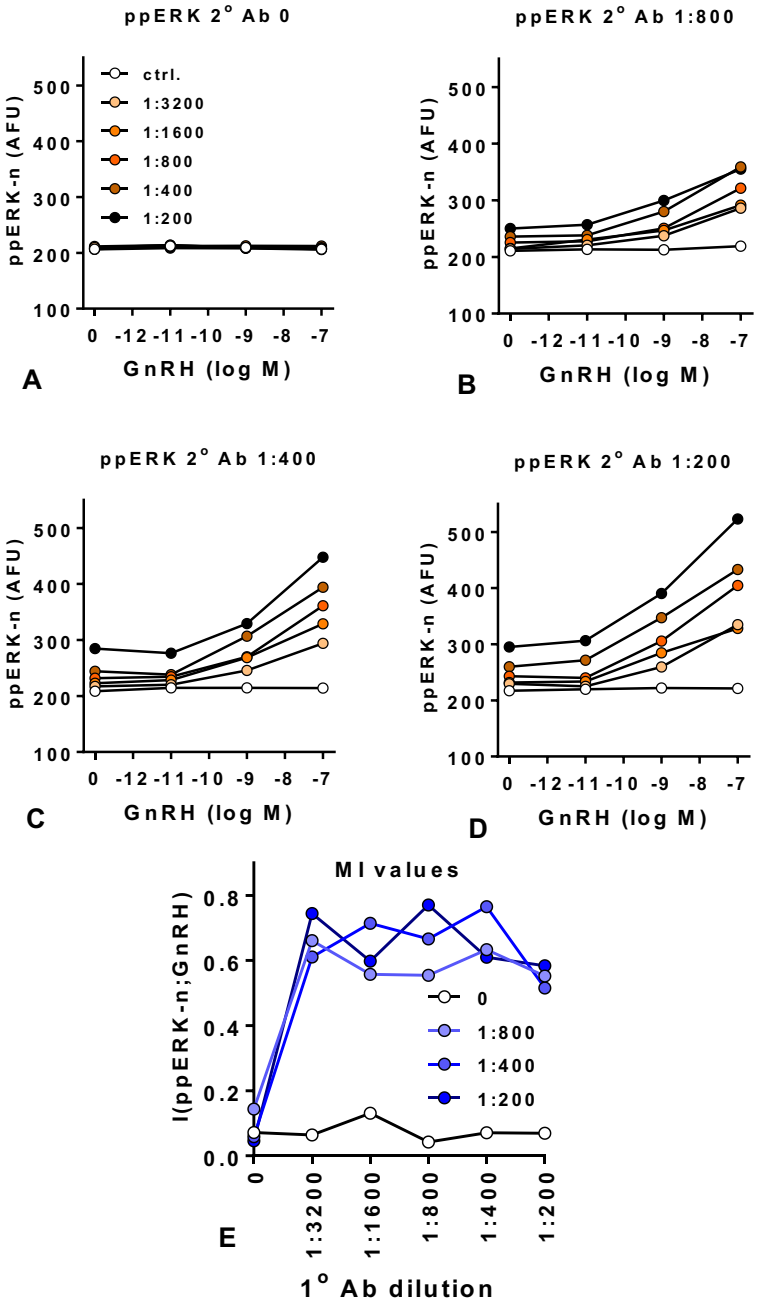

Figure 5.7. Optimizing antibodies for an ERK activation assay using MI measurements

LßT2 cells were cultured and stimulated with 0 or 10^{-7} M GnRH. Cells were then fixed and stained for ppERK with varied dilution of 1°Ab and 2°Ab (as shown in the figures). Cells were then imaged with 10x objective and at 1000 msec. A-D show population average ppERK-n in AFU, (means ± SEMs, n=3). The single cell data measures were used for the calculation of MI (shown in E).

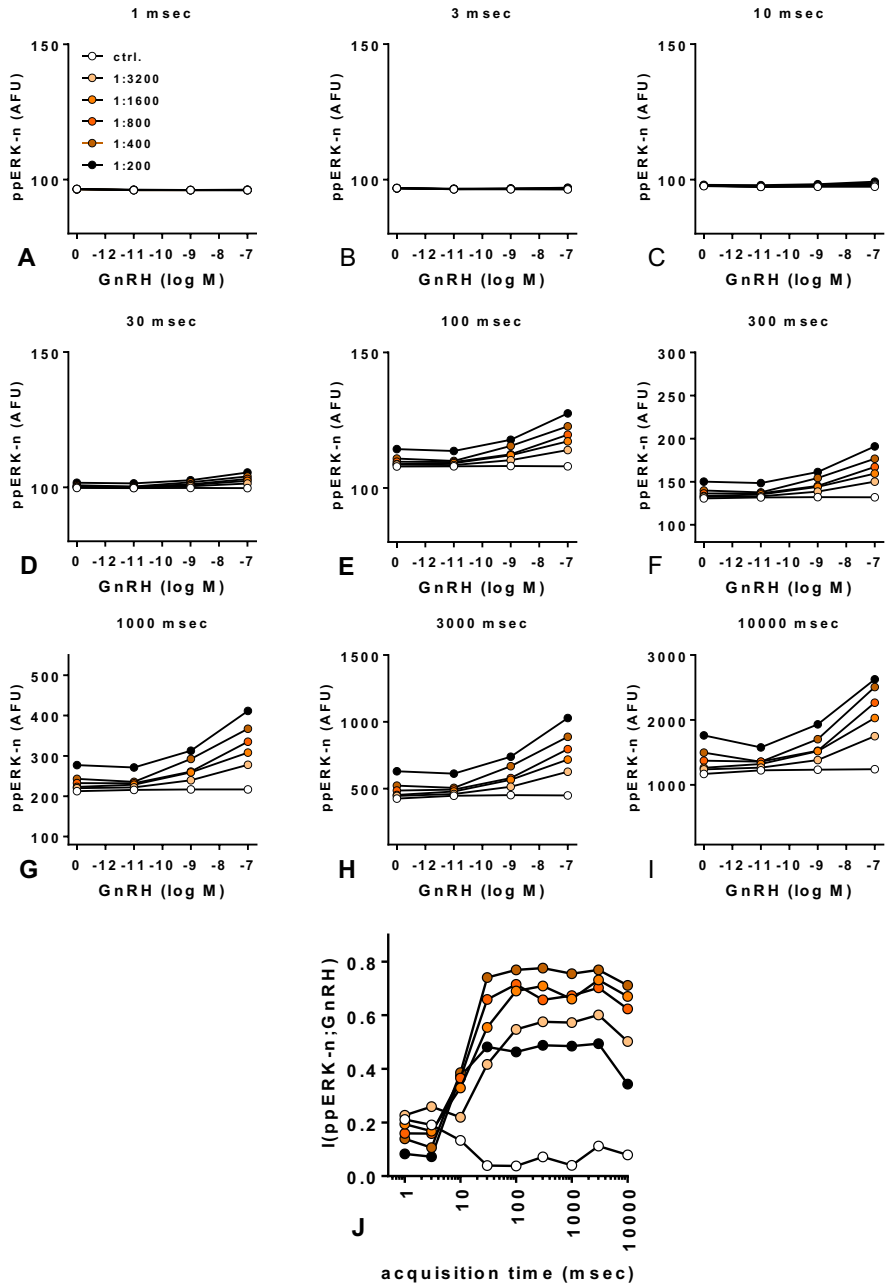

Figure 5.8. Optimizing the acquisition time for an ERK activation assay using MI measurements

LßT2 cells were cultured as described in Chapter 2. Cells were stimulated with 0 or 10^{-11} -10^{-7} M GnRH, they were then fixed and stained for ppERK with the indicated dilutions. Cells were then imaged with the 10x objective at varied acquisition time (1 to 10000 msec). A-I show population average ppERK-n in AFU with the indicated exposure times (means ± SEMs, n=3). The single cell data measures were used for the calculation of MI (J).

5.4. Discussion

Mutual information (MI) that takes cell-cell variability into account [292] is widely applied in cell biology [153]. It can measure the quality of the inference of the signal from the response [274]. The previous chapter (Chapter 4) used methods that were useful in mapping the signalling pathways but did not tell us how much information is transferred through any of the examined pathways. Thus, here MI was used to estimate information transfer via GnRHR to ERK or NFAT and their transcriptional readouts using the same cellular models that were used in Chapter 4.

The key findings are summarized in figure 5.9, as shown more information about GnRH concentration is transferred to the transcriptome via ERK than via NFAT in LßT2 cells, but the opposite is true for both HeLa and MCF-7 cells. For both effectors and effectors driven transcriptions, it was found that a significant amount of information was lost through signalling (i.e. 3 Bits of information was available, and <1 Bit was transferred).

Even though GnRHR signalling is cell context dependent, the data obtained here revealed a loss of information irrespective of the cellular model used (Figure 5.9). Another possibility is that the low MI might be related to the additional variability that introduced by Ad mGnRHR transduction for receptor expression in HeLa cells. However, the data obtained from LβT2 cells that endogenously express GnRHR argue against this possibility. As shown in figure 5.9 the measured information transfer between GnRHR and all experimental readouts was comparable for both endogenous GnRHRs (LβT2 cells) and heterologously expressed GnRHR (HeLa and MCF-7 cells). The MI values were always <1Bit.

In both heterologous GnRHR expression systems HeLa and MCF-7 cells we routinely transduced with Ad mGnRHRs at 25 pfu/nl providing around 70.000 sites/per cell for receptor expression [152]. The GnRHRs number was previously estimated from radioligand binding by transducing HeLa cells with Ad mGnRHR at varied titters (0.8–25 pfu/nl) [22, 180, 324], and found to be in the range of 20.000 to 75.000 sites/per cell. The variation between cells in expressing the receptors could be related to the cell-cell heterogeneity [22, 180, 324]. Gonadotrope-derived cell lines and mouse gonadotrophs express around 25–75 × 10^3 GnRHR [22, 180, 324]. Thus, do the number of receptors influence sensing information? Previous work studied the relationship between receptor number and transferred information to ppERK by transducing HeLa cells with varied titters of Ad mGnRHR [152]. This revealed that I(ppERK; GnRH) can be increased by increasing GnRHR number [152]. The MI values were increased from ~0.4 Bits to ~0.6 Bits in the range of 20-75 x 10^3 GnRHRs per cell, and no further increase beyond that [152]. The same study also recorded a loss of information between ppERK and PDBu (PKC activator) [152], suggesting that factors other than GnRHRs number influence information transfer in this pathways.

GnRHR engage a bifurcating signalling system where activation of PLC mediates the activation of Ca^{2+} effectors (like NFAT) as well as PKCs and their effectors (like ERK) (11). Thus, sensing multiple pathways within networks could be an alternative possibility for mitigating information loss (11). This was addressed by measuring ppERK and NFAT translocation responses or Egr1-zsGreen and NFAT-RE-asRed in the same cells. The data revealed that estimated MI values can be increased by sensing multiple pathways within GnRHR signalling network. A study on growth factor stimulated signalling showed the important role of concomitant activation of pathways in compensation of information transmission (when one pathway was inhibited,

transferred information via another was retained) [300]. However, in respect of information transfer, it is important to know that this robustness does not equate to biological redundancy. The emphasis on the amount of information transfer via signalling networks not on cell decision. Consider a case where a stimulus elicits single cell ERK and NFAT responses that are perfectly correlated with one another but mediate activation of different effectors. In that case, ablation of ERK or NFAT would not affect the information that cell was provided about hormone concentration in its environment, it would affect their responses to the stimulus. Thus, the robustness in information transfer that results from concomitant activation tells us nothing about the transferred information downstream of ERK or NFAT [153].

Interestingly, the MI values for each response alone and join MI values showed different time dependencies in the three cellular models. For instance, in HeLa cells, I(ppERK; GnRH) decreased from 0.48 to 0.17 Bits from 5 to 60 min, whereas I(NFAT-NF; GnRH) showed a small increase (from 0.16 to 0.2 Bits), and joint MI dropped from 0.5 to 0.2 Bit, during the same period. A similar time course pattern was observed in MCF-7 cells. On the contrary, in LßT2 cells, the I(NFAT1c-EFP; GnRH) values increased from 0.2 to 0.5 Bits from 5 to 60 min, whereas I(ppERK; GnRH) remained unaltered. This is another demonstration of cell context-dependent signalling.

Notably, in some cell types (HeLa cell for example, Figure 5.1), the estimated MI value was high at 10 min and reduced by 60 min. This clearly does not mean that the cells gain less information from a 60 min GnRH stimulation than from a 10 min one, instead it just shows that the 60 min snapshot data underestimate the information gained over the entire stimulation period. In the same manner, the 10 min snapshot

data could underestimate the information transferred over this period. Another interesting observation is that in LβT2 cells the I(Egr1-zsGreen; GnRH) value was higher than I(ppERK; GnRH) value. If the information is lost as it goes through the cascade, it would be expected that the information transferred to the Egr1-zsGreen (the downstream of ERK) would be lower than information transferred to ERK. However, this is not the case (Figure 5.3 and Figure 5.4). The higher Egr1-zsGreen value is consistent with the idea that the snapshots underestimate information transfer via GnRHR to ERK. Another possible explanation is that the measured MI value to GnRHR signalling to ppERK is the minimum possible value that can be obtained during the 60 min and the value could be higher. While Egr1-zsGreen readout is accumulated gradually over time (8 hr) giving us a better estimate of transferred information. This means that the amount of measured information could differ by using different experimental readouts. Therefore, our experimental procedures (assays) were optimized to minimize the lost information that could be due to the used technique. So, the transferred information via signalling can be maximized in order to improve MI estimation. The work was done by using different readouts, varied antibodies dilution and different exposure times (Figure 5.7 and Figure 5.8) and objectives (data are not shown). The obtained results revealed that the choices of assay's conditions that we routinely work with do not underestimate our MI values

Further, to mitigate the loss in information through signalling, few studies suggested negative feedback as a mechanism that can protect against information loss. For example, a study by Chong et al., 2011 showed that the information transferred between tumour necrosis factor (TNF) and nuclear factor-kB (NF-κB) was enhanced by negative feedback that reduced noise [299]. Another study demonstrated that by reducing the basal activity, negative feedback could enhance information transfer

through protein kinase signalling systems [298]. A recent study of ERK signalling considering the effect of rapid and slow negative feedback on increasing or reducing information transfer in the ERK pathway [152]. The study revealed that negative feedback can reduce information transfer by reducing the dynamic range for the system output and can also protect information transfer by reducing cell-cell variability [152].

Few studies have reported a mark loss of information through other receptors and signalling pathways including NF-κB and pituitary adenylate cyclase-activating peptide (PACAP) [198, 199]. The work here is investigating signalling mechanism in different cell types. It was shown, in the first two chapters, that these cells can signal to ERK and/or NFAT via other receptors than GnRHR. For example, the activation of TKRs by EGF caused the activation of both ERK and NFAT pathways in LβT2 cells and ERK pathway in HeLa and MCF-7 cells. A recent study measured transferred information via EGF to ERK in HeLa cells provided with 3 Bits and revealed that ~0.2 Bits of information was transferred to ERK over 5 min [298]. Comparing this value with the obtained values here via GnRHR (0.5 Bits, Figure 5.1) make it interesting to explore the reliability of these cells in sensing their environment via other receptors.

In summary, using single-cell measures to quantify transferred information to ERK or NFAT via GnRHRs showed that signalling is inefficient (<1 Bit of information transferred to ERK or NFAT). Most information was lost through signalling as system inputs were 3 Bits for most experiments. Although, cells gained additional information by simultaneous sensing of ERK and NFAT pathways, the increase was small. Similar data were obtained in the three cell types, revealing similar information transfer via endogenous and heterologous expressed GnRHR. Notably, in some cell types, the

estimated MI value was high at early time point and reduced thereafter, indicating that snapshot data might underestimate the information gained over the entire stimulation period, and cell could gain information over time. Thus, this possibility is explored in the following chapter.

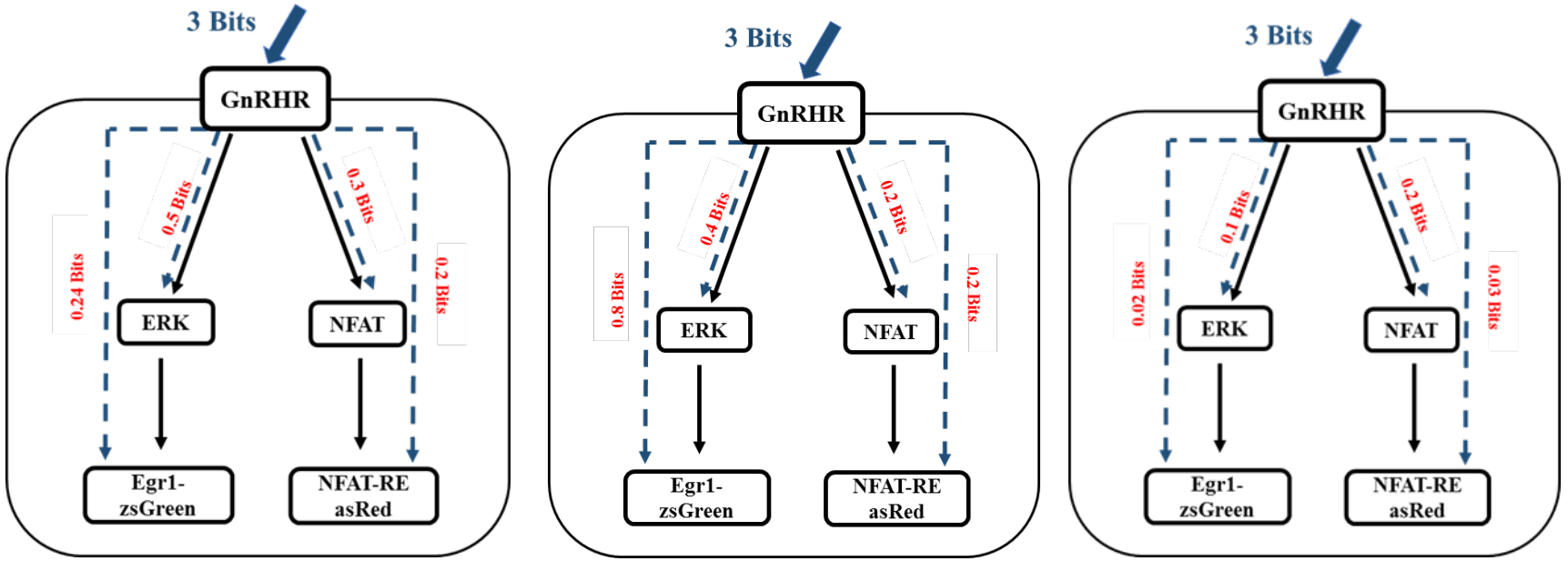

Figure 5.9. Summary of transferred information via GnRHRs to ERK or NFAT and their transcription readouts in three cellular models.

The figures show that providing the system with 3 Bits of information, less than 1 Bit was transferred. For example, around 0.5 Bits of information transfer to ERK in HeLa and LβT2 cells and just 0.1 Bit in MCF-7 cells. However, in MCF-7 the estimated MI values to the transcriptional readouts were much lower than MI values obtained in the other cellular models. These observations extend the idea of cell-context-dependent GnRH signalling to the amount of information transferred via the GnRHR.

Chapter 6- Live cell imaging and sensing dynamics

6.1. Background

Single cell measures reveal high cell-cell variability, and information theoretical approaches can be used to explore the influence of such heterogeneity on information transfer. The previous chapter (Chapter 5) explored the transmitted information via GRHRs to ERK and NFAT and their transcriptions readouts in three cellular models (HeLa, MCF-7 and LβT2 cells). The data obtained revealed loss of information through signalling networks irrespective of the cell type or response measured (Figure 5.9). One Bit of information can resolve two different signal values, but at single time-points, MI values were always <1Bit, despite 3 Bits system inputs. Sensing multiple pathways as a mechanism that cells might do to mitigate such any loss was explored as well. This revealed that cells indeed gained additional information by sensing joint pathways, but the increase was always modest <1Bit. This implies that the available information might be underestimated by using snapshot data, and sensing response dynamics could be an alternative possibility to increase information.

In this chapter, this possibility was explored by live cell imaging of NFAT1c-EFP translocation responses in GnRH stimulated LβT2 cells. MI was also calculated taking response trajectory into account. Also, since, nuclear translocation of NFAT is mediated by elevation of cytoplasmic Ca^{2+}, similar experiments were undertaken using Ca^{2+} responses measured with Ca^{2+} sensor dyes (Fluo-4 or Rhod-3). As GnRH is secreted in a pulsatile manner, the amount of additional information gained by sensing repeated pulses of GnRH was also considered.

6.2. Materials and methods

LβT2 cells were cultured and imaged as detailed in Chapter 2. Briefly, for a single pulse of GnRH experiment, LβT2 cells were maintained at 37^{o}C on the imaging stage of the INCell 2200 and GnRH was added automatically from a compound plate. This enabled cell images to be acquired before and after stimulation without having to remove the culture plate from the INCell.

For dual pulse of GnRH experiments, the first pulse was as above and was terminated by removing the plate from the stage and washing the stimulus before the plate was returned to the INCell for the second stimulus. For data analysis, the image stacks obtained for the first and second imaging period were stitched together manually using Notepad^{++} (Text editor, Microsoft). InCell Analyzer was then used for image analysis to determine fluorophore intensities in regions of interest. The nuclear perimeter was determined from the Hoechst stain and the x-y position of the centre of each nucleus was used to track individual cells over time. This was achieved using a MatLab algorithm (Kindly provided by Dr. Margaritis Voliotis). Time-courses of responses were plotted for each individual tracked cell and were inspected to aid removal of incorrectly tracked cells and outliers as described in Chapter 2.

6.3. Results

6.3.1. Live cell NFAT1c-EFP imaging in LβT2 cells

Ad NFAT1c-EFP transduced LßT2 cells were stimulated with a single pulse of 0 or 10^{-11}-10^{-7} M GnRH in PSS buffer. The cells were then imaged for 50 min. The response of the individual cells to GnRH was variable (Figure 6.1). Some of the cells

showed no response to GnRH (grey shade traces) whereas in >80% GnRH caused a sustained response in the nuclear fraction (NF) of NFAT1c-EFP (Figure 6.1B).

Population averaged data (pooled from all tracked cells) revealed that GnRH causes a concentration and time-dependent increase in nuclear translocation of NFAT1c-EFP in LβT2 cells (Figure 6.1E). Maximum responses were obtained with 10^{-9} M 10^{-8} M and 10^{-7} M GnRH and by 20-30 min. They were then sustained to 50 min (the last time-point measured).

Binning individual cells according to the NF of the NFAT1c-EFP (Figure 6.1F) revealed pronounced cell-cell variation and that GnRH increased the population averaged NFAT1c-EFP levels by shifting the FD plots rightward. There was no evidence for such distinct cell populations, as cells showed a graded response, rather than an all-or-nothing response.

The pronounced overlaps between the FD plots for stimulated and unstimulated cells immediately suggest that MI values will be low. As shown in figure 6.1 G, calculated MI values for each time points followed a very similar time-course to the NFAT1c-EFP-NF translocation responses, increasing to a maximum of 0.38 ± 0.01 Bits by 20-30 min and remaining at this level until 50 min. MI was also calculated taking response trajectories of individual cells into account using 10, 30 and 50 min, and this was 0.54 ± 0.01 Bits. Calculation of MI values at a wide range of time points (Figure 6.1D) reveals that we have not underestimated MI by simply choosing the wrong time-point for analysis. However, the increase in MI seen when trajectory is considered demonstrates that the snapshot data do indeed underestimate information transfer via GnRHRs to NFAT in LβT2 cells.

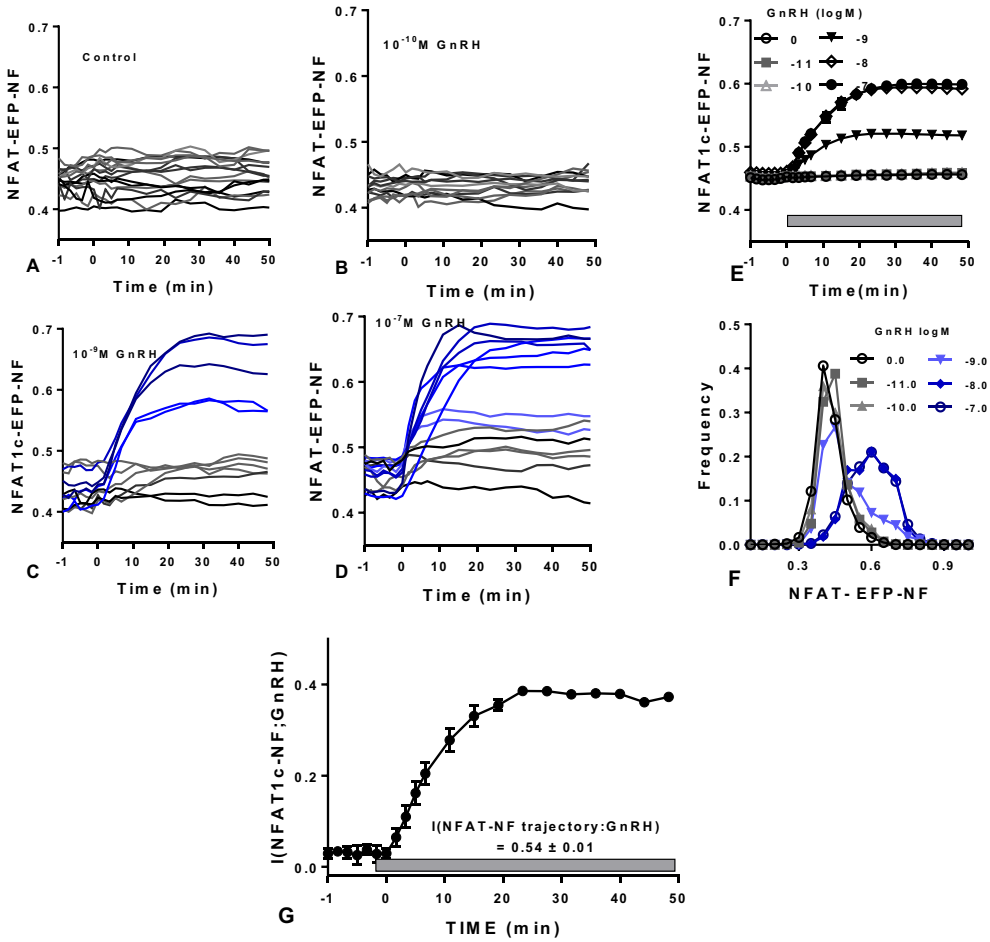

Figure 6.1. Sensing dynamics and live cell NFAT1c-EFP imaging in LßT2 cells

LβT2 cells were culture and treated as described in Chapter 2. Cells were imaged at 37°C both before and during continuous stimulation with varied concentrations of GnRH as shown. Images were acquired at the indicated times, and automated image analysis algorithm was used to calculate the NFAT1c-EFP-NF. A MatLab tracking algorithm was used to follow individual cell responses over time. The cells that had a failed tracking or had at time 0 NFAT1c-EFP-NF values of <0.4 or >0.55 were removed (around 2% defined as outliers). Representative single cells responses are shown for control cells (A) for cells stimulated from time 0 with 10^{-10} M GnRH (B) with 10^{-9} M GnRH (C) and with 10^{-7} M GnRH (D). Population average responses for all tracked cells are shown as the means ± SEMs, from 3 separate experiments (n=3), with duplicate wells (E). The total number of cells tracked for each GnRH concentration was between 70 and 320. Single cell data were used to generate FD plots. Representative FD plots shown for cells stimulated 20 min (F) with the indicated concentrations of GnRH. The I(NFAT-NF; GnRH) values for all tracked cells at each time point are shown in panel G. Also, panel G shows the MI between GnRH and the translocation response when single cell response trajectories are considered (10, 30 and 50 min).

6.3.2. Sensing dynamics and live cell Fluo-4 imaging in LβT2 cells.

In the next series of experiments, the Ca^{2+} sensitive fluorescent dye Fluo-4 was used for live cell imaging of GnRH effects on the cytoplasmic Ca^{2+} concentration in LβT2 cells. As shown in figure 6.2A, in control cells, cytoplasmic Ca^{2+} concentrations (indicated by Fluo-4 fluorescence) were relatively stable over time, although clear oscillations were seen in a small proportion (<20%) of cells imaged (Figure 6.2A). 10^{-7} M GnRH caused a rapid increase in Ca^{2+} (Figure 6.2B). These responses varied markedly from cell to cell although most cells responded to this concentration of GnRH (>90%). The maximum responses were typically achieved within 30 sec of stimulation with a gradual reduction toward plateau levels after 4-10 min. Interestingly, some cells showed a clear delay between GnRH addition and Ca^{2+} elevation (light blue shade traces in Figure 6.2D), an effect that was also seen in cells stimulated with lower GnRH concentrations (Figure 6.2B and C). At lower GnRH concentrations, the single cell data revealed a tendency for lower maximal responses (Figure 6.2B and C).

The population averaged data (Figure 6.2E) revealed that the maximum GnRH effect and response kinetics were both dependent upon GnRH concentration. Notably, the highest concentration of GnRH caused the most transient response (i.e. maximum response: plateau response ratio was greater with 10^{-7} M than with 10^{-9} M GnRH and the time taken to achieve the maximum response was less with 10^{-7} M GnRH than with 10^{-9} M GnRH (Figure 6.3C and D).

Binning individual cells according to the log of the nuclear Fluo-4 stain intensity (Figure 6.2F) revealed pronounced cell-cell variation in the Fluo-4 levels and that GnRH increased the population averaged Fluo-4 levels by shifting the FD plots

rightward. No evidence was found for GnRH responsive and GnRH non-responsive cell populations, as a graded response rather than an all-or-nothing response was shown. The overlaps between the FD plots for stimulated and unstimulated cells immediately suggest that MI values will be low. As shown in figure 6.2G, MI values were calculated for each time points and these followed a very similar time-course to the population averaged Fluo-4 responses. The MI values increased to a maximum of 0.74 ± 0.01 Bits within 30 sec of stimulation, then reduced gradually to 0.58 ± 0.1 after 2 min and remained at this level for 10 min (the last time-point measured).

It is important to note that the data in figure 6.2G are normalised to the individual cell Fluo-4 level before stimulus addition in order to correct for cell-cell variation in Fluo-4 loading. MI values were calculated for both the raw data (Fluo-4 fluorescence in AFU) and the normalised data. For raw data, the MI values were 0.60 ± 0.05 Bits within 30 sec of stimulation then gradually decreased to 0.35 ± 0.04 within 10 min. The values obtained were a little higher with the normalised data, indicating that this technical source of variation causes MI values to be underestimated with the raw data. With the normalized data the maximum MI value was 0.74 ± 0.10 Bits at 30 sec, but when trajectory was considered using 140, 160 and 300 sec responses, the MI value was increased to 1.01 ± 0.04 Bits.

Thus, maximum estimates for information transfer via GnRHR are greater with the Ca^{2+} sensor (Figure 6.2H) than with the NFAT1c-EFP translocation reporter (Figure 6.1.G) and, although MI values are increased by consideration of response trajectory for both readouts, the majority of information available still appears to be lost through signalling with both experimental readouts.

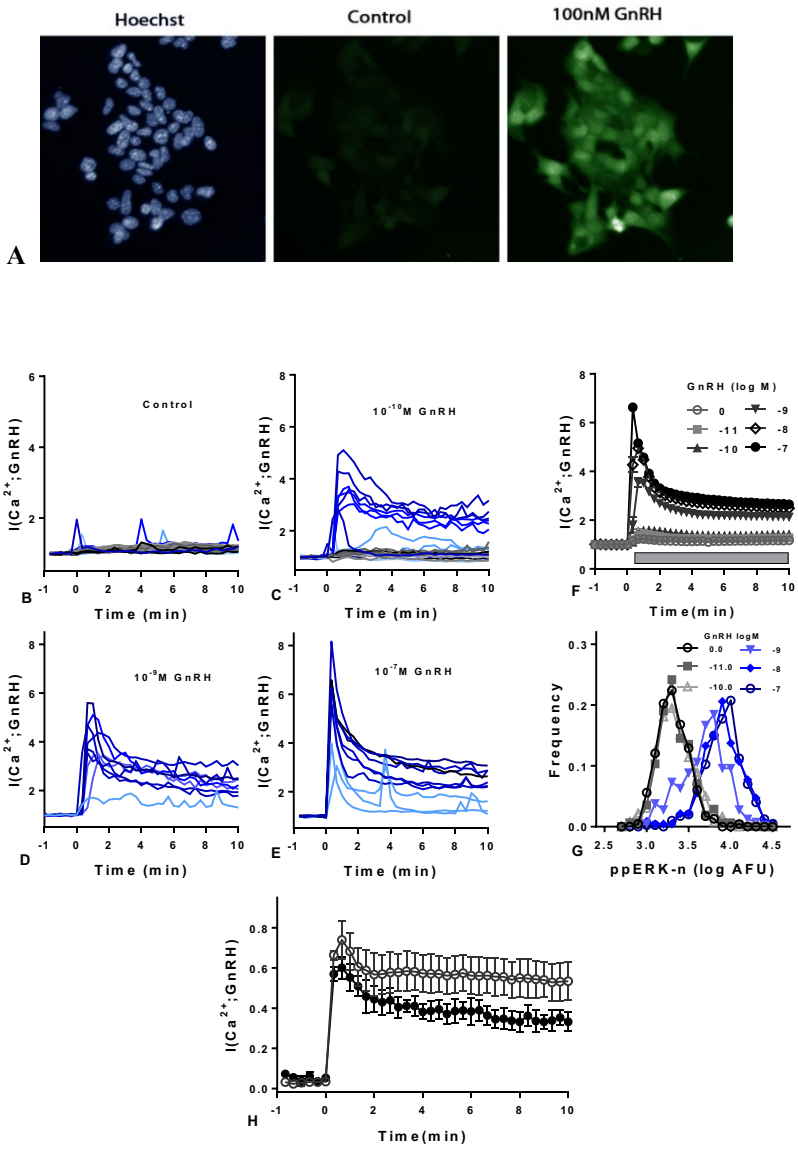

Figure 6.2. Sensing dynamics and live cell Fluo-4 imaging in LβT2 cells

Cells were cultured and treated as described in Chapter 2. Images were collected every 20 sec, and a Matlab tracking algorithm was used to follow individual cell responses over time. The cells that had a fail tracking were removed (around 2% of cells, defined as outliers). Panel A shows representative images of Hoechst, nuclear Fluo-4 stained cells cultured under control condition or stimulated for 1 min with 10^{-7} M GnRH (3). Representative single cells responses are shown for control cells (B) for cells stimulated from time 0 with 10^{-10} M GnRH (C), with 10^{-9} M GnRH (D) and for 10^{-7} M GnRH (E). Population average responses for all tracked cells are shown as the means ± SEMs, n=3 (F). The total number of cells tracked for each GnRH concentration was between 130 and 320 cells. Representative FD plots are shown for cells stimulated 1 min (G) with the indicated concentrations of GnRH. The I(Ca^{2+}; GnRH) values for all tracked cells at each time point were calculated for both the raw data (Fluo-4 fluorescence in AFU, closed circles) and the normalised data (open circles) and are shown in H.

6.3.3. Live cell Fluo-4 imaging in HeLa cells

GnRH effect on the cytoplasmic Ca^{2+} concentration was also measured in HeLa cells as an alternative model. The cells were cultured and treated as LβT2 cells were treated with the exception that HeLa cells were transduced with Ad mGnRHRs for the expression of heterogenous receptors. As shown in figure 6.3B, in control cells, cytoplasmic Ca^{2+} concentrations were relatively stable over time. However, a small transient response was observed following fluid addition (PSS alone without GnRH). As shown in figure 6.3, GnRH induced a rapid increase in Ca^{2+}. The maximum responses achieved with 10^{-7} M GnRH and within 30 sec of stimulation, followed by a gradual reduction toward plateau levels after 4-10 min (Figure 6.3E). Although most cells responded to this concentration of GnRH (>90%), the responses were varied from cell to cell. Some cells exhibited a low response to the stimulus (grey shade traces), whereas other cells showed a spike response to GnRH (dark orange shade traces), and around 10% showed clear oscillations. At lower GnRH concentrations, the single cell data revealed a tendency for lower maximal responses (Figure 6.3D).

The population averaged responses (Figure 6.3F) were consistent with the single cell responses. The maximum GnRH effect and response kinetics were both dependent upon GnRH concentration. The maximum response: plateau response ratio was greater with 10^{-7} M than with 10^{-9} M GnRH and the time taken to achieve the maximum response was less with 10^{-7} M GnRH than with 10^{-9} M GnRH. Like the single cell observation, a transient response was observed in control cells (Figure 6.3F, open circle) following the addition of fluid (PSS alone), which might be an effect of mechanical stimulation in this cell line.

Binning individual cells according to the log of the nuclear Fluo-4 stain intensity revealed pronounced cell-cell variation in the Fluo-4 levels. GnRH increased the population averaged Fluo-4 levels by shifting the FD plots rightward. No evidence was seen for GnRH responsive and GnRH non-responsive cell populations, as a graded response rather than an all-or-nothing response occurred (Figure 6.3G).

The pronounced overlaps between the FD plots for stimulated and unstimulated cells suggest that MI values will be low. This is shown in figure 6.3H. MI values were calculated for single-time-point data and these followed a quite similar time pattern to the population averaged Fluo-4 responses. The MI values were maximum of 0.56 ± 0.03 Bits at 24 sec, followed by a small reduction of 0.49 ± 0.03 Bits within 1 min then again increased gradually to 0.66 ± 0.01 after 3 min where it remained sustained for 10 min (the last time-point measured). MI values were calculated for both the raw data (Fluo-4 fluorescence in AFU, closed circles) and the normalised data (open circles) and found to be higher in the latter (Figure 6.3H), suggesting that this technical source of variation causes underestimation of MI values in the raw data. The maximum MI value obtained in normalised data was 0.56 ± 0.03 Bits at 24 sec, but when trajectory was considered (using 140, 160 and 300 sec responses) the MI value was increased to 1.01 ± 0.05 Bits. However, despite the increase in MI values by consideration of response trajectory, still most of the information available appears to be lost through signalling.

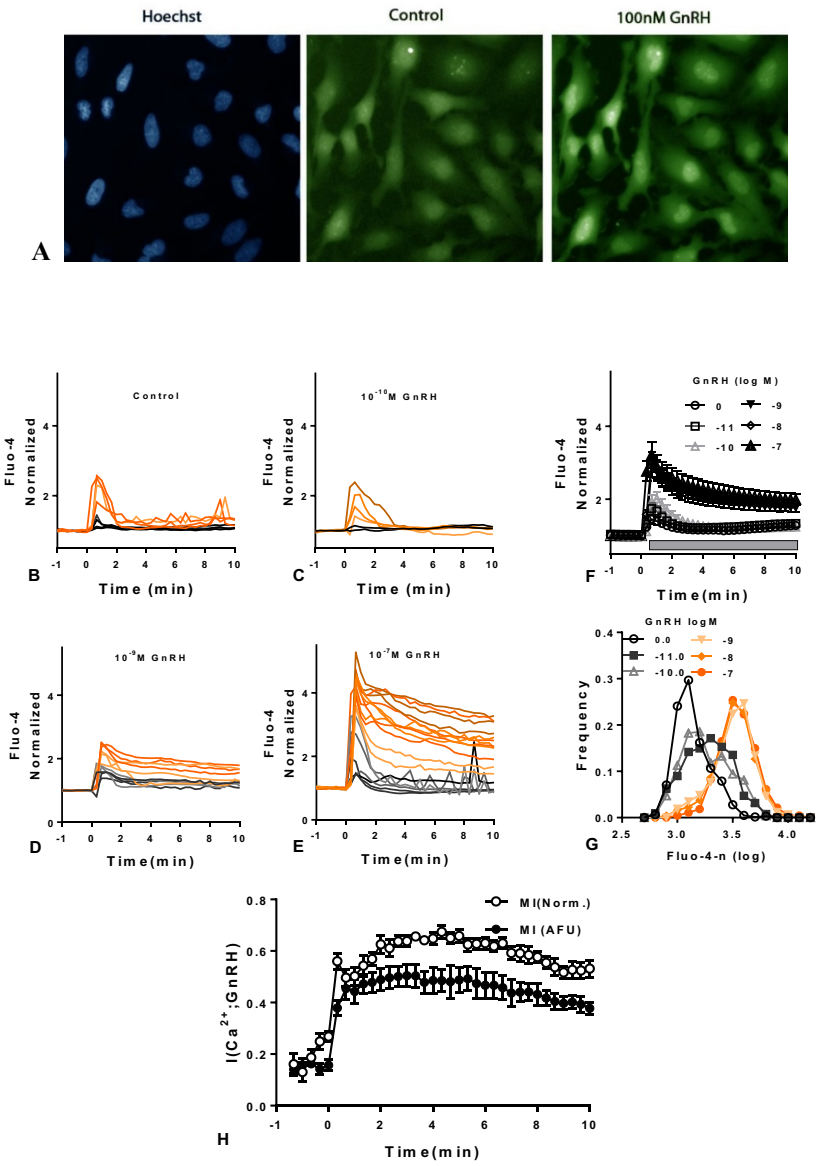

Figure 6.3. Sensing dynamics and live cell Fluo-4 imaging in HeLa cells

Cells were treated as described in Chapter 2. Images were acquired every 20 sec, and a Matlab tracking algorithm was used to follow individual cell responses over time. The cells that had a fail tracking were removed (around 5% of cells defined as outliers). Panel A shows representative images of Hoechst, nuclear Fluo-4 stained cells cultured under control condition or stimulated for 24 sec with 10^{-7} M GnRH. Representative single cells responses are shown for control cells (B), for cells stimulated from time 0 with 10^{-10} M GnRH (C), with 10^{-9} M GnRH (D) and with 10^{-7} M GnRH (E). Population average responses for all tracked cells are shown as the means ± SEMs, n=4 (F). The total number of cells tracked for each GnRH concentration was between 150 and 300 cells. Representative FD plots are shown for cells stimulated 24 sec (G) with the indicated concentrations of GnRH. Panel H shows the I(Ca^{2+}; GnRH) values for all tracked cells at each time point calculated for both the raw data (Fluo-4 fluorescence in AFU, closed circles) and the normalised data (open circles).

6.3.4. Joint sensing of Ca^{2+} and NFAT signalling

Transferred information might be increase by joint sensing of Ca^{2+} and NFAT translocation responses, so this possibility was explored. However, Fluo-4 and NFAT1c-EFP cannot be imaged in the same cells. This is because of that the excitation of both Fluo-4 and EFP are similar (see Chapter 2), which will cause the emission spectra to overlap. Accordingly, an alternative Ca^{2+} sensitive fluorophore, Rhod-3, was used. Rhod-3 is a red-shifted calcium indicator providing a means to avoid bypass the overlap.

Imaging the response of both NFAT and Rhod-3 (Figure 6.4) in the same cells revealed that cytoplasmic Ca^{2+} concentrations were relatively stable over time in control cells. A rapid increase in Ca^{2+} in cells stimulated by10^{-7} M GnRH was observed, with a maximum response achieved within 1 min of stimulation, followed by a gradual reduction toward plateau levels after 4-10 min. A delay between GnRH addition and Ca^{2+} elevation was seen in cells stimulated by 10^{-9} M GnRH (Figure 6.4B), At lower GnRH concentrations, the single cell data revealed a tendency for lower maximal responses.

Consistent with single cell responses, the population averaged data showed that the maximal GnRH effect and response kinetics were both dependent upon GnRH concentration. The maximum response: plateau response ratio was greater with 10^{-7}M than with 10^{-9}M GnRH (Figure 6.4B and C). MI values calculated for each time point followed a very similar time-course to the Rhdo-3 responses (a maximum of ~0.7 Bits within 30 sec of stimulation then a gradual reduction to control values over 25 min.

For NFAT1c-EFP translocation, the single cell responses in figure 6.4 demonstrate that small proportion of cells (<20%) showed no response to GnRH (grey shade traces), and more than 80% of cells showed a sustained response (green shade traces. Population averaged data revealed that GnRH causes a concentration and time-dependent increase in NFAT1c-EFP- NF translocation. Maximum response was obtained with 10^{-9} M, 10^{-8} M, and 10^{-7}M GnRH and by 10-20 min. They were then sustained to 25 min (the last time-point measured). MI values calculated for each time point followed a very similar time-course to the NFAT1c-EFP-NF translocation responses (a maximum of ~0.4 Bits by 10 min and remaining at this level until 25 min). No much additional information was gained by sensing joint pathways, the MI value was 0.97 ± 0.05 Bits.

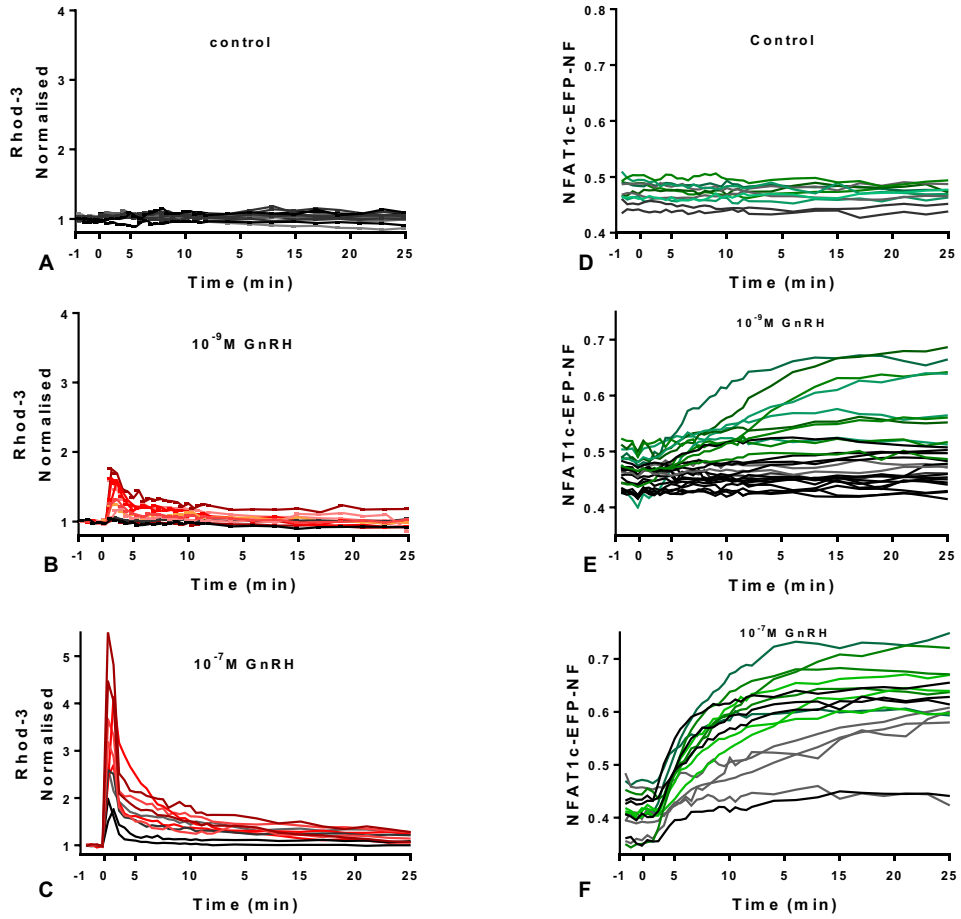

Figure 6.4. Imaging Rhod-3 and NFAT1c-EFP in the same cells: single cell data.

Cells were cultured as described in Chapter 2. Cells were imaged at 37°C both before and during continuous stimulation with varied concentrations of GnRH as shown in the figures. Images were collected every 45 sec, and a MatLab tracking algorithm was used to follow individual cell responses over time. The cells that had a failed tracking were removed (around 3% of cells, defined as outliers). Representative single cells responses of Rhod-3 or NFAT1c-EFP are shown for control cells (A and D) for cells stimulated from time 0 with 10^{-9} M GnRH (B and E) and with 10^{-7} M GnRH (C and F).

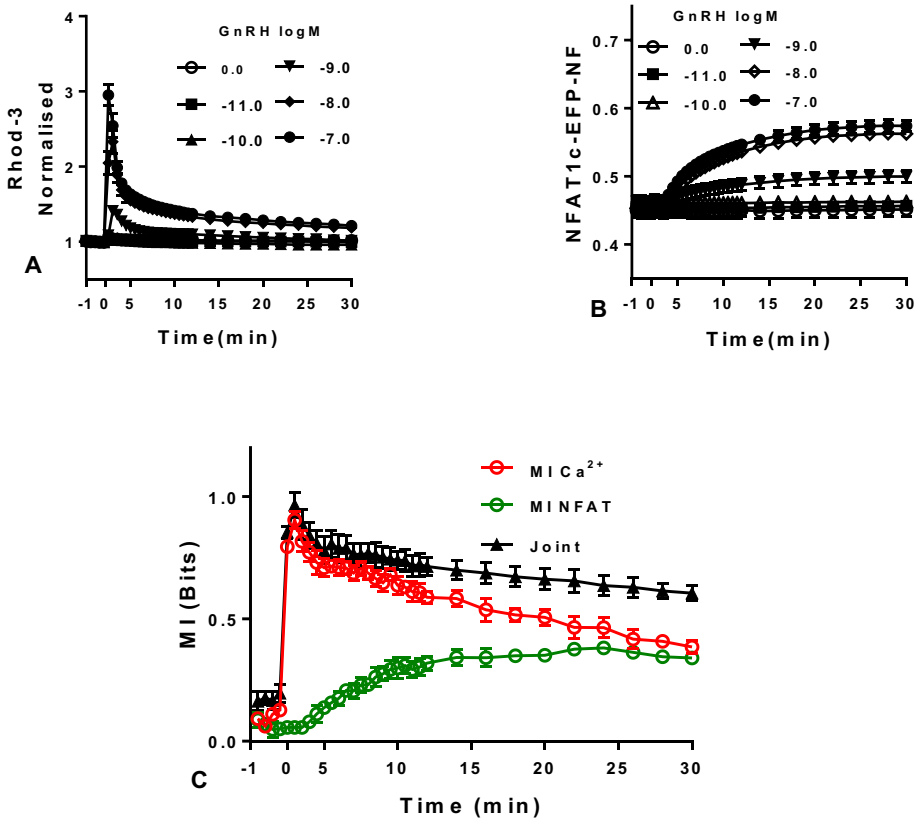

Figure 6.5. Imaging Rhod-3 and NFAT1c-EFP in the same cells: population averaged data and MI values

Cells were cultured as described in Chapter 2. Cells were imaged at 37°C both before and during continuous stimulation with varied concentrations of GnRH as shown in the figures. Images were collected every 45 sec, and a Matlab tracking algorithm was used to follow individual cell responses over time. Representative single cells responses of Rhod-3 or NFAT1c-EFP are shown in Figure 6.4. Population average responses for all tracked cells are shown here as means ± SEMs, n=4. Panel A and B show population average responses for Rhod-3, and NFAT-1c-EFP-NF respectively. Panel C shows the MI values for all tracked cells at each time point. The maximum MI values were ~0.4 Bits for NFAT1c-EFP-NF, ~ 0.9 Bits for Ca^{2+} and these values were increased to ~1Bit by sensing both pathways.

6.3.5. Sensing repeated pulses

GnRH is secreted in a pulsatile manner which is critical for normal reproductive function [23]. Signalling also continues after GnRH pulses are terminated and this raises two related questions. First how much information transfer occurs after the GnRH pulse. Second, how much additional information is gained by sensing a second pulse of GnRH. Here these questions were addressed by live cell imaging of NFAT1c-EFP expressing in LβT2 cells with two pulses of GnRH and using the tracked cells to calculate MI values.

The response of the individual cells to GnRH was remarkably variable as shown in figure 6.5. Small proportion of cells (<10%) showed no response to GnRH, some cells showed a clear delay between GnRH addition and NFAT1c-EFP translocation. However, most of the cells responded to GnRH. The maximum response was seen with the highest concentration of GnRH (10^{-7} M and 10^{-8} M) which was achieved within 10-15 min of GnRH stimulation for each pulse (Figure 6.5B and C). Consistent with the single cell observations above, the population averaged data revealed that the maximum GnRH effect and response kinetics were both dependent upon GnRH concentration. The maximum response was seen with higher GnRH concentrations (10^{-7} M and 10^{-8} M).

MI values were calculated for the responses to GnRH in the 1st and 2nd pulse, and these shown in figure 6.5E. The MI values were 0.38 ± 0.02 Bits for the 1st pulse and 0.23 ± 0.03 Bits for the 2nd pulse. The MI value between the 1st pulse and 2nd pulse responses was calculated, and this increased to ~0.46 Bits. The additional information that cells could gain by sensing the 2nd pulse was also calculated, and this revealed that ~0.1 Bits was gained by sensing the 2nd pulse of GnRH. When trajectory was

considered using all time points (MDS as described in Chapter 2), the MI value was increased to 0.55 ± 0.02 Bits.

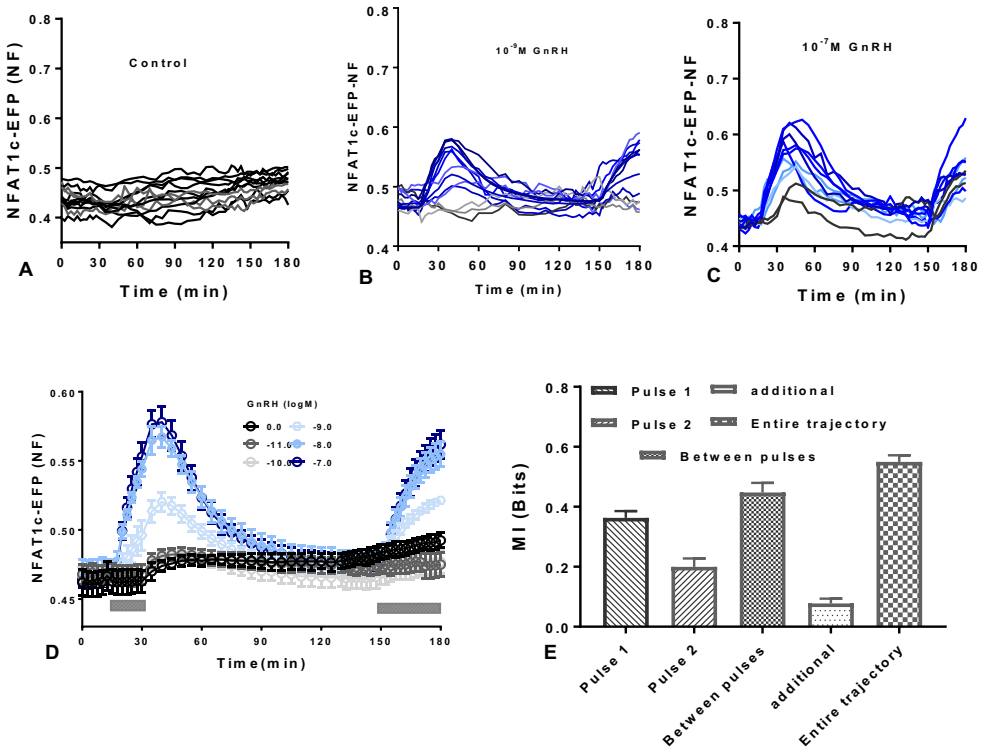

Figure 6.6. Sensing dynamics with repeated stimulation and live cell NFAT1c-EFP imaging

Ad NFAT1c-EFP transduced cells were stimulated with GnRH as shown for 15 min (first grey bar). The cells were then washed 3x over 5 min with PPS, and then imaged for a further two hours before repeat stimulation (second grey bar) for 30 min using the same concentrations. Images were acquired at the indicated times, and a Matlab tracking algorithm was used to follow individual cell responses over time. The cells that had a failed tracking or had at time 0 NFAT-NF values of <0.4 or >0.55 were removed (around 5% of cells defined as outliers). Panel A, B and C are shown representative single cell responses (control and cells stimulated with 10^{-9} M GnRH or 10^{-7} M GnRH). Population average responses for all tracked cells are shown as the means ± SEMs, n=4, with data from duplicate wells. The total number of cells tracked for each GnRH concentration was between 80 and 200. The MI values were calculated and for the first pulse were 0.45 Bits and 0.23 Bits for the second pulse. Little information additional was gained by sensing both pulses (~0.1 Bits). These values were increased to ~0.6 Bits with trajectory consideration.

6.3.6. Varying a time between two pulses

Cell-cell variability in cellular responses could reflect differences in the expression of key signalling effectors. In a recent model of the GnRH signalling pathway [153], the expression level of two effectors (GnRHRs and calmodulin) could fluctuate across different time-scales (fluctuation half-times from 10 min- representing unstable effectors- to 10.000 min representing stable effector). The results revealed that additional information could be gained from sensing a second pulse in the former scenario and little or no information in the latter one. A prediction from these simulations is that increasing the time between two pulses could increase information gained from sensing the second pulse. Here this hypothesis was investigated by loading LβT2 cells with Fluo-4 (as calcium indicator). Cells were then received two pulses of GnRH, with varying times between pulses (10, 20, 60 and 90 min). The first one lasted for 7 min with 20 sec intervals for imaging and was terminated by removing the plate from the stage and washing the stimulus with PSS buffer (4x 100µl over 3 min). The plate was then returned to the INCell for the second stimulus. Cells were then imaged for 10, 20, 60 or 90 min, before receiving the second pulse of GnRH and again imaged for 7 min with 20 sec intervals.

The population averaged data revealed that the maximum GnRH effect and response kinetics were both dependent upon GnRH concentration. GnRH caused a rapid increase in Ca^{2+} (Figure 6.2A). The maximum responses were typically achieved within 1 min of stimulation for each pulse. The responses to 1st pulse and 2nd pulse of GnRH were typical. The highest concentrations of GnRH caused the most transient response (10^{-8} M and 10^{-7} M). A tendency for lower maximal responses was seen at lower GnRH concentrations (10^{-9} M GnRH). The time taken to achieve the maximum

response was less with 10^{-8} M and 10^{-7} M GnRH than with 10^{-9} M GnRH (Figure 6.3C and D).

MI values were calculated for 1st and 2nd pulse of GnRH, and these are shown in Figure 6.7. For each case, the MI values were ~0.7 Bits for the 1st pulse and ~0.6 Bits for the 2nd pulse, and little information was gained by sensing the 2nd pulse (~0.1Bit). Note that, were stimulated with 0 or 10^{-10}-10^{-7} M GnRH, providing 2.2 Bits of information as the system input. The information transferred between pulses where also calculated and these were comparable under all test condition (Figure 6.7). Two-way ANOVAs of the MI values between pulses revealed that varying the time between pulses are not significant sources of variation ($P>0.05$). Very little information was gained by sensing the second pulse and the amount of information gained was not dependent on the pulse interval, implying that the sources of variation in this model are relatively stable over the time-course of the experiments. Also, MI was calculated taking the entire trajectory into account, and this increased the MI values to approximately 1Bit under all tested conditions.

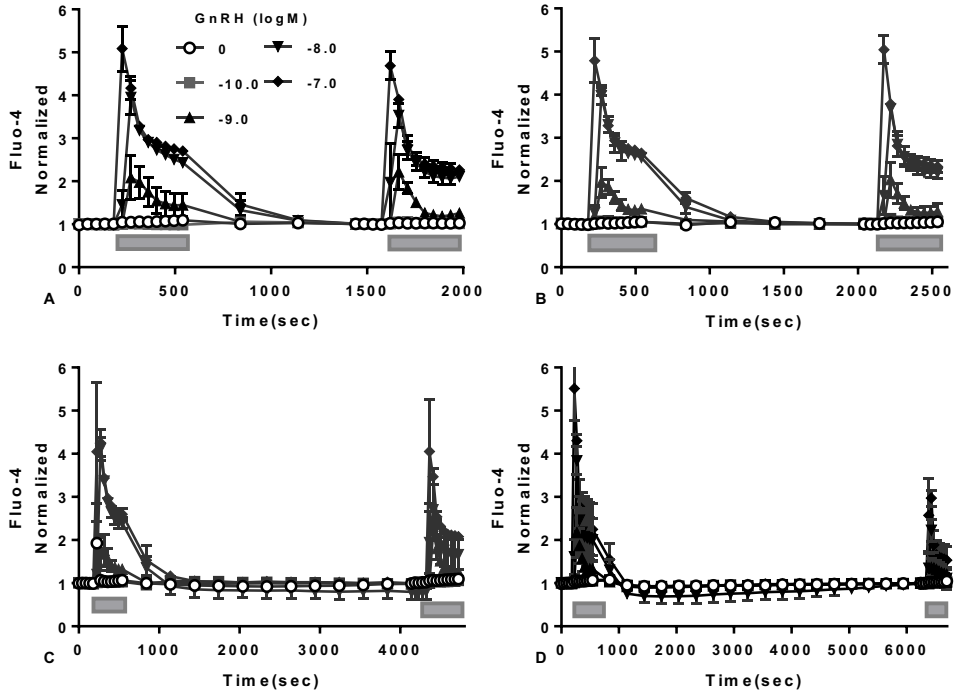

Intervals between pulses	Between pulses	GnRH and the response to 1st pulse	GnRH and the response to 2nd pulse	Additional information	Entire trajectory
10 min	1.03 ± 0.18	0.70 ± 0.07	0.68 ± 0.04	0.13 ± 0.04	1.10 ± 0.01
20 min	0.92 ± 0.02	0.61 ± 0.04	0.57 ± 0.05	0.12 ± 0.03	1.02 ± 0.1
60 min	0.92 ± 0.13	0.61 ± 0.01	0.64 ± 0.08	0.20 ± 0.12	1.10 ± 0.1
90 min	0.78 ± 0.01	0.63 ± 0.06	0.51 ± 0.04	0.06 ± 0.02	0.97 ± 0.1

Figure 6.7. Sensing dynamics with repeated stimulation and live cell [Ca^{2+}] imaging

LβT2 cells were incubated with Fluo-4 for 30 min at 37°C then washed 3x with PSS prior to stimulation with 0 or 10^{-10}-10^{-7} M GnRH for 7 min (1st grey bar). The cells were then washed 4x over 3 min with PPS, and then imaged for a further 10 min (A), 20 min (B) 60 min (C) or 90 min (D) before repeat stimulation (2nd grey bar) for 7 min using the same concentration as used with the first pulse. Panels A-D show the population average responses for all tracked cells. The results show the means ± SEMs, n=3. A MatLab tracking algorithm was used to follow individual cell responses over the time and the total number of cells tracked was between 100- 340 cells. MI values in response to 1st, 2nd pulse and between pulses with different inter-pulse intervals are calculated and are shown in the table. The inset text box shows MI values between GnRH concentration and the maximum response for the 1st and 2nd pulses. It also shows the additional information gained by sensing both pulses, the MI between pulses, and I(Fluo-4; GnRH) when the entire response trajectory is taken into consideration.

In the previous experiments, it was noted that the population averaged Fluo-4 responses were lower in the 2nd pulse than the 1st, particularly with the higher inter-pulse intervals. This could conceivably reflect down-regulation of GnRHR caused by the 1st GnRH pulse, but this seems unlikely as agonist induced internalisation of type I mammalian GnRH is slow and recovery would be expected to occur between the pulses. It could also be related to leakage of Fluo-4 from the cells, or chemical modifications of the Fluo-4 that impair chemical sensing, occurring over time. In order to distinguish between these possibilities, related experiments were undertaken in which cells were treated with10^{-7} M GnRH (group C) or without GnRH (group B) in the 1st pulse, then washed and incubated for another 90 min before stimulation with 0 or 10^{-7} M GnRH. As shown (Figure 6.8), the response of cells to the 2nd pulse of GnRH was similar in both groups. Accordingly, there was a time-dependent reduction in Fluo-4 response rather than a GnRH-induced reduction in response to GnRH.

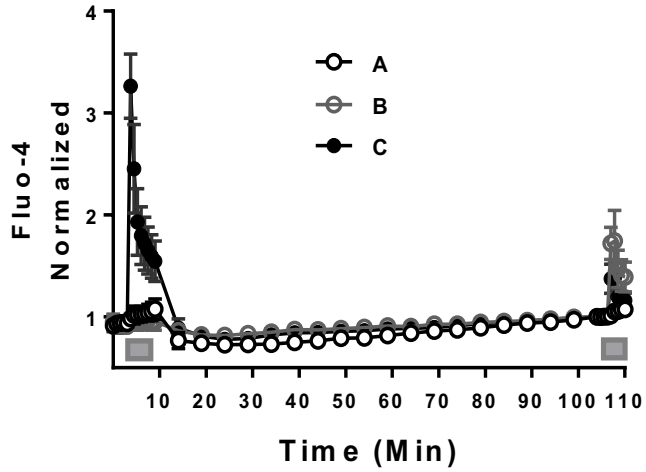

Figure 6.8. Exploring reasons for the reduction in [Ca^{2+}] response with a 2nd pulse of GnRH.

LßT2 cells were treated as described in figure 6.7. Group A represents control, cells in group B were injected with PSS only and cells in group C were received 10^{-7}M GnRH (1st grey bar). Cells were imaged for 7 min, then GnRH effect was terminated by washing cells 4x over 3 min with PPS. Cells were then imaged for 90 min before both groups (B and C) receiving a second pulse of GnRH (2nd grey bar). The figure shows the population average responses for all tracked cells. The results show the means ± SEMs, n=3. The normalised Fluo-4 value of the 2nd pulse was calculated using the AUCs and these values were comparable 1.38 ± 0.29 (B) and 1.745 ± 0.59 (C). The t-test of the second pulse reveals no significant differences in response to GnRH between group B and C ($P<0.05$).

6.3.7. GnRHR-independent Ca^{2+} mobilisation

The maximal MI values reported in this chapter are approximately 1 Bit (irrespective of the experimental end-point and whether response trajectory is taken into consideration). The implication is that a marked loss of information through signalling occurs early in the GnRHR signalling cascade, perhaps at the level of GnRHR coupling to its G-protein, or G-protein activation of PLC. If so, we might expect higher MI values with a GnRHR-independent stimulus for Ca^{2+} mobilisation so, in the final experiments, this was addressed using a Ca^{2+} ionophore (ionomycin). Fluo-4AM

loaded LβT2 cells were stimulated with 0 or 10^{-5}-10^{-7} M ionomycin, providing 2.45 Bits of information as the system input.

As shown in figure 6.8, in control cells receiving no ionomycin, cytoplasmic Ca^{2+} concentrations were relatively stable over time. Clear oscillations were observed in a small proportion (<20%) of cells imaged (Figure 6.8A). 10^{-5} M ionomycin caused a rapid increase in Ca^{2+} (Figure 6.8D). These responses varied markedly from cell to cell although almost all cells responded to this concentration of ionomycin (>90%). The maximum responses were typically achieved within 30 sec of stimulation with a gradual reduction toward plateau levels after 3-10 min. At lower ionomycin concentrations, the single cell data revealed a tendency for lower maximal responses and delays between ionomycin addition and Ca^{2+} elevation (Figure 6.8B).

Consistent with the single cell observations above, the population averaged data revealed that the maximum ionomycin effect and response kinetics were both dependent upon ionomycin concentration. Notably, the maximum response: plateau response ratio was greater with 10^{-5} M ionomycin than with 10^{-6} M ionomycin and the time taken to achieve the maximum response was less with former than with latter.

Binning individual cells according to the log of the nuclear Fluo-4 stain intensity revealed pronounced cell to cell variation in the Fluo-4 levels. Ionomycin increased the population averaged Fluo-4 levels by shifting the FD plots rightward. No evidence was obtained for ionomycin responsive and non-responsive cell populations, as a graded response rather than an all-or-nothing response was seen (Figure 6.8G). The pronounced overlaps between the FD plots for stimulated and unstimulated cells suggest that MI values will be low. This is shown in figure 6.8H. MI values were calculated for single-time-point data, and these followed a very similar time-course to

the Fluo-4 responses. They increased to a maximum of 1.3 ± 0.06 Bits at 24 sec and then reducing gradually. MI was also calculated taking response trajectories of individual cells into account using 140, 160, 300 sec, and this was increased to 1.5 ± 0.03 Bits. The MI values are greater in cells stimulated with ionomycin than with GnRH (compare Figure 6.2 and Figure 6.8).

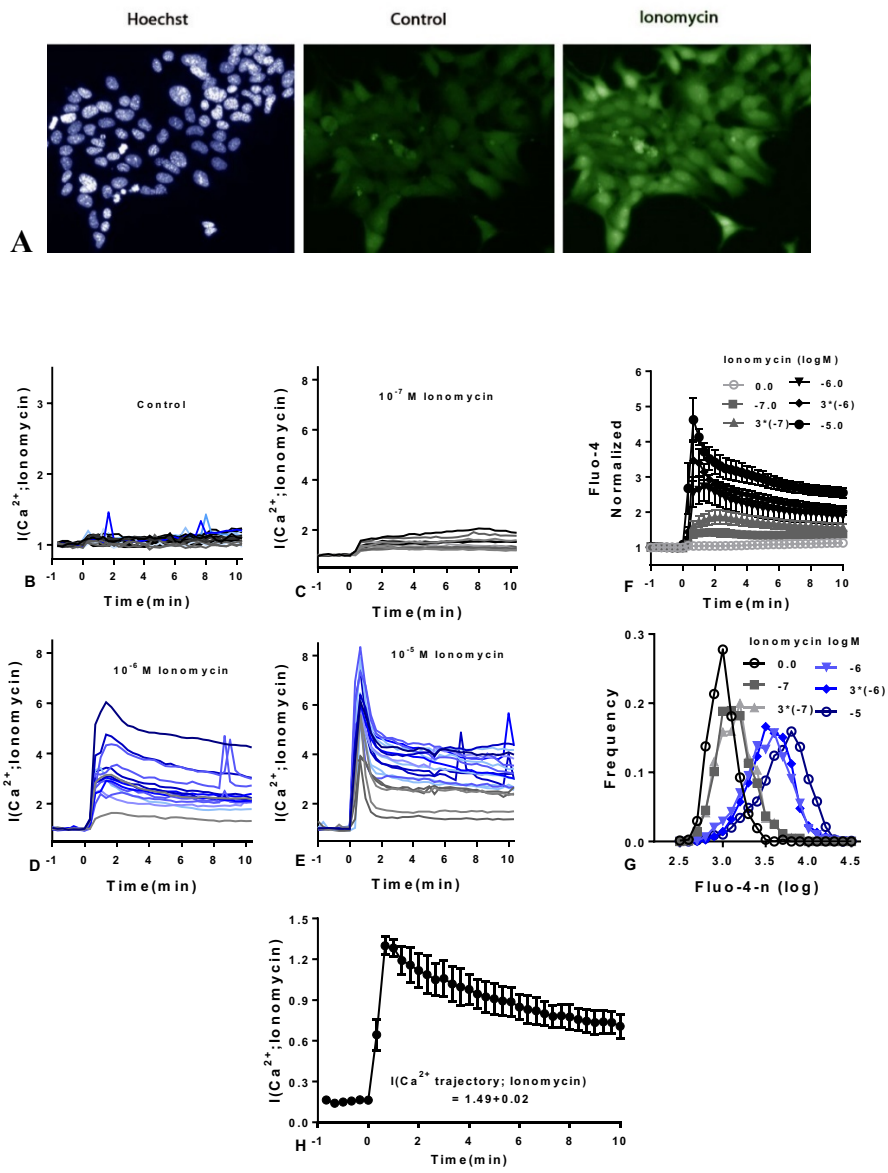

Figure 6.9. Ionomycin-mediated Ca^{2+} mobilisation

Cells were cultured and treated as described in Chapter 2. Images were collected every 20 sec, and a Matlab tracking algorithm was used to follow individual cell responses over time. The cells that had a failed tracking were removed (around 2% of cells, defined as outliers). Panel A shows representative images of Hoechst, nuclear stain and Fluo-4 stained cells cultured under control condition or stimulated with 10^{-5} M ionomycin for 24 sec. Representative single cells responses are shown for control cells (B) for cells stimulated from time 0 with 10^{-7} M ionomycin (C), with 10^{-6}M ionomycin (D) and with 10^{-5}M ionomycin (D). Population average responses for all tracked cells are shown as the means ± SEMs, n=4 (E). The total number of cells tracked for each GnRH concentration was between 130 and 320 cells. The I(Ca^{2+}; ionomycin) values for all tracked cells at each time point are calculated shown in D. It also (D) shows MI calculated taking trajectory into account (140, 160, 300 sec).

6.3.8. Discussion

Single cell measures of the amount and/or activity of signalling protein reveal high cell-cell variability. Information theory-derived statistical approaches can be used to explore the influence of such heterogeneity on information transfer [274, 283, 296, 298]. The signalling experiments in the previous chapter showed that the MI values used to measure information transfer via GnRHRs were always <1 Bit regardless of the experimental measure, and cell type studied. This indicates that GnRHRs engage noisy communication channels with most of the information lost through signalling. However, the obtained data were by imaging fixed cells, and such snapshot data might underestimate information transfer. The effects of GnRH are usually dependent on temporal aspects of the stimulus, such as stimulus duration with constant stimulation, or pulse characteristics with intermittent stimulation. Thus, an obvious possibility is that cells gain additional information by sensing over time.

This chapter aimed to determine if additional information is gained by sensing response trajectories over time. This was achieved by live cell monitoring of Ca^{2+} responses and Ca^{2+}-driven NFAT1c-EFP translocation in cells stimulated by GnRH. In addition, and as GnRH is secreted in pulses, the second aim was exploring if additional information is gained by repeated GnRH pulses. Sensing ionomycin was also considered.

The main findings were that GnRH caused concentration and time-dependent increases in NFAT1c-EFP-NF in live LβT2 cells (Figure 6.1). It also caused a similar effect in Ca^{2+} in both LβT2 and HeLa cells (Figure 6.2 and Figure 6.3). The calculated MI at each time point for both measurements were relatively low (<0.4 Bits for NFAT1c-EFP responses and <0.8 Bits for Ca^{2+} responses). Notably, the time-courses

for GnRH effects on MI were largely similar with time-course for the population averaged to the NFAT1c-EFP and Fluo-4 responses. This observation indicates that the dynamic range is the main factor of the observed MI values and implies that cell-cell variability does not simply scale with any of these population averaged responses.

The obtained results here also revealed that information was underestimated by having snapshot data. For each of these experiments, MI values were calculated taking response trajectories in individual tracked cells into account and this increased MI values from 0.38 Bits to 0.54 Bits for the NFAT1c-EFP translocation response in LβT2 cells, from 0.74 Bits to 1Bit for Ca^{2+} responses in LβT2 cells and from 0.56 Bits to 1Bit for Ca^{2+} response in HeLa cells. Here, the key observation is that for each cell type and/or experimental readout, additional information is gained by sensing over time. However, still most available information is lost through signalling, even when trajectories are considered (as system inputs were 2.45 Bits).

These data extend (and in part contribute to) a recent study in which GnRH effects on NFAT1c-EFP translocation was studied in Ad GnRHRs transduced HeLa cells [153]. That work revealed a similar effect of GnRH on NFAT1c-EFP. The response was sustained and marked cell-cell variability was observed. The MI values were higher with I(NFAT1c-EFP; GnRH) approximately 0.6 Bits in HeLa cells, as compared to 0.39 Bits in LβT2 cells. Interestingly some differences were observed, and these are that a) responses were more rapid in HeLa cells than in LβT2 cells and b) that consideration of trajectory increased MI estimates for LβT2 (from 0.38 Bits to 0.54 Bits) but not for HeLa cells [153].

The response of Ca^{2+} to GnRH has been extensively characterised in different cell lines [140, 369-371]. In pituitary gonadotrophs, GnRH causes biphasic increases in

[Ca^{2+}]i [371]. Oscillatory responses were described in male mice, and transient responses at both lower and higher concentrations were recorded from acute pituitary slices *in vitro* [369]. A similar study, in mouse gonadotrophs described the responses in individual cells and revealed that responses are varied in duration, magnitude, and frequency of oscillation [370]. Here in this work, a small proportion of oscillatory pattern was seen under the control condition (< 20%) in both LβT2 and HeLa cells. In both cell types, the highest concentrations of GnRH caused biphasic (spike-plateau) responses, while at lower GnRH concentrations more gradual elevation was observed. The time taken to achieve the maximum response was longer than the time taken with highest GnRH concentrations.

MI was calculated, and obtained results revealed that the I(Fluo-4; GnRH) values were ~0.8 Bits in LβT2 cells and ~0.6 Bits in HeLa cells. These increased to a maximum of ~1Bit with trajectory consideration. This is the first study to quantify information transfer via GnRHRs using Ca^{2+}-sensitive dyes, and it reveals that information appears to be lost early in the GnRH signalling network (i.e. prior Ca^{2+} mobilisation). Noteworthy, although single cell responses in both cell lines were relatively similar, some differences where observed. These are that in HeLa cells (Figure 6.3), a small and transient response occurred in the control group after fluid addition (PSS buffer without GnRH), such a response did not observe in the endogenous expression system (LßT2 cell line, Figure 6.2). When MI values were calculated, different time dependencies between HeLa and LßT2 cells was clearly observed. (Compare Figure 6.2 H and Figure 6.3 H). In HeLa cells, the MI values peaked to 0.54 Bits within 30 sec of GnRH addition, then dropped to ~0.4 Bits a minute later, before peaking again to 0.65 Bits over 4 minutes then again reduced to 0.5 Bit at 10 min.

For LßT2 cells, MI value was ~ 0.8 Bit 30 sec of GnRH stimulation, reduced to 0.6 Bit over 2 minutes and remained unaltered during the examined period. Likewise, when trajectory was considered using different time points (see appendix, table 3). MI values were relatively higher when late time points consider in HeLa cells, and the opposite was for LβT2 cells. These differences could reflect the differences in mechanical stimulation on cytoplasmic Ca^{2+} concentration in these cell lines.

The observed difference in time-courses for GnRH effects on I(NFAT1c-EFP-NF; GnRH) and I(Ca^{2+}; GnRH) are best illustrated by the experiments in which NFAT1c-EFP translocation and Rhod-3 were imaged in the same cells (Figure 6.4 and Figure 6.5), with I(NFAT-EFP-NF; GnRH) increasing gradually to a maximum of 0.4 Bits at 10-20 min and I(Ca^{2+}; GnRH) peaking to ~0.9 Bits within 1 min. Similar differences were observed for the population averaged responses that were rapid and transient for Rhod-3 as compared to the slower and more sustained NFAT1c-EFP translocation response (Figure 6.5). For these experiments joint MI was also calculated, reasoning that if the NFAT translocation response was modulated by GnRH effects other than Ca^{2+} elevation, there might be a poor correlation between the two responses and a substantial increase in MI by consideration of both. However, the maximum joint sensing MI value was very similar to that for Ca^{2+}alone arguing against this possibility. Joint MI exceeded that for either response alone at later time-points implying that the correlation between the NFAT and Ca^{2+} responses reduces at later time-points.

GnRH caused a concentration and time-dependent increase in NFAT1c-EFP-NF in LβT2 cells. The effect was reversed when the stimulus was washed off and repeated when a 2nd stimulus was added. Calculated MI values were similar in the 1st and 2nd

pulse and little additional information was gained by sensing the second pulse (0.08 Bit). Similar results were obtained in previous work done in HeLa cells [153].The additional information from sensing the 2nd pulse suggests a good correlation between individual cell responses in 1st and 2nd pulse. This was confirmed in the previous study by showing the response in one pulse could be predicted from the response in the other (MI 1 Bit) [153]. An important difference between this and the earlier study is that the use of the INCell 2200 here enabled automated stimulus addition so that a pre-stimulation control could be established. Also, washing the 1st from HeLa cells caused a major increase in NFAT1c-EFP-NF that is presumably an artifact caused by mechanical stimulation and was much less prevalent in the LβT2 data shown here. Remarkably, the MI value calculated from NFAT1c-EFP-NF after the 1st GnRH pulse and during the pulse was comparable. This is in line with the idea that GnRH signalling continues between GnRH pulses and that such inter-pulse signalling contributes to downstream responses during GnRH pulses. This would require that the stimulus can be sensed from the inter-pulse signal, precisely as shown here.

A similar two pulse protocol was used to examine the amount of additional information that could be gained by a 2nd GnRH pulse using Fluo-4 as the signalling readout. The main difference is that the interval between pulses was varied to explore the amount of additional information gained by a 2nd GnRH pulse. The responses of Ca^{2+} are more rapid in onset compared to NFAT1c-EFP translocation responses so that the duration of the 1st pulse can be decreased, and rapidly reversed. Thus, the interval between pulses can be reduced and varied. The expected concentration-dependent and time-dependent increases in Ca^{2+} during the 1st and 2nd pulse with GnRH was seen. Unexpectedly, a smaller response to the 2nd pulse of GnRH was seen with longer inter-pulse intervals (Compare 1st and 2nd pulses in Figure 6.7A and C).

However, the reduction does not reflect desensitisation to GnRH as a similar response was observed in cells treated with PSS alone without GnRH and imaged for further 90 min before stimulation with GnRH (Figure 6.8). A possible explanation is that during the extended incubations period a proportion of the Ca^{2+} sensor is lost from the cells. It may also be that the sensor is altered chemically that reduced its Ca^{2+} sensitivity. Nevertheless, as MI values are not affected by transformations of the output or input, theoretically, this should not impact the calculated MI values. As shown in Figure 6.7, MI values calculated for 1st pulse and 2nd pulse were comparable regardless of the time interval between them (~0.7 Bits and ~0.6 Bits for 1st pulse and 2nd pulse respectively). It was previously predicted that cells would gain additional information as the interval between the pulses increased [153]. Yet, this is not the case here as the additional MI values were low (0.06-0.2 Bits) irrespective of the pulse interval (10-90 min). Therefore, both NFAT1c-EFP translocation data and Ca^{2+} imaging data argue against the possibility of repeated pulses could increase the reliability of GnRH sensing.

The fact that signalling pathways act as noisy communication systems with much information lost through signalling is increasingly recognised, but the sites at which information is lost is very poorly defined. As shown, I(Ca^{2+}; GnRH) values were typically <1 Bit implying that most information is lost prior Ca^{2+} mobilisation. Thus, in the final experiments, ionomycin (a Ca^{2+} ionophore) was used. It enhances Ca^{2+} influx by stimulating store-regulated cation entry [372]. As expected, ionomycin caused concentration and time-dependent increases in Ca^{2+} (like GnRH, Figure 6.8). However, the I(Ca^{2+}; ionomycin) value was maximum at 1.25 Bits within 30 sec of stimulation and was increased to 1.5 Bits by consideration of trajectory.

Interestingly, the MI value with this GnRHR-independent stimulus is greater than any MI value reported here for GnRH signalling. This suggests that the GnRHR and its upstream effectors are a signalling node at which significant information loss occurs. Similarly, the fact that I(Ca^{2+}; GnRH) values exceed I(NFAT-NF; GnRH) values and that these in turn exceed I(NFAT-RE values) in both the HeLa and LβT2 cell models, implies that information is lost at each step through the signalling cascade (Figure 5.1 and Figure 5.3). The recorded loss of information could be a result of engaging the stimulus with IP_3R on endoplasmic reticulum for calcium mobilisation. A study by Lestas *et* all., in 2010, showed that there is a correlation between the number of components that mediates a specific target and the efficiencies of signalling networks. More generally, increasing the number of mediators would provide more opportunities for the noise to suppress information transmission through the networks [373].

Sensing other receptors was also considered in this study. Oxytocin receptors have been implicated in regulation of gonadotrophin expression. Oxytocin stimulates gonadotrophin secretion from pituitary cell cultures and increases the Ca^{2+} concentration [374, 375]. However, when LßT2 cells were loaded with Fluo-4 and stimulated with 10^{-6} M-10^{-10} M oxytocin, no response was seen (data not shown). This could be because this cell line does not express the endogenous oxytocin receptors. In fact, a study has revealed that although oxytocin receptors are present in the anterior pituitary, its expression appears to occur on lactotroph cells rather than gonadotroph cells [376]. On the other hand, another research showed the oxytocin increased the cytosolic Ca^{2+} concentration in αT3-1 cell line (a murine gonadotroph-derived cell line) [374].

As mentioned above, the sources of cell-cell variation that effect information transfer are very poorly defined. A recent publication described a model of GnRH signalling to NFAT (a mixed mechanistic and probabilistic model) [153]. In that model the expression level of two effectors (GnRHR and CaM) were fluctuated across different time-scales to introduce heterogeneity. The main conclusion was that if the introduced variations are relatively constant over time, the response in the 2nd pulse can be predicted from that in the 1st pulse, and thus cells can gain little or no information by sensing both. On the other hand, if the effector concentrations vary rapidly the response of the 2nd pulse cannot be inferred from the 1st pulse (or vice versa). Consequently, a marked increase in information will be gained from sensing both pulses [153]. The published HeLa cell NFTAT1c-EFP translocation data were in accord with the former possibility (little information gain from sensing the 2nd pulse). This is also true for the LβT2 cell NFAT1c-EFP translocation data described here. Thus, although the main reason for the heterogeneity in the NFAT1c-EFP translocation response is not clear, it appears not to be dependent on any component of a network that varies markedly in the time-frame of these experiments (approximately 2 hr). Interestingly, here the responses of Ca^{2+} are rapid in onset and offset, and rapid oscillatory responses are seen in some cells [140, 369, 370]. These indicate that the relevant network components could be less stable. Therefore, we expected that by increasing the interval between the pulses, the estimated MI from sensing both pulses might increase. Nevertheless, this was not the case, as we can see in Figure 6.8, the additional MI values were low irrespective of the pulse interval (10, 20, 60 and 90 min).

Overall, the reasons behind the variability in single cell Ca^{2+} responses still unknown. It could be related to the differences between cells in the signalling network features

that are relatively stable over time, such as variations in concentration of component proteins or their compartmentalisation.

Chapter 7 – Conclusion

7.1. Background and scope of the study

Since the isolation of GnRH from the hypothalamus four decades ago, landmark studies have been conducted identifying its structure [12, 19, 61, 112], secretion and regulation [377, 378]. In addition to that, the structure of GnRHRs and their mechanisms of action have been extensively characterised [76, 120, 190, 240, 256]. Notably, the mammalian type I GnRHRs lack COOH-terminal tails that are found in other GPCRs and contribute to their rapid desensitisation [190]. Signalling pathways are initiated following the activation of receptors by GnRH [152, 153]. The interaction of these pathways within the networks create complex systems, allowing for high coordination of cellular responses. However, it has been reported experimentally [379] and theoretically [380] that cellular systems are heterogeneous. GnRH is secreted in a pulsatile manner, and *in vivo* studies demonstrated that individual gonadotrophin genes respond differentially to GnRH pulses [317, 381, 382]. Therefore, the intracellular signalling network should decode the received information to ensure an appropriate physiological response of the gonadotroph cell.

Several studies have revealed that GnRH effects are cell context-dependent, suggesting different signalling mechanisms in different cell types. Therefore, the overall aim of the work here was to advance our understanding of GnRH signalling by exploring differences in responses between different cell types as well as between individual cells of a given cell type. First, the work focused on identifying the optimal cellular model for studying the mechanisms of GnRH action. This was done using a conventional approach to compare GnRH signalling in three cell types HeLa and MCF-7 cells (extra-pituitary cell lines) and LβT2 cells (a gonadotroph-derived cell line). Due to the complexity of GnRHRs signalling mechanisms, the work was

extended beyond just describing structure of biological networks to using a mathematical approach that allowed us to examine the reliability of signalling networks in transferring information about the extracellular environment to the cells. Recently, this approach was used to quantify transferred information via different signalling pathways [152, 153, 298-300, 383]. These combined methodologies have advanced our understanding of signalling mechanisms. The main findings for each results chapter are summarised below.

The first two chapters studied the cell context-dependence of GnRHR signalling to the ERK and NFAT pathways in the three cell types. Measures were collected from the population average, and the emphasis was on the response kinetics in Chapter 3, and the sensitivity of ERK and NFAT pathways to pharmacological inhibition in Chapter 4. Chapter 3 begun by monitoring the effect of GnRH on ERK and NFAT signalling pathways that was achieved using a high content imaging system (an INCell 1000 or an INCell 2200). Another aim was to characterise the responses of both ERK and NFAT to EGF and a PKC activator as EGF receptors and PKC are both implicated in GnRH signalling. The main findings were that a) ERK activation is stimulus-specific (sustained activation by PDBu and transient activation by EGF), and b) that GnRH effects on ppERK were cell context-dependent (transient in extra-pituitary cell lines and sustained in the pituitary-derived cell line, Figure 3.11, Figure 3.12, and Figure 3.13). GnRH-mediated Egr1-driven zsGreen expression (a readout for ERK driven gene expression), and NFAT-RE- driven asRed expression (a readout for NFAT-driven gene expression) were found to be comparable in both LßT2 and HeLa cells. However, in MCF-7 cells, the effect of GnRH on NFAT-RE- driven asRed expression was relatively weak, and no effect was seen on Egr1-zsGreen expression in this cell line (Figure 3.14 and Figure 3.15). Overall, the work on Chapter 3

confirmed that GnRHR signalling is indeed dependent on the cellular context and emphasised the importance of examining different cell lines in signalling pathway studies. It also helped to optimize the protocols for examining ERK and NFAT signalling, that were further examined in the next chapter with the additional use of pharmacological inhibitors.

Chapter 4 aimed to use distinct pharmacological inhibitors in order to further delineation of the network architecture of ERK and NFAT. The experimental results revealed that GnRH acts via type I GnRHRs in all three cellular models examined because cetrorelix prevented GnRH signalling to ERK and NFAT (Figure 4.1, Figure 4.4 and Figure 4.7). Endogenous GnRHR expression is reported in some hormone-dependent cancer cells [351, 384-387] but not in MCF-7 cells [199]. It has been thought that context-dependence of GnRH effects in hormone-dependent cancer cells can reflect activation of endogenous type II GnRHR [388-390]. Yet, when cetrorelix was applied in MCF-7 cells transduced with Ad mGnRHR for functional GnRHR, the antagonist blocked GnRH effect on ERK or NFAT revealing that GnRH is acting via the type I GnRHR. GnRH-mediated ERK activation was PKC and MEK dependent and EGFR independent in all three cell lines. Moreover, GnRH caused Ca^{2+} dependent activation of NFAT1c-EFP in all cell types examined. Although the EC_{50} values of GnRH effects on the receptors were similar in the three cell types, results here revealed that signalling is cell-context dependent. For example, the PKC inhibitor caused a marked reduction in ppERK in LβT2 cells compared to HeLa or MCF-7 cells. There was no evidence for EGFR transactivation mediating GnRH signalling to ERK. EGFR undergoes a rapid agonist-induced internalisation [280, 391] that presumably contributes to the transient responses observed in these cells. EGF-mediated NFAT1c-EFP activation is also context dependent, as stimulation with EGF resulted in nuclear

translocation of NFAT1c-EFP in HeLa cells, but not in the other two cellular models used. On the other hand, the PKC activator (PDBu), failed to activate NFAT1c-EFP (a readout for Ca^{2+}/CaM/Cn) in any of the cellular models (Figure 3.11, Figure 3.12 and Figure 3.13). Although early work by Jobin and Chang used PKC activator (12-O-Tetradecanoylphorbol-13-acetate TPA) and reported that the TPA increases Ca^{2+} in goldfish pituitary cells [345]. The experimental results in this work contrast with the earlier finding in that PDBu does not increase the Ca^{2+} level in these contexts.

Taken together these data revealed that GnRHR signalling is dependent upon cellular model, as demonstrated by the differences in response kinetics (compare ppERK responses in HeLa or MCF-7 to LβT2 cells) and by the sensitivity to pharmacological inhibition (Figure 4.10). The idea of cell-context dependent GnRHR signalling is not novel [6, 110, 120, 145, 392-398]. However, interpreting published results are complicated. This is because GnRH effects have been monitored using different methods, in different cell types and by different groups. The work here was performed by a single experimentalist, using similar methods, and it was conducted as internally controlled comparisons of different cell lines, different stimuli and different inhibitors. The obtained results from these better-controlled studies revealed that the concept of cell context-dependency was not limited to GnRHR signalling but it was also seen for EGF signalling.

Signalling through mouse GnRHR can be differently constructed in these genetically different cell lines. HeLa and MCF-7 cells had to be transduced with the Ad for GnRHR expression. An implication of this is the possibility that GnRHR signalling mechanism could be affected, especially, these cells are derived from cancer cells that are genetically different from normal human cells. LβT2 cells are gonadotroph cells

that express the endogenous GnRHR in addition to αGSU and LHβ. Thus, this cell seems to be optimal for GnRHR signalling mechanism study, but the use of SV-40 oncogenes to drive their proliferation could impact GnRHR signalling. Therefore, it could be concluded that there is no single ideal cellular model for GnRHR signalling studies and that the optimal approach could be to use different cell types, primary cultures, studies on animal models (*in vivo*), and clinical data.

To sum up, the data in Chapters 3 and 4 show that GnRH signalling is, in fact, dependent upon cellular model, extending earlier work by showing that this is the case in internally controlled experiments using identical experimental measures. The cell context-dependency was observed by comparing response kinetics (Figure 3.4 and Figure 3.7), and sensitivity to pharmacological inhibition (Figure 4.1, Figure 4.4 and Figure 4.7) and was also seen in responses to EGF (Figure 3.12). However, although using different inhibitors have helped us in mapping the signaling network, it tells us nothing about the amount of information transferring through specific pathways or effectors in the GnRHR signalling system. Thus, an information theoretic approaches to investigation of GnRHR signalling were used in the following chapter.

7.2. Exploring cell-cell variability and its impact on information transfer with fixed cells.

The work described in Chapters 3 and 4 address context-dependence of GnRH signalling in population averaged responses and compared its effect in genetically distinct cell lines. However, studies on single cells revealed marked cell-cell variation in response to GnRH [153], suggesting difference in the arrangement of GnRHR signalling network between genetically identical cells within a given cell type. The

0experiments reported in Chapters 5 and 6 were performed to evaluate this variability and mainly its impact on information transfer [152].

The high content imaging platform used in this study provides the possibility to obtain the same experimental measures for each individual cell. These individual cell responses were used to quantify transferred information via GnRHRs to ERK or NFAT. Transmitted information was quantified using MI which is a statistical measure that takes cell-cell variability into account [283, 298]. The results revealed that most available information about GnRH concentration in the environment was lost through signalling. This is consistent with other studies that reported loss of information via other signalling pathways in other systems [298-300, 399], but it is nevertheless surprising as it indicates that a single gonadotrope cannot even unambiguously distinguish between two GnRH concentrations, despite the fact that GnRH concentration-response curves are graded over a broad range of hormone concentrations. The low MI values were recorded in the three cellular models revealing comparable information transfer via endogenous and heterologous expressed GnRHR. The loss of information was not limited to the ppERK cascade as similar results were obtained from consideration of information transfer between GnRHRs and NFAT irrespective of the cellular model used (Figure 5.9). A recent work studied the impact of GnRHR number on transferred information to ppERK in Ad mGnRHR transduced HeLa cells, and the transmitted information between PDBu and ppERK [152]. The main conclusion was that I(ppERK; GnRH) could be increased by increasing the GnRHR number [152]. Furthermore, a loss of information was reported between ppERK and PDBu (PKC activator), implying that factors other than GnRHR number could harm information transfer in these pathways.

The low MI values raised two distinct questions a) how do cells mitigate the loss of information? and b) do the experimental conditions contribute to underestimation of information transfer. For the former question, and as GnRHR engage a bifurcating signalling system, cells might gain additional information by sensing multiple pathways within the network. However, although sensing both pathways showed a significant increase in information transferred (Figure 5.1 and Figure 5.2 as an example), the increases were small, and still, most available information about GnRH concentration in the environment is lost through the cascade. Thus, the other concerned (the technical issue) was considered and the methods used (e.g. 1°Ab and 2°Ab dilution, acquisition time and cell number) were optimised to maximise MI estimates. This revealed that MI values were not underestimated by using sub-optimal assay conditions (Figure 5.7 and Figure 5.8). As described in Chapter 3, activating TKRs by EGF caused the activation of both ERK and NFAT cascades in HeLa cells. It is possible that cells could sense their environment more reliably via other pathways/receptors than the once considered. This model has been applied before to estimate information transfer via EGF receptor to ERK [298]. Thus, the introduced model here can be used to consider other pathways or receptors (e.g. PACAP, Oxytocin) for further research in signalling mechanism.

The main conclusion drawn from the data in Chapter 5 is that a significant amount of information is lost through GnRHR signalling to ERK and NFAT, irrespective of the cellular model used and although information transfer was increased by joint sensing, the increases were limited. As shown in HeLa cells (For example, Figure 5.1), the estimated MI value was high at early time point (5 min) and reduced thereafter (by 60 min), and this means that the 60 min snapshot data underestimate the information gained over the entire stimulation period. The 5 min snapshot data could also

underestimate the information transferred over this period. In other words, by ignoring response dynamics, information transfer might be underestimated, and cells could sense information over time. This was the focus of the work documented in Chapter 6.

7.3. Exploring cell-cell variability and its impact on information transfer in live cells

The experimental results at the previous chapter have indicated three key points; 1) the loss of information is not restricted to ERK or NFAT cascade, 2) joint sensing is a mechanism that cells could use to mitigate such loss, 3) the low MI values are not related to the techniques used. However, it is possible that the use of fixed cells and snapshot data had caused underestimation of information transfer. Indeed a stochastic modelling was proposed by Margaritis and et al., where they predicted I(ppERK; S) using snapshot data and compared with I(ppERK; S) value taking trajectory into count [152]. The system input was 3 Bits, and the snapshot MI value had a maximum of 1.4 Bits, but this was increased to 2.8 Bits with trajectory consideration [152].

This possibility was explored using live cell monitoring of Ca^{2+} responses and Ca^{2+} driven NFAT1c-EFP translocation in LβT2 cells. In fact, gaining additional information by sensing responses dynamics over time was explored previously in HeLa cells by our group [153]. The main differences here are that LβT2 cells express the endogenous receptor, so the variability that might be introduced due to Ad mGnRHR transduction is avoided. Another difference is that in this study cells were stimulated automatically rather than manually using INCell analyser 2200, therefore, a technical source of variation is removed. However, the most important and novel

aspect of the work here is that using the automated injection allowed us also to follow rapid Ca^{2+} responses. The experimental results revealed that such snapshot data do indeed underestimate information transfer. This is evident from calculated MI value that was a maximum of ~0.4 Bits at 30 min for NFAT1c-EFP-NF and increased to ~0.6 Bits with trajectory consideration (Figure 6.1).

For Ca^{2+} imaging data, cell-cell variability was seen in the LβT2 cell responses to GnRH and clear oscillations were observed in a small number of cells. Rapid and transient responses were induced by the highest concentrations of GnRH (Figure 6.2). The maximum responses were at 24 sec of stimulation followed by a gradual reduction toward plateau levels. The population averaged responses were consistent with the single cell responses. With 2.45 Bits of system input, calculated MI values were ~0.8 Bits at 24 sec and increased to 1 Bit with trajectory consideration. Accordingly, the maximum estimates for information transfer via GnRHR are higher with the Ca^{2+} sensor than with the NFAT1c-EFP translocation reporter. The Ca^{2+} imaging data like the NFAT1c-EFP translocation data suggest that most information is lost through signalling. However, comparison of the two results indicates that most information is lost through signalling, and most likely occurs early in the GnRH signalling network, prior to Ca^{2+} mobilisation.

The data above suggest that GnRHRs engage noisy communication channels with most available information lost through signalling, and most likely at the level of GnRHR coupling to its G-protein or G-protein activation of PLC. If this was true, we would expect to have higher MI values with a GnRHR-independent stimulus for Ca^{2+} mobilisation. The obtained results that are presented in Figure 6.9 confirmed the above possibility. Stimulation of LβT2 cells with ionomycin caused concentration and time-

dependent increases in Ca^{2+}. The single cell responses to ionomycin were like those described for GnRH. The maximum response was achieved within 30 sec, and the population averaged data were consistent with the single cell observations. The MI values were greater than MI values for GnRH sensing. They were maximum of 1.25 Bits within 30 sec of stimulation and increased to 1.5 Bits by consideration of trajectory (Figure 6.9).

GnRH is secreted in a pulsatile manner that is critical for normal reproductive function [19, 23, 261, 266], and signalling continues after GnRH pulses. This pattern of GnRH secretion raises two questions, 1) how much information transfer occurs after the GnRH pulse, and 2) how much additional information do cells gain by sensing a second pulse of GnRH. These questions were explored by imaging of NFAT1c-EFP as shown in Figure 6.6. The MI values for snapshot data in the 1st and 2nd pulses were ~0.4 Bits and ~0.3 Bits respectively. Cells did gain a little information by sensing a repeated pulse but not much (~0.1 Bit), and with the consideration of response trajectory, these values were increased to a maximum of 0.55 Bits.

The sources of cell-cell variation that harm transmitted information are unknown. Recent work developed a mixed mechanistic and probabilistic model suggested that if the sources of variations are relatively stable over time, the response in the 2nd pulse would be predicted from the response in the 1st pulse, and that cells would gain little or no additional information by sensing both pulses. In contrast, if the sources of variations are unstable over time the response of the 2nd pulse cannot be inferred from the 1st pulse. In this case cells would gain more information from sensing both pulses [153]. The LβT2 cell NFAT1c-EFP translocation data described here are in accord with the former possibility, and similar work was published in HeLa cells [153].

The above hypothesis was explored experimentally here by loading LβT2 cells with Fluo-4 (as Ca^{2+} indicator), then cells were received two pulses of GnRH, and the time between pulses was varied (10, 20, 60 and 90 min). The population averaged responses were dependent on GnRH concentration. As expected, GnRH caused a rapid increase in Ca^{2+} (Figure 6.2), and the maximum responses typically occurred within 1 min of stimulation for each pulse. However, the MI values calculated for the 1st and 2nd pulse were comparable and did not differ significantly with different inter-pulse intervals. Most importantly, the additional information from sensing a 2nd pulse was low (0.06-0.2 Bits) for all time intervals, as summarised in Figure 6.7. Consequently, from the NFAT1c-EFP translocation data and Ca^{2+} imaging data, we can argue against the possibility that repeated pulses increase the reliability of GnRH sensing.

7.4. The meaning of MI

Information theory-derived statistical approaches are the novel aspect used in this work to quantify the amount of information transfer through signalling pathways. This approach came to eminence in 2011/2012 with a number of publications that explained the use of computational approaches for such quantification [124, 265, 266, 273, 274, 289-291, 367, 368]. The main aspect of this approach is that information can be defined as uncertainty [292]. The term information had been previously used in the field of signal transduction but in an undefined way. There was a common assumption that when an inhibitor reduces a response, this equates to a reduction in information transfer through signalling network. However, it is possible that the reduction in the population averaged response is mirrored by a reduction in cell-cell variability. In this case, the inhibitor would not have affected the reliability with which

the system input can be inferred from the output (i.e. information transfer would not be reduced). Thus, experimental work is needed to investigate if the partial reduction of GnRH effects on pERK by PKC inhibition is correlated with a reduction in information transfer. In a similar way, it would be of interest to pre-treat cells with GnRH and investigate if homologous desensitisation (as measured by population averaged responses) is associated with impaired GnRH sensing (as measured by MI). Generally, the use of information theory in signalling studies has highlighted a fundamental point, which is that response size cannot safely be equated to information transfer as it "information transferred" is also affected by noise in biochemical signalling networks.

Here, the MI between system inputs and outputs has been used to measure information transfer between stimulus (e.g. GnRH concentrations) and responses (e.g. ppERK). The merits of this measure are that MI does consider cell-cell variability and response size. It also, unaffected by non-linear input-output relationships that are common in signal-transduction pathways providing us with more reliable measures [125]. However, MI values are dependent on the input distribution. For example, in this work, we have used 8 different concentrations of GnRH to provide the full range of the concentration-response curve (e.g. 0 and 10^{-12}-10^{-6} M GnRH). MI is measured in Bits where I Bit of information can resolve two different values (8 different concentration provides 3 Bits). However, MI values would be expected to be lower with a lower concentration of GnRH (e.g. 0 and 10^{-18}-10^{-12} M GnRH) and higher with a higher concentration of GnRH (e.g. 0 and 10^{-7}-10^{-2} M GnRH). The main point is that MI values measured are input distribution dependent. Thus, an alternative approach would be quantifying the information transduction capacity of a signalling channel. In other words, using an approach to define the maximum amount of information that a

signalling network can transfer with any input distribution. This is computationally demanding, but a recent approach named SLEMI (Statistical Learning Based Estimation of Mutual Information) provides algorithms to do this (i.e. for quantifying information capacity of a signalling channel) [400]. It would certainly be of interest in future work to estimate the capacity of GnRHR signalling channels, as opposed to information transfer.

The underestimation of snapshot data (in MI estimates) has highlighted the requirement for live cell imaging in order to take response trajectories into account. This is evident in Chapter 6, where live cell imaging revealed maximal I(NFAT1c-EFP; GnRH) values of approximately 0.4 Bits, whereas estimates taking trajectory into account increased to >0.5 Bits (Figure 6.1). However, consideration of the response trajectory was limited to 3-4 time points (see appendix, table 3). This, in turn, may lead to significant underestimation of the potential information available from sensing response trajectories. The aforementioned SLEMI approach simplifies the computation, facilitating the consideration of multidimensional system outputs. It may therefore be advantageous to use this technique in estimating MI as this should enable consideration of more or all time points. Alternatively, transcriptional reporters could be developed further. Here, the responses of NFAT-RE-asRed were imaged after a period of 8 hr GnRH stimulation. This 8 hr NFAT-RE-asRed transcriptional response could be sensitive to the time-course of NFAT translocation in each cell. So, although correction for the expression level of the reporter construct would be needed, further research could be undertaken to ask if MI values and information capacity calculated for upstream readouts and consideration of trajectory are any higher than those calculated for a single time-point transcriptional readout.

The work on this thesis was focusing on sensing GnRH although pituitary gonadotrophs and gonadotroph-derived cell lines are regulated by many other endocrine, paracrine and autocrine factors (e.g. growth factors, nucleotides, gonadal steroids, and other peptides like oxytocin and PACAP). The significance of such stimuli for the physiology of gonadotrophs and the pathways through which they act, are often poorly defined. Therefore, in future work, it would be of interest to use MI and information capacity to explore the ability of gonadotrophs to sense these inputs. Preliminary attempts using oxytocin and PACAP yielded unexpected results as both stimuli failed to increase Ca^{2+} in LβT2 cells (unpublished data). The SLEMI approach mentioned earlier has been developed to consider multiple variables (i.e. inputs and outputs). This can be many time points (as outlined above), and it could also be different responses. Thus, the consideration of joint sensing could be extended to consider more than two pathways or various inputs.

The reasons for cell-cell heterogeneity is unknown. Regarding GnRH signalling, the most likely possibilities are that it reflects cell-cell variation in concentrations of GnRHR or its effectors. In fact, in this work, the I(Ca^{2+}; ionomycin) values were found to be higher than I(Ca^{2+}; GnRH) values, as shown in Figure 6.2 and Figure 6.7. These findings revealed that loss of information is related to noise upstream (i.e. at the level of the GnRHR and its upstream effectors). Moreover, the obtained results here showed that cells gained little information from sensing a 2^{nd} pulse of GnRH (Figure 6.4), suggesting that the features that cause cell-cell heterogeneity are relatively stable at least during the time-course examined in this work. Apart from these conclusions, nothing is really known about the reasons for cell-cell variability in responses to GnRH. This is an important issue for future research, and the work could be extended to examine the relevance of GnRHR, ERK and NFAT concentrations. To date, there

is no reliable antibody for GnRHR quantification (McArdle, personal communication), accordingly, the work could be performed in a heterologous expression system (HeLa cells) using epitope-tagged GnRHR (e.g. HA-tagged GnRHR). HA-GnRHR, total ERK, and ppERK could then be measured in the same cells, and the cells could be binned according to the expression level of GnRHR and ERK. This would help in defining their effect on the I(ppERK; GnRH). Alternatively, the expression level of ppERK could be normalised to total ERK (on a cell by cell basis) to ask if this would increase MI values. A more advanced statistical approach would be to consider the response to GnRH in samples of the cell population selected to have identical average total ERK concentrations, but with different variation in total ERK concentrations. By doing this we could define the robustness of transfer information to heterogeneity in the concentration of ERK. Such a method could actually be applied for any other effector that can be measured in single cells. In fact, this was the aim of a preliminary study (MSc student project Christopher Benson, supervised by McArdle and Alobaid) although, at the time of writing, the data analysis has not yet been undertaken.

A recurring observation in this work is that most available information about GnRH concentration is lost through signalling network, raising the question of whether information transfer had been underestimated. Sensing joint pathways and trajectory have been considered here. Cells might also gain additional information by sensing signalling in neighbouring cells, and the mathematical approach can be used to calculate the MI between ppERK levels (as an example) in adjacent cells. In fact, this was performed in LβT2 cells where cells were stimulated with GnRH and MI values were calculated for neighbour sensing. These values were higher for pairs of cells that are close to one-another than for pairs of cells that were more distant from one-another

(unpublished data). This is consistent with cells obtaining information by sensing their neighbours, but in these experiments, there were technical problems (most probably related to uneven illumination of the cells). Thus, in future experiments it would be worthwhile repeating the experiment with better control of illumination.

As final consideration, the concern about loss information (i.e. how and where it is underestimated) could be misplaced. It is possible that the maximum amount of information transferred through GnRHR signalling is only 1 Bit. Most cellular decisions made by cells are binary [401], and these require only 1Bit of information. In the case of gonadotrophs, and as gonadotropin secretion is the most important activity, it is not clear if this activity is binary (all or nothing response) at the level of single cells. As explained early, the population average measures are graded over a broad range of stimulus concentration, but at the single cell, it might be still be binary. Furthermore, GnRH is secreted in a pulsatile manner, and blood circulation studies revealed that low nM GnRH pulses are interrupted by intervals of low pM concentrations. Thus, it might be that gonadotrophs *in vivo* only need to distinguish between these two states and have adapted to convey just the 1 Bit of information needed to do so.

7.5. Summary of the general conclusion

The main aim of the work performed here was to advance our understanding of GnRH signalling by exploring differences in responses between different cell types as well as between individual cells of a given cell type. The use of the mathematical approach (MI calculation) in addition to the conventional approach has provided us with promising results that advanced our knowledge in the mechanism of GnRHR

signalling. GnRH effects mediated by GnRHR are dependent upon cellular model, as shown by the differences in response kinetics and by the sensitivity to pharmacological inhibition. Most information about GnRH concentration in the environment is lost through GnRHR signalling. The MI values differed between HeLa cells and LβT2 cells, extending the concept of cell context-dependent GnRH signalling to the amount of information transferred through GnRHR. The live cell imaging revealed that snapshot data underestimated information transfer over time and that cells gain more information when the trajectory is considered. The repeated pulse experiments data revealed that cells did not gain much information by sensing additional GnRH pulses. The most striking data were probably those from the live cells Ca^{2+} imaging experiments. These data suggest that the GnRHR and its upstream effectors are a signalling node at which information loss occurs, and that the unknown sources of cell-cell variation are relatively stable over time.

Further experiments have been suggested here and further research should be undertaken to investigate (for example) the reasons underlying the cell-cell heterogeneity, which would shed further light on the mechanism of GnRHR signalling. Finally, in future experiments, it would also be of value to define the maximum amount of information that the GnRHR signalling network can transfer (using SLEMI or a related computational approach).

Appendix.

1. Optimisation of cell tracking protocols.

For live cell imaging experiments, cells were loaded with Ca^{2+}-sensitive dye and/or transduced with Ad NFAT1c-EFP. They were then imaged at different time points before, during and after stimulation as described in Chapter 2. Then, a cell tracking algorithm (provided by Dr. Margaritis Voliotis) was used to track individual cells over time. In its simplest form, the tracking algorithm matches the geometric centre of the nuclei between sequential images in the time stack (i.e. tracking is based on the x-y position of the nuclei) but in preliminary experiments, the use of alternative cell measures (nuclear area and nuclear stain intensity) were also considered. The tracking algorithm also includes a "probability of error" function. When this function is set too low there is a higher probability of errors in tracking. On the other hand, when it is set too high, there is higher confidence in the accuracy of the tracking but fewer cells are tracked. Table 1 shows the number of cells tracked using different cell measures and at different error probabilities in LβT2 cells receiving a single pulse of GnRH. Table 2 shows similar data but for cells receiving two pulses of GnRH. Note that, the tracked cells number is lower with two pulses than with single pulse. This is related to the physical movement associated with removing the plate and washing the cells (compare tables 1 and 2). Furthermore, the tracked cells number is not increased by consideration of nuclear measures. Consequently, for the experiments shown in this thesis cells were tracked based on the x- and y-co-ordinate alone, and with a probability of 0.1.

Measurement	Probability (0.0)	Probability (0.1)	Probability (0.2)	Probability (0.3)
x-coordinate y-coordinate Nuclear area Nuclear intensity	80-230	0-100	0-40	0-9
x-coordinate y-coordinate Nuclear area	8-150	0-57	0-23	0-3
x-coordinate y-coordinate Nuclear intensity	88-188	0-90	0-30	0-6
x-coordinate y-coordinate	280-370	230-300	120-200	30-80

Table 1. Number of cells tracked after a single pulse of GnRH. Data from a representative experiment where cells received a single pulse of 0-10^{-12}-10^{-7} M GnRH and were tracked with probability of varied, and on the basis of the cell measures indicated. These were all calculated from the nuclear stain (Hoechst) using the INCell workstation algorithm

Measurement	Probability (0.0)	Probability (0.1)	Probability (0.2)	Probability (0.3)
x-coordinate y-coordinate Nuclear area Nuclear intensity	5-33	0	0	0
x-coordinate y-coordinate Nuclear area	1-8	1	0	0
x-coordinate y-coordinate Nuclear intensity	6-34	0	0	0
x-coordinate y-coordinate	116-180	51-80	2-23	3

Table 2. Number of cells tracked after a single pulse of GnRH. Data from a representative experiment where cells received a two pulse of 0-10^{-12}-10^{-7} M GnRH and were tracked with probability error of varied and based on the cell measures indicated.

2. Optimising assessments of MI taking response trajectory into account.

For Ca^{2+} imaging experiments, LβT2 cells or Ad GnRHR transduced HeLa cells were loaded with Fluo-4 AM or Rhod-3 AM and stimulated with varied concentrations of GnRH. Cells were then imaged at different time points and the response of each individual cells were tracked. MI values were then calculated from Fluo-4 AM or Rhod-3 AM fluorescence at individual time-points using either single cell measures of raw fluorescence intensities or fluorescence normalised to the control (pre-stimulation) value in any given cell. In addition, MI calculated taking trajectory into account. To do so the response was considered to be an "N" dimensional vector, where N is the number of sampling points. Different time points were compared in order to get maximum estimates of MI. As shown in table 3, MI values were consistently higher with the normalised data. The consideration of 3 or 4 time-points did not considerably increase MI values above those obtained with 2 time-points.

.

Time in sec		LβT2	HeLa
140, 160	a	1.041 ± 0.055	0.867 ± 040
	b	0.813 ± 0.007	0.639 ± 0.053
140, 180	a	1.023 ± 0.051	0.889 ± 050
	b	0.829 ± 0.029	0.712 ± 0.084
140,300	a	0.986 ± 0.036	1.015 ± 054
	b	0.791 ± 0.044	0.808 ± 0.064
140,700	a	0.977 ± 0.039	0.955 ± 0.027
	b	0.813 ± 0.057	0.738 ± 0.053
140,160,300	a	1.013 ± 0.049	0.838 ± 0.069
	b	0.661 ± 0.035	0.531 ± 0.065
140,160,700	a	0.928 ± 0.067	0.907 ± 0.039
	b	0.691 ± 0.052	0.607 ± 0.047
140, 180, 300	a	0.931 ± 0.044	0.867 ± 040
	b	0.584 ± 0.025	0.639 ± 0.053
140, 180, 700	a	0.946 ± 0.050	0.955 ± 0.063
	b	0.669 ± 0.016	0.683 ± 0.048
140,300,700	a	0.881 ± 0.071	1.007 ± 0.054
	b	0.535 ± 0.015	0.260 ± 0.153
140,160,180,300	a	0.752±0.061	0.631 ± 0.079
	b	0.250 ± 0.020	0.229 ± 0.097
140,160,180,700	a	0.781 ± 0.061	0.725 ± 0.067
	b	0.301 ± 0.046	0.329 ± 0.077
140,160,300,700	a	0.844 ± 0.055	0.819 ± 0.058
	b	0.360 ± 0.025	0.360 ± 0.079
140,180,300,700	a	0.797 ± 0.030	0.849 ± 0.071
	b	0.335 ± 0.031	0.438 ± 0.087

Table 3. Preliminary experiments for selection of time-points to be used in MI calculations for live cell Ca^{2+} imaging experiments.

MI values were calculated using raw (b) or normalised (a) Fluo-4 fluorescence values in HeLa or LβT2 cells stimulated with varied concentrations of GnRH. The MI values were calculated taking trajectory into account by using measures at 2, 3 or 4 time-points as specified. The values shown are the means ± SEMs from 3 separate experiments (these experiments are also documented in Figure 6.3 and Figure 6.4).

3. Tracking and exclusion in live cell experiments.

The movement of cells during live cell experiments makes the tracking complicated. Accordingly, the responses of all individual tracked cells were plotted and inspected to remove cells that were not tracked precisely. Inspection of image stacks suggested that the tracking was not precise for cells that were poorly attached (i.e. cells that moved rapidly and did not stay in a fixed plane) and for cells that had moved close to one-another and indeed overlapped. Therefore, tracking algorithm allocated the wrong data to the cells before and after this point. Those type of cells were excluded from further analysis. In the case of the NFAT1c-EFP translocation experiments cells with very high or low starting NFAT1c-EFP ratios were also excluded because on image inspection they often appeared to be unhealthy (or even to be just debris from dead cells). By doing that around 2% or "tracked cells" were excluded from the analyses in Chapter 6. The figure below shows examples of NFAT1c-EFP traces in cells that were included (panels C and D) or excluded (panels A and B) from further analysis.

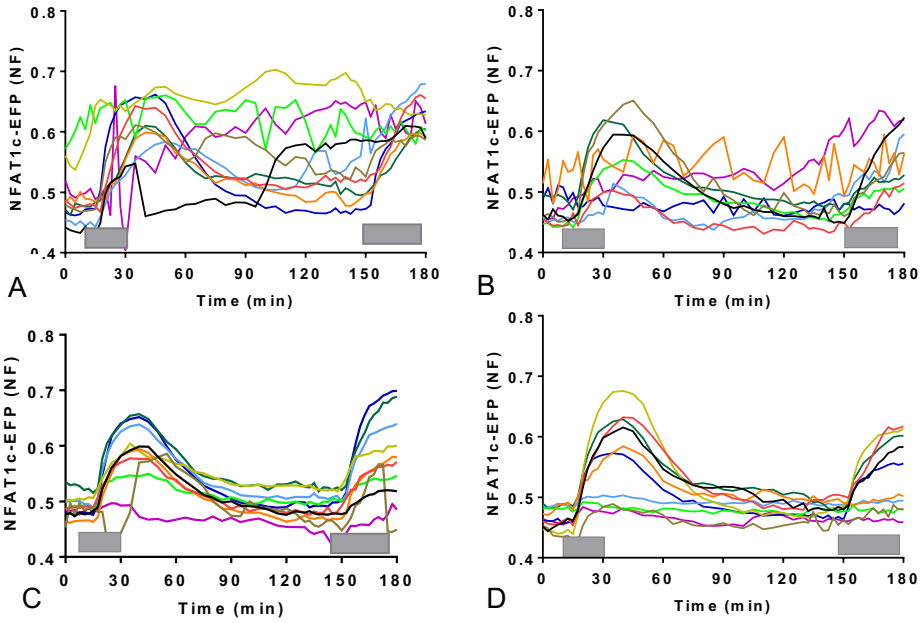

Figure 1. Representative single cell NFAT1c-EFP traces illustrating exclusion.

This figure shows time-courses of NFAT1c-EFP-NF for individual tracked LβT2 cells stimulated twice with 10^{-7} M GnRH. The duration of the 1st and 2nd pulse of GnRH is illustrated by the grey bars. Panels A and B show examples of cells that were excluded, either because inspection of the cells or the raw images indicated that tracking had failed, or because the time 0 NFAT1c-EFP-NF values were <0.4 or >0.55. Approximately 5% of cells were removed in this way. Panels C and D show examples of the responses of cells that were considered to have been successfully tracked. These data are from one of the experiments incorporated in Figure 6.4.

References

1. Clarke, I.J., *Hypothalamus as an Endocrine Organ.* Comprehensive Physiology, 2015. **5**(1): p. 217-253.
2. Bliss, S.P., et al., *GnRH signaling, the gonadotrope and endocrine control of fertility.* Front Neuroendocrinol, 2010. **31**(3): p. 322-40.
3. Maggi, R., et al., *GnRH and GnRH receptors in the pathophysiology of the human female reproductive system.* Hum Reprod Update, 2016. **22**(3): p. 358-81.
4. Halasz, B., *Neurohormonal mechanisms controlling trophic hormone secretion of the anterior pituitary.* J Neurovisc Relat, 1969. **31**: p. Suppl 9:329+.
5. Perrett, R.M. and C.A. McArdle, *Molecular mechanisms of gonadotropin-releasing hormone signaling: integrating cyclic nucleotides into the network.* Front Endocrinol (Lausanne), 2013. **4**: p. 180.
6. Naor, Z., D. Harris, and S. Shacham, *Mechanism of GnRH receptor signaling: combinatorial cross-talk of Ca2+ and protein kinase C.* Front Neuroendocrinol, 1998. **19**(1): p. 1-19.
7. Ferris, H.A. and M.A. Shupnik, *Mechanisms for pulsatile regulation of the gonadotropin subunit genes by GNRH1.* Biol Reprod, 2006. **74**(6): p. 993-8.
8. Seeburg, P.H., et al., *The mammalian GnRH gene and its pivotal role in reproduction.* Recent Prog Horm Res, 1987. **43**: p. 69-98.
9. Glode, L.M., *The biology of gonadotropin-releasing hormone and its analogs.* Urology, 1986. **27**(1 Suppl): p. 16-20.
10. Plant, T.M., *60 YEARS OF NEUROENDOCRINOLOGY: The hypothalamo-pituitary-gonadal axis.* J Endocrinol, 2015. **226**(2): p. T41-54.
11. Wierman, M.E., K. Kiseljak-Vassiliades, and S. Tobet, *Gonadotropin-releasing hormone (GnRH) neuron migration: Initiation, maintenance and cessation as critical*

steps to ensure normal reproductive function. Frontiers in Neuroendocrinology, 2011. **32**(1): p. 43-52.

12. Millar, R.P., et al., *Gonadotropin-releasing hormone receptors.* Endocr Rev, 2004. **25**(2): p. 235-75.
13. Mitchell, A.L., et al., *Genetic basis and variable phenotypic expression of Kallmann syndrome: towards a unifying theory.* Trends Endocrinol Metab, 2011. **22**(7): p. 249-58.
14. King, J.C. and E.L.P. Anthony, *Lhrh Neurons and Their Projections in Humans and Other Mammals - Species Comparisons.* Peptides, 1984. **5**: p. 195-207.
15. Oakley, A.E., D.K. Clifton, and R.A. Steiner, *Kisspeptin signaling in the brain.* Endocr Rev, 2009. **30**(6): p. 713-43.
16. Campbell, R.E. and A.E. Herbison, *Definition of brainstem afferents to gonadotropin-releasing hormone neurons in the mouse using conditional viral tract tracing.* Endocrinology, 2007. **148**(12): p. 5884-5890.
17. Boehm, U., Z. Zou, and L.B. Buck, *Feedback loops link odor and pheromone signaling with reproduction.* Cell, 2005. **123**(4): p. 683-95.
18. Simerly, R.B., *Wired for reproduction: organization and development of sexually dimorphic circuits in the mammalian forebrain.* Annu Rev Neurosci, 2002. **25**: p. 507-36.
19. Millar, R.P., *GnRHs and GnRH receptors.* Anim Reprod Sci, 2005. **88**(1-2): p. 5-28.
20. Balasubramanian, R., et al., *Human GnRH deficiency: a unique disease model to unravel the ontogeny of GnRH neurons.* Neuroendocrinology, 2010. **92**(2): p. 81-99.
21. Moenter, S.M., R.C. Brand, and F.J. Karsch, *Dynamics of gonadotropin-releasing hormone (GnRH) secretion during the GnRH surge: insights into the mechanism of GnRH surge induction.* Endocrinology, 1992. **130**(5): p. 2978-84.

22. Loumaye, E. and K.J. Catt, *Agonist-induced regulation of pituitary receptors for gonadotropin-releasing hormone. Dissociation of receptor recruitment from hormone release in cultured gonadotrophs.* J Biol Chem, 1983. **258**(19): p. 12002-9.

23. Ciccone, N.A. and U.B. Kaiser, *The biology of gonadotroph regulation.* Curr Opin Endocrinol Diabetes Obes, 2009. **16**(4): p. 321-7.

24. Conn, P.M. and W.F. Crowley, Jr., *Gonadotropin-releasing hormone and its analogs.* Annu Rev Med, 1994. **45**: p. 391-405.

25. Merkley, C.M., et al., *KNDy (kisspeptin/neurokinin B/dynorphin) neurons are activated during both pulsatile and surge secretion of LH in the ewe.* Endocrinology, 2012. **153**(11): p. 5406-14.

26. Marques, P., et al., *Physiology of GNRH and Gonadotropin Secretion*, in *Endotext*, K.R. Feingold, et al., Editors. 2000: South Dartmouth (MA).

27. Crowley, W.F., Jr., et al., *The physiology of gonadotropin-releasing hormone (GnRH) secretion in men and women.* Recent Prog Horm Res, 1985. **41**: p. 473-531.

28. Beltramo, M., et al., *Cellular mechanisms and integrative timing of neuroendocrine control of GnRH secretion by kisspeptin.* Mol Cell Endocrinol, 2014. **382**(1): p. 387-399.

29. Skorupskaite, K., J.T. George, and R.A. Anderson, *The kisspeptin-GnRH pathway in human reproductive health and disease.* Human Reproduction Update, 2014. **20, NUMB 4**: p. 485-500.

30. Lee, D.K., et al., *Discovery of a receptor related to the galanin receptors.* FEBS Lett, 1999. **446**(1): p. 103-7.

31. Kotani, M., et al., *The metastasis suppressor gene KiSS-1 encodes kisspeptins, the natural ligands of the orphan G protein-coupled receptor GPR54.* J Biol Chem, 2001. **276**(37): p. 34631-6.

32. Clarke, H., W.S. Dhillo, and C.N. Jayasena, *Comprehensive Review on Kisspeptin and Its Role in Reproductive Disorders.* Endocrinol Metab (Seoul), 2015. **30**(2): p. 124-41.

33. Pielecka-Fortuna, J., Z. Chu, and S.M. Moenter, *Kisspeptin acts directly and indirectly to increase gonadotropin-releasing hormone neuron activity and its effects are modulated by estradiol.* Endocrinology, 2008. **149**(4): p. 1979-86.

34. Roa, J., V.M. Navarro, and M. Tena-Sempere, *Kisspeptins in reproductive biology: consensus knowledge and recent developments.* Biol Reprod, 2011. **85**(4): p. 650-60.

35. Tena-Sempere, M., *Timeline: the role of kisspeptins in reproductive biology.* Nat Med, 2008. **14**(11): p. 1196.

36. Gutierrez-Pascual, E., et al., *Direct pituitary effects of kisspeptin: activation of gonadotrophs and somatotrophs and stimulation of luteinising hormone and growth hormone secretion.* J Neuroendocrinol, 2007. **19**(7): p. 521-30.

37. Tena-Sempere, M., *Roles of kisspeptins in the control of hypothalamic-gonadotropic function: focus on sexual differentiation and puberty onset.* Endocr Dev, 2010. **17**: p. 52-62.

38. Seminara, S.B., et al., *The GPR54 gene as a regulator of puberty.* New England Journal of Medicine, 2003. **349**(17): p. 1614-U8.

39. de Roux, N., et al., *Hypogonadotropic hypogonadism due to loss of function of the KiSS1-derived peptide receptor GPR54.* Proceedings of the National Academy of Sciences of the United States of America, 2003. **100**(19): p. 10972-10976.

40. Teles, M.G., et al., *A GPR54-activating mutation in a patient with central precocious puberty.* N Engl J Med, 2008. **358**(7): p. 709-15.

41. Chan, Y.M., et al., *Kisspeptin/Gpr54-independent gonadotrophin-releasing hormone activity in Kiss1 and Gpr54 mutant mice.* J Neuroendocrinol, 2009. **21**(12): p. 1015-23.

42. Lapatto, R., et al., *Kiss1-/- mice exhibit more variable hypogonadism than Gpr54-/- mice.* Endocrinology, 2007. **148**(10): p. 4927-36.

43. Funes, S., et al., *The KiSS-1 receptor GPR54 is essential for the development of the murine reproductive system.* Biochemical and Biophysical Research Communications, 2003. **312**(4): p. 1357-1363.

44. Topaloglu, A.K., et al., *TAC3 and TACR3 mutations in familial hypogonadotropic hypogonadism reveal a key role for Neurokinin B in the central control of reproduction.* Nat Genet, 2009. **41**(3): p. 354-358.

45. Jayasena, C.N., et al., *Neurokinin B administration induces hot flushes in women.* Sci Rep, 2015. **5**: p. 8466.

46. Seifer, D.B. and R.L. Collins, *Current concepts of beta-endorphin physiology in female reproductive dysfunction.* Fertil Steril, 1990. **54**(5): p. 757-71.

47. Veldhuis, J.D., et al., *Role of endogenous opiates in the expression of negative feedback actions of androgen and estrogen on pulsatile properties of luteinizing hormone secretion in man.* J Clin Invest, 1984. **74**(1): p. 47-55.

48. Wilkes, M.M., et al., *Localization and quantitation of beta-endorphin in human brain and pituitary.* Neuroendocrinology, 1980. **30**(2): p. 113-21.

49. Quigley, M.E. and S.S. Yen, *The role of endogenous opiates in LH secretion during the menstrual cycle.* J Clin Endocrinol Metab, 1980. **51**(1): p. 179-81.

50. Cheng, G., et al., *The kisspeptin/neurokinin B/dynorphin (KNDy) cell population of the arcuate nucleus: sex differences and effects of prenatal testosterone in sheep.* Endocrinology, 2010. **151**(1): p. 301-11.

51. Goodman, R.L., et al., *Kisspeptin neurons in the arcuate nucleus of the ewe express both dynorphin A and neurokinin B.* Endocrinology, 2007. **148**(12): p. 5752-60.

52. Watanabe, M., A. Fukuda, and J. Nabekura, *The role of GABA in the regulation of GnRH neurons.* Front Neurosci, 2014. **8**: p. 387.

53. Hatef, A. and S. Unniappan, *Gonadotropin-releasing hormone, kisspeptin, and gonadal steroids directly modulate nucleobindin-2/nesfatin-1 in murine hypothalamic gonadotropin-releasing hormone neurons and gonadotropes.* Biol Reprod, 2017. **96**(3): p. 635-651.

54. Herbison, A.E. and D.T. Theodosis, *Localization of oestrogen receptors in preoptic neurons containing neurotensin but not tyrosine hydroxylase, cholecystokinin or luteinizing hormone-releasing hormone in the male and female rat.* Neuroscience, 1992. **50**(2): p. 283-98.

55. Matsuo, H., et al., *Structure of the porcine LH- and FSH-releasing hormone. I. The proposed amino acid sequence.* Biochem Biophys Res Commun, 1971. **43**(6): p. 1334-9.

56. Baba, Y., H. Matsuo, and A.V. Schally, *Structure of the porcine LH- and FSH-releasing hormone. II. Confirmation of the proposed structure by conventional sequential analyses.* Biochem Biophys Res Commun, 1971. **44**(2): p. 459-63.

57. Schally, A.V., et al., *Isolation and properties of the FSH and LH-releasing hormone.* Biochem Biophys Res Commun, 1971. **43**(2): p. 393-9.

58. Hayflick, J.S., J.P. Adelman, and P.H. Seeburg, *The complete nucleotide sequence of the human gonadotropin-releasing hormone gene.* Nucleic Acids Res, 1989. **17**(15): p. 6403-4.

59. Radovick, S., et al., *Isolation and characterization of the human gonadotropin-releasing hormone gene in the hypothalamus and placenta.* Mol Endocrinol, 1990. **4**(3): p. 476-80.

60. Cheng, C.K. and P.C. Leung, *Molecular biology of gonadotropin-releasing hormone (GnRH)-I, GnRH-II, and their receptors in humans.* Endocr Rev, 2005. **26**(2): p. 283-306.

61. Schneider, J.S. and E.F. Rissman, *Gonadotropin-releasing hormone II: a multi-purpose neuropeptide.* Integr Comp Biol, 2008. **48**(5): p. 588-95.

62. Sealfon, S.C., H. Weinstein, and R.P. Millar, *Molecular mechanisms of ligand interaction with the gonadotropin-releasing hormone receptor.* Endocr Rev, 1997. **18**(2): p. 180-205.

63. Carolsfeld, J., et al., *Primary structure and function of three gonadotropin-releasing hormones, including a novel form, from an ancient teleost, herring.* Endocrinology, 2000. **141**(2): p. 505-12.

64. Roch, G.J., E.R. Busby, and N.M. Sherwood, *Evolution of GnRH: diving deeper.* Gen Comp Endocrinol, 2011. **171**(1): p. 1-16.

65. Powell, J.F., et al., *Two new forms of gonadotropin-releasing hormone in a protochordate and the evolutionary implications.* Proc Natl Acad Sci U S A, 1996. **93**(19): p. 10461-4.

66. Miyamoto, K., et al., *Identification of the second gonadotropin-releasing hormone in chicken hypothalamus: evidence that gonadotropin secretion is probably controlled by two distinct gonadotropin-releasing hormones in avian species.* Proc Natl Acad Sci U S A, 1984. **81**(12): p. 3874-8.

67. White, R.B., et al., *Second gene for gonadotropin-releasing hormone in humans.* Proc Natl Acad Sci U S A, 1998. **95**(1): p. 305-9.

68. Chen, A., et al., *A second isoform of gonadotropin-releasing hormone is present in the brain of human and rodents.* Febs Letters, 1998. **435**(2-3): p. 199-203.

69. Millar, R.P., et al., *Receptor binding and gonadotropin-releasing activity of a novel chicken gonadotropin-releasing hormone ([His5, Trp7, Tyr8]GnRH) and a D-Arg6 analog.* Endocrinology, 1986. **119**(1): p. 224-31.

70. Andreyko, J.L., et al., *Therapeutic uses of gonadotropin-releasing hormone analogs.* Obstet Gynecol Surv, 1987. **42**(1): p. 1-21.

71. Harrison, G.S., et al., *Gonadotropin-releasing hormone and its receptor in normal and malignant cells.* Endocr Relat Cancer, 2004. **11**(4): p. 725-48.

72. Currie, A.J., H.M. Fraser, and R.M. Sharpe, *Human placental receptors for luteinizing hormone releasing hormone.* Biochem Biophys Res Commun, 1981. **99**(1): p. 332-8.

73. Lin, L.S., V.J. Roberts, and S.S. Yen, *Expression of human gonadotropin-releasing hormone receptor gene in the placenta and its functional relationship to human chorionic gonadotropin secretion.* J Clin Endocrinol Metab, 1995. **80**(2): p. 580-5.

74. Aguilar-Rojas, A. and M. Huerta-Reyes, *Human gonadotropin-releasing hormone receptor-activated cellular functions and signaling pathways in extra-pituitary tissues and cancer cells (Review).* Oncol Rep, 2009. **22**(5): p. 981-90.

75. Kakar, S.S. and L. Jennes, *Expression of gonadotropin-releasing hormone and gonadotropin-releasing hormone receptor mRNAs in various non-reproductive human tissues.* Cancer Letters, 1995. **98**(1): p. 57-62.

76. Cheung, L.W. and A.S. Wong, *Gonadotropin-releasing hormone: GnRH receptor signaling in extrapituitary tissues.* FEBS J, 2008. **275**(22): p. 5479-95.

77. Leung, P.C., C.K. Cheng, and X.M. Zhu, *Multi-factorial role of GnRH-I and GnRH-II in the human ovary.* Mol Cell Endocrinol, 2003. **202**(1-2): p. 145-53.

78. Khodr, G.S. and T.M. Siler-Khodr, *Placental luteinizing hormone-releasing factor and its synthesis.* Science, 1980. **207**(4428): p. 315-7.

79. Morales, P., et al., *Sperm binding to the human zona pellucida and calcium influx in response to GnRH and progesterone.* Andrologia, 2002. **34**(5): p. 301-7.

80. Morales, P., et al., *Gonadotropin-releasing hormone-stimulated sperm binding to the human zona is mediated by a calcium influx.* Biology of Reproduction, 2000. **63**(2): p. 635-642.

81. Huhtaniemi, I.T., K.J. Catt, and R.N. Clayton, *Newborn and Immature Rat Testes Contain Gonadotropin-Releasing Hormone (Gnrh) Receptors, and Their Testosterone Production Is Stimulated by a Gnrh Agonist Invitro.* Molecular and Cellular Endocrinology, 1985. **40**(1): p. 41-44.

82. Huhtaniemi, I.T., et al., *Blockade of rat testicular gonadotropin releasing hormone (GnRH) receptors by infusion of a GnRH antagonist has no major effects of Leydig cell function in vivo.* Mol Cell Endocrinol, 1987. **49**(2-3): p. 89-97.

83. Clayton, R.N. and I.T. Huhtaniemi, *Absence of gonadotropin-releasing hormone receptors in human gonadal tissue.* Nature, 1982. **299**(5878): p. 56-9.

84. Skinner, D.C., et al., *Effects of gonadotrophin-releasing hormone outside the hypothalamic-pituitary-reproductive axis.* J Neuroendocrinol, 2009. **21**(4): p. 282-92.

85. Boyle, T.A., D.I. Belt-Davis, and T.M. Duello, *Nucleotide sequence analyses predict that human pituitary and human placental gonadotropin-releasing hormone receptors have identical primary structures.* Endocrine, 1998. **9**(3): p. 281-287.

86. Limonta, P., et al., *The luteinizing hormone-releasing hormone receptor in human prostate cancer cells: messenger ribonucleic acid expression, molecular size, and signal transduction pathway.* Endocrinology, 1999. **140**(11): p. 5250-6.

87. Kakar, S.S., W.E. Grizzle, and J.D. Neill, *The nucleotide sequences of human GnRH receptors in breast and ovarian tumors are identical with that found in pituitary.* Mol Cell Endocrinol, 1994. **106**(1-2): p. 145-9.

88. Chatzaki, E., et al., *The expression of gonadotropin-releasing hormone and its receptor in endometrial cancer, and its relevance as an autocrine growth factor.* Cancer Research, 1996. **56**(9): p. 2059-2065.

89. Tieva, A., et al., *Gonadotropin-releasing hormone receptor expression in the human prostate.* Prostate, 2001. **47**(4): p. 276-84.

90. Everest, H.M., et al., *Signaling and antiproliferative effects mediated by GnRH receptors after expression in breast cancer cells using recombinant adenovirus.* Endocrinology, 2001. **142**(11): p. 4663-72.

91. Franklin, J., et al., *Signalling and anti-proliferative effects mediated by gonadotrophin-releasing hormone receptors after expression in prostate cancer cells using recombinant adenovirus.* Journal of Endocrinology, 2003. **176**(2): p. 275-284.

92. Delemarre, E.M., B. Felius, and H.A. Delemarre-van de Waal, *Inducing puberty.* Eur J Endocrinol, 2008. **159 Suppl 1**: p. S9-15.

93. Raivio, T., et al., *Reversal of idiopathic hypogonadotropic hypogonadism.* N Engl J Med, 2007. **357**(9): p. 863-73.

94. Limonta, P., et al., *GnRH in the Human Female Reproductive Axis.* Vitam Horm, 2018. **107**: p. 27-66.

95. Kumar, P. and A. Sharma, *Gonadotropin-releasing hormone analogs: Understanding advantages and limitations.* J Hum Reprod Sci, 2014. **7**(3): p. 170-4.

96. Labrie, F., et al., *Gonadotropin-releasing hormone agonists in the treatment of prostate cancer.* Endocr Rev, 2005. **26**(3): p. 361-79.

97. van Loenen, A.C., et al., *GnRH agonists, antagonists, and assisted conception.* Semin Reprod Med, 2002. **20**(4): p. 349-64.

98. Copperman, A.B. and C. Benadiva, *Optimal usage of the GnRH antagonists: a review of the literature.* Reprod Biol Endocrinol, 2013. **11**: p. 20.

99. Kiesel, L.A., et al., *Clinical use of GnRH analogues.* Clinical Endocrinology, 2002. **56**(6): p. 677-687.

100. Huirne, J.A., R. Homburg, and C.B. Lambalk, *Are GnRH antagonists comparable to agonists for use in IVF?* Human Reproduction, 2007. **22**(11): p. 2805-2813.

101. Grundker, C. and G. Emons, *The Role of Gonadotropin-Releasing Hormone in Cancer Cell Proliferation and Metastasis.* Front Endocrinol (Lausanne), 2017. **8**: p. 187.

102. Rosario, D.J., et al., *The role of gonadotrophin-releasing hormone antagonists in the treatment of patients with advanced hormone-dependent prostate cancer in the UK.* World J Urol, 2016. **34**(12): p. 1601-1609.

103. Magon, N., *Gonadotropin releasing hormone agonists: Expanding vistas.* Indian J Endocrinol Metab, 2011. **15**(4): p. 261-7.

104. Reinhart, J., L.M. Mertz, and K.J. Catt, *Molecular cloning and expression of cDNA encoding the murine gonadotropin-releasing hormone receptor.* J Biol Chem, 1992. **267**(30): p. 21281-4.

105. Huang, C.C. and J.J. Tesmer, *Recognition in the face of diversity: interactions of heterotrimeric G proteins and G protein-coupled receptor (GPCR) kinases with activated GPCRs.* J Biol Chem, 2011. **286**(10): p. 7715-21.

106. Fredriksson, R., et al., *The G-protein-coupled receptors in the human genome form five main families. Phylogenetic analysis, paralogon groups, and fingerprints.* Mol Pharmacol, 2003. **63**(6): p. 1256-72.

107. Wise, A., K. Gearing, and S. Rees, *Target validation of G-protein coupled receptors.* Drug Discov Today, 2002. **7**(4): p. 235-46.

108. Granier, S. and B. Kobilka, *A new era of GPCR structural and chemical biology.* Nature Chemical Biology, 2012. **8**(8): p. 670-673.

109. Ruf, F., M.Y. Fink, and S.C. Sealfon, *Structure of the GnRH receptor-stimulated signaling network: insights from genomics.* Front Neuroendocrinol, 2003. **24**(3): p. 181-99.

110. McArdle, C.A., et al., *The gonadotrophin-releasing hormone receptor: signalling, cycling and desensitisation.* Arch Physiol Biochem, 2002. **110**(1-2): p. 113-22.

111. Rispoli, L.A. and T.M. Nett, *Pituitary gonadotropin-releasing hormone (GnRH) receptor: structure, distribution and regulation of expression.* Anim Reprod Sci, 2005. **88**(1-2): p. 57-74.

112. Millar, R.P., *GnRH II and type II GnRH receptors.* Trends Endocrinol Metab, 2003. **14**(1): p. 35-43.

113. Hapgood, J.P., et al., *Regulation of expression of mammalian gonadotrophin-releasing hormone receptor genes.* J Neuroendocrinol, 2005. **17**(10): p. 619-38.

114. Pawson, A.J., et al., *Inhibition of human type i gonadotropin-releasing hormone receptor (GnRHR) function by expression of a human type II GnRHR gene fragment.* Endocrinology, 2005. **146**(6): p. 2639-49.

115. Wess, J., *Molecular basis of receptor/G-protein-coupling selectivity.* Pharmacol Ther, 1998. **80**(3): p. 231-64.

116. Rosenbaum, D.M., S.G. Rasmussen, and B.K. Kobilka, *The structure and function of G-protein-coupled receptors.* Nature, 2009. **459**(7245): p. 356-63.

117. Peeters, M.C., et al., *Importance of the extracellular loops in G protein-coupled receptors for ligand recognition and receptor activation.* Trends Pharmacol Sci, 2011. **32**(1): p. 35-42.

118. Tan, C.M., et al., *Membrane trafficking of G protein-coupled receptors.* Annu Rev Pharmacol Toxicol, 2004. **44**: p. 559-609.

119. Tikhonova, I.G. and S. Costanzi, *Unraveling the structure and function of G protein-coupled receptors through NMR spectroscopy.* Curr Pharm Des, 2009. **15**(35): p. 4003-16.

120. Naor, Z., *Signaling by G-protein-coupled receptor (GPCR): studies on the GnRH receptor.* Front Neuroendocrinol, 2009. **30**(1): p. 10-29.

121. Ferguson, S.S., et al., *Molecular mechanisms of G protein-coupled receptor desensitization and resensitization.* Life Sci, 1998. **62**(17-18): p. 1561-5.

122. Vrecl, M., et al., *Internalization kinetics of the gonadotropin-releasing hormone (GnRH) receptor.* Pflugers Arch, 2000. **439**(Suppl 1): p. r019-r020.

123. Tsaneva-Atanasova, K., et al., *Decoding GnRH neurohormone pulse frequency by convergent signalling modules.* J R Soc Interface, 2012. **9**(66): p. 170-82.

124. Finch, A.R., et al., *Agonist-induced internalization and downregulation of gonadotropin-releasing hormone receptors.* Am J Physiol Cell Physiol, 2009. **297**(3): p. C591-600.

125. Pawson, A.J., et al., *Mammalian type I gonadotropin-releasing hormone receptors undergo slow, constitutive, agonist-independent internalization.* Endocrinology, 2008. **149**(3): p. 1415-22.

126. Heding, A., et al., *Gonadotropin-releasing hormone receptors with intracellular carboxyl-terminal tails undergo acute desensitization of total inositol phosphate production and exhibit accelerated internalization kinetics.* J Biol Chem, 1998. **273**(19): p. 11472-7.

127. Hanyaloglu, A.C., et al., *Casein kinase II sites in the intracellular C-terminal domain of the thyrotropin-releasing hormone receptor and chimeric gonadotropin-releasing hormone receptors contribute to beta-arrestin-dependent internalization.* J Biol Chem, 2001. **276**(21): p. 18066-74.

128. Aguilar-Rojas, A., M.A. Perez-Solis, and G. Maya-Nunez, *The gonadotropin-releasing hormone system: Perspectives from reproduction to cancer (Review).* Int J Oncol, 2016. **48**(3): p. 861-8.

129. Sealfon, S.C., *Teaching resources. G-protein-coupled receptors.* Sci STKE, 2005. **2005**(279): p. tr11.

130. Blaukat, A., et al., *G protein-coupled receptor-mediated mitogen-activated protein kinase activation through cooperation of G alpha(q), and G alpha(i) signals.* Molecular and Cellular Biology, 2000. **20**(18): p. 6837-6848.

131. Millar, R.P. and C.L. Newton, *The year in G protein-coupled receptor research.* Mol Endocrinol, 2010. **24**(1): p. 261-74.

132. Choi, S.G., et al., *G proteins and autocrine signaling differentially regulate gonadotropin subunit expression in pituitary gonadotrope.* J Biol Chem, 2012. **287**(25): p. 21550-60.

133. Caunt, C.J., et al., *GnRH receptor signalling to ERK: kinetics and compartmentalization.* Trends Endocrinol Metab, 2006. **17**(8): p. 308-13.

134. Liu, F.J., et al., *Involvement of both G(q/11) and G(s) proteins in gonadotropin-releasing hormone receptor-mediated signaling in L beta T2 cells.* Journal of Biological Chemistry, 2002. **277**(35): p. 32099-32108.

135. Tsutsumi, R., D. Mistry, and N.J. Webster, *Signaling responses to pulsatile gonadotropin-releasing hormone in LbetaT2 gonadotrope cells.* J Biol Chem, 2010. **285**(26): p. 20262-72.

136. Grundker, C., P. Volker, and G. Emons, *Antiproliferative signaling of luteinizing hormone-releasing hormone in human endometrial and ovarian cancer cells through G protein alpha(I)-mediated activation of phosphotyrosine phosphatase.* Endocrinology, 2001. **142**(6): p. 2369-80.

137. Krsmanovic, L.Z., et al., *An agonist-induced switch in G protein coupling of the gonadotropin-releasing hormone receptor regulates pulsatile neuropeptide secretion.* Proc Natl Acad Sci U S A, 2003. **100**(5): p. 2969-74.

138. Stamatiades, G.A. and U.B. Kaiser, *Gonadotropin regulation by pulsatile GnRH: Signaling and gene expression.* Molecular and Cellular Endocrinology, 2018. **463**(C): p. 131-141.

139. Kanasaki, H., et al., *Extracellular Signal-Regulated Kinase (ERK) Activation and Mitogen-Activated Protein Kinase Phosphatase 1 Induction by Pulsatile Gonadotropin-Releasing Hormone in Pituitary Gonadotrophs.* J Signal Transduct, 2012. **2012**: p. 198527.

140. Armstrong, S.P., et al., *Pulsatile and sustained gonadotropin-releasing hormone (GnRH) receptor signaling: does the Ca2+/NFAT signaling pathway decode GnRH pulse frequency?* J Biol Chem, 2009. **284**(51): p. 35746-57.

141. Armstrong, S.P., et al., *Pulsatile and sustained gonadotropin-releasing hormone (GnRH) receptor signaling: does the ERK signaling pathway decode GnRH pulse frequency?* J Biol Chem, 2010. **285**(32): p. 24360-71.

142. Harris, D., et al., *Activation of MAPK cascades by GnRH: ERK and Jun N-terminal kinase are involved in basal and GnRH-stimulated activity of the glycoprotein hormone LHbeta-subunit promoter.* Endocrinology, 2002. **143**(3): p. 1018-25.

143. Roberson, M.S., et al., *Activation of the p38 mitogen-activated protein kinase pathway by gonadotropin-releasing hormone.* Endocrinology, 1999. **140**(3): p. 1310-8.

144. Cowan, K.J. and K.B. Storey, *Mitogen-activated protein kinases: new signaling pathways functioning in cellular responses to environmental stress.* J Exp Biol, 2003. **206**(Pt 7): p. 1107-15.

145. Naor, Z., O. Benard, and R. Seger, *Activation of MAPK cascades by G-protein-coupled receptors: the case of gonadotropin-releasing hormone receptor.* Trends Endocrinol Metab, 2000. **11**(3): p. 91-9.

146. McCain, J., *The MAPK (ERK) Pathway: Investigational Combinations for the Treatment Of BRAF-Mutated Metastatic Melanoma.* P T, 2013. **38**(2): p. 96-108.

147. Eandi, J.A., J.C. Yang, and C.P. Evans, *Signal transduction-mediated regulation of urokinase gene expression in human prostate cancer.* Biochem Biophys Res Commun, 2001. **288**(3): p. 521-7.

148. Kato, Y., et al., *Role of BMK1 in regulation of growth factor-induced cellular responses.* Immunol Res, 2000. **21**(2-3): p. 233-7.

149. Nithianandarajah-Jones, G.N., et al., *ERK5: structure, regulation and function.* Cell Signal, 2012. **24**(11): p. 2187-96.

150. Kanasaki, H., et al., *Gonadotropin-releasing hormone pulse frequency-dependent activation of extracellular signal-regulated kinase pathways in perifused LbetaT2 cells.* Endocrinology, 2005. **146**(12): p. 5503-13.

151. Bonfil, D., et al., *Extracellular signal-regulated kinase, Jun N-terminal kinase, p38, and c-Src are involved in gonadotropin-releasing hormone-stimulated activity of the glycoprotein hormone follicle-stimulating hormone beta-subunit promoter.* Endocrinology, 2004. **145**(5): p. 2228-44.

152. Garner, K.L., et al., *Information Transfer in Gonadotropin-releasing Hormone (GnRH) Signaling: EXTRACELLULAR SIGNAL-REGULATED KINASE (ERK)-MEDIATED FEEDBACK LOOPS CONTROL HORMONE SENSING.* J Biol Chem, 2016. **291**(5): p. 2246-59.

153. Garner, K.L., et al., *Information Transfer via Gonadotropin-Releasing Hormone Receptors to ERK and NFAT: Sensing GnRH and Sensing Dynamics.* J Endocr Soc, 2017. **1**(4): p. 260-277.

154. Lim, S., et al., *Negative feedback governs gonadotrope frequency-decoding of gonadotropin releasing hormone pulse-frequency.* PLoS One, 2009. **4**(9): p. e7244.

155. Bliss, S.P., et al., *ERK Signaling, But Not c-Raf, Is Required for Gonadotropin-Releasing Hormone (GnRH)-Induced Regulation of Nur77 in Pituitary Gonadotropes.* Endocrinology, 2012. **153**(2): p. 700-711.

156. Johnson, G.L. and R. Lapadat, *Mitogen-activated protein kinase pathways mediated by ERK, JNK, and p38 protein kinases.* Science, 2002. **298**(5600): p. 1911-2.

157. Molkentin, J.D., *Calcineurin-NFAT signaling regulates the cardiac hypertrophic response in coordination with the MAPKs.* Cardiovasc Res, 2004. **63**(3): p. 467-75.

158. Tomida, T., et al., *NFAT functions as a working memory of Ca2+ signals in decoding Ca2+ oscillation.* Embo Journal, 2003. **22**(15): p. 3825-3832.

159. Duran-Pasten, M.L. and T. Fiordelisio, *GnRH-Induced Ca(2+) Signaling Patterns and Gonadotropin Secretion in Pituitary Gonadotrophs. Functional Adaptations to Both Ordinary and Extraordinary Physiological Demands.* Front Endocrinol (Lausanne), 2013. **4**: p. 127.

160. Natarajan, K., et al., *Specific identification and subcellular localization of three calmodulin-binding proteins in the rat gonadotrope: spectrin, caldesmon, and calcineurin.* Biol Reprod, 1991. **44**(1): p. 43-52.

161. Haisenleder, D.J., et al., *Gonadotropin-releasing hormone stimulation of gonadotropin subunit transcription: evidence for the involvement of calcium/calmodulin-dependent kinase II (Ca/CAMK II) activation in rat pituitaries.* Endocrinology, 2003. **144**(7): p. 2768-74.

162. Haisenleder, D.J., H.A. Ferris, and M.A. Shupnik, *The calcium component of gonadotropin-releasing hormone-stimulated luteinizing hormone subunit gene transcription is mediated by calcium/calmodulin-dependent protein kinase type II.* Endocrinology, 2003. **144**(6): p. 2409-2416.

163. Binder, A.K., et al., *GnRH regulation of Jun and Atf3 requires calcium, calcineurin, and NFAT.* Mol Endocrinol, 2012. **26**(5): p. 873-86.

164. Lim, S., et al., *Distinct mechanisms involving diverse histone deacetylases repress expression of the two gonadotropin beta-subunit genes in immature gonadotropes, and their actions are overcome by gonadotropin-releasing hormone.* Molecular and Cellular Biology, 2007. **27**(11): p. 4105-4120.

165. Macian, F., *NFAT proteins: key regulators of T-cell development and function.* Nat Rev Immunol, 2005. **5**(6): p. 472-84.

166. Ronacher, K., et al., *Serine residues 338 and 339 in the carboxyl-terminal tail of the type II gonadotropin-releasing hormone receptor are critical for beta-arrestin-independent internalization.* Endocrinology, 2004. **145**(10): p. 4480-8.

167. McArdle CA, Roberson MS. Gonadotropes and gonadotropin-releasing hormone signaling. In: Plant TM, editor. Knobil and Neill's physiology of reproduction. 4th ed. Amsterdam: Elsevier; 2015. p. 335–97

168. Kakar, S.S., et al., *Identification of distinct gene expression profiles associated with treatment of L beta T2 cells with gonadotropin-releasing hormone agonist using microarray analysis.* Gene, 2003. **308**: p. 67-77.

169. Wurmbach, E., et al., *Gonadotropin-releasing hormone receptor-coupled gene network organization.* J Biol Chem, 2001. **276**(50): p. 47195-201.

170. Salisbury, T.B., A.K. Binder, and J.H. Nilson, *Welcoming beta-catenin to the gonadotropin-releasing hormone transcriptional network in gonadotropes.* Mol Endocrinol, 2008. **22**(6): p. 1295-303.

171. Jorgensen, J.S., C.C. Quirk, and J.H. Nilson, *Multiple and overlapping combinatorial codes orchestrate hormonal responsiveness and dictate cell-specific expression of the genes encoding luteinizing hormone.* Endocr Rev, 2004. **25**(4): p. 521-42.

172. Burger, L.L., et al., *Regulation of gonadotropin subunit gene transcription.* J Mol Endocrinol, 2004. **33**(3): p. 559-84.

173. Schang, A.L., et al., *Mechanisms underlying the tissue-specific and regulated activity of the Gnrhr promoter in mammals.* Front Endocrinol (Lausanne), 2012. **3**: p. 162.

174. Gregory, S.J. and U.B. Kaiser, *Regulation of gonadotropins by inhibin and activin.* Semin Reprod Med, 2004. **22**(3): p. 253-67.

175. Nathwani, P.S., et al., *Regulation of gonadotropin-releasing hormone and its receptor gene expression by 17beta-estradiol in cultured human granulosa-luteal cells.* Endocrinology, 2000. **141**(5): p. 1754-63.

176. Yasin, M., et al., *Gonadotropin-releasing hormone (GnRH) pulse pattern regulates GnRH receptor gene expression: augmentation by estradiol.* Endocrinology, 1995. **136**(4): p. 1559-64.

177. Kaiser, U.B., P.M. Conn, and W.W. Chin, *Studies of gonadotropin-releasing hormone (GnRH) action using GnRH receptor-expressing pituitary cell lines.* Endocrine Reviews, 1997. **18**(1): p. 46-70.

178. Katt, J.A., et al., *The frequency of gonadotropin-releasing hormone stimulation determines the number of pituitary gonadotropin-releasing hormone receptors.* Endocrinology, 1985. **116**(5): p. 2113-5.

179. Turzillo, A.M., J.L. Juengel, and T.M. Nett, *Pulsatile gonadotropin-releasing hormone (GnRH) increases concentrations of GnRH receptor messenger ribonucleic acid and numbers of GnRH receptors during luteolysis in the ewe.* Biol Reprod, 1995. **53**(2): p. 418-23.

180. Hislop, J.N., et al., *Desensitization and internalization of human and xenopus gonadotropin-releasing hormone receptors expressed in alphaT4 pituitary cells using recombinant adenovirus.* Endocrinology, 2000. **141**(12): p. 4564-75.

181. Hislop, J.N., et al., *Internalization of gonadotropin-releasing hormone receptors (GnRHRs): does arrestin binding to the C-terminal tail target GnRHRs for dynamin-dependent internalization?* J Mol Endocrinol, 2005. **35**(1): p. 177-89.

182. Schirman-Hildesheim, T.D., et al., *Differential gonadotropin-releasing hormone (GnRH) and GnRH receptor messenger ribonucleic acid expression patterns in different tissues of the female rat across the estrous cycle.* Endocrinology, 2005. **146**(8): p. 3401-8.

183. Bauer-Dantoin, A.C., A.N. Hollenberg, and J.L. Jameson, *Dynamic regulation of gonadotropin-releasing hormone receptor mRNA levels in the anterior pituitary gland during the rat estrous cycle.* Endocrinology, 1993. **133**(4): p. 1911-4.

184. Bedecarrats, G.Y. and U.B. Kaiser, *Differential regulation of gonadotropin subunit gene promoter activity by pulsatile gonadotropin-releasing hormone (GnRH) in perifused L beta T2 cells: role of GnRH receptor concentration.* Endocrinology, 2003. **144**(5): p. 1802-11.

185. Kaiser, U.B., et al., *A mechanism for the differential regulation of gonadotropin subunit gene expression by gonadotropin-releasing hormone.* Proc Natl Acad Sci U S A, 1995. **92**(26): p. 12280-4.

186. Bjelobaba, I., et al., *The relationship between basal and regulated Gnrhr expression in rodent pituitary gonadotrophs.* Molecular and Cellular Endocrinology, 2016. **437**(C): p. 302-311.

187. Cattanach, B.M., et al., *Gonadotrophin-releasing hormone deficiency in a mutant mouse with hypogonadism.* Nature, 1977. **269**(5626): p. 338-40.

188. Mason, A.J., et al., *A deletion truncating the gonadotropin-releasing hormone gene is responsible for hypogonadism in the hpg mouse.* Science, 1986. **234**(4782): p. 1366-71.

189. de Roux, N., et al., *A family with hypogonadotropic hypogonadism and mutations in the gonadotropin-releasing hormone receptor.* N Engl J Med, 1997. **337**(22): p. 1597-602.

190. Cheng, K.W. and P.C.K. Leung, *The expression, regulation and signal transduction pathways of the mammalian gonadotropin-releasing hormone receptor.* Canadian Journal of Physiology and Pharmacology, 2000. **78**(12): p. 1029-1052.

191. Pincas, H., et al., *Multiple elements in the distal part of the 1.2 kb 5'-flanking region of the rat GnRH receptor gene regulate gonadotrope-specific expression conferred by proximal domain.* Mol Cell Endocrinol, 1998. **144**(1-2): p. 95-108.

192. Granger, A., et al., *The promoter of the rat gonadotropin-releasing hormone receptor gene directs the expression of the human placental alkaline phosphatase reporter gene in gonadotrope cells in the anterior pituitary gland as well as in multiple extrapituitary tissues.* Endocrinology, 2004. **145**(2): p. 983-993.

193. Granger, A., et al., *The LIM-homeodomain proteins Isl-1 and Lhx3 act with steroidogenic factor 1 to enhance gonadotrope-specific activity of the gonadotropin-releasing hormone receptor gene promoter.* Mol Endocrinol, 2006. **20**(9): p. 2093-108.

194. Aylwin, S.J. and J.M. Burrin, *The role of transcription factors in the pituitary expression of the glycoprotein hormone alpha-subunit gene.* J Mol Endocrinol, 1995. **15**(3): p. 221-31.

195. Maurer, R.A., et al., *Regulation of glycoprotein hormone alpha-subunit gene expression.* Recent Prog Horm Res, 1999. **54**: p. 455-84; discussion 485.

196. Brayman, M.J., et al., *Androgen Receptor Repression of GnRH Gene Transcription.* Molecular Endocrinology, 2012. **26**(1): p. 2-13.

197. Windle, J.J., R.I. Weiner, and P.L. Mellon, *Cell lines of the pituitary gonadotrope lineage derived by targeted oncogenesis in transgenic mice.* Mol Endocrinol, 1990. **4**(4): p. 597-603.

198. Morgan, K., et al., *Gonadotropin-releasing hormone receptor levels and cell context affect tumor cell responses to agonist in vitro and in vivo.* Cancer Res, 2008. **68**(15): p. 6331-40.

199. Finch, A.R., et al., *Signaling and antiproliferative effects of type I and II gonadotropin-releasing hormone receptors in breast cancer cells.* J Clin Endocrinol Metab, 2004. **89**(4): p. 1823-32.

200. Holdstock, J.G., S.J. Aylwin, and J.M. Burrin, *Calcium and glycoprotein hormone alpha-subunit gene expression and secretion in alpha T3-1 gonadotropes.* Mol Endocrinol, 1996. **10**(11): p. 1308-17.

201. Fowkes, R.C., P. King, and J.M. Burrin, *Regulation of human glycoprotein hormone alpha-subunit gene transcription in L beta T2 gonadotropes by protein kinase C and extracellular signal-regulated kinase 1/2.* Biology of Reproduction, 2002. **67**(3): p. 725-734.

202. Roberson, M.S., et al., *A role for mitogen-activated protein kinase in mediating activation of the glycoprotein hormone alpha-subunit promoter by gonadotropin-releasing hormone.* Mol Cell Biol, 1995. **15**(7): p. 3531-9.

203. Burger, L.L., et al., *Regulation of Lhb and Egr1 gene expression by GNRH pulses in rat pituitaries is both c-Jun N-terminal kinase (JNK)- and extracellular signal-regulated kinase (ERK)-dependent.* Biol Reprod, 2009. **81**(6): p. 1206-15.

204. Haisenleder, D.J., et al., *Pulsatile gonadotropin-releasing hormone stimulation of gonadotropin subunit transcription in rat pituitaries: Evidence for the involvement of Jun N-terminal kinase but not p38.* Endocrinology, 2008. **149**(1): p. 139-145.

205. Weck, J., et al., *Differential gonadotropin-releasing hormone stimulation of rat luteinizing hormone subunit gene transcription by calcium influx and mitogen-activated protein kinase-signaling pathways.* Mol Endocrinol, 1998. **12**(3): p. 451-7.

206. Fowkes, R.C., P. King, and J.M. Burrin, *Regulation of human glycoprotein hormone alpha-subunit gene transcription in LbetaT2 gonadotropes by protein kinase C and extracellular signal-regulated kinase 1/2.* Biol Reprod, 2002. **67**(3): p. 725-34.

207. Kay, T.W., P.J. Chedrese, and J.L. Jameson, *Gonadotropin-releasing hormone causes transcriptional stimulation followed by desensitization of the glycoprotein hormone alpha promoter in transfected alpha T3 gonadotrope cells.* Endocrinology, 1994. **134**(2): p. 568-73.

208. Burrin, J.M., et al., *Mechanism of action of pituitary adenylate cyclase-activating polypeptide on human glycoprotein hormone alpha-subunit transcription in alphaT3-1 gonadotropes.* Endocrinology, 1998. **139**(4): p. 1731-7.

209. Zhang, P. and S.H. Mellon, *The orphan nuclear receptor steroidogenic factor-1 regulates the cyclic adenosine 3',5'-monophosphate-mediated transcriptional*

activation of rat cytochrome P450c17 (17 alpha-hydroxylase/c17-20 lyase). Mol Endocrinol, 1996. **10**(2): p. 147-58.

210. Gyles, S.L., et al., *ERKs regulate cyclic AMP-induced steroid synthesis through transcription of the steroidogenic acute regulatory (StAR) gene.* J Biol Chem, 2001. **276**(37): p. 34888-95.

211. Keri, R.A., et al., *Estradiol inhibits transcription of the human glycoprotein hormone alpha-subunit gene despite the absence of a high affinity binding site for estrogen receptor.* Mol Endocrinol, 1991. **5**(5): p. 725-33.

212. Jorgensen, J.S. and J.H. Nilson, *AR suppresses transcription of the alpha glycoprotein hormone subunit gene through protein-protein interactions with cJun and activation transcription factor 2.* Mol Endocrinol, 2001. **15**(9): p. 1496-504.

213. Halvorson, L.M., U.B. Kaiser, and W.W. Chin, *Stimulation of luteinizing hormone beta gene promoter activity by the orphan nuclear receptor, steroidogenic factor-1.* J Biol Chem, 1996. **271**(12): p. 6645-50.

214. Quirk, C.C., et al., *A single Pitx1 binding site is essential for activity of the LH beta promoter in transgenic mice.* Molecular Endocrinology, 2001. **15**(5): p. 734-746.

215. Lanctot, C., B. Lamolet, and J. Drouin, *The bicoid-related homeoprotein Ptx1 defines the most anterior domain of the embryo and differentiates posterior from anterior lateral mesoderm.* Development, 1997. **124**(14): p. 2807-2817.

216. Dorn, C., et al., *Activation of luteinizing hormone beta gene by gonadotropin-releasing hormone requires the synergy of early growth response-1 and steroidogenic factor-1.* J Biol Chem, 1999. **274**(20): p. 13870-6.

217. Jameson, L., et al., *The gene encoding the beta-subunit of rat luteinizing hormone. Analysis of gene structure and evolution of nucleotide sequence.* J Biol Chem, 1984. **259**(24): p. 15474-80.

218. Wu, F.C.W., et al., *Patterns of Pulsatile Luteinizing-Hormone Secretion before and during the Onset of Puberty in Boys - a Study Using an Immunoradiometric Assay.* Journal of Clinical Endocrinology & Metabolism, 1990. **70**(3): p. 629-637.

219. Haisenleder, D.J., et al., *Regulation of Gonadotropin Subunit Messenger-Ribonucleic-Acid Expression by Gonadotropin-Releasing-Hormone Pulse Amplitude Invitro.* Endocrinology, 1993. **132**(3): p. 1292-1296.

220. Shupnik, M.A., S.D. Gharib, and W.W. Chin, *Divergent Effects of Estradiol on Gonadotropin Gene-Transcription in Pituitary Fragments.* Molecular Endocrinology, 1989. **3**(3): p. 474-480.

221. Levine, J.E. and V.D. Ramirez, *Luteinizing-Hormone-Releasing Hormone-Release during the Rat Estrous-Cycle and after Ovariectomy, as Estimated with Push-Pull Cannulae.* Endocrinology, 1982. **111**(5): p. 1439-1448.

222. Lee, S.L., et al., *Luteinizing hormone deficiency and female infertility in mice lacking the transcription factor NGFI-A (Egr-1).* Science, 1996. **273**(5279): p. 1219-21.

223. Topilko, P., et al., *Multiple pituitary and ovarian defects in Krox-24 (NGFI-A, Egr-1)-targeted mice.* Mol Endocrinol, 1998. **12**(1): p. 107-22.

224. Zhao, L.P., et al., *Steroidogenic factor 1 (SF1) is essential for pituitary gonadotrope function.* Development, 2001. **128**(2): p. 147-154.

225. Zhao, L., M. Bakke, and K.L. Parker, *Pituitary-specific knockout of steroidogenic factor 1.* Mol Cell Endocrinol, 2001. **185**(1-2): p. 27-32.

226. Bliss, S.P., et al., *ERK Signaling in the Pituitary Is Required for Female But Not Male Fertility.* Molecular Endocrinology, 2009. **23**(7): p. 1092-1101.

227. Melamed, P., *Hormonal signaling to follicle stimulating hormone beta-subunit gene expression.* Mol Cell Endocrinol, 2010. **314**(2): p. 204-12.

228. Melamed, P., et al., *Transcription of gonadotropin beta subunit genes involves cross-talk between the transcription factors and co-regulators that mediate actions of the regulatory hormones.* Mol Cell Endocrinol, 2006. **252**(1-2): p. 167-83.

229. Choi, S.G., et al., *Characterization of Gonadotrope Secretoproteome Identifies Neurosecretory Protein VGF-derived Peptide Suppression of Follicle-stimulating Hormone Gene Expression.* J Biol Chem, 2016. **291**(40): p. 21322-21334.

230. Thompson, T.B., et al., *The structure of the follistatin:activin complex reveals antagonism of both type I and type II receptor binding.* Dev Cell, 2005. **9**(4): p. 535-43.

231. Ciccone, N.A., et al., *A composite element that binds basic helix loop helix and basic leucine zipper transcription factors is important for gonadotropin-releasing hormone regulation of the follicle-stimulating hormone beta gene.* Molecular Endocrinology, 2008. **22**(8): p. 1908-1923.

232. Coss, D., et al., *A novel AP-1 site is critical for maximal induction of the follicle-stimulating hormone beta gene by gonadotropin-releasing hormone.* Journal of Biological Chemistry, 2004. **279**(1): p. 152-162.

233. Wang, Y., et al., *Activator protein-1 and smad proteins synergistically regulate human follicle-stimulating hormone beta-promoter activity.* Endocrinology, 2008. **149**(11): p. 5577-91.

234. Strahl, B.D., et al., *Two proximal activating protein-1-binding sites are sufficient to stimulate transcription of the ovine follicle-stimulating hormone-beta gene.* Endocrinology, 1997. **138**(6): p. 2621-31.

235. Huang, H.J., et al., *Transcriptional regulation of the ovine follicle-stimulating hormone-beta gene by activin and gonadotropin-releasing hormone (GnRH):*

involvement of two proximal activator protein-1 sites for GnRH stimulation. Endocrinology, 2001. **142**(6): p. 2267-74.

236. Strahl, B.D., et al., *Transcriptional activation of the ovine follicle-stimulating hormone beta-subunit gene by gonadotropin-releasing hormone: involvement of two activating protein-1-binding sites and protein kinase C.* Endocrinology, 1998. **139**(11): p. 4455-65.

237. Ciccone, N.A., et al., *Frequency-Dependent Regulation of Follicle-Stimulating Hormone beta by Pulsatile Gonadotropin-Releasing Hormone Is Mediated by Functional Antagonism of bZIP Transcription Factors.* Molecular and Cellular Biology, 2010. **30**(4): p. 1028-1040.

238. Xie, C.C., et al., *Gonadotropin and kisspeptin gene expression, but not GnRH, are impaired in cFOS deficient mice.* Molecular and Cellular Endocrinology, 2015. **411**(C): p. 223-231.

239. Jonak, C.R., et al., *c-JUN Dimerization Protein 2 (JDP2) Is a Transcriptional Repressor of Follicle-stimulating Hormone beta (FSHbeta) and Is Required for Preventing Premature Reproductive Senescence in Female Mice.* J Biol Chem, 2017. **292**(7): p. 2646-2659.

240. Janjic, M.M., S.S. Stojilkovic, and I. Bjelobaba, *Intrinsic and Regulated Gonadotropin-Releasing Hormone Receptor Gene Transcription in Mammalian Pituitary Gonadotrophs.* Front Endocrinol (Lausanne), 2017. **8**: p. 221.

241. Gong, Q., C. Huntsman, and D. Ma, *Clathrin-independent internalization and recycling.* J Cell Mol Med, 2008. **12**(1): p. 126-44.

242. Chini, B. and M. Parenti, *G-protein coupled receptors in lipid rafts and caveolae: how, when and why do they go there?* Journal of Molecular Endocrinology, 2004. **32**(2): p. 325-338.

243. Hanyaloglu, A.C. and M. von Zastrow, *Regulation of GPCRs by endocytic membrane trafficking and its potential implications.* Annu Rev Pharmacol Toxicol, 2008. **48**: p. 537-68.

244. Luttrell, L.M. and R.J. Lefkowitz, *The role of beta-arrestins in the termination and transduction of G-protein-coupled receptor signals.* J Cell Sci, 2002. **115**(Pt 3): p. 455-65.

245. Pierce, K.L. and R.J. Lefkowitz, *Classical and new roles of beta-arrestins in the regulation of G-protein-coupled receptors.* Nat Rev Neurosci, 2001. **2**(10): p. 727-33.

246. Kaksonen, M., C.P. Toret, and D.G. Drubin, *Harnessing actin dynamics for clathrin-mediated endocytosis.* Nat Rev Mol Cell Biol, 2006. **7**(6): p. 404-14.

247. Roux, A., et al., *GTP-dependent twisting of dynamin implicates constriction and tension in membrane fission.* Nature, 2006. **441**(7092): p. 528-31.

248. Mundell, S.J., et al., *Distinct clathrin-coated pits sort different G protein-coupled receptor cargo.* Traffic, 2006. **7**(10): p. 1420-31.

249. Hazum, E., et al., *Receptor-mediated internalization of fluorescent gonadotropin-releasing hormone by pituitary gonadotropes.* Proc Natl Acad Sci U S A, 1980. **77**(11): p. 6692-5.

250. Jennes, L., W.E. Stumpf, and P.M. Conn, *Intracellular Pathways of Electron-Opaque Gonadotropin-Releasing Hormone Derivatives Bound by Cultured Gonadotropes.* Endocrinology, 1983. **113**(5): p. 1683-1689.

251. Heding, A., et al., *The rat gonadotropin-releasing hormone receptor internalizes via a beta-arrestin-independent, but dynamin-dependent, pathway: addition of a carboxyl-terminal tail confers beta-arrestin dependency.* Endocrinology, 2000. **141**(1): p. 299-306.

252. Pawson, A.J., et al., *Multiple determinants for rapid agonist-induced internalization of a nonmammalian gonadotropin-releasing hormone receptor: a putative palmitoylation site and threonine doublet within the carboxyl-terminal tail Are critical.* Endocrinology, 2003. **144**(9): p. 3860-71.

253. Ulloa-Aguirre, A. and P.M. Conn, *Targeting of G protein-coupled receptors to the plasma membrane in health and disease.* Front Biosci (Landmark Ed), 2009. **14**: p. 973-94.

254. Aridor, M. and W.E. Balch, *Integration of endoplasmic reticulum signaling in health and disease.* Nat Med, 1999. **5**(7): p. 745-51.

255. Trombetta, E.S. and A.J. Parodi, *Quality control and protein folding in the secretory pathway.* Annu Rev Cell Dev Biol, 2003. **19**: p. 649-76.

256. Finch, A.R., et al., *Trafficking and signalling of gonadotrophin-releasing hormone receptors: an automated imaging approach.* Br J Pharmacol, 2010. **159**(4): p. 751-60.

257. Brooks, D.A., *Introduction: Molecular chaperones of the ER: their role in protein folding and genetic disease.* Seminars in Cell & Developmental Biology, 1999. **10**(5): p. 441-442.

258. Finch, A.R., et al., *Plasma membrane expression of GnRH receptors: regulation by antagonists in breast, prostate, and gonadotrope cell lines.* J Endocrinol, 2008. **196**(2): p. 353-67.

259. Davidson, J.S., et al., *Incorporation of an additional glycosylation site enhances expression of functional human gonadotropin-releasing hormone receptor.* Endocrine, 1996. **4**(3): p. 207-12.

260. Weiner, R.I., *Cellular basis of the GnRH pulse generator.* Nihon Sanka Fujinka Gakkai Zasshi, 1996. **48**(8): p. 573-7.

261. Tsutsumi, R. and N.J. Webster, *GnRH pulsatility, the pituitary response and reproductive dysfunction.* Endocr J, 2009. **56**(6): p. 729-37.

262. Belchetz, P.E., et al., *Hypophyseal Responses to Continuous and Intermittent Delivery of Hypothalamic Gonadotropin-Releasing Hormone.* Science, 1978. **202**(4368): p. 631-633.

263. Knobil, E., *The neuroendocrine control of the menstrual cycle.* Recent Prog Horm Res, 1980. **36**: p. 53-88.

264. Wildt, L., et al., *Frequency and amplitude of gonadotropin-releasing hormone stimulation and gonadotropin secretion in the rhesus monkey.* Endocrinology, 1981. **109**(2): p. 376-85.

265. Bennett, H.P.J. and C. Mcmartin, *Peptide-Hormones and Their Analogs - Distribution, Clearance from the Circulation, and Inactivation Invivo.* Pharmacological Reviews, 1978. **30**(3): p. 247-292.

266. Grachev, P. and R.L. Goodman, *The GnRH Pulse Generator.* Aims Medical Science, 2016. **3**(4): p. 359-385.

267. Carmel, P.W., S. Araki, and M. Ferin, *Pituitary stalk portal blood collection in rhesus monkeys: evidence for pulsatile release of gonadotropin-releasing hormone (GnRH).* Endocrinology, 1976. **99**(1): p. 243-8.

268. Voogt, J.L., et al., *In vivo release of dopamine, luteinizing hormone-releasing hormone and thyrotropin-releasing hormone in male rats bearing a prolactin-secreting tumor.* Neuroendocrinology, 1987. **46**(2): p. 110-6.

269. Clarke, I.J. and J.T. Cummins, *The Temporal Relationship between Gonadotropin-Releasing Hormone (Gnrh) and Luteinizing-Hormone (Lh) Secretion in Ovariectomized Ewes.* Endocrinology, 1982. **111**(5): p. 1737-1739.

270. Van Vugt, D.A., et al., *Gonadotropin-releasing hormone pulses in third ventricular cerebrospinal fluid of ovariectomized rhesus monkeys: correlation with luteinizing hormone pulses.* Endocrinology, 1985. **117**(4): p. 1550-8.

271. Sisk, C.L. and D.L. Foster, *The neural basis of puberty and adolescence.* Nat Neurosci, 2004. **7**(10): p. 1040-7.

272. Halban, P.A. and J.C. Irminger, *Sorting and processing of secretory proteins.* Biochem J, 1994. **299 (Pt 1)**: p. 1-18.

273. Clarke, I., L. Moore, and J. Veldhuis, *Intensive direct cavernous sinus sampling identifies high-frequency, nearly random patterns of FSH secretion in ovariectomized ewes: combined appraisal by RIA and bioassay.* Endocrinology, 2002. **143**(1): p. 117-29.

274. Bowsher, C.G. and P.S. Swain, *Environmental sensing, information transfer, and cellular decision-making.* Curr Opin Biotechnol, 2014. **28**: p. 149-55.

275. Levchenko, A. and I. Nemenman, *Cellular noise and information transmission.* Curr Opin Biotechnol, 2014. **28**: p. 156-64.

276. Lewis, C.E., P.S.M. Richards, and J.F. Morris, *Heterogeneity of Responses to Lh-Releasing Hormone and Phorbol Ester among Rat Gonadotrophs - a Study Using a Reverse Hemolytic Plaque-Assay for Lh.* Journal of Molecular Endocrinology, 1989. **2**(1): p. 55-63.

277. McArdle, C.A., R. Bunting, and W.T. Mason, *Dynamic video imaging of cystolic Ca(2+) in the alphaT3-1, gonadotrope-derived cell line.* Mol Cell Neurosci, 1992. **3**(2): p. 124-32.

278. Stojilkovic, S.S. and K.J. Catt, *Novel aspects of GnRH-induced intracellular signaling and secretion in pituitary gonadotrophs.* J Neuroendocrinol, 1995. **7**(10): p. 739-57.

279. Geva-Zatorsky, N., et al., *Oscillations and variability in the p53 system.* Molecular Systems Biology, 2006. **2**.

280. Cohen-Saidon, C., et al., *Dynamics and variability of ERK2 response to EGF in individual living cells.* Mol Cell, 2009. **36**(5): p. 885-93.

281. Tay, S., et al., *Single-cell NF-kappaB dynamics reveal digital activation and analogue information processing.* Nature, 2010. **466**(7303): p. 267-71.

282. Selimkhanov, J., et al., *Accurate information transmission through dynamic biochemical signaling networks.* Science, 2014. **346**(6215): p. 1370-1373.

283. Rhee, A., R. Cheong, and A. Levchenko, *The application of information theory to biochemical signaling systems.* Phys Biol, 2012. **9**(4): p. 045011.

284. Levens, D. and A. Gupta, *Molecular biology. Reliable noise.* Science, 2010. **327**(5969): p. 1088-9.

285. Tsimring, L.S., *Noise in biology.* Rep Prog Phys, 2014. **77**(2): p. 026601.

286. Ladbury, J.E. and S.T. Arold, *Noise in cellular signaling pathways: causes and effects.* Trends Biochem Sci, 2012. **37**(5): p. 173-8.

287. Chang, A.Y. and W.F. Marshall, *Organelles - understanding noise and heterogeneity in cell biology at an intermediate scale.* J Cell Sci, 2017. **130**(5): p. 819-826.

288. Kim, E., et al., *Cell signaling heterogeneity is modulated by both cell-intrinsic and -extrinsic mechanisms: An integrated approach to understanding targeted therapy.* Plos Biology, 2018. **16**(3).

289. Bandiera, L., S. Furini, and E. Giordano, *Phenotypic Variability in Synthetic Biology Applications: Dealing with Noise in Microbial Gene Expression.* Front Microbiol, 2016. **7**: p. 479.

290. Chen, J.Y., et al., *A two-dimensional ERK-AKT signaling code for an NGF-triggered cell-fate decision.* Mol Cell, 2012. **45**(2): p. 196-209.

291. Dean, M., T. Fojo, and S. Bates, *Tumour stem cells and drug resistance.* Nat Rev Cancer, 2005. **5**(4): p. 275-84.

292. Fink, G., *Mathematical modeling of gonadotropin-releasing hormone signaling.* Mol Cell Endocrinol, 2018. **470**: p. 34-35.

293. Raser, J.M. and E.K. O'Shea, *Noise in gene expression: origins, consequences, and control.* Science, 2005. **309**(5743): p. 2010-3.

294. Kaern, M., et al., *Stochasticity in gene expression: from theories to phenotypes.* Nat Rev Genet, 2005. **6**(6): p. 451-64.

295. Lu, T., et al., *Phenotypic variability of growing cellular populations.* Proc Natl Acad Sci U S A, 2007. **104**(48): p. 18982-7.

296. Brennan, M.D., R. Cheong, and A. Levchenko, *How Information Theory Handles Cell Signaling and Uncertainty.* Science, 2012. **338**(6105): p. 334-335.

297. Gage, J.S., *The concept of meaning and the mathematical theory of communication.* MD Comput, 1992. **9**(3): p. 146-8.

298. Voliotis, M., et al., *Information transfer by leaky, heterogeneous, protein kinase signaling systems.* Proc Natl Acad Sci U S A, 2014. **111**(3): p. E326-33.

299. Cheong, R., et al., *Information transduction capacity of noisy biochemical signaling networks.* Science, 2011. **334**(6054): p. 354-8.

300. Uda, S., et al., *Robustness and compensation of information transmission of signaling pathways.* Science, 2013. **341**(6145): p. 558-61.

301. Landry, J.J., et al., *The genomic and transcriptomic landscape of a HeLa cell line.* G3 (Bethesda), 2013. **3**(8): p. 1213-24.

302. Armstrong, S.P., et al., *Using automated imaging to interrogate gonadotrophin-releasing hormone receptor trafficking and function.* Molecular and Cellular Endocrinology, 2011. **331**(2): p. 194-204.

303. Masters, J.R., *HeLa cells 50 years on: the good, the bad and the ugly.* Nat Rev Cancer, 2002. **2**(4): p. 315-9.

304. Scherer, W.F., J.T. Syverton, and G.O. Gey, *Studies on the propagation in vitro of poliomyelitis viruses. IV. Viral multiplication in a stable strain of human malignant epithelial cells (strain HeLa) derived from an epidermoid carcinoma of the cervix.* J Exp Med, 1953. **97**(5): p. 695-710.

305. Turner, T., *Development of the polio vaccine: a historical perspective of Tuskegee University's role in mass production and distribution of HeLa cells.* J Health Care Poor Underserved, 2012. **23**(4 Suppl): p. 5-10.

306. Comsa, S., A.M. Cimpean, and M. Raica, *The Story of MCF-7 Breast Cancer Cell Line: 40 years of Experience in Research.* Anticancer Res, 2015. **35**(6): p. 3147-54.

307. Soule, H.D., et al., *A human cell line from a pleural effusion derived from a breast carcinoma.* J Natl Cancer Inst, 1973. **51**(5): p. 1409-16.

308. Levenson, A.S. and V.C. Jordan, *MCF-7: the first hormone-responsive breast cancer cell line.* Cancer Res, 1997. **57**(15): p. 3071-8.

309. Holliday, D.L. and V. Speirs, *Choosing the right cell line for breast cancer research.* Breast Cancer Res, 2011. **13**(4): p. 215.

310. Ebi, H., et al., *PI3K regulates MEK/ERK signaling in breast cancer via the Rac-GEF, P-Rex1.* Proc Natl Acad Sci U S A, 2013. **110**(52): p. 21124-9.

311. Suvarna, V., et al., *Phytochemicals and PI3K Inhibitors in Cancer-An Insight.* Front Pharmacol, 2017. **8**: p. 916.

312. Sedgley, K.R., et al., *Intracellular gonadotropin-releasing hormone receptors in breast cancer and gonadotrope lineage cells.* J Endocrinol, 2006. **191**(3): p. 625-36.

313. Burdall, S.E., et al., *Breast cancer cell lines: friend or foe?* Breast Cancer Res, 2003. **5**(2): p. 89-95.

314. Bahia, H., et al., *Karyotypic variation between independently cultured strains of the cell line MCF-7 identified by multicolour fluorescence in situ hybridization.* International Journal of Oncology, 2002. **20**(3): p. 489-494.

315. Voliotis, M., et al., *Exploring Dynamics and Noise in Gonadotropin-Releasing Hormone (GnRH) Signaling.* Methods Mol Biol, 2018. **1819**: p. 405-429.

316. Armstrong, S.P., C.J. Caunt, and C.A. McArdle, *Gonadotropin-releasing hormone and protein kinase C signaling to ERK: spatiotemporal regulation of ERK by docking domains and dual-specificity phosphatases.* Mol Endocrinol, 2009. **23**(4): p. 510-9.

317. Fink, M.Y., et al., *Research resource: Gonadotropin-releasing hormone receptor-mediated signaling network in LbetaT2 cells: a pathway-based web-accessible knowledgebase.* Mol Endocrinol, 2010. **24**(9): p. 1863-71.

318. Alarid, E.T., et al., *Immortalization of pituitary cells at discrete stages of development by directed oncogenesis in transgenic mice.* Development, 1996. **122**(10): p. 3319-29.

319. Arroyo, J.D. and W.C. Hahn, *Involvement of PP2A in viral and cellular transformation.* Oncogene, 2005. **24**(52): p. 7746-55.

320. Sablina, A.A. and W.C. Hahn, *SV40 small T antigen and PP2A phosphatase in cell transformation.* Cancer Metastasis Rev, 2008. **27**(2): p. 137-46.

321. Larder, R., et al., *Gonadotropin-releasing hormone regulates expression of the DNA damage repair gene, Fanconi anemia A, in pituitary gonadotroph cells.* Biol Reprod, 2004. **71**(3): p. 828-36.

322. Liu, F., D.A. Austin, and N.J. Webster, *Gonadotropin-releasing hormone-desensitized LbetaT2 gonadotrope cells are refractory to acute protein kinase C, cyclic AMP, and calcium-dependent signaling.* Endocrinology, 2003. **144**(10): p. 4354-65.

323. Thomas, P., et al., *The L beta T2 clonal gonadotrope: a model for single cell studies of endocrine cell secretion.* Endocrinology, 1996. **137**(7): p. 2979-89.

324. McArdle, C.A., et al., *Estradiol regulates gonadotropin-releasing hormone receptor number, growth and inositol phosphate production in alpha T3-1 cells.* Mol Cell Endocrinol, 1992. **87**(1-3): p. 95-103.

325. Everest, H.M., et al., *Signaling and antiproliferative effects mediated by GnRH receptors after expression in breast cancer cells using recombinant adenovirus.* Endocrinology, 2001. **142**(11): p. 4663-4672.

326. Re, M., et al., *The Human Gonadotropin Releasing Hormone Type I Receptor Is a Functional Intracellular GPCR Expressed on the Nuclear Membrane.* Plos One, 2010. **5**(7).

327. Caunt, C.J., et al., *Arrestin-mediated ERK activation by gonadotropin-releasing hormone receptors: receptor-specific activation mechanisms and compartmentalization.* J Biol Chem, 2006. **281**(5): p. 2701-10.

328. Hsyu, P.H., et al., *Interactions of organic anions with the organic cation transporter in renal BBMV.* Am J Physiol, 1988. **254**(1 Pt 2): p. F56-61.

329. Oheim, M., et al., *New red-fluorescent calcium indicators for optogenetics, photoactivation and multi-color imaging.* Biochim Biophys Acta, 2014. **1843**(10): p. 2284-306.

330. Bootman, M.D., et al., *Ca2+-sensitive fluorescent dyes and intracellular Ca2+ imaging.* Cold Spring Harb Protoc, 2013. **2013**(2): p. 83-99.

331. Nemenman, I., F. Shafee, and W. Bialek, *Entropy and inference, revisited.* Advances in Neural Information Processing Systems 14, Vols 1 and 2, 2002. **14**: p. 471-478.

332. Shah, B.H., et al., *Roles of Src and epidermal growth factor receptor transactivation in transient and sustained ERK1/2 responses to gonadotropin-releasing hormone receptor activation.* J Biol Chem, 2003. **278**(21): p. 19118-26.

333. Ueda, Y., et al., *Protein kinase C activates the MEK-ERK pathway in a manner independent of Ras and dependent on Raf.* J Biol Chem, 1996. **271**(38): p. 23512-9.

334. Emons, G., et al., *High affinity binding and direct antiproliferative effects of LHRH analogues in human ovarian cancer cell lines.* Cancer Res, 1993. **53**(22): p. 5439-46.

335. Macville, M., et al., *Comprehensive and definitive molecular cytogenetic characterization of HeLa cells by spectral karyotyping.* Cancer Res, 1999. **59**(1): p. 141-50.

336. Das, M.R. and M.M. Mink, *Sequence homology of nucleic acids from human breast cancer cells and complementary DNA's from murine mammary tumor virus and Mason-Pfizer monkey virus.* Cancer Res, 1979. **39**(12): p. 5106-13.

337. Mok, M.T., et al., *Mouse mammary tumor virus-like env sequences in human breast cancer.* Int J Cancer, 2008. **122**(12): p. 2864-70.

338. Sontag, E., et al., *The interaction of SV40 small tumor antigen with protein phosphatase 2A stimulates the map kinase pathway and induces cell proliferation.* Cell, 1993. **75**(5): p. 887-97.

339. Sharma, R., et al., *Australian mental health care practitioners' practices and attitudes for encouraging smoking cessation and tobacco harm reduction in smokers with severe mental illness.* International Journal of Mental Health Nursing, 2018. **27**(1): p. 247-257.

340. Chen, J., et al., *Gonadotropin-releasing hormone-mediated phosphorylation of estrogen receptor-alpha contributes to fosB expression in mouse gonadotrophs.* Endocrinology, 2009. **150**(10): p. 4583-93.

341. Murphy, L.O., et al., *Molecular interpretation of ERK signal duration by immediate early gene products.* Nat Cell Biol, 2002. **4**(8): p. 556-64.

342. Murphy, L.O., J.P. MacKeigan, and J. Blenis, *A network of immediate early gene products propagates subtle differences in mitogen-activated protein kinase signal amplitude and duration.* Mol Cell Biol, 2004. **24**(1): p. 144-53.

343. Shaul, Y.D. and R. Seger, *The MEK/ERK cascade: from signaling specificity to diverse functions.* Biochim Biophys Acta, 2007. **1773**(8): p. 1213-26.

344. Perlson, E., et al., *Vimentin-dependent spatial translocation of an activated MAP kinase in injured nerve.* Neuron, 2005. **45**(5): p. 715-26.

345. Jobin, R.M. and J.P. Chang, *Actions of two native GnRHs and protein kinase C modulators on goldfish pituitary cells. Studies on intracellular calcium levels and gonadotropin release.* Cell Calcium, 1992. **13**(8): p. 531-40.

346. Naor, Z., et al., *Reciprocal cross talk between gonadotropin-releasing hormone (GnRH) and prostaglandin receptors regulates GnRH receptor expression and differential gonadotropin secretion.* Molecular Endocrinology, 2007. **21**(2): p. 524-537.

347. Millar, R.P. and C.L. Newton, *Current and future applications of GnRH, kisspeptin and neurokinin B analogues.* Nat Rev Endocrinol, 2013. **9**(8): p. 451-66.

348. Ebisuya, M., K. Kondoh, and E. Nishida, *The duration, magnitude and compartmentalization of ERK MAP kinase activity: mechanisms for providing signaling specificity.* J Cell Sci, 2005. **118**(Pt 14): p. 2997-3002.

349. Zehorai, E., et al., *The subcellular localization of MEK and ERK--a novel nuclear translocation signal (NTS) paves a way to the nucleus.* Mol Cell Endocrinol, 2010. **314**(2): p. 213-20.

350. Caunt, C.J., et al., *Seven-transmembrane receptor signalling and ERK compartmentalization.* Trends Endocrinol Metab, 2006. **17**(7): p. 276-83.

351. Eidne, K.A., et al., *Gonadotropin-releasing hormone (GnRH)-binding sites in human breast cancer cell lines and inhibitory effects of GnRH antagonists.* J Clin Endocrinol Metab, 1987. **64**(3): p. 425-32.

352. Limonta, P., M.M. Marelli, and R.M. Moretti, *LHRH analogues as anticancer agents: pituitary and extrapituitary sites of action.* Expert Opinion on Investigational Drugs, 2001. **10**(4): p. 709-720.

353. Lake, D., S.A. Correa, and J. Muller, *Negative feedback regulation of the ERK1/2 MAPK pathway.* Cell Mol Life Sci, 2016. **73**(23): p. 4397-4413.

354. Santos, S.D., P.J. Verveer, and P.I. Bastiaens, *Growth factor-induced MAPK network topology shapes Erk response determining PC-12 cell fate.* Nat Cell Biol, 2007. **9**(3): p. 324-30.

355. Shankaran, H. and H.S. Wiley, *Oscillatory dynamics of the extracellular signal-regulated kinase pathway.* Curr Opin Genet Dev, 2010. **20**(6): p. 650-5.

356. Herbert, C.A. and T.E. Trigg, *Applications of GnRH in the control and management of fertility in female animals.* Anim Reprod Sci, 2005. **88**(1-2): p. 141-53.

357. Gan, H.K., et al., *The epidermal growth factor receptor (EGFR) tyrosine kinase inhibitor AG1478 increases the formation of inactive untethered EGFR dimers. Implications for combination therapy with monoclonal antibody 806.* J Biol Chem, 2007. **282**(5): p. 2840-50.

358. D'Anneo, A., et al., *Parthenolide induces superoxide anion production by stimulating EGF receptor in MDA-MB-231 breast cancer cells.* Int J Oncol, 2013. **43**(6): p. 1895-900.

359. Wilkinson, S.E., P.J. Parker, and J.S. Nixon, *Isoenzyme Specificity of Bisindolylmaleimides, Selective Inhibitors of Protein-Kinase-C.* Biochemical Journal, 1993. **294**: p. 335-337.

360. Matsuda, S. and S. Koyasu, *Mechanisms of action of cyclosporine.* Immunopharmacology, 2000. **47**(2-3): p. 119-25.

361. Kiani, A., A. Rao, and J. Aramburu, *Manipulating immune responses with immunosuppressive agents that target NFAT.* Immunity, 2000. **12**(4): p. 359-72.

362. Imai, A., et al., *Gi protein activation of gonadotropin-releasing hormone-mediated protein dephosphorylation in human endometrial carcinoma.* Am J Obstet Gynecol, 1997. **176**(2): p. 371-6.

363. Emons, G., et al., *Effects of LHRH-analogues on mitogenic signal transduction in cancer cells.* J Steroid Biochem Mol Biol, 1998. **65**(1-6): p. 199-206.

364. Limonta, P., et al., *The biology of gonadotropin hormone-releasing hormone: role in the control of tumor growth and progression in humans.* Front Neuroendocrinol, 2003. **24**(4): p. 279-95.

365. Moretti, R.M., et al., *Inhibitory activity of luteinizing hormone-releasing hormone on tumor growth and progression.* Endocr Relat Cancer, 2003. **10**(2): p. 161-7.

366. Maudsley, S., et al., *Gonadotropin-releasing hormone (GnRH) antagonists promote proapoptotic signaling in peripheral reproductive tumor cells by activating a Galphai-coupling state of the type I GnRH receptor.* Cancer Res, 2004. **64**(20): p. 7533-44.

367. Cho-Clark, M., et al., *GnRH-(1-5) transactivates EGFR in Ishikawa human endometrial cells via an orphan G protein-coupled receptor.* Mol Endocrinol, 2014. **28**(1): p. 80-98.

368. Lazar, M.A., *Nuclear receptor corepressors.* Nucl Recept Signal, 2003. **1**: p. e001.

369. Duran-Pasten, M.L., T. Fiordelisio-Coll, and A. Hernandez-Cruz, *Castration-induced modifications of GnRH-elicited [Ca2+](i) signaling patterns in male mouse pituitary gonadotrophs in situ: studies in the acute pituitary slice preparation.* Biol Reprod, 2013. **88**(2): p. 38.

370. Sanchez-Cardenas, C. and A. Hernandez-Cruz, *GnRH-Induced [Ca2+]i-signalling patterns in mouse gonadotrophs recorded from acute pituitary slices in vitro.* Neuroendocrinology, 2010. **91**(3): p. 239-55.

371. McArdle, C.A., et al., *Ca2+ entry in gonadotrophs and alpha T3-1 cells: Does store-dependent Ca2+ influx mediate gonadotrophin-releasing hormone action?* Journal of Endocrinology, 1996. **149**(1): p. 155-169.

372. Morgan, A.J. and R. Jacob, *Ionomycin enhances Ca2+ influx by stimulating store-regulated cation entry and not by a direct action at the plasma membrane.* Biochem J, 1994. **300 (Pt 3)**: p. 665-72.

373. Lestas, I., G. Vinnicombe, and J. Paulsson, *Fundamental limits on the suppression of molecular fluctuations.* Nature, 2010. **467**(7312): p. 174-8.

374. Evans, J.J., W. Forrest-Owen, and C.A. McArdle, *Oxytocin receptor-mediated activation of phosphoinositidase C and elevation of cytosolic calcium in the gonadotrope-derived alphaT3-1 cell line.* Endocrinology, 1997. **138**(5): p. 2049-55.

375. Veening, J.G., et al., *The role of oxytocin in male and female reproductive behavior.* Eur J Pharmacol, 2015. **753**: p. 209-28.

376. Breton, C., et al., *Oxytocin receptor messenger ribonucleic acid: characterization, regulation, and cellular localization in the rat pituitary gland.* Endocrinology, 1995. **136**(7): p. 2928-36.

377. Krsmanovic, L.Z., et al., *The hypothalamic GnRH pulse generator: multiple regulatory mechanisms.* Trends Endocrinol Metab, 2009. **20**(8): p. 402-8.

378. Kanasaki, H., et al., *How is GnRH regulated in GnRH-producing neurons? Studies using GT1-7 cells as a GnRH-producing cell model.* General and Comparative Endocrinology, 2017. **247**: p. 138-142.

379. Altschuler, S.J. and L.F. Wu, *Cellular heterogeneity: do differences make a difference?* Cell, 2010. **141**(4): p. 559-63.

380. Elsasser, W.M., *Outline of a theory of cellular heterogeneity.* Proc Natl Acad Sci U S A, 1984. **81**(16): p. 5126-9.

381. Dalkin, A.C., et al., *The frequency of gonadotropin-releasing-hormone stimulation differentially regulates gonadotropin subunit messenger ribonucleic acid expression.* Endocrinology, 1989. **125**(2): p. 917-24.

382. Burger, L.L., et al., *GnRH pulse frequency modulation of gonadotropin subunit gene transcription in normal gonadotropes-assessment by primary transcript assay provides evidence for roles of GnRH and follistatin.* Endocrinology, 2002. **143**(9): p. 3243-9.

383. Bowsher, C.G. and P.S. Swain, *Identifying sources of variation and the flow of information in biochemical networks.* Proc Natl Acad Sci U S A, 2012. **109**(20): p. E1320-8.

384. Dondi, D., et al., *Antiproliferative effects of luteinizing hormone-releasing hormone (LHRH) agonists on human androgen-independent prostate cancer cell line DU 145: evidence for an autocrine-inhibitory LHRH loop.* Cancer Res, 1994. **54**(15): p. 4091-5.

385. Limonta, P., et al., *Antiproliferative effects of luteinizing hormone-releasing hormone agonists on the human prostatic cancer cell line LNCaP.* J Clin Endocrinol Metab, 1992. **75**(1): p. 207-12.

386. Emons, G. and A.V. Schally, *The Use of Luteinizing-Hormone-Releasing Hormone Agonists and Antagonists in Gynecological Cancers.* Human Reproduction, 1994. **9**(7): p. 1364-1379.

387. Schally, A.V. and A. Nagy, *Cancer chemotherapy based on targeting of cytotoxic peptide conjugates to their receptors on tumors.* European Journal of Endocrinology, 1999. **141**(1): p. 1-14.

388. Millar, R., et al., *A novel mammalian receptor for the evolutionarily conserved type II GnRH.* Proc Natl Acad Sci U S A, 2001. **98**(17): p. 9636-41.

389. Neill, J.D., et al., *A gonadotropin-releasing hormone (GnRH) receptor specific for GnRH II in primates.* Biochem Biophys Res Commun, 2001. **282**(4): p. 1012-8.

390. Morgan, K., et al., *A transcriptionally active human type II gonadotropin-releasing hormone receptor gene homolog overlaps two genes in the antisense orientation on chromosome 1q.12.* Endocrinology, 2003. **144**(2): p. 423-36.

391. Wells, A., *EGF receptor.* Int J Biochem Cell Biol, 1999. **31**(6): p. 637-43.

392. Sviridonov, L., et al., *Differential signaling of the GnRH receptor in pituitary gonadotrope cell lines and prostate cancer cell lines.* Mol Cell Endocrinol, 2013. **369**(1-2): p. 107-18.

393. Dobkin-Bekman, M., et al., *Activation of Mitogen-activated protein kinase (MAPK) by GnRH is cell-context dependent.* Molecular and Cellular Endocrinology, 2006. **252**(1-2): p. 184-190.

394. Stojilkovic, S.S., J. Reinhart, and K.J. Catt, *Gonadotropin-releasing hormone receptors: structure and signal transduction pathways.* Endocr Rev, 1994. **15**(4): p. 462-99.

395. Shacham, S., et al., *Mechanism of GnRH receptor signaling: from the membrane to the nucleus.* Ann Endocrinol (Paris), 1999. **60**(2): p. 79-88.

396. Naor, Z., *Signal transduction mechanisms of Ca2+ mobilizing hormones: the case of gonadotropin-releasing hormone.* Endocr Rev, 1990. **11**(2): p. 326-53.

397. Naor, Z., *GnRH receptor signaling: cross-talk of Ca2+ and protein kinase C.* Eur J Endocrinol, 1997. **136**(2): p. 123-7.

398. Dobkin-Bekman, M., et al., *Differential role of PKC isoforms in GnRH and phorbol 12-myristate 13-acetate activation of extracellular signal-regulated kinase and Jun N-terminal kinase.* Endocrinology, 2010. **151**(10): p. 4894-907.

399. Selimkhanov, J., et al., *Systems biology. Accurate information transmission through dynamic biochemical signaling networks.* Science, 2014. **346**(6215): p. 1370-3.

400. Tomasz J, Tomasx W, Karol N, Slawomi B, Michal K. *information-theoretic analysis of multivariate single - cell signaling responses using SLEMI.* arXiv:1808.05581[q-bio.QM], 16.08.2018.

401. Porter, J.R., B.W. Andrews, and P.A. Iglesias, *A framework for designing and analyzing binary decision-making strategies in cellular systems.* Integr Biol (Camb), 2012. **4**(3): p. 310-7.